

The Effect of Inorganic Components on Organic Matter Transformation under Hydrothermal Conditions

–

Constraints from Laboratory Experiments Studying the Abiotic Oxidation of *n*-Octane in Presence of Iron Mineral Assemblages, Additional Transition Metals and Dissolved Sulfate

Von der Naturwissenschaftlichen Fakultät der
Gottfried Wilhelm Leibniz Universität Hannover

zur Erlangung des Grades
Doktorin der Naturwissenschaften, Dr. rer. nat.
genehmigte Dissertation

von

Dipl.-Geow. Svenja Erdmann (geb. Germerott)

geboren am 22.11.1982 in Gehrden

2015

Referent: Prof. Dr. rer. nat. Harald Behrens

Korreferent: Prof. Dr. rer. nat. Wolfgang Bach

Tag der Promotion: 15.01.2015

Acknowledgments

First of all, I thank my supervisors Dr. Christian Ostertag-Henning and Prof. Dr. Harald Behrens for initiating the present PhD thesis through the combined research project 200-4500044471 between the Leibniz University of Hanover and the Federal Institute for Natural Resources and Geosciences (BGR). I appreciate their support during my PhD. I also want to thank my current managers Stefan Wessling and Ansgar Cartellieri for their support during the final phase.

Furthermore, I want to thank all my colleagues from the mineralogy department who created a friendly work atmosphere. Special thanks are addressed to the workshop team at the university, including Ulrich Kroll, Fabian Christ, Manuel Christ and Björn Ecks, for technical assistance with the cold-seal pressure vessels. From the BGR side, I want to extend my thanks to Christian Seeger for his input and help with the experimental setup. I thank Michael Hinze for contributing to this work in the frame of his Bachelor thesis and his work as research assistant. Then, I want to thank Sören Wilke for his help during sample preparation.

Major thanks are addressed to Sabrina Hohls who provided gas chromatography measurements in a very attentive and thorough way. X-ray diffraction data were supplied, by Dr. Reiner Dohrmann, Dr. Stephan Kaufhold and Dieter Weck from the BGR. Ute Bauer performed CS analyses at the university. I thank Annegret Tietjen, Georg Scheeder and Christian Wöhr, who always had a helping hand during method development and lab work at the BGR. I also want to thank Dr. Jan Schüssler, who shared his knowledge on how to determine the activity of pyrrhotite. I am much obliged to Laurent Richard who introduced me to thermodynamic modeling with the SUPCRT program. Furthermore, I want to thank Michael Hentscher who performed geochemical modeling using the Geochemist's Workbench software. I am grateful for constructive comments on a manuscript by Jeffrey Seewald and an anonymous reviewer that strongly helped to improve data interpretation. I thank Amer Hakki from the technical chemistry department at the Leibniz University of Hanover for discussion on transition metal catalysis. Props are given to Bastian Joachim for proof-reading the thesis.

Last but not least, I thank my family and friends who supported me the whole way. I especially thank my adorable husband for loving me as I am with all my moods, and my lovely daughter Paulina who made it easy to forget work sometimes.

Abstract

Numerous possibilities exist for reactions of inorganic and organic compounds in nature, like for example in petroleum systems, submarine hydrothermal systems and sulfide ore deposits if associated with organic matter. The understanding of the effect of inorganic components on the stability of organic compounds in these settings is, however, limited. In order to contribute to a better understanding of these potential reactions, three internally consistent series of experiments (300-350°C, 13 and 35 MPa, 72-336 h) were conducted to study the reaction of *n*-octane (C₈H₁₈) with two defined mineral assemblages (pyrite-pyrrhotite-magnetite = PPM and hematite-magnetite = HM), Na₂SO₄ and various transition metal sulfates (CuSO₄, FeSO₄, Fe₂(SO₄)₃, NiSO₄ and ZnSO₄). After the experiments, solids were analyzed via X-ray diffraction and organic reaction products were analyzed via headspace gas chromatography. Quantified organic products comprise CO₂, *n*- and *iso*-alkanes, alkenes, ketones and aromatics. An extended calibration allowed the determination of three organosulfur compounds (thiophene, 2- and 3-methylthiophene) for samples containing transition metal sulfates.

Overall, the distribution pattern of organic products is similar for all samples, indicating that cracking and aqueous oxidation are the major controlling factors for *n*-octane decomposition during the experiments. Despite this good general agreement, results clearly show that the examined inorganic compounds can affect the thermal decomposition of *n*-octane to various, non-negligible degrees. This is for example illustrated by the observation that different additives cause various *n*-octane conversions, which range from 0.24 mol% (PPM+H₂O+C₈H₁₈ 300°C) to 28 mol% (CuSO₄+H₂O+C₈H₁₈ 315°C). Furthermore, generated products reflect more oxidizing conditions in presence of HM than in presence of the PPM, which is in line with the redox buffering ability of these mineral assemblages. Thermodynamic evaluation of organic products provide evidence that alkanes and alkenes, but not alkenes and ketones, attained or closely approached thermodynamic equilibrium with respect to the aqueous hydrogen concentration, which is regulated by the buffers during the experiments.

Addition of Na₂SO₄ reduces the oxidation of *n*-octane to CO₂ in the HM, PPM and buffer-free experiments, which were processed at 350°C. This is in contrast to previous studies, which investigate the thermochemical reduction of sulfate (TSR), a redox reaction in which hydrocarbons are oxidized and sulfate is reduced. Based on the results of the present study, especially those for the PPM experiments, it is hypothesized that TSR may still have proceeded at a subordinate rate and that a shift in the reaction network toward a pathway involving organosulfur compounds may successfully explain this observation.

Clear evidence for TSR without the initial presence of low valence sulfur is provided by detection of organosulfur compounds in the Fe₂(SO₄)₃, FeSO₄ and CuSO₄ containing samples, which were processed at 315°C. Moreover, this is the first time that occurrence of TSR without initial presence of low valence sulfur is demonstrated at pH ≥ 4. Based on the generated amount of organosulfur compounds (thiophene, 2- and 3-methylthiophene), the following relative reactivity of the transition metal sulfates can be inferred: Fe₃(SO₄)₂ >> FeSO₄ > CuSO₄. No organosulfur compounds were detected for the NiSO₄ and ZnSO₄ containing samples.

Results of this study highlight the potential of well-constrained experiments, which allow us to investigate the effect of inorganic species on organic matter transformation. Combination of such experiments with thermodynamic evaluations will have significant implications for our understanding of the occurrence and stability of hydrocarbons in nature.

Keywords: Thermochemical sulfate reduction, transition metals, redox buffers, *n*-alkanes, fluid-rock interaction

Zusammenfassung

In der Natur gibt es zahlreiche Möglichkeiten für die Reaktion von organischen und anorganischen Verbindungen, wie zum Beispiel in Erdöl- und Erdgaslagerstätten, submarinen hydrothermal Systemen oder Sulfidzylinderstätten, wenn diese mit organischem Material assoziiert sind. Das Verständnis des Einflusses von anorganischen Verbindungen auf die Stabilität von organischen Verbindungen in diesen Milieus ist jedoch limitiert. Um ein besseres Verständnis zu erzielen, wurden in dieser Studie drei in sich konsistente experimentelle Serien (300-350°C, 13 und 35 MPa, 72-336 h) durchgeführt, um die Reaktion von *n*-Oktan (C₈H₁₈) mit zwei definierten Mineralvergesellschaftungen (Pyrit-Pyrrhotin-Magnetit = PPM und Hämatit-Magnetit = HM), Na₂SO₄ und verschiedenen Übergangsmetallsulfaten (CuSO₄, FeSO₄, Fe₂(SO₄)₃, NiSO₄ und ZnSO₄) zu untersuchen. Nach den Experimenten wurden die Feststoffe mittels Röntgenbeugung und organische Reaktionsprodukte mittels Headspace-Gaschromatographie analysiert. Quantifizierte organische Produkte umfassen CO₂, *n*- und *iso*-Alkane, Alkene, Ketone und Aromaten. Eine erweiterte Kalibration ermöglichte es für die Proben mit den Übergangsmetallsulfaten auch Organoschwefelverbindungen (Thiophen, 2- und 3-Methylthiophen) zu messen.

Prinzipiell ist das Verteilungsmuster der organischen Reaktionsprodukte für alle Proben sehr ähnlich. Dies zeigt, dass während der Experimente Cracking und aquatische Oxidation die Hauptkontrollfaktoren für die Zersetzung von Oktan sind. Trotz dieser guten generellen Übereinstimmung, zeigen die Ergebnisse deutlich, dass die untersuchten anorganischen Verbindungen die thermische Zersetzung von *n*-Oktan in unterschiedlichem, nicht zu vernachlässigbarem Maße, beeinflussen können. Dies zeigt sich beispielsweise dadurch, dass die verschiedenen anorganischen Additive zu einem unterschiedlich hohen Umsatz an *n*-Oktan führen. Dieser reicht von 0.24 mol% (PPM+H₂O+C₈H₁₈ 300°C) bis 28 mol% (CuSO₄+H₂O+C₈H₁₈ 315°C). Außerdem spiegeln die Produkte in Gegenwart von HM stärker oxidierende Bedingungen wider als in Gegenwart von PPM. Dies ist im Einklang mit der Pufferwirkung dieser Mineralvergesellschaftungen. Eine thermodynamische Betrachtung der organischen Produkte liefert Anzeichen dafür, dass Alkane und Alkene, aber nicht Alkene und Ketone, sich im thermodynamischen Gleichgewicht bezüglich der vom Puffer eingestellten aquatischen Wasserstoffkonzentration befinden, beziehungsweise sich diesem annähern.

In den 350°C Experimenten, führte die Zugabe von Na₂SO₄ in allen drei untersuchten Systemen (HM, PPM und ohne Puffer) zu einer verringerten Oxidation von *n*-Oktan zu CO₂. Dies steht im Widerspruch zu früheren Studien, welche die thermochemische Reduktion von Sulfat (TSR) untersucht haben. TSR bezieht sich auf eine Redoxreaktion bei der Kohlenwasserstoffe oxidiert und Sulfat reduziert werden. Basierend auf den Ergebnissen dieser Studie, speziell denen für die PPM Experimente, wird die Hypothese aufgestellt, dass TSR dennoch, wenn auch mit sehr niedriger Rate, abgelaufen sein könnte. Eine damit verbundene Verschiebung im Reaktionsnetzwerk hin zu einem Reaktionsweg mit Organoschwefelverbindungen als Zwischenstufen, könnte die Beobachtungen erfolgreich erklären.

Ein eindeutiger Beweis für TSR ohne anfängliche Anwesenheit von reduziertem Schwefel, ist für die Fe₂(SO₄)₃, FeSO₄ and CuSO₄ haltigen Proben, die bei 315°C prozessiert wurden, durch den Nachweis von Organoschwefelverbindungen gegeben. Darüber hinaus ist dies die erste Studie, welche das Auftreten TSR ohne initiale Anwesenheit von reduziertem Schwefel bei einem pH von ≥4 nachweist. Anhand der gebildeten Mengen an Organoschwefelverbindungen (Thiophen, 2- und 3-Methylthiophen) lässt sich die folgende relative Reaktivität der Übergangsmetallsulfate ableiten: Fe₃(SO₄)₂ >> FeSO₄ > CuSO₄. Für die Versuche mit NiSO₄ und ZnSO₄ wurden keine Organoschwefelverbindungen detektiert.

Ergebnisse dieser Arbeit zeigen das Potential auf, welches gut definierte Experimente haben um den Einfluss anorganischer Stoffe auf die Umwandlung von organischem Material zu untersuchen. Eine Kombination solcher Experimente mit thermodynamischen Betrachtungen kann eine erhebliche Auswirkung auf unser Verständnis bezüglich des Auftretens und der Stabilität von Kohlenwasserstoffen in der Natur haben.

Schlagwörter: Thermochemische Sulfatreduktion, Übergangsmetalle, Redox Puffer, *n*-Alkane, Fluid-Gesteins Interaktion

Table of Contents

1.	Motivation and Overview	1
2.	Theoretical Background.....	6
2.1	Thermal Cracking	6
2.2	Influence of Inorganic Components on Organic Matter Transformation	9
2.2.1	Role of Water During Pyrolysis	10
2.2.1.1	<i>Aqueous Oxidation of n-Alkanes</i>	<i>10</i>
2.2.2	Role of Minerals during Hydrocarbon Conversion	13
2.2.2.1	<i>Redox Buffering Ability of Mineral Assemblages</i>	<i>13</i>
2.2.2.2	<i>Transition Metal Minerals as Reactants and Catalysts During Aqueous Oxidation of Hydrocarbons.....</i>	<i>19</i>
2.2.3	Role of Sulfate – Possibility of Thermochemical Sulfate Reduction.....	25
3.	Materials and Methods.....	33
3.1	Experimental Strategy	33
3.2	Starting Materials	34
3.3	Sample Preparation	35
3.4	Experimental Procedure	37
3.4.1	Setting of the Experimental Parameters Time and Temperature	37
3.4.2	Cold-Seal Pressure Vessel Setup.....	39

3.4.3	Parr Hydrothermal Reactor.....	40
3.5	Analytical Methods.....	41
3.5.1	Static Headspace Gas Chromatography.....	41
3.5.2	X-ray Diffraction Analysis and Total Carbon Determination	43
3.6	Thermodynamic Calculations	44
3.6.1	Activities of Aqueous H ₂ and H ₂ S Regulated by the HM and PPM Buffers.....	44
3.6.2	Aqueous Solubility of <i>n</i> -Octane at Experimental Conditions	47
3.6.3	Aqueous Solubility of Metal Sulfates at Experimental Conditions and Modeling of In Situ pH	48
4.	Part I-A.....	51
	Investigating the Effect of the PPM and HM Mineral Buffers, and the Effect of Dissolved Sulfate on the Product Distribution Generated from <i>n</i> -Octane Under Hydrothermal Conditions	
4.1	Results – Solid phase	52
4.2	Results – Organic Products.....	53
4.2.1	300°C Experiments Processed for 168 h.....	55
4.2.2	350°C Experiments Processed for 168 h.....	56
4.2.3	Time Series Data for Samples of the Type PPM+H ₂ O+C ₈ H ₁₈ +Na ₂ SO ₄ Processed at 350°C	61
4.3	Discussion	62
4.3.1	Starting Conditions.....	62

4.3.2	Changes in Mineral Buffer Composition.....	66
4.3.2.1	<i>Is the Buffer Capable of Controlling Redox?.....</i>	70
4.3.2.2	<i>Mineral Buffers as Catalysts and Reactants.....</i>	72
4.3.3	Evaluating Contributions from Cracking and Aqueous Oxidation.....	73
4.3.3.1	<i>Cracking.....</i>	73
4.3.3.2	<i>Aqueous Oxidation.....</i>	75
4.3.4	Effect of the PPM and HM Mineral Buffers, as well as the Effect of Dissolved Sulfate on the Hydrothermal Degradation of <i>n</i> -Octane.....	80
4.3.4.1	<i>Elevated Gas Dryness for the Sulfate-Containing PPM Samples.....</i>	80
4.3.4.2	<i>Sulfate Addition Lowers Total Oxidation to CO₂.....</i>	85
4.3.4.3	<i>Similarity of the Sulfate-Containing Buffer-Free and HM Samples....</i>	90
4.4	Conclusions.....	92
5.	Part I-B.....	95
	Metastable Thermodynamic Equilibrium of the Alkane-Alkene and Alkene-Ketone Reactions	
5.1	Results.....	98
5.1.1	Molar Alkane/Alkene Ratios.....	98
5.1.2	Molar Ketone/Alkene Ratios.....	98
5.2	Discussion.....	100
5.2.1	Evaluating the Attainment of Equilibrium From Comparison of Predicted and Experimental Ratios.....	100
5.2.2	Evaluating the Thermodynamic Drive for the Reactions.....	101
5.2.3	The Role of the Starting Compound and of the Reaction Network.....	104
5.3	Conclusions.....	106

6.	Part II	108
	Effect of Dissolved Transition Metal Sulfates on the Degradation of <i>n</i> -Octane Under Hydrothermal Conditions	
6.1	Starting Conditions	109
6.2	Results and Discussion.....	117
6.2.1	Product Distribution and Estimate of Conversion	117
6.2.2	Evidence for TSR.....	120
6.2.3	Effect of pH and Additional Factors on TSR.....	122
6.3	Conclusions	127
7.	Implications for Natural Systems.....	129
7.1	Petroleum Systems	129
7.1.1	Transferability of Experimental Results.....	129
7.1.2	Implication I: Thermochemical Sulfate Reduction.....	133
7.1.3	Implication II: Conversion of Hydrocarbons to Dry Gas	134
7.2	Submarine Hydrothermal Systems.....	134
7.2.1	Transferability of Experimental Results.....	135
7.2.2	Implications III: Petroleum Alteration in Submarine Hydrothermal Systems.....	136
7.3	Sulfide Ore Deposits	138
7.3.1	Implication IV: Thermochemical Sulfate Reduction in the Kupferschiefer	138

8. Conclusions	141
References	145
Appendix.....	153

1.

MOTIVATION AND OVERVIEW

Organic-inorganic associations are abundant in diverse geologic environments (Fig. 1) including, but not limited to petroleum systems (Seewald, 1994, 2001, 2003), sulfide ore deposits (Powell and Macqueen, 1984; Leventhal, 1990; Sun and Püttmann, 2000; Bechtel et al., 2001; Sun and Püttmann, 2003) and submarine hydrothermal systems (McCollom and Seewald, 2007; Proskurowski et al., 2008). The reaction between inorganic components (e.g. minerals, dissolved sulfate and aqueous metal cations) and organic matter can play a crucial role in a wide range of geochemical processes that include, for example, the generation of oil and gas, as well as the transport and deposition of ore-forming metals. Despite this impact, understanding of inorganic-organic reactions is limited (Price and DeWitt, 2001).

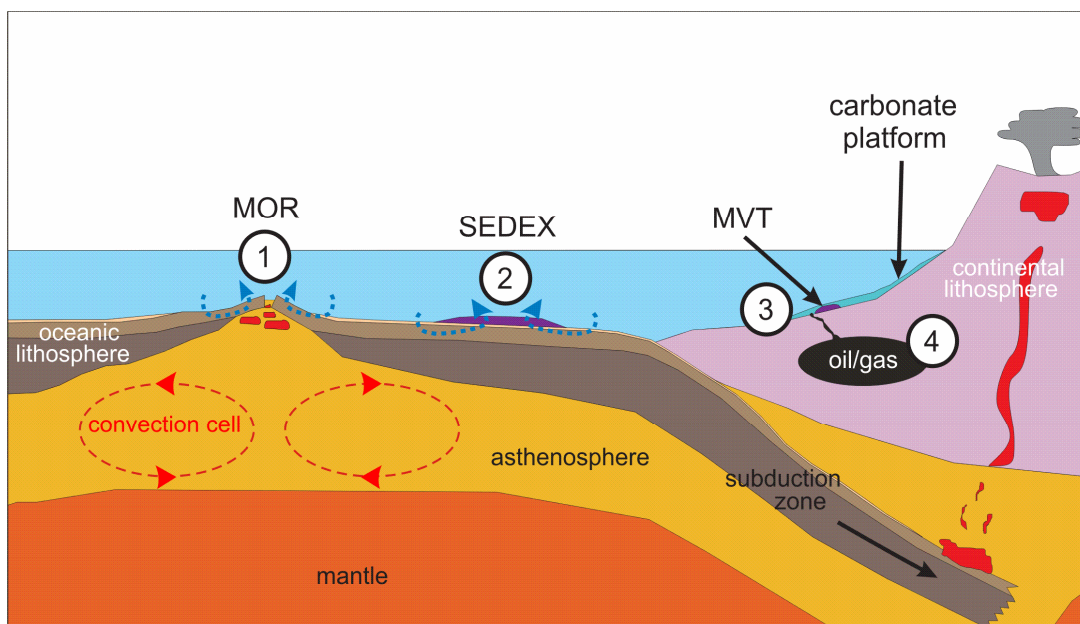


Fig. 1: Schematic illustration of possible geologic environments, in which inorganic-organic interactions can be encountered: 1 = Mid Ocean Ridges (MOR), 2 = Sedimentary exhalative deposits (SEDEX), 3 = Mississippi Valley type deposits (MVT), and 4 = Petroleum systems.

Natural Observations

Two sulfide ore deposits that are associated with organic matter are for example the Kupferschiefer and the Mississippi Valley type deposits. They both owe their origin to fluid circulation in sedimentary basins. The Kupferschiefer is a stratabound polymetallic sulfide deposit in Central Europe characterized by copper enrichment. It consists of black and marly

shales, which are intercalated between underlying Zechstein sandstones and overlying Zechstein carbonates (Sun, 1998). Sun and Püttmann (2000) showed that reduction of sulfate by organic matter, the so-called thermochemical sulfate reduction (TSR), is responsible for up to 60% of the Kupferschiefer mineralization in the Sangerhausen basin in Germany. Mississippi Valley type deposits (MVT), on the other hand, are stratabound, mainly carbonate-hosted sulfide ore deposits dominated by high concentrations in Pb, Zn and Cu (Robb, 2009). Analysis of natural samples from such deposits in Canada (Powell and Macqueen, 1984) and SE Missouri (Leventhal, 1990) confirmed the involvement of TSR in ore formation processes.

In context of petroleum reservoirs, TSR has been addressed as possible cause for severe gas souring with up to 90 vol% H₂S in the gas phase (Orr, 1977). In addition to that, numerous geological and geochemical studies have presented convincing arguments that inorganic components like water, minerals and transition metals in the solid or dissolved state, have the ability to influence hydrocarbons during generation, expulsion, migration and storage (Siskin and Katritzky, 1991; Mango et al., 1994; Machel, 2001; Price, 2001; Price and DeWitt, 2001; Seewald, 2001; Lu et al., 2011). Apart from that, the impact of inorganic components on organic matter transformation is often neglected in petroleum maturation studies. Conventional petroleum models, for example, which are generally used to predict stability and maturation of hydrocarbons, only consider burial temperature, geologic time and the organic starting material as controlling factors (Price, 2001). Price (2001) noted that such models greatly underestimate the thermal stability of oil. Thus, it is a challenge to predict what is happening “down there”. Prediction of processes influencing the quality of hydrocarbon reservoirs becomes, however, more and more important at an early exploration stage to avoid problems during recovery as well as to save exploration and production costs (Hoffmann et al., 1995; Huc, 2003).

Experimental Investigations

Laboratory experiments represent a powerful tool to gain insight into inorganic-organic interactions in a confined system. Their results have the potential to contribute to a better understanding of petroleum generation and evolution in nature. Consequently, experimental studies are strongly required for the improvement of prediction models.

During the last three decades increasing number of experimental studies were published that emphasize the critical role that water (Winters et al., 1981; Lewan, 1997; Leif and Simoneit, 2000), minerals (Horsfield and Douglas, 1980; Seewald, 2001; McCollom and Seewald, 2003), dissolved sulfate (Zhang et al., 2007; Zhang et al., 2008a; Lu et al., 2011), and transition metals (Mango et al., 1994; Mango and Hightower, 1997b) can play for the conversion of organic matter. Extrapolation of many experimental results to natural systems is, however, questionable because key chemical variables such as redox conditions were not controlled at geologically reasonable values (Helgeson et al., 1993; Seewald, 2001). Helgeson et al. (1993) makes a strong point in his conclusion, stating that redox-controlled experiments reflecting conditions prevailing in hydrocarbon reservoirs are crucially needed to understand oil and gas generation in nature. To the best of my knowledge, there are to this point only studies by Jeffrey Seewald and two of his former PhD students (Tom McCollom and Eoghan Reeves), who used redox-controlled experiments to investigate the stability of low molecular weight hydrocarbons ($\leq C_7$) and organic acids ($\leq C_5$) under hydrothermal conditions (Seewald, 1994, 2001; McCollom and Seewald, 2003; Seewald, 2003; McCollom and Seewald, 2003a; McCollom, 2010; Reeves et al., 2012). From these studies, only three focus on the conversion of *n*-alkanes (Seewald, 1994, 2001; Reeves et al., 2012), which are the major constituents of oil and gas (Kissin, 1987). Seewald (1994, 2001) presents results for three experiments with ethane and three with *n*-heptane at 300 and 325°C using the hematite-magnetite-pyrite (HMP) and the pyrite-pyrrhotite-magnetite (PPM) mineral redox buffers. Reeves et al. (2012) presents results for experiments with a mixture of C_1 to C_5 *n*-alkanes at 325°C with the PPM mineral buffer.

This PhD Thesis

Driving factors for initiating the present PhD thesis were scarcity of data for redox-controlled experiments studying hydrocarbon stability in presence of sulfate, on the one side, and insufficient data for studies investigating the effect of inorganic components on the reaction network associated with hydrocarbon transformation at elevated temperature, on the other side. The central goal of this thesis is to stress the impact inorganic components can have on organic matter transformation under hydrothermal conditions, which can be of fundamental importance in the context of petroleum reservoirs, sulfide ore deposits and

submarine hydrothermal systems. Due to complexity of natural systems, a simplified synthetic system is used for the experiments in this study. Three experimental series were conducted in the course of the present PhD thesis in order to study the effect of minerals, dissolved sulfate and dissolved transition metals on the conversion of *n*-octane in the temperature range of 300 to 350°C. The effect of minerals on *n*-octane conversion was explored using the hematite-magnetite and the pyrite-pyrrhotite-magnetite mineral buffer assemblages. Sodium sulfate and five different transition metal sulfates (CuSO₄, FeSO₄, Fe₂(SO₄)₃, NiSO₄ and ZnSO₄) were used as sulfate sources, with the latter also being a source for transition metals. For all experiments, special attention was drawn to the organic product distribution (*n*-alkanes, alkenens, ketones and CO₂).

The thesis is structured in eight chapters. The first one is this introductory chapter, which is followed by a chapter summarizing the theoretical background relevant for this study. It summarizes important chemical reactions and principals, and gives a brief literature review on today's state of knowledge regarding inorganic-organic reactions under hydrothermal conditions. *Chapter 3* represents the foundation of the thesis. Here, the experimental strategy is described and details on materials and methods are provided. *Chapters 4 to 6* form the core of the thesis and contain experimental results, as well as their discussion. Basically, the experiments discussed in these chapters can be divided into two main parts (Part I and II): Experiments presented in *chapter 4* (Part I-A) and *chapter 5* (Part I-B) focus on the effect of mineral-buffers on the thermal decomposition of *n*-octane, and those presented in *chapter 6* (Part II) elucidate the effect of transition metal sulfates on the thermal decomposition of *n*-octane. In detail, the objectives of the individual chapters are as follows:

Part I-A (*chapter 4*) focuses on the interpretation of the data for the HM and PPM samples processed at 300°C and 350°C in presence and absence of sulfate. The objective is to evaluate the effect of these inorganic components on the product distribution and to determine possible processes responsible for the degradation of *n*-octane during the experiments.

Part I-B (*chapter 5*) ties in with part I-A. Here, data for experiments with the HM and PPM redox buffers are evaluated in a thermodynamic framework in order to explore possible equilibration of redox-dependent organic reactions like the alkane-alkene and alkene-ketone reactions.

Part II (*chapter 6*) presents first results for samples with transition metal sulfates, which were processed at 315°C and 13 MPa for 168 h in absence of mineral buffers. The ability of dissolved transition metals to initiate and catalyze TSR is evaluated.

The three results and discussion chapters are followed by an implications chapter (*chapter 7*), which highlights the broad spectrum of natural environments where results might be applicable. Last but not least, the thesis is concluded in *chapter 8*.

2.

THEORETICAL BACKGROUND

2.1 THERMAL CRACKING

Thermal cracking is investigated in pyrolysis studies. The compound of interest (e.g. *n*-alkanes) is heated to a desired temperature, usually $>300^{\circ}\text{C}$, and reaction products are monitored in order to gain insight into the product distribution and associated reactions. During thermal cracking the starting material is mainly cleaved into shorter molecules and the products are dominated by straight-chain *n*-alkanes and alkenes (Moldoveanu, 2010). Pure pyrolysis is studied in an oxygen-free atmosphere and without additives. Such studies provide information on basic reaction mechanisms for *n*-alkane conversion and results are valuable for a better understanding of refining processes.

The Radical Chain Mechanism

The generally accepted standard mode of *n*-alkane decomposition during pyrolysis is the radical chain mechanism. It was first described by pioneering studies in the early 1930s (Rice, 1931; Rice and Herzfeld, 1934). The principal concept of this mechanism, which is also known as the Rice-Kossiakoff concept (Kossiakoff and Rice, 1943), is summarized here using the example of *n*-octane, a straight chain hydrocarbon with eight carbon atoms (Fig. 2). The interested reader is referred to Safarik and Strausz (1996), Olah and Molnár (2003) and Moldoveanu (2010), for thorough reviews and detailed information on the process.

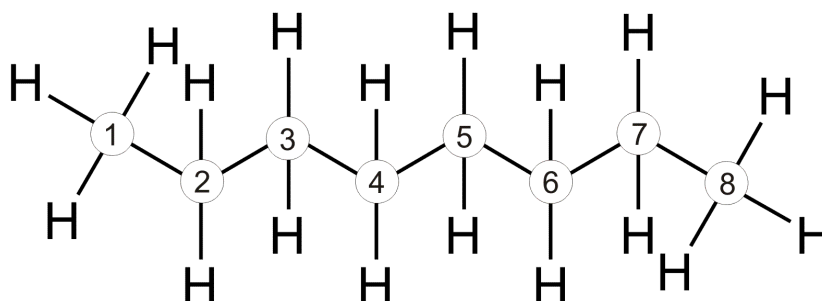


Fig. 2: Structural formula of *n*-octane (C_8H_{18}). Circles represent carbon atoms; numbers refer to the carbon position.

The concept of the free-radical chain mechanism can be divided into four steps: i) initiation reaction, ii) chain propagation through hydrogen abstraction, iii) radical transformation by C-C bond homolysis (β scission), i.e. cleavage of the C-C bond by splitting the binding electron pair, and iv) termination reactions.

Step 1: Initiation reaction

The initiation takes place by homolytic scission of a C-C bond in *n*-octane, producing two radicals (Table 1). The probability for cleavage of a C-C bond varies for the different positions in the C₈ molecule, depending mainly on the bond energies. Bond dissociation energies summarized by Moldoveanu (2010) show that the C-C bonds are less stable the

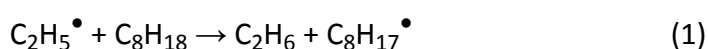
Table 1: Possible initiation reactions for *n*-octane.

Cleavage between C positions	Generated radicals
1-2 or 7-8	CH ₃ [•] + C ₇ H ₁₅ [•] (rather unlikely)
2-3 or 6-7	C ₂ H ₅ [•] + C ₆ H ₁₃ [•]
3-4 or 5-6	C ₃ H ₇ [•] + C ₅ H ₁₁ [•]
4-5	C ₄ H ₉ [•] + C ₄ H ₉ [•]

greater the alkyl-groups are, which are attached to the two carbon atoms. An alkyl-group is usually abbreviated with the symbol R and consists solely of single-bonded carbon and hydrogen atoms, for example a methyl (-CH₃) or ethyl (-CH₂-CH₃) group. The different bond strengths indicate that the probability of cleaving *n*-octane between carbon positions 1-2 and 7-8 is rather unlikely – although not excluded. As shown in Table 1, eight different radicals may be produced from *n*-octane by C-C bond scission.

Step 2: Chain propagation through hydrogen abstraction

The initially formed radicals can then abstract hydrogen from *n*-octane, the reactant molecule, which is exemplified using an ethyl radical in the following reaction:



With progressing reaction, more and more radicals can form and may also abstract hydrogen from other product hydrocarbons. Non-terminal hydrogen atoms are preferentially removed over those bonded to a primary carbon atom (Kossiakoff and Rice, 1943). According to the authors, the probability to remove hydrogen from a tertiary carbon is greater than for removal from a secondary carbon atom.

Step 3: Radical decomposition by C-C homolysis (β scission)

If a radical is composed of at least three carbon atoms, it has the possibility to decompose by β scission. The greek letter refers to the discrete position of the carbon atom in the chain, that means that in this case the cleavage of the C-C bond occurs between the second and the third carbon adjacent to the radical site (Fig. 3). As a result, an α -alkene, i.e. an alkene with the double bond between the two outermost carbon atoms (e.g. 1-butene $\text{CH}_2=\text{CH}-\text{CH}_2-\text{CH}_3$), and a radical of shorter chain length than the starting compound are produced. In Reaction (2) an example of β scission for a terminal n -octyl radical is given:

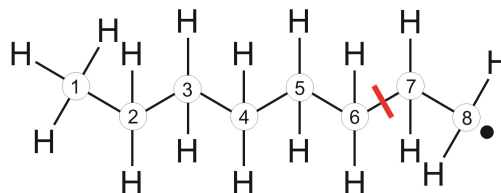
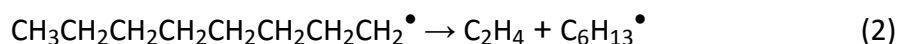
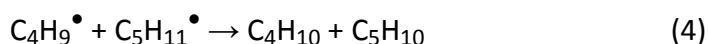


Fig. 3: The red bar marks the C-C bond in β position to the radical site in a n -octyl radical. The carbon atom (8) with the unpaired electron (radical) is named α carbon, the next carbon atom in the chain (7) is the β carbon, and the following carbon atoms are named consecutively using greek letters. Thus the C-C bond in β position to the radical site is the bond between the β (=7) and γ (=6) carbon.



Step 4: Termination reactions

There are two kinds of termination reactions: i) termination by combination of two radicals (Reaction 3), and ii) termination with disproportionation (Reaction 4) (Moldoveanu, 2010); both possibilities are illustrated using the example of the n -butyl and n -pentyl radicals:



Termination according to Reaction (3) opens the possibility to produce larger n -alkanes than the starting material. In contrast, termination with disproportionation always results in shorter molecules than the starting compound, with an n -alkane and an alkene being the products.

Note that the radical chain mechanism shows pressure dependence. With increasing pressure, bimolecular reactions are favored over unimolecular reactions (Rice and Herzfeld,

1934; Fabuss et al., 1964). As a result, cracking products obtained at higher pressures, like in the present study (13-35 MPa), are significantly different from normal pyrolysis studies at lower pressures ($P \approx 0.1$ MPa), in the way that: i) larger *n*-alkanes are more abundant, and ii) the alkane/alkene ratios are significantly higher.

In addition to the radical chain mechanism, ionic mechanisms may also play a role for hydrocarbon decomposition. Carbonium-ion mechanisms (those involving positively charged intermediates), for example, are proposed to be responsible for the generation of branched hydrocarbons (Greensfelder et al., 1949). Organic reaction products generated from *n*-octane during experiments performed in the course of the present study, are, however, dominated by straight-chain alkanes. According to Seewald (2001), this observation indicates that ionic mechanisms play only a subordinate role.

2.2 INFLUENCE OF INORGANIC COMPONENTS ON ORGANIC MATTER TRANSFORMATION

In natural systems, temperature is not the only controlling factor for *n*-alkane conversion and organic matter transformation in general. The reason is that inorganic components, like water, transition metals and minerals, are ubiquitous compounds in subsurface environments, which may all alter hydrocarbons during generation, expulsion, migration and storage to various degrees (Mango, 1997a; Seewald, 2001, 2003). Especially the effect of sulfate on petroleum alteration attracted great interest because it may minimize hydrocarbon quality severely (Zhang et al., 2007; 2008; Zhang et al., 2008a; Zhang et al., 2008b; Zhang et al., 2012). In the context of sulfide ore deposits, the reaction of dissolved transition metals, sulfate and organic matter may play a crucial role for ore transport and deposition. This subchapter provides a brief review on today's state of knowledge about the effect of inorganic species on organic matter transformation under hydrothermal conditions.

2.2.1 ROLE OF WATER DURING PYROLYSIS

In contrast to dry pyrolysis, hydrous pyrolysis – i.e. pyrolysis in presence of water – has been shown to closely simulate petroleum generation in natural systems (Lewan et al., 1985; Price, 2001), for example the characteristic low-olefin (high saturates) content of natural petroleum oils (Winters et al., 1981). The role of water is manifold. Water can act as solvent and thus facilitate reactions not available in dry environments. Furthermore, it may act as oxygen and hydrogen donor (Seewald, 2001). Stalker et al. (1994) used ^{18}O labeled water in their experiments to show that oxygen addition from water to sedimentary organic matter can occur at hydrothermal conditions (150-330°C) during kerogen degradation. At about the same time, Lewan (1997) could proof extensive hydrocarbon deuteration as a result of hydrous pyrolysis of Woodford shale in presence of D_2O at 330°C. Recently, Reeves et al. (2012) studied the hydrogen isotope exchange between *n*-alkanes ($\leq\text{C}_5$) and water at 323°C. They could verify that hydrogen exchange between water and hydrocarbons with more than two carbon atoms (C_{2+}) occurs on the timescale of days under hydrothermal conditions. The study of Seewald (2003) strengthens these observations claiming that conventional models, which neglect water as hydrogen donor, may significantly underestimate the amount of oil and natural gas that can be generated (Fig. 4).

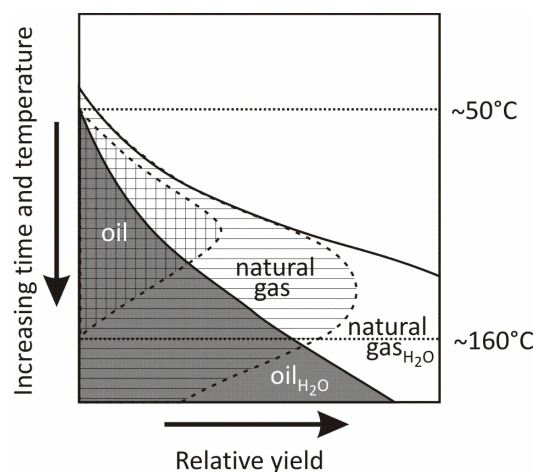


Fig. 4: Schematic illustration of the oil and gas generation potential from kerogen during thermal maturation in sedimentary basins. Presence of water and minerals (indicated by solid fields) significantly affects the amount and timing of oil and gas formation when compared to predicted amounts by traditional petroleum generation models (hatched fields), which treat temperature as the only controlling factor (modified after Seewald, 2003).

2.2.1.1 AQUEOUS OXIDATION OF *N*-ALKANES

In 2001, Seewald published a reaction network for the stepwise aqueous oxidation of hydrocarbons in a sulfate-free system. With that, Seewald (2001) provided a new interpretational approach for hydrocarbon decomposition in natural environments and contributed to a better understanding of associated processes. He established the reaction network based on results from experiments studying the reaction of *n*-alkanes (ethane and

n-heptane) and alkenes (ethene, propene and 1-butene) with the HM, HMP and PPM mineral assemblages under hydrothermal conditions (300-350°C, 35 MPa). Seewald (2001) notes that, besides a thermodynamic drive, presence of a suitable oxidizing agent or a mechanism to remove H₂ is a prerequisite for the process to occur. The reaction sequence involves reduction, hydration and oxidation reactions, of which some are clearly sequential, whereas others may proceed in parallel. The alteration assemblage obtained by aqueous oxidation is compositionally distinct from that by pure thermal cracking, e.g. oxygenated organic compounds are more abundant. The final products in the sequence are methane and CO₂. This reaction scheme is of fundamental importance for the discussion of results presented in the present PhD thesis and is referred to as the “Seewald model”. In detail, the reaction scheme is structured as follows:

In the first step of the reaction scheme (Fig. 5) an *n*-alkane is oxidized to an alkene. Specific hydration of the interior carbon associated with the double bond generates an alcohol, a process known as Markownikoff addition in chemistry. Seewald (2001) noted that hydration of the alkene in step (2) may also occur at the terminal carbon, but at a rate substantially slower than hydration following the Markownikoff rule. Further oxidation of the alcohol produces a ketone (step 3). The first three steps in this sequence are analogous to the reaction scheme postulated by Leif and Simoneit (1995; 2000). Oxidation in step (4) forces a decrease in carbon chain length. The interior C-C bond of the ketone that is adjacent to the carbonyl (C=O) functional group is cleaved, and two organic acids are produced. Seewald (2001) suggests that the largest organic acid that can be generated in step (4) has usually two carbons less than the starting *n*-alkane, due to the fact that alkene oxidation in step (2) is not likely to occur at terminal carbons. This also implicates that formation of formic acid (CH₂O₂) is generally not a preferred product in step (4). Formic acid may also be generated in step (5) if C₂₊ organic acids generated in step (4) undergo “deformylation” (McCollom and Seewald, 2003). However, results from McCollom and Seewald (2003) for experiments with valeric acid (C₅H₁₀O₂) performed under identical conditions than the experiments conducted by Seewald (2001), i.e. in presence of water and the same mineral buffers (HM, HMP and PPM) and at a temperature of 325°C and a pressure of 35 MPa, indicate that formic acid is not stable and will instantly react to CO₂ and H₂. Apart from deformylation two more likely possibilities exist how reactions continue in step (5): decarboxylation and oxidation. Oxidation promotes the formation of CO₂, whereas

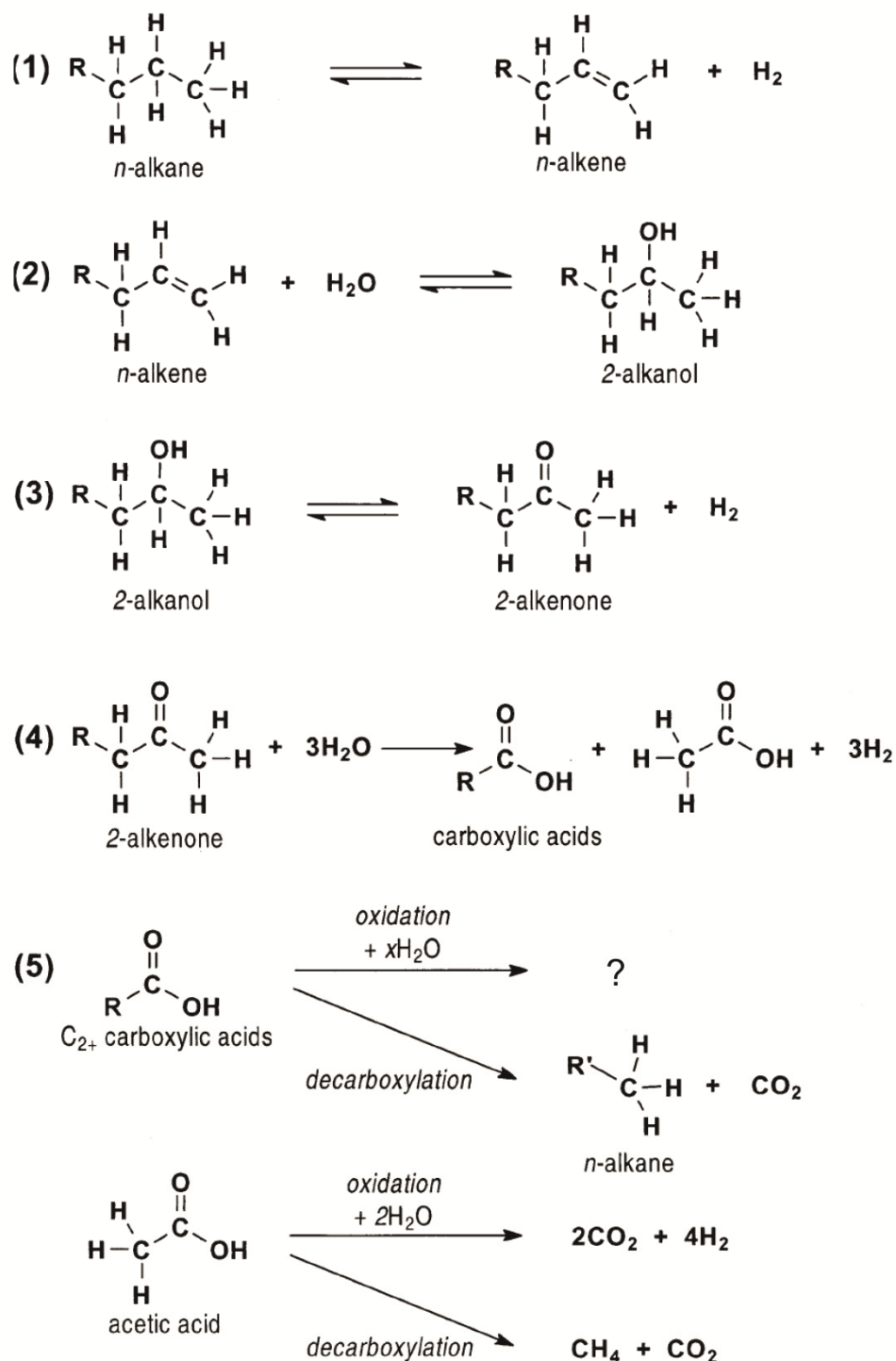


Fig. 5: Schematic representation of the reaction scheme postulated by Seewald (2001) for the oxidative decomposition of aqueous *n*-alkanes. The formation of a terminal alkene in the first step is for illustrative purpose only and formation of other alkene isomers is also possible. Products generated by C_{2+} carboxylic acid oxidation (step 5) could not be specified. Adapted from Seewald (2001) with kind permission of Pergamon.

decarboxylation produces equimolar amounts of CO₂ and a short-chain *n*-alkane. The *n*-alkanes produced in step (5) are mainly composed of three carbons less than the starting *n*-alkane, because hydration of alkenes at the terminal carbon is negligible in step (2). Generated *n*-alkanes may re-enter the reaction scheme at step (1), which shows that the reaction scheme is interwoven.

Even though some products, like for example alkenes, might only be present at low concentrations, they still form a crucial link in the reaction scheme and are important intermediates for oxidative *n*-alkane decomposition. At all steps in the sequence, the thermodynamic drive becomes stronger the higher the chain length is (see Fig. 10 in Seewald, 2001).

2.2.2 ROLE OF MINERALS DURING HYDROCARBON CONVERSION

2.2.2.1 REDOX BUFFERING ABILITY OF MINERAL ASSEMBLAGES

The HM, HMP and PPM mineral assemblages that Seewald (2001) used during the experiments have the characteristic that they can act as redox mineral buffers. Such mineral assemblages can constrain redox conditions as a function of temperature, which may have implications for hydrocarbon transformations. The buffering ability can be attributed to the fact that the minerals may consume or supply molecular oxygen, i.e. their capability to function as oxygen buffers. If, in presence of water, conditions get more oxidizing the fraction of the oxidized mineral increases whereby the hydrogen activity in the system is kept constant if equilibrium is attained (see *chapter 3.6.1* for detailed buffer reactions). Therefore, the activity of aqueous hydrogen can be used to characterize the redox conditions adjusted by the mineral buffers under hydrothermal conditions. For dilute solutions, the activity of any component *i* in solution is defined as:

$$a_i = \frac{c_i}{c_0} \quad (5)$$

with c_i being the molal (mol/kg_{H₂O}) concentration of the species *i* in water, and c_0 refers to the standard state of a dilute solution, which shows ideal behavior. The standard state for aqueous species other than water is a hypothetical 1 molal solution referenced to infinite dilution at any temperature and pressure. The standard state adopted for water is unit

activity of the pure liquid at any temperature and pressure. The activity of an aqueous species can be computed from thermodynamic models. Furthermore, the concentration of the aqueous species of interest can be measured during hydrothermal experiments. For dilute solution, this then corresponds to the aqueous activity (cf. Equation 5).

In addition to the hydrogen activity, the oxygen fugacity ($f_{O_2(g)}$ in bar) is commonly used to characterize redox conditions. It refers to the effective partial pressure of oxygen in the system and can be defined as:

$$f_{O_2(g)} = \phi_{O_2(g)} \cdot X_{O_2(g)} \cdot P_{tot} \quad (6)$$

with P_{tot} being the total pressure in the system, $X_{O_2(g)}$ is the molar fraction of oxygen in the gas phase, and ϕ stands for the fugacity coefficient. Because the disproportionation of water rapidly attains a state of thermodynamic equilibrium under hydrothermal conditions, the fugacity of oxygen can be directly related to the activity of aqueous hydrogen via:

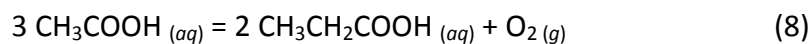


Note, that this does not necessarily mean that free oxygen is present in the reacting system, because oxygen generated by the reaction can be readily stored in minerals and other available reactants (Helgeson et al., 1993).

In experimental petrology, redox buffers are widely used to fix redox conditions at realistic geological conditions during experiments. In doing so, experiments can closely mirror natural processes and their results can be interpreted in a thermodynamic framework. Depending on the desired redox conditions different mineral assemblages are used. Up to this point, the use of mineral redox buffers in experimental organic geochemistry is scarce, despite the fact that many organic-organic and inorganic-organic reactions clearly involve changes in the nominal oxidation state of carbon and may be redox-dependent (Seewald, 2001).

Natural Observations for Petroleum Reservoirs

Shock (1988; 1989) performed a thermodynamic study of data reported by Carothers and Kharaka (1978) for concentrations of short-chain organic acid anions (acetate, propionate, butyrate, and valerate) in 95 formation-water samples from 15 oil and gas fields in the San Joaquin Valley, California, and in the Houston and Corpus Christi areas, Texas, covering subsurface temperatures of 40-200°C. These fields all represent calcite-bearing sandstone reservoirs. Shock (1988; 1989) used this data to compute oxygen fugacity based on the law of mass action for the reaction:



assuming equilibrium between aqueous propanoic ($\text{CH}_3\text{CH}_2\text{COOH}$) and acetic acid (CH_3COOH) (details see Shock, 1988; 1989). As shown in Fig. 6 calculated oxygen fugacities fall between the stability line of the HM and the field of the pyrite-pyrrhotite-magnetite PPM mineral assemblages. Calculated $\log f_{\text{O}_2}$ values of -59 to -55 in the temperature range of 90 to 110°C are in line with expectations for typical hydrocarbon reservoirs in nature (Pokrovskii and Helgeson, 1994).

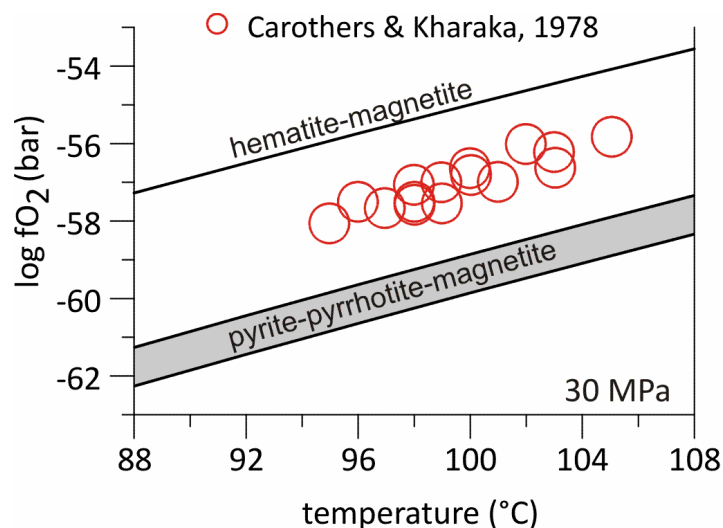


Fig. 6: Log fugacity of oxygen ($\log f_{\text{O}_2}$) as a function of temperature (modified after Shock, 1988). The symbols represent $\log f_{\text{O}_2}$ values computed by Shock (1988) for metastable equilibrium between aqueous propanoic ($\text{CH}_3\text{CH}_2\text{COOH}$) and acetic acid (CH_3COOH) in formation-water samples from calcite-bearing sandstone reservoirs (details see Shock, 1988; 1989). Data used for the calculation is taken from Carothers and Kharaka (1978). Calculated values fall between the line of the hematite-magnetite (HM) and the field for the pyrite-pyrrhotite-magnetite (PPM) mineral assemblages. Owing to the non-stoichiometry of pyrrhotite the PPM buffer can fix f_{O_2} in a certain range (see *chapter 3.6.1* for details).

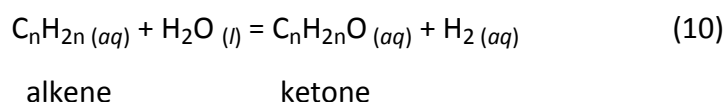
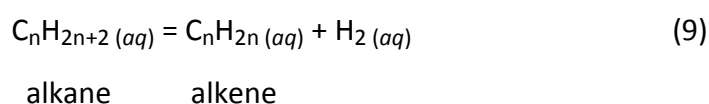
Implications for Reactions Between Organic Compounds

As discussed in the previous section, thermodynamic investigation of data for natural samples provide evidence that organic-organic reactions can be controlled by redox and that individual reactions may attain a thermodynamic equilibrium state although the global system may not have attained total thermodynamic equilibrium. According to Seewald (2001), this is possible because of kinetic barriers. He uses the expression “metastable thermodynamic equilibrium” for such partial thermodynamic equilibria of individual reactions. The expression is adopted in the present study.

Seewald (2001), investigated the possible attainment of metastable thermodynamic equilibria for the alkane-alkene and alkene-ketone reactions in sulfate-free experiments with *n*-alkanes (ethane and *n*-heptane) and alkenes (ethene, propene and 1-butene) in presence of the HM, HMP and PPM mineral assemblages under hydrothermal conditions (300-350°C, 35 MPa), the same that were already referred to in *chapter 2.2.1.1*. He used a flexible-cell hydrothermal apparatus for the experiments (cf. Fig. 1 in McCollom and Seewald, 2003), which allows sampling and injection of fluids without interruption of experiments. This offers a great advantage for studying reversibility of reactions. The effectiveness of the mineral buffers was confirmed by monitoring the concentration of aqueous hydrogen during the course of the experiments and comparing it with thermodynamic predictions for equilibrium values. In all three buffering systems the hydrogen activity quickly readjusted, i.e. within 24 h, to the nominal value after perturbation of the chemical system. Results by Seewald (2001) highlight that redox can play a crucial role for stability and reactivity of organic compounds. In presence of the more oxidizing HM and HMP buffers, with both adjusting the same hydrogen activity, aqueous oxidation of hydrocarbons to CO₂ is enhanced if compared to the more reducing conditions obtained with the PPM mineral buffer. In fact, results of experiments by Seewald (2001) indicate that the relative abundance of the whole set of reaction products generated by oxidation and reduction reactions associated with aqueous oxidation (Fig. 5) may be controlled by the redox conditions imposed by the mineral buffers. This seems self-explanatory, but such interaction between inorganic and organic compounds is often not considered in organic chemistry.

Experimental Evidence for Possible Metastable Thermodynamic Equilibrium of the *Alkane-Alkene* and the *Alkene-Ketone* Reactions

Seewald (1994, 2001) was the first one who provided *experimental* evidence that individual redox-dependent organic reactions, such as the alkane-alkene (Reaction 9) or alkene-ketone (Reaction 10) reactions, are reversible and can attain a redox-dependent metastable thermodynamic equilibrium state.



As indicated by Reactions (9) and (10), more reducing conditions, i.e. higher hydrogen activity, favor *n*-alkanes with respect to alkenes, and alkenes with respect to ketones. Seewald (2001) showed that injected alkenes (propene and 1-butene) attain a metastable thermodynamic equilibrium state with corresponding ketones within <200 h in presence of the HMP and PPM mineral buffer at 300, 325 and 350°C, whereas this is not the case in presence of the HM mineral buffer (compare Seewald, 2001 Fig. 11). This is surprising because identical redox conditions are expected in presence of both, the HM and HMP mineral buffer. One crucial difference between these two buffers is, however, the presence of sulfur in the HMP system, which might possibly explain observed differences.

A positive effect of sulfur on equilibration was observed by Seewald for alkane-alkene equilibria in the HM system if sodiumthiosulfate ($\text{Na}_2\text{S}_2\text{O}_3$) is added to the experiment containing 1-butene. Without sulfur being present in the system, 1-butene did not achieve a metastable equilibrium state with *n*-butane during the course of the experiments (see Fig. 12 in Seewald, 2001). However, the adjustment of metastable equilibrium states is quite complex and influenced by many other factors as shown in the following section.

In presence of the HMP mineral buffer alkane/alkene ratios reach equilibrium values within ≤ 100 h after ethane, propene and 1-butene injection at 300°C, but continuing reaction results in a departure from equilibrium conditions, indicating a reversal in the

direction for Reaction (12) (see Seewald, 2001 Fig. 12). According to Seewald (2001), “metastable thermodynamic equilibrium was not attained because the rate of alkene production by alkane oxidation was insufficient to keep pace with alkene consumption due to ketone formation (acetaldehyde in the case of ethane)”. The finding points out that the attainment of metastable equilibria can be severely influenced by reaction rates as well as the effect of preceding and subsequent reactions in the reaction network.

During experiments performed at 325°C in presence of the same mineral buffer (HMP), ethene and ethane equilibrate within <200 h after ethene injection. In contrast to the 300°C experiments with ethene, the equilibrium persists even with continuing reaction. This highlights that the experimental temperature does have an influence on alkane/alkene equilibration, which is also confirmed by Seewald’s experiments in the PPM system. Here, injected alkenes (propene and 1-butene) could only attain metastable equilibrium at the highest temperature (350°C). The experimental duration is also critical. The PPM experiments at 350°C show that butene-butane equilibration happened within <100 h, but the starting butane/butene ratio was already close to equilibrium. In case of propene, prolonged reaction times (>2500 h) were needed to reach metastable equilibrium (see Fig. 12 in Seewald, 2001) at the same experimental conditions.

In addition to experiments with alkenes as starting compounds, Seewald (2001) also presents data for two experiments (HMP and PPM) at 300°C with *n*-heptane – an *n*-alkane – as reactant. In both buffer systems metastable thermodynamic equilibrium for neither the ethane-ethene nor the propane-propene reaction could be reached within 3000 hours.

The results of Seewald (2001), which were presented above are summarized in Table 2. They highlight the possibility of metastable thermodynamic equilibrium states for individual redox-dependent organic reactions. Even though these equilibria are not necessarily fixed once they are attained, they may, however, prevail for a certain duration, which can have implications for the reacting system. The attainment of such metastable equilibrium states may be influenced by various factors, which may be interdependent: redox, temperature, reaction rate, time, availability of catalytic species (e.g. intermediate sulfur species), as well as the interdependency on preceding and subsequent reactions in the reaction network.

Table 2: Overview of reactions for which metastable thermodynamic equilibrium has (+) or has not been (-) observed during experiments performed by Seewald, 2001. Limitations exist if sign is bracketed. For explanations see text. Experimental conditions: 300, 325 and 350°C, 35 MPa and run durations of up to 8000 hours.

Compound injected Mineral buffer used	alkane-alkene	alkene-ketone
<u>alkene</u> (ethene, propene or 1-butene)		
PPM	(+)	+
HMP	(+)	+
HM	-	-
HM + Na ₂ S ₂ O ₃	+	-
<u>n-heptane</u> (only 300°C experiments)		
PPM	-	no data
HMP	-	no data

HMP – hematite-magnetite-pyrite; PPM – pyrite-pyrrhotite-magnetite;
HM – hematite-magnetite

2.2.2.2 TRANSITION METAL MINERALS AS REACTANTS AND CATALYSTS DURING AQUEOUS OXIDATION OF HYDROCARBONS

Apart from the fact that certain mineral assemblages may act as redox buffers, individual minerals have the ability to act as reactants. Hematite, for example, has been reported to directly supply oxygen during the oxidation of hydrocarbons (Surdam et al., 1989; Surdam et al., 1993; Bell et al., 1994). In nature, the reduction of hematite by organic matter can lead to significant bleaching of sandstones (PhD thesis of Meier, 2012 and references therein).

In presence of water pyrite has been shown to supply sulfur to the reacting system (Seewald, 2001) by generating H₂S. According to Seewald (2001), this enhances the rate for the conversion of alkanes to alkenes, but he notes that “the specific mechanisms and species responsible for the catalytic activity of sulfur are unclear”.

The catalytic activity of transition metals is well known in petrochemistry and used there to improve desired outcome of thermal cracking operations (Olah and Molnár, 2003). The potential of transition metal minerals to act as catalysts during hydrocarbon

transformation under hydrothermal conditions has been explored by various authors. Below, a brief summary of the studies by Shipp et al. (2010), Mango (Mango, 1992; Mango et al., 1994; Mango, 1997a; Mango and Hightower, 1997b) and Bell et al. (1994) is given. The general conclusion among the authors is consistent. They state that the behavior of a mineral to act as catalyst depends on its accessibility, as well as on the structure and chemical composition of the minerals, which both affect the strength of the chemisorption potential at the mineral surface. A detailed mechanistic model how this works on a molecular scale is often not provided. Only Mango (1992) proposes a schematic catalytic cycle for the hydrogenolysis of an alkene to methane.

Effect of Minerals on the Interconversion Between Alkanes and Alkenes in Hydrothermal Systems (Shipp et al., 2010)

The interconversion of alkanes and alkenes represents the initial step of the reaction scheme proposed for aqueous oxidation by Seewald (2001) (Fig. 5). In order to elucidate if mineral surfaces might be catalytically active for this reaction, Shipp et al. (2010) performed experiments with *trans*-1,2-dimethylcyclohexane as educt at 300°C and 100 MPa in presence of pyrite, pyrrhotite, magnetite and hematite. All samples contained water. Gold tubes were used as sample container. The authors put a special focus on the analysis of *cis*- and *trans*-hydrocarbon products in order to identify whether reactions took place on the mineral surface or rather in solution. A dominance of *cis* products provides strong evidence that the reactions occur on the mineral surface. Based on the results the authors conclude that the different minerals affect the amount of conversion and relative abundance of reaction products differently, suggesting that the structure and chemical composition of the mineral has an effect on the reaction mechanism. Detailed information is not given, because the reference is just a conference abstract. In a recent paper that presents data for the transformation of organic functional groups under hydrothermal conditions in a mineral free system (Shipp et al., 2013), the authors emphasize, however, that the research investigating the effect of minerals on such reactions is still ongoing in their group.

Transition Metal Catalysis in the Generation of Natural Gas (studies by Mango et al., 1992 – 1997)

Alkenes are generated during cracking and as intermediate products during aqueous oxidation. They may be hydrogenated on the surface of solid transition metals. This catalytic process is well known in petrochemistry, mainly in the context of refining operations (Vollhardt and Schore, 2005) (Fig. 7).

Based on natural observations, Mango (1992) proposed that this process may also play a key role for the generation of dry, i.e. methane-rich, natural gas. He states that cracking of oil and kerogen without the aid of transition metal catalysts is not able to mimic the high methane content observed in natural thermogenic gas, which equals 85 %wt methane in the C₁ to C₄ fraction on average (Mango, 1997a).

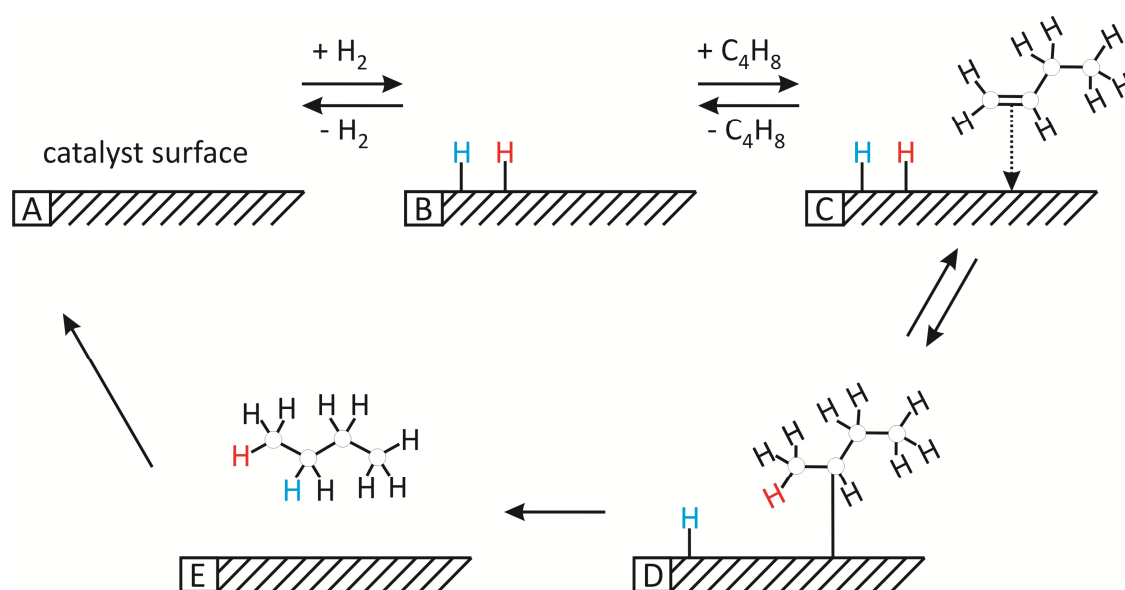


Fig. 7: Hydrogenation of 1-butene on a transition metal catalyst (modified after Fig. 12-1 in Vollhardt and Schore, 2005). The first step involves activation of hydrogen (H_2) by forming metal-hydrogen bonds on the catalyst surface. In the second step, the pi bond of the alkene interacts with the metal weakening the bond (Weisshaar, 1993). As a result, a hydrogen atom from the metal surface is transferred to one of the carbon atoms from the double bond forming a new C-H bond. The other carbon atom from the double bond forms a bond with the metal. In the final step, the second hydrogen atom is transferred to the alkene. The newly formed alkane, in this case *n*-butane, is released from the catalyst's surface allowing the catalyst to accept hydrogen and alkene molecules again. Because of the physical arrangement of the alkene and hydrogen on the metal surface, the reaction produces *cis*-alkanes (Shipp et al., 2010). That means that hydrogen atoms are added to the same face of the double bond.

In his 1992 paper Mango proposes a catalytic cycle for the hydrogenolysis of an alkene to methane (Fig. 8). Within the following five years he, together with co-workers, published experimental results consolidating his hypothesis (Mango et al., 1994; Mango and

Hightower, 1997b). Active transition metal catalysts in this cycle can be transition metal oxides (e.g. Fe_3O_4) and organometallic complexes (e.g. Ni-porphyrins), which may become catalytically active under the reducing conditions of diagenesis (Mango, 1997a). A limitation under natural conditions may be that “low concentrations of contaminants, such as humic acids or H_2S , could reduce the levels of catalytic activity” of the transition metals (Mango, 1992).

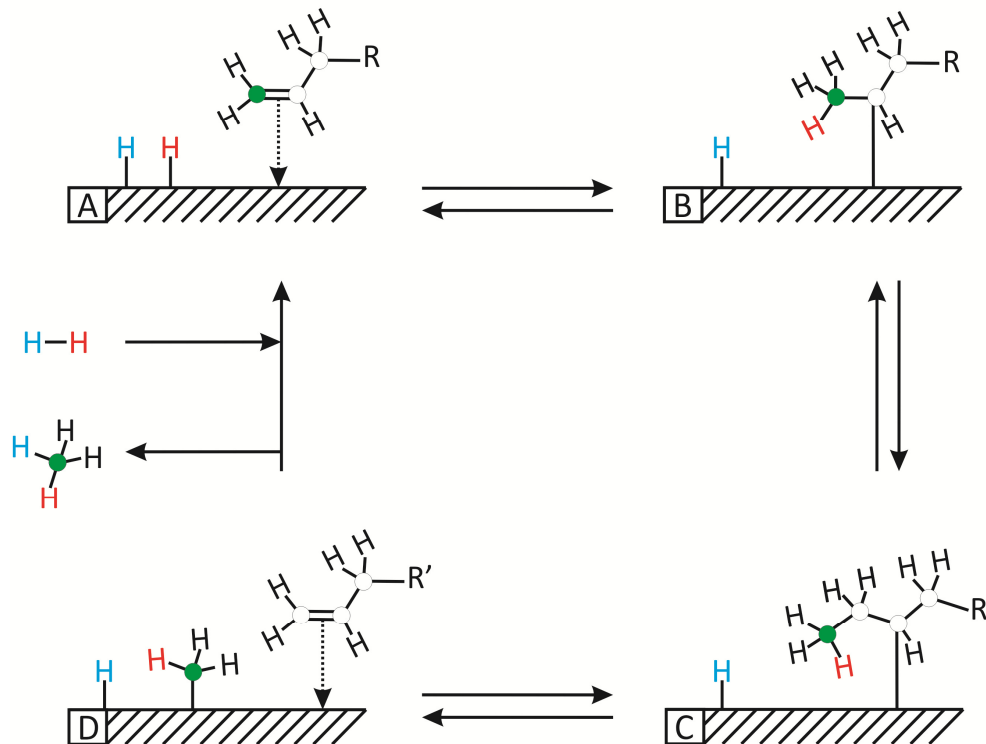


Fig. 8: Cycle proposed for the hydrogenolysis of a long-chain alkene to methane on the surface of a solid transition metal catalyst (modified after Mango, 1992). R represents an alkyl group, with the chain length of R' being one methylene unit (CH_2) shorter than R. Steps A to B are consistent with steps A to D in Fig. 7.

In the first step of the cycle [A], hydrogen (H_2) and an alkene, both for example generated from decomposing kerogen, are activated on the catalyst's surface. A weak coordinate bond forms between the double bond and the metal, which is indicated by a downward pointing arrow. In the next step [B], a hydrogen atom from the metal surface is transferred to one of the carbon atoms from the double bond forming a new C-H bond. The other carbon atom from the double bond forms a bond with the metal. According to Mango (1997a) the metal-carbon bond is free to move up or down the carbon chain by sequential addition-elimination steps, but he does not provide more mechanistic detail. In step C of the scheme, the metal-carbon bond shifted by one position, wherefore the alkyl chain (R) is shortened by one methylene unit (CH_2). The carbon bond in β position to the metal-carbon bond, i.e. the bond between the green and white carbon atom in step C, can cleave easily. As a result, a methyl (CH_3) group and an alkene are generated, with the chain length of the alkene being one carbon atom shorter than the starting alkene. The methyl group adsorbs on the metal surface and the double bond of the alkene forms a weak coordinate bond with the metal [step D]. The second hydrogen atom adsorbed on the metal surface can now combine with the methyl group to generate methane. If additional hydrogen is available, the cycle can start over again, but the new starting alkene will contain one methylene unit less than the starting alkene from the previous cycle.

In addition to the studies by Mango (Mango, 1992; Mango et al., 1994; Mango, 1997a; Mango and Hightower, 1997b; Mango et al., 2010), experimental work by Ott et al. (2006) show that aqueous transition metals, like $\text{Zn}^{2+}_{(aq)}$, $\text{Ni}^{2+}_{(aq)}$ and $\text{Cu}^{2+}_{(aq)}$, may also display

catalytic potential. In their study, they investigated the influence of metal sulfates on the dehydration of polyols, i.e. an alcohol with multiple hydroxyl groups (e.g. 1,2-propanediol), under hydrothermal conditions (280-400°C, 25-34 MPa, 10-180 s).

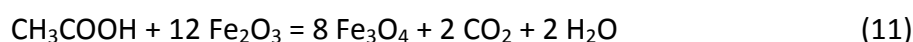
Thermal Decomposition of Acetate Catalyzed by Mineral Surfaces (Bell et al., 1994)

Transition metal minerals may not only affect the conversion of *n*-alkanes and alkenes, but also that of other products generated during aqueous oxidation, like for example organic acids (step 4 in Fig. 5). The effect of minerals on the stability of organic acids under hydrothermal conditions has been the focus of quite many studies (Palmer and Drummond, 1986; Bell et al., 1994; McCollom and Seewald, 2003; McCollom and Seewald, 2003a), because it may have severe implications for reservoir porosity and metal transport.

The study by Bell et al. (1994) is presented in more detail, because they investigated a broad variety of common sedimentary minerals, comprising quartz, calcite, natural pyrite, Ca-montmorillonite, Fe-bearing montmorillonite, hematite, synthetic pyrite and magnetite. In addition to that, they investigated the catalytic potential of typical reaction vessel materials used in experimental studies, i.e. gold, Pyrex, fused quartz and titanium oxide. Bell et al. (1994) studied the thermal decarboxylation of aqueous solutions of acetic acid and sodium acetate in contact with these minerals and reaction vessel materials. Experiments were conducted in a Ti vessel or gold bag at 335°C and 355°C, with the experimental pressure being fixed to the vapor/liquid boundary of water at the given temperature. Run durations were ≤ 3000 hours.

Regarding the reaction vessel materials, it should be emphasized that Pyrex was the only one that catalyzed decarboxylation. Based on this observation, I suggest that experiments performed in Pyrex glass tubes (e.g. Kiyosu, 1980; Kiyosu and Krouse, 1993) should be viewed critical.

Concerning the minerals relevant for the present PhD study, Bell et al. (1994) showed that hematite promotes oxidation according to:



They state that defected magnetite, i.e. with some Fe(III) in the structure, also promotes oxidation. I want to emphasize that the oxygen supply by the minerals can, however, not be regarded as a true catalytic trait because the mineral is transformed. Magnetite containing lower amounts of Fe(III) may catalyze decarboxylation, with the cleavage of the C-C bond occurring while the acetate molecule is adsorbed onto the surface. But as noted above, details for the mechanism are not presented. Decarboxylation may also be catalyzed by synthetic pyrite, but the natural pyrite used in the study by Bell et al. (1994) did not show catalytic activity.

Effect of Minerals on Abiotic Synthesis of Organic Compounds Under Reducing Conditions

The counterpart of aqueous oxidation is abiotic organic synthesis, during which low molecular weight hydrocarbons may be synthesized from inorganic carbon sources such as CO_2 , CO and HCO_3^- (Shock, 1992). This process may only proceed under highly reducing conditions and temperatures below 350°C (Fig. 9). These are conditions which are not encountered during experiments conducted in the course of the present PhD study. The information is still provided in order to provide guidance for planning of follow-up experiments. The objective is to make the reader aware of the possibility of this process if experimental conditions moved to conditions displayed as shaded region in Fig. 9.

In nature, such conditions may, for example be encountered in submarine hydrothermal systems if the circulation reaches deep into the crust (>1.3 km, cf. chapter 7.2.2). In the scientific community, the process of abiotic

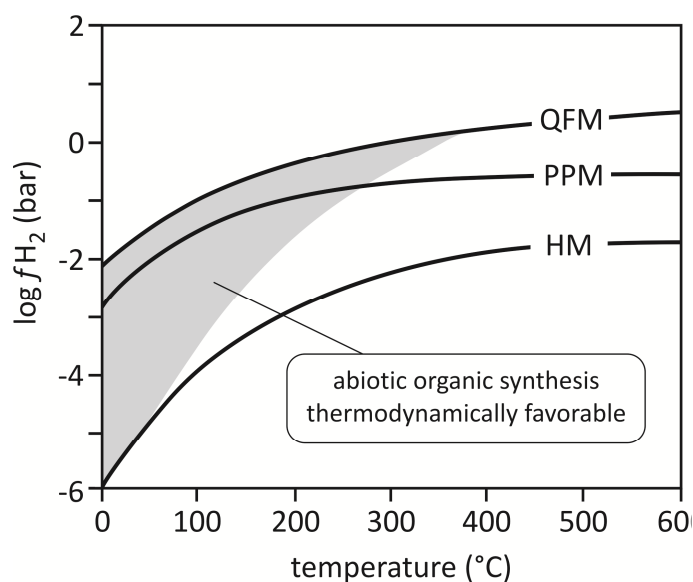


Fig. 9: Curves for the hydrogen fugacity adjusted by the quartz-fayalite-magnetite (QFM), the pyrite-pyrrhotite-magnetite (PPM) and the hematite-magnetite (HM) mineral assemblages as a function of temperature. The grey area represents conditions at which abiotic organic synthesis may occur. (modified after Shock, 1992)

organic synthesis is generally discussed in the context of the debate on the origin of life. Experimental studies showed that transition metals may catalyze the reaction. Results of McCollom et al. (2010) indicate for example that the reduction of CO and CH₂O₂ (formic acid) to methane and other short-chain *n*-alkanes is promoted on the surface of magnetite (Fe₃O₄) under extremely reducing and hydrothermal conditions (250°C, 17 MPa, 0 - 400 h). They propose that catalysis by magnetite occurs according to reactions encountered during Fischer-Tropsch synthesis, a process, which can be used commercially to convert a mixture of carbon monoxide and hydrogen into liquid hydrocarbons (Dry, 1990).

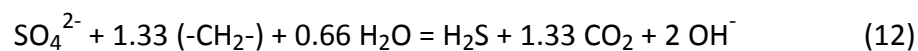
2.2.3 ROLE OF SULFATE – POSSIBILITY OF THERMOCHEMICAL SULFATE REDUCTION

In environments where organic matter gets in contact with sulfate, thermochemical sulfate reduction (TSR) may be initiated. Two natural TSR laboratories are for example the Smackover formation in the Gulf of Mexico (Sassen, 1988; Rooney, 1995; Amrani et al., 2012; Wei et al., 2012) and the Khuff formation in Abu Dhabi (Worden and Smalley, 1996; Worden et al., 2000). TSR is a redox reaction, which is commonly defined as the abiological¹, thermally-driven oxidation of organic compounds by reduction of sulfate, with CO₂ and H₂S as main reaction products (Orr, 1974; Machel, 2001; Zhang et al., 2007; Zhang et al., 2008a; Zhang et al., 2008b; Lu et al., 2011). Especially, the high H₂S contents (up to 80 vol%; Orr, 1977) encountered with TSR altered reservoirs caught the interest of the oil and gas industry that asked for a better understanding of the reaction, because H₂S contents >10% in natural gases increase production cost substantially (Hoffmann et al., 1995; Nöth, 1997; Cross et al., 2004). Additionally, TSR products lead to the dilution of remaining hydrocarbon gases, which minimizes reservoir quality (Goldstein and Aizenshtat, 1994; Cross et al., 2004). If transition or base metals are present, H₂S generated by TSR can initiate metal sulfide precipitation and thus contribute to the formation of sulfide ore deposits (Powell and Macqueen, 1984; Machel et al., 1995; Sun and Püttmann, 2000). Geological and geochemical investigations of Kupferschiefer samples from the Sangerhausen Basin (Germany) indicate, for example, that 60% of the copper-sulfide mineralization in this location can be attributed to the TSR

¹ No bacteria are involved in TSR, wherefore it has to be distinguished from bacterial sulfate reduction (BSR). Machel (2001) presents a comparison of BSR and TSR.

reaction (Sun and Püttmann, 2000). Extensive reviews on TSR are presented by Trudinger et al. (1985), Goldstein and Aizenshtat (1994) and Machel (2001). In addition to that, a thorough PhD study on the molecular geochemical signature of TSR is provided by Hanin (2002), but it is only available in French language. Despite these and other TSR studies, many open questions remain regarding TSR reaction mechanisms and controlling factors. This chapter summarizes the current state of knowledge.

In 1974 Orr proposed a model reaction for TSR, in which methylene groups (-CH₂-) represent the organic reducing agent:



This reaction is simplified and more recent studies showed that TSR is a multistep reaction, which involves many parallel and sequential steps (Seewald, 2003; Amrani et al., 2008; Zhang et al., 2008b). Seewald (2001) emphasized that there is a striking similarity between reaction products derived from TSR and aqueous oxidation, indicating that aqueous oxidation of hydrocarbons probably contributes to TSR.

The confirmed temperature for TSR occurring in nature ranges from 127°C (Rooney, 1995) to 300°C (Giuliani et al., 2000). Thermodynamic modeling indicates that direct reduction of sulfate by most organic molecules is energetically favorable at temperatures above 20°C, but due to the high activation energy the direct reduction of sulfate by organic matter is not considered to be important in most oil field waters (Goldstein and Aizenshtat, 1994). Amrani et al. (2008) point out that the activation of sulfate is the critical step for initiating TSR and that the rupture of the first S–O bond, i.e. the reduction of SO₄²⁻ (with S having a valence of +6) to SO₃²⁻ (with S having a valence of +4), requires the greatest activation energy. In order to overcome the high activation energy for TSR initiation, experimental studies are usually performed at higher temperature (>300°C) or catalysts, like reduced sulfur species are used (Goldstein and Aizenshtat, 1994; Cross et al., 2004; Ma et al., 2008).

Machel (2001) noted that there is not the *one* parameter, which can be used to identify TSR in nature, and he suggests that as many petrographic and geochemical criteria as possible should be combined. The following list comprises an excerpt of possible indicators for TSR involvement that have been reported:

Compounds with sulfur

- High H₂S concentrations, at least in carbonate reservoirs, because in environments with clastic rocks H₂S can be sequestered in mineral phases (Worden et al., 2003), leading to low H₂S concentrations in such settings despite TSR.
- Sulfur incorporation in organic matter is promoted (Zhang et al., 2008b).
- Recent work by Amrani et al. (2012) demonstrate that the $\delta^{34}\text{S}$ values of benzothiophenes and dibenzothiophenes seem to be a promising proxy for TSR.

Compounds without sulfur

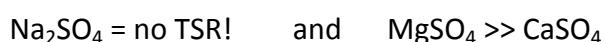
- Increased gas dryness, i.e. high methane content (Orr, 1977; Pan et al., 2006).
- Residual organic matter shows a lower H/C ratio and more aromatic structure, both indicating a loss of hydrogen (Leventhal, 1990).
- Wei et al. (2012) showed that an increase in concentration of thiadiazonoids correlates positively with the extent of TSR.

In contrast to natural observations, experimental studies offer a powerful tool for a better understanding of TSR, because reaction mechanisms, kinetics and controlling factors can be studied in a confined system. Often the H₂S yield is used as measure of the extent of TSR in these studies (Zhang et al., 2007; Amrani et al., 2008; Zhang et al., 2008a; Zhang et al., 2008b; Lu et al., 2010a; Lu et al., 2011). The first experiments on TSR have been presented half a century ago (Harrison and Thode, 1957; Toland, 1960) and during the last two decades numerous experimental works followed (Kiyosu and Krouse, 1993; Cross et al., 2004; Yue et al., 2006; Zhang et al., 2007; Amrani et al., 2008; Zhang et al., 2008a; Zhang et al., 2008b; Chen et al., 2009; Truche et al., 2009; Lu et al., 2010b; Lu et al., 2011; Zhang et al., 2012). Despite these approaches specific reaction mechanisms could to date not be determined (Pryor, 1962; Kiyosu, 1980; Yue et al., 2006). The upside is, however, that experimental studies were successful in identifying various influencing factors for TSR, such as:

i) availability and nature of reactants, ii) inorganic and organic sulfur species, and iii) temperature and pH.

Availability and Nature of Reactants

The initiation and continuation of TSR requires that sulfate and organic matter obviously have to be available, and in contact. Nature of sulfate and organic reactants significantly influence reaction rate and products. Lu et al. (2011) investigated the reaction of three different sulfates (Na_2SO_4 , CaSO_4 and MgSO_4) with *n*-tetracosane ($\text{C}_{24}\text{H}_{50}$) in presence of water at 420°C and 50 MPa using sealed gold tube reactors. Run duration ranged between 12 and 48 h. According to Lu et al. (2011), the sulfates display the following reactivity during TSR:



The significantly higher rate for TSR with MgSO_4 is consistent with results of Zhang et al. (2008a), who studied the reaction of MgSO_4 with *n*-octane (C_8H_{18}) at 350°C and 24 MPa for 24 h using gold tube reactors. They suggested that precipitation of a magnesium hydroxide sulfate mineral might have lowered the pH significantly during experiments (Zhang et al., 2008a; p. 321). This in turn leads to an increase of the concentration of HSO_4^- ion, which has been shown to be more reactive than the fully-solvated SO_4^{2-} anion (Ma et al., 2008). Another possibility for the enhanced TSR rate is the formation of MgSO_4 contact ion pairs (CIP), which seem to be equally reactive compared to the HSO_4^- ion, as indicated by molecular modeling calculations (Ma et al., 2008). Calculated activation energies of the HSO_4^- ion, MgSO_4 CIP, CaSO_4 CIP and free sulfate ion reacting with ethane are 54.21 kcal/mol, 54.95 kcal/mol, 62.53 kcal/mol and 77.60 kcal/mol respectively (Ma et al., 2008).

Although Lu et al. (2011) observed no evidence for reduction of Na_2SO_4 with *n*-alkanes under his experimental conditions, Hoffmann et al. (1995) showed that TSR of Na_2SO_4 by crude oil is possible. They investigated the potential of TSR with Na_2SO_4 and crude oil in glass cylinder experiments ($250\text{-}320^\circ\text{C}$, 6 to 20 MPa, 70-530 h). At the highest temperature and after 500 h, 36% of initial sulfate was reduced. However, reduction may have been catalyzed by organic sulfur compounds (see next paragraph) present in the crude

oil or by the glass used as sample container. A third study (Kiyosu, 1980) investigated the possibility of TSR with Na_2SO_4 and dextrose in presence of water at temperatures between 300 and 340°C in Pyrex (boric-silica glass) tubes. Only at the highest temperature evidence for TSR was observed after 170 h, indicated by a slight decrease of sulfate and a slight increase of H_2S concentrations. However, the TSR process was very sluggish and it cannot be excluded that the reaction was catalyzed by PYREX (Bell et al., 1994). Thus, it remains open if TSR is possible with Na_2SO_4 as sulfate source.

In addition to sulfate, the organic reactant influences TSR rate. Zhang et al. (2007) investigated the effect of hydrocarbon type on TSR with MgSO_4 in presence of water at 350°C and 24.1 MPa for 24 h using gold tube reactors. Based on the H_2S yields (Fig. 10), they inferred that the relative reactivity during TSR for the synthetic model compounds studied is:

1-octene > 1-octanol > 1-octanone > *n*-octane > octanoic acid > octylbenzene > xylene

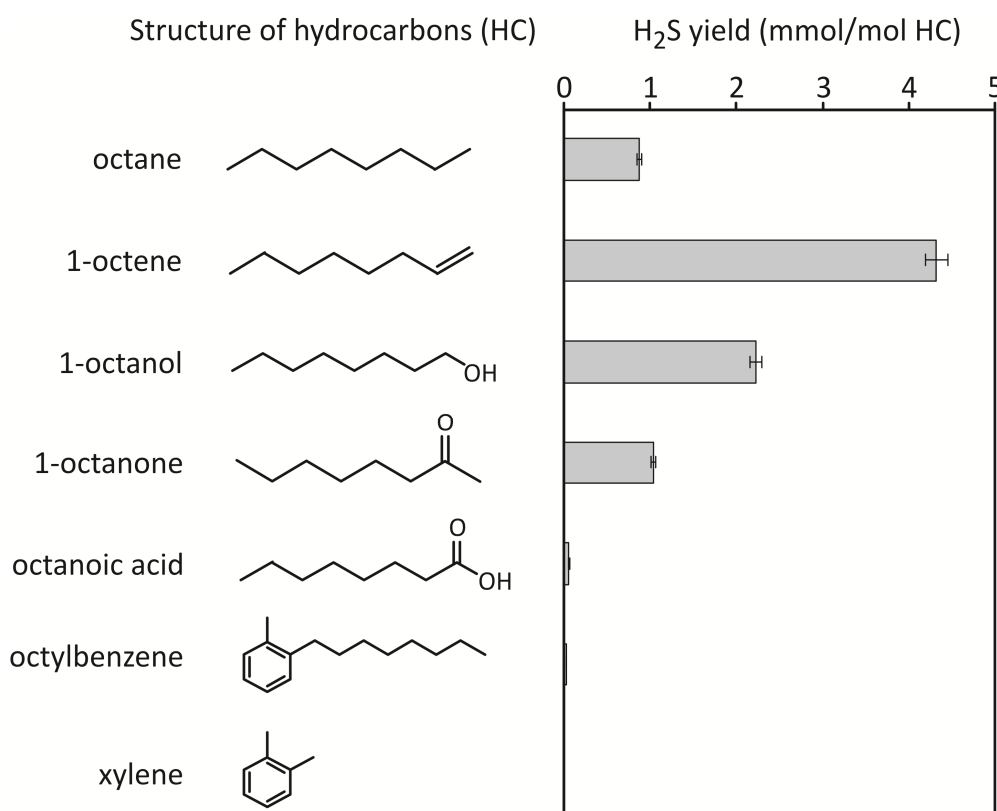


Fig. 10: H_2S yield from reduction of MgSO_4 by model compounds after 24 h at 350°C and 24.1 MPa. Adapted from Zhang et al. (2007) with kind permission by Pergamon.

A similar trend in reactivity is observed by Lu et al. (2010a) for experiments simulating TSR with MgSO_4 and four fractions (saturated, aromatic, polar² and asphaltene) of a crude oil from well Che571 in the Dongying Depression (China). Experiments were performed in presence of water at 420°C and 50 MPa for 24 h in gold tube reactors. They showed that TSR is possible with all four fractions, which is manifested by increased H_2S yields upon sulfate addition (compare *Fig.1h* in Lu et al., 2010a). Based on H_2S yields, generated amounts of C_1 to C_5 alkanes (especially methane), and the $\delta^{13}\text{C}$ values for methane, ethane and propane, Lu et al. (2010a) inferred the following relative reactivity for the individual petroleum fractions with MgSO_4 :

saturated > asphaltene > polar > aromatic

Inorganic and Organic Sulfur Species

In 1960, Toland addressed the positive effect of H_2S and other low valence sulfur species on the TSR rate. As a result, H_2S or elemental S are often used to initiate the reaction in experimental studies (Kiyosu and Krouse, 1993; Cross et al., 2004). Once initiated, increasing H_2S partial pressures lead to increasing TSR rates, which is an autocatalytic process. The nature of the active sulfur species responsible for the oxidation of organic matter in TSR is still subject of speculation. Goldstein and Aizenshtat (1994) proposed that polysulfides are likely the most active species for TSR. More recently it has been suggested that H_2S and other inorganic low valence sulfur species play only a subordinate role and that labile organosulfur compounds (LSC) are more likely the key intermediate species for early stage TSR catalysis (see Amrani et al., 2008 and Zhang et al., 2008b for details). Labile organosulfur compounds stands for organic compounds that contain sulfur and show a relatively low thermal stability, like thiols ($\text{C}_n\text{H}_{2n+1}\text{SH}$), some organosulfides and organopolysulfides. Amrani et al. (2008)³ showed that minute amounts of LSCs can significantly enhance the rate of TSR; e.g. addition of 0.03 wt% S (as 1-pentanethiol = LSC) doubles the rate of TSR over that of TSR without LSCs. The authors used density functional

² The polar fraction is composed of NSO compounds, i.e. organic molecules that contain nitrogen, sulfur and/or oxygen.

³ Amrani et al. (2008) performed gold-tube hydrous pyrolysis experiments with *n*-octane and CaSO_4 in presence of reduced sulfur (H_2S , S^0 and organic sulfur compounds like e.g. 1-pentanethiol) at 330 and 356°C, 24.1 MPa for 5 to 405 h. The pH during the experiments was buffered to 3.5 with talc and silica.

theory-based molecular modeling in order to gain insight into possible reaction mechanisms responsible for the catalytic effect of LSCs. They propose that “1-pentanethiol or its thermal degradation products may directly react with sulfate and reduce the activation energy required to rupture the first S-O bond through the formation of a sulfate ester” (Amrani et al., 2008, p. 2960), but they state at the same time that “further study, both theoretical and experimental, is needed to confirm this suggested mechanism” (Amrani et al., 2008, p. 2970).

Reaction Kinetics of TSR, and the Effect of Temperature and pH

TSR without presence of initial low valence sulfur, has been successfully simulated in laboratory experiments at temperatures $\geq 241^{\circ}\text{C}$ with either H_2SO_4 , CaSO_4 or MgSO_4 , which were reacted with different organic compounds, like dextrose, acetic acid and hydrocarbons (Zhang et al., 2012 and references therein). The reaction shows strong temperature dependence, with higher temperatures increasing the reaction rate. Zhang et al. (2012) provide new experimental data for kinetics of TSR, as well as a thorough review on published TSR kinetic data. There is general agreement amongst the authors (Zhang et al., 2012 and references therein) that H_2S generation from sulfate is a first-order reaction and that the activation of the sulfate is the critical first step. However, Zhang et al. (2012) also emphasize that “further work is needed to quantify the effect of different reductants on the rate of sulfate reduction” and that only then a comprehensive model can be developed for the prediction of TSR in geologic settings.

The pH can be critical for the TSR reaction rate. Kiyosu (1980) and Zhang et al. (2012) showed that acidic pH (<4) significantly enhance the TSR rate and lower the onset temperature for the reaction. This is due to activation of sulfate by increasing the HSO_4^- activity with decreasing pH values (Toland, 1960; Goldstein and Aizenshtat, 1994; Zhang et al., 2008b). As noted above, the bisulfate ion (HSO_4^-) has been shown to be more reactive than the free sulfate ion (SO_4^{2-}) (Ma et al., 2008). It is, however, noteworthy that acidic pH values are rather uncommon in petroleum systems. Here the pH usually ranges from 5.5 to 7 (cf. Helgeson et al., 1993, Fig. 10). In this pH range, the TSR rate seems to be independent of pH (Cross et al., 2004). In experimental studies, the pH may be controlled by using suitable pH mineral buffers. Zhang et al. (2012) used, for example, the talc-silica pH buffer to control

the pH during TSR experiments, but other effects of the minerals on the reacting system are not addressed.

Despite the availability of numerous studies investigating inorganic-organic reactions, they all have serious limitations. The major one being that the effect of inorganic components on isolated reactions is often studied in great detail, but not their effect on the whole reaction network responsible for hydrocarbon conversion and associated processes like cracking and aqueous oxidation. This is especially true for TSR experiments. A second limitation is that the effect of redox buffers on TSR reactions has not been studied in detail, although TSR is obviously a redox-dependent process. A third limitation is that the effect of dissolved transition metals is barely studied, which may, however, have severe implications for the stability of hydrocarbons.

In order to contribute to a better understanding of these open points, an internally consistent set of experiments was conducted investigating the reaction of *n*-octane with two mineral buffers (HM and PPM) in presence and absence of sulfate. Furthermore, experiments with a variety of transition metal sulfates were conducted to investigate the effect of dissolved transition metal cations on the product distribution generated from *n*-octane.

3.

MATERIALS AND METHODS

3.1 EXPERIMENTAL STRATEGY

Three experimental series were conducted in the course of the present PhD thesis (Table 3). The objective of the first series was to investigate the effect of the hematite-magnetite and the pyrite-pyrrhotite-magnetite mineral assemblages on the hydrothermal conversion of *n*-octane. For this, experiments with *n*-octane and water in presence of these two mineral buffers were carried out in the temperature range of 300 - 350°C and at a pressure of 35 MPa for a duration of 168 h. In the sample names, presence of *n*-octane is indicated by the subscript C_8 whereas *HM* and *PPM* denote presence of the hematite-magnetite and the pyrite-pyrrhotite-magnetite mineral buffers respectively. For comparison identical experiments were performed without any mineral buffer being present, which is denoted by the label *-buf* in the sample name. Furthermore, one experiment with only *n*-octane (labeled by $C_{8*350^\circ C}$) was carried out at 350°C and 35 MPa for 168 h with the intention to assess contributions from pure thermal cracking at these conditions.

The second experimental series ties in with the first one. The objective was to explore the effect of sodium sulfate (Na_2SO_4) on the product distribution generated from *n*-octane thermal decomposition in presence and absence of the HM and PPM mineral buffers. Presence of sodium sulfate in the experimental charge is highlighted by the subscript *+Na* in the sample name. The experiments were run at identical conditions as the first series. In addition to that, time series experiments with run durations ranging from 72-336 h were conducted for sulfate-containing samples processed in presence of the PPM mineral buffer at 300°C and 350°C. In the course of the time series experiments, one blank sample of the type PPM+H₂O+Na₂SO₄ was processed at each temperature for 168 h in order to determine possible hydrocarbon contributions from the PPM mineral buffer.

The objective for the third experimental series was to investigate the influence of five transition metal sulfates ($NiSO_4$, $ZnSO_4$, $FeSO_4$, $Fe_2(SO_4)_3$ and $CuSO_4$) on reaction outcome of thermal *n*-octane decomposition. Four different concentrations of the metal sulfates were tested, ranging from 0 to 0.5 mol/kg_{H₂O}. Presence of transition metals is indicated in the sample name via the following subscripts: *Ni*, *Zn*, *Fe(II)*, *Fe(III)* and *Cu*. Experiments were carried out at a temperature of 315°C and at a pressure of 13 MPa for a run duration of

168 h. For comparison, a sample with a Na_2SO_4 solution and *n*-octane was processed at identical conditions.

Table 3: Overview of the variety of experiments conducted in the course of the present PhD thesis. The duration of most experiments was 168 h, with the exception of the time series. Here, samples were processed for 72 to 336 h.

Experimental conditions	300°C & 35 MPa	315°C & 13 MPa	350°C & 35 MPa
C_8H_{18} only			x
-buf <i>with/without Na₂SO₄</i>			x/x
HM <i>with/without Na₂SO₄</i>			x/x
PPM <i>with/without Na₂SO₄</i>	x/x		x/x
PPM Blank <i>(PPM+H₂O+Na₂SO₄)</i>	x		x
PPM time series <i>(PPM+H₂O+Na₂SO₄)</i>			x
-buf <i>with transition metals*</i>		x	

-buf, HM and PPM stand for: no buffer, hematite-magnetite and pyrite-pyrrhotite-magnetite respectively

*the following transition metal sulfate solutions were investigated: FeSO_4 , $\text{Fe}_2(\text{SO}_4)_3$, NiSO_4 , CuSO_4 & ZnSO_4

3.2 STARTING MATERIALS

Synthetic *n*-octane (Sigma-Aldrich, anhydrous, >99% pure) was used as model organic compound. Minerals were purchased from Sigma Aldrich in case of hematite (Fe_2O_3 , >99 wt% pure on metal basis), and from Alfa Aesar in case of pyrite, pyrrhotite and magnetite (all >99.997 wt% pure on a metal basis). For each mineral buffer, equal amounts (on a weight basis) of powdered minerals with a grain size of <150 μm for iron sulfides and <840 μm for hematite and magnetite were thoroughly mixed in a mortar. For the PPM buffer this was done under an argon atmosphere to prevent oxidation of minerals. Two Na_2SO_4 solutions, one with a concentration of 1.7 mol/kg $_{\text{H}_2\text{O}}$ (300°C and 350°C experiments) and one with a concentration of 0.5 mol/kg $_{\text{H}_2\text{O}}$ (315°C experiments), were used to study the effect of sulfate on the hydrothermal decomposition of *n*-octane. The solutions were

prepared by dissolving Na_2SO_4 powder (Merck, anhydrous, >99%) in HPLC-grade water (Lab-Scan Analytical Sciences). Stock solutions of transition metal sulfates, namely $\text{FeSO}_4 \cdot 7\text{H}_2\text{O}$ (Sigma Aldrich, 99+%), $\text{Fe}_2(\text{SO}_4)_3 \cdot x\text{H}_2\text{O}$ (Sigma Aldrich, 97%), NiSO_4 (Sigma Aldrich, 99.99%), CuSO_4 (Sigma Aldrich, 99.99+%) and $\text{ZnSO}_4 \cdot \text{H}_2\text{O}$ (Sigma Aldrich, 99.9+%), were prepared in the same manner to adjust a sulfate concentration of $0.5 \text{ mol/kg}_{\text{H}_2\text{O}}$. In case of $\text{FeSO}_4 \cdot 7\text{H}_2\text{O}$ the prepared stock solution had a sulfate concentration of $0.3 \text{ mol/kg}_{\text{H}_2\text{O}}$.

3.3 SAMPLE PREPARATION

Arc welded gold tubes were used as sample containers for all experiments. The dimension of the containers were as follows: inner diameter of 4 or 5 mm, wall thickness of 0.2 mm and length between 25 and 40 mm ($V = 440$ to $503 \mu\text{l}$). A schematic picture of the general sample layout is given in Fig. 11.

Gold was chosen as material for sample containers because of its chemical inertness, good thermal conductivity and flexibility. Prior to the experiments, gold tubes were cleaned with acetone and dried. In order to remove residual organic material and to soften the gold, the tubes were then annealed at 850°C for 10 min. After that, one end of each gold tube was crimped and sealed by arcwelding using a "PUK 3 professional plus" welding plant from Lampert Werktechnik GmbH. Next, $5 \mu\text{l}$ of *n*-octane ($=31 \mu\text{mol}$) and $90 \mu\text{l}$ HPLC-grade water or $90 \mu\text{l}$ of the Na_2SO_4 solution ($c_{\text{Na}_2\text{SO}_4} = 1.7 \text{ mol/kg}_{\text{H}_2\text{O}}$) were injected with a syringe. In case of the transition metal samples, the procedure was different. In this series four different concentrations of transition metal sulfates were investigated, ranging from 0 to $0.50 \text{ mol/kg}_{\text{H}_2\text{O}}$. That means that either $200 \mu\text{l}$ of the pure Na_2SO_4 solution ($c_{\text{Na}_2\text{SO}_4} = 0.50 \text{ mol/kg}_{\text{H}_2\text{O}}$), $200 \mu\text{l}$ of the pure transition metal sulfate solution or a mix of both was added to the sample container (Table 4). The amount of *n*-octane, which was added to the sample container ($5 \mu\text{l}$), was the same as in the other samples.

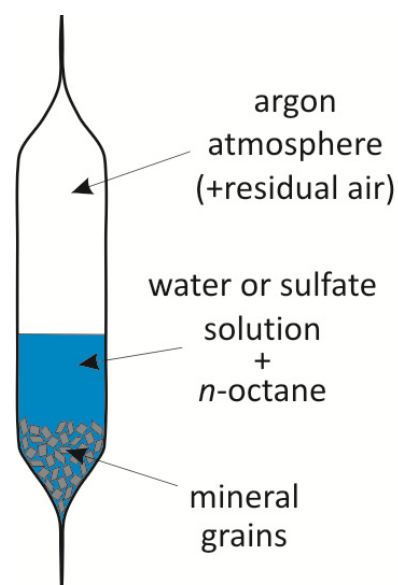


Fig. 11: Sketch of a typical sample layout as used for samples processed in the course of the present PhD study.

After the liquids have been introduced to the sample container, solids were added by means of a funnel. Weights were recorded with an uncertainty below $\pm 2\%$ for all compounds. Immediately after loading, the gold containers were flushed with argon for 30 seconds to remove air, crimped, welded shut and weighted to check for any loss. Reduction in weight is usually below $\pm 5\%$ and cannot be linked to a specific compound, wherefore correction is not possible. Directly before the experiments, the gold capsules were compressed at room temperature in a steel autoclave at 20 MPa argon pressure. Compaction of the capsule was taken as indication for efficient sealing.

Table 4: Compositions employed for transition metal samples. The mixing ratios used for the individual transition metal sulfate solutions and the sodium sulfate solution ($c_{\text{Na}_2\text{SO}_4} = 0.5 \text{ mol/kg}_{\text{H}_2\text{O}}$) are given. Due to inverse solubilities of the metal sulfates (except NiSO_4) the actual amount of sulfate and the concentration of the transition metal cation in solution are lowered at experimental conditions (cf. *chapter 6.1*).

Transition metal sulfate (TMS)	Concentration of stock solution (mol/kg _{H₂O})	Ratio TMS/Na ₂ SO ₄ (μl/μl)	Sample ID
Na ₂ SO ₄	0.50	0/200	Na
FeSO ₄	0.27	40/160	Fe(II)_mix1
		100/100	Fe(II)_mix2
		200/0	Fe(II)
Fe ₂ (SO ₄) ₃	0.17	42/158	Fe(III)_mix1
		84/116	Fe(III)_mix2
		200/0	Fe(III)
NiSO ₄	0.50	40/160	Ni_mix1
		100/100	Ni_mix2
		200/0	Ni
CuSO ₄	0.48	40/160	Cu_mix1
		100/100	Cu_mix2
		200/0	Cu
ZnSO ₄	0.45	40/160	Zn_mix1
		100/100	Zn_mix2
		200/0	Zn

3.4 EXPERIMENTAL PROCEDURE

3.4.1 SETTING OF THE EXPERIMENTAL PARAMETERS TIME AND TEMPERATURE

Experimental parameters were set based on time series data for samples of the type PPM+H₂O+C₈H₁₈+Na₂SO₄ processed at temperatures of 300 and 350°C, and at a pressure of 35 MPa for 72 to 336 hours. In order to make the decision transparent, it is necessary to forestall some results. Data for generated *n*-alkanes show that their concentrations remain roughly constant at 300°C (Fig. 12 A), even if the reaction time is doubled from 168 h to 336 h. The conversion of *n*-octane is very low. A temperature increase from 300 to 350°C significantly promotes *n*-octane decomposition, which is indicated by *n*-alkane yields that increase by one to two orders of magnitude (Fig. 12 B). This is in line with previous experimental studies (e.g. Behar and Vandembroucke, 1996) that demonstrate the positive effect of temperature on *n*-alkane degradation in a sulfate- and mineral-free system. Time series data at 350°C (Fig. 12 B) show that generated amounts of *n*-alkanes continuously increase with increasing run duration from 72 to 336 h. Time series data provided by Seewald (2001) for similar experiments with *n*-heptane and the PPM buffer indicate, however, that decomposition of *n*-heptane is still ongoing in this time frame and that the whole system has not reached a final state after 3022 h (cf. Fig. 26).

The objective of the experiments performed in the present study is to investigate the effect of inorganic components on the conversion of *n*-octane at an early stage. Based on the results for the 350°C experiments (Fig. 12 B and Table A1 in the appendix) it was decided to choose a constant run duration of 168 h for the majority of the experiments, as a compromise of acceptable run duration and well measurable product concentrations. I am aware that the experiments only represent a snap shot on the reaction and that equilibrium for the whole system has not been reached, although in question if this is possible at all. At 300°C, concentration of reaction products are still small after 168 h, but will only increase with very long run durations. Thus, a temperature of 350°C was chosen for most samples in order to overcome low product concentrations generated at the lower temperatures. In this way the “resolution” was improved so that effects of the inorganic components could be identified.

In case of the transition metal samples, the focus was to process a large quantity of samples simultaneously in order to get an overview of the effect of different transition metals on *n*-octane decomposition. Therefore the Parr hydrothermal reactor (cf. *chapter 3.4.3*) was used, which constrains the maximum possible experimental temperature to 315°C. The pressure was adjusted to 13 MPa for these experiments.

Note that the pressure is well above the vapor pressure curve of water for all experiments in order to keep the reaction in the liquid state.

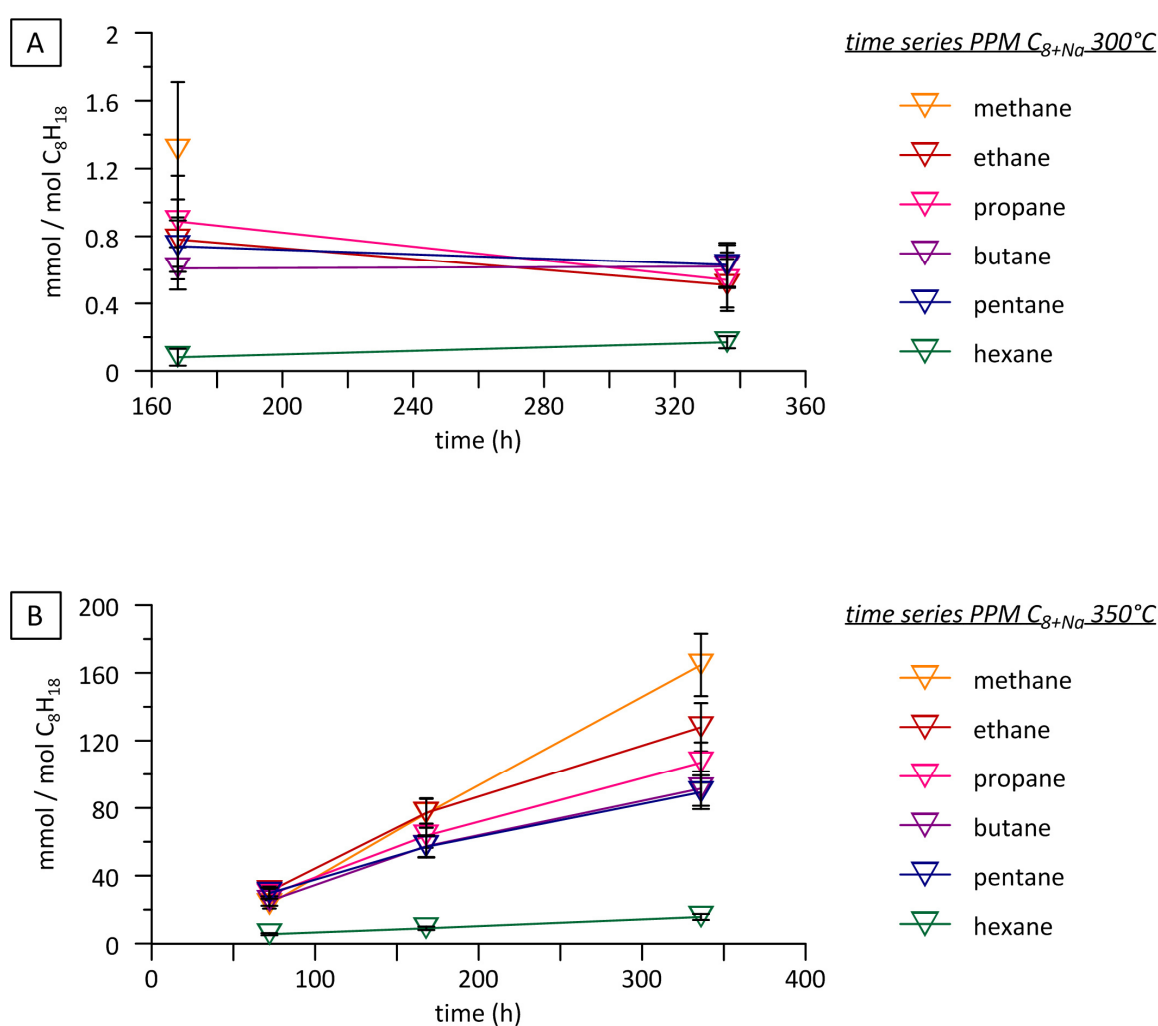


Fig. 12: Variations of *n*-alkane concentrations as a function of time during heating of *n*-octane at (A) 300°C and (B) 350°C in presence of the pyrite-pyrrhotite-magnetite (PPM) mineral assemblage and sodium sulfate. Pressure was kept at 35 MPa for all experiments. Error bars represent uncertainties, which results from error propagation of the analytical error and the total weighing error of initial *n*-octane.

3.4.2 COLD-SEAL PRESSURE VESSEL SETUP

A cold-seal pressure vessel (CSPV, Fig. 13) was used for most experiments conducted in the course of the present PhD thesis. With this setup, it was possible to process up to six samples simultaneously. After loading, the autoclave was pressurized with argon and inserted into a vertical oven. Pressure was maintained constant at 35 ± 1 MPa during experiments. Desired run temperatures of 300 and $350 \pm 5^\circ\text{C}$ were reached within 70 to 90 min. Temperature was kept within $\pm 5^\circ\text{C}$ and monitored with three K-type thermocouples evenly distributed along the sample (indicated by T_A , T_B and T_C in Fig. 13). At the end of the experiments, the CSPV was withdrawn from the oven and rapidly cooled (<10 min) to room temperature by compressed air, resulting in a cooling rate of $30^\circ\text{C}/\text{min}$. During quenching, the confining pressure was maintained constant to prevent rupturing of sealed gold tubes. After cooling, pressure was released and samples were recovered from the autoclave.

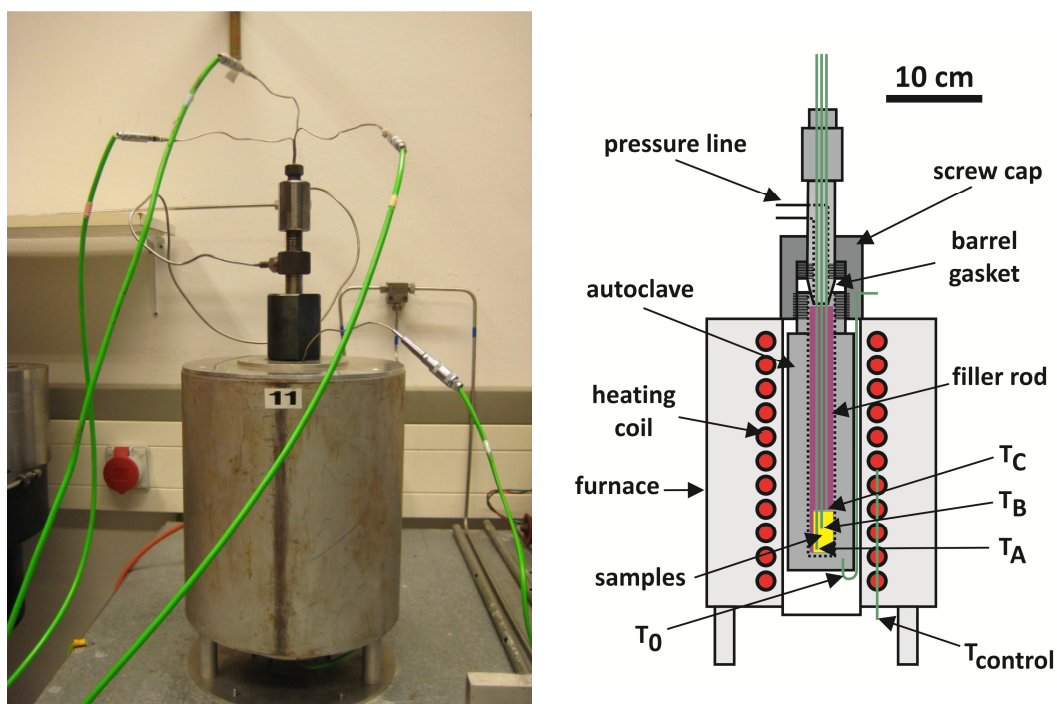


Fig. 13: Cold-seal pressure vessel used for the experiments at the lab of the mineralogy department at the Leibniz University of Hanover (left). The right side shows a schematic picture of the experimental setup. T_A , T_B , T_C , T_0 and T_{control} refer to individual thermocouples used to accurately monitor and control the temperature during the experiments.

3.4.3 PARR HYDROTHERMAL REACTOR

The Parr hydrothermal reactor (Fig. 14) was used for experiments of the transition metal series. Owing to its large volume ($V = 450 \text{ mL}$), it was possible to process up to 34 samples simultaneously. The samples were placed in a sample holder and then loaded in the autoclave that is externally heated. The reactor was completely filled with water, which was used as pressure medium. During the experiments the pressure was kept within $13.00 \pm 0.05 \text{ MPa}$ using an ISCO high pressure syringe pump. Temperature was monitored using a thermocouple, which is located in the lower third of the reactor. The desired run temperature of $315 \pm 5^\circ\text{C}$ was reached within 80 min and maintained in this range during the experiments. The line of action at the end of an experiment is identical to that for experiments with the CSPV, with the exception that the autoclave was cooled by room air and water, instead of compressed air. Room temperature was reached within 60 min, which results in a cooling rate that is 6 times lower than for experiments with the CSPV. Method tests performed in the course of my PhD work showed, however, that both cooling procedures are sufficient enough to avoid detectable changes in product distribution caused by potential retrograde reactions.



Fig. 14: Samples in the sample holder (left), which can be loaded into the Parr hydrothermal reactor (right). In the right picture all reactors are not running. This is represented by the ovens that are not covering the reactors. (photographs taken by Christian Ostertag-Henning)

3.5 ANALYTICAL METHODS

A weight difference of less than 0.4 mg before and after the experiments was taken to indicate no leak, and only these samples were taken for detailed analysis. Subsequent to experiments, the outside of sealed gold tubes was cleaned with dichloromethane (DCM) to remove any grease, which can be carried over from the autoclave. After complete vaporization of DCM, individual samples were placed into separate 22 ml vials, which were sealed with a PTFE/butyl septum. Vials were flushed with helium for 5 min to remove air using a double needle technique, which ensured that no over pressurization of vials occurred. Next, either 1.5 ml (for samples labelled by *-buf C₈*, *-buf C_{8+N_a}* and *PPM C_{8+N_a}*) or 1.0 ml (for all other samples) of nitrogen-purged water was injected. The gold capsules were pierced at two ends with an awl to allow release of reaction products. Vials containing 1.0 ml water were directly measured by headspace gas chromatography (HSGC), whereas a 500 µl fluid aliquot was taken for high performance liquid chromatography (data not presented here) from vials containing 1.5 ml water, before these samples were analyzed by HSGC. Method tests showed that only ketone concentrations were significantly affected by this difference in dilution because of their high solubility in water. Thus measured ketone values for samples *-buf C₈*, *-buf C_{8+N_a}* and *PPM C_{8+N_a}* were corrected according to:

$$[C_nH_{2n}O]_{corrected} = [C_nH_{2n}O]_{quantified} \times (1590 \mu\text{l} / 1090 \mu\text{l}) \quad (13)$$

After HSGC analysis, vials were immediately opened, fluid was removed and the solid sample was lyophilized for X-ray diffraction (XRD) analysis.

3.5.1 STATIC HEADSPACE GAS CHROMATOGRAPHY

A comprehensive analysis of selected hydrocarbons (<C₈H₁₈) and oxygen-containing compounds was performed by headspace gas chromatography (HSGC) using a two-channel Hewlett-Packard 6890 GC equipped with a PerkinElmer TurboMatrix 40 headspace autosampler. The gas chromatograph was fitted with a HP-Plot/Q column (30 m x 0.53 mm i.d.) connected to a flame ionization detector (FID) and a CP-PoraPlot Q column (27.5 m x 0.32 mm i.d.), which is linked to a thermal conductivity detector (TCD). Helium was used as carrier gas at a constant flow rate of 8.2 ml/min and 2.2 ml/min respectively for the two columns. The initial temperature of the GC oven was kept constant at 50°C for 2 min,

followed by a temperature ramp of 10°C/min up to 230°C, which was held for 20 min. Prior to analysis, each vial was equilibrated and shaken at 80°C for 25 min in the auto sampler oven. For calibration, five standards, covering the full sample range, were prepared using a solution of pure *n*- and *iso*-alkanes, alkenes, ketones and aromatics in methanol and a standard gas from Air Products (CO₂ + gaseous *n*-alkanes and alkenes). In addition to that, organosulfur compounds, i.e. thiophene, 2- and 3-methylthiophene, were calibrated for the series of the transition metal sulfate samples, i.e. samples of the third experimental series.

Retention times of individual compounds were used for compound identification. Peak integration was performed with the Agilent ChemStation software and all major peaks were considered for data evaluation. An example of a typical chromatogram is shown in Fig. 15. In all samples, quantified products were at least one order of magnitude above detection limits (cf. Table A1 & A2 in the appendix). At low product concentrations, background noise of the chromatogram as well as coelution complicated integration of peaks. Significant coelution occurred around the retention times for *iso*-butane, 1-butene, *iso*-pentane, benzene, *n*-heptane and toluene.

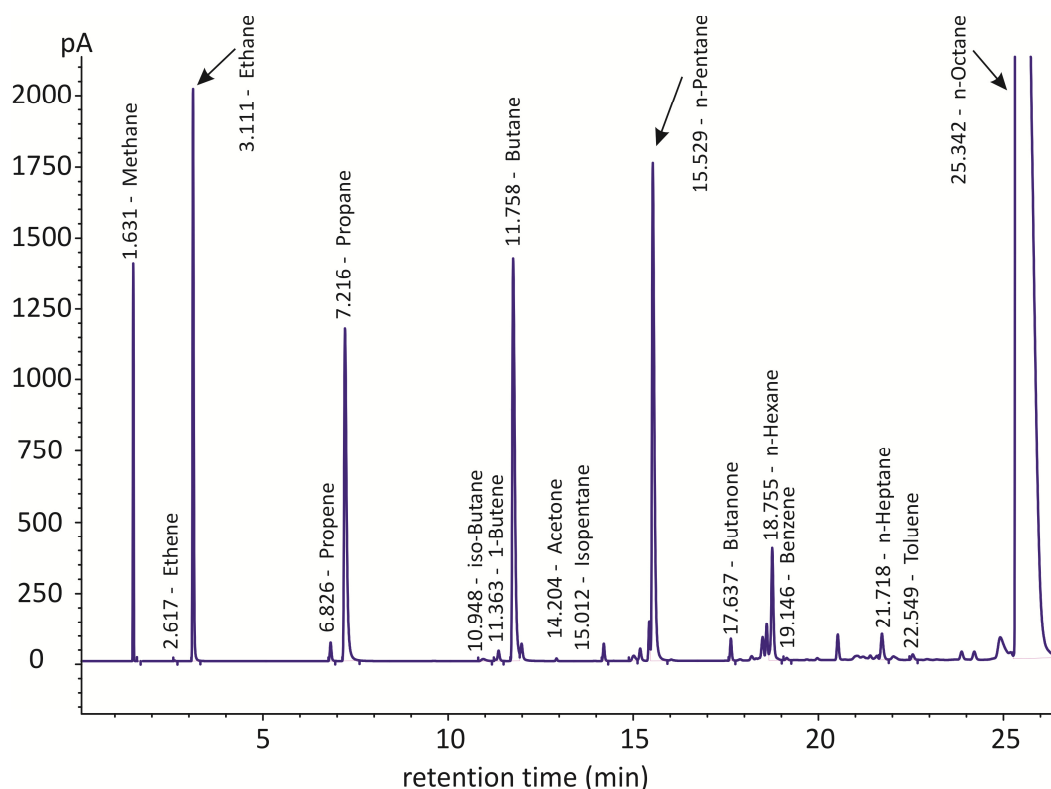


Fig. 15: Chromatogram for one of the PPM C_{8+Na} 350°C samples. Only the trace of the flame ionization detector (FID) is shown. The FID signal is recorded in picoampere (pA).

The analytical uncertainty was estimated from the comparison of standards between individual analytical sequences and multiple measurements (>10) of standards within one sequence. These data indicate that the uncertainty (1σ) of the HSGC method is 10 % for most concentrations in the range of the 350°C samples. It increases to 20 % at lower concentrations, which is the case for some alkene and all the benzene measurements at 350°C. This is also true for the products generated at 300°C and some of the data obtained for the 315°C samples.

3.5.2 X-RAY DIFFRACTION ANALYSIS AND TOTAL CARBON DETERMINATION

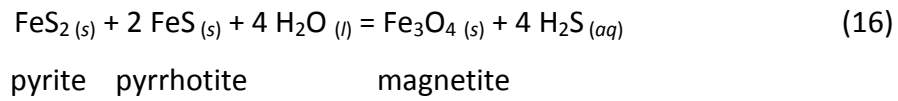
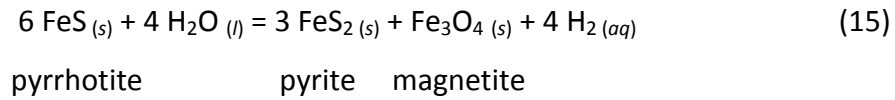
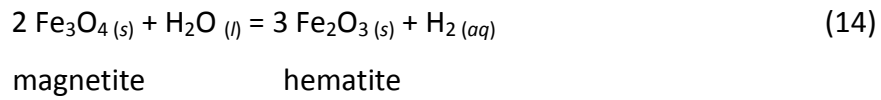
X-ray diffraction (XRD) patterns of powdered samples were recorded using a PANalytical X'Pert PRO MPD Θ - Θ diffractometer (Co-K α radiation generated at 40 kV and 40 mA), equipped with a variable divergence slit (10 mm irradiated length), primary and secondary soller, Scientific X'Celerator detector (active length 0.59°), and a sample changer (sample diameter 16 mm). The samples were investigated in the 2Θ range from 2° to 90° with a step size of 0.0167° and a measuring time of 10 seconds per step. All diffractograms had a low baseline, indicating that no detectable amount of an amorphous phase was present. Amounts of individual minerals were quantified by Rietveld refinement of XRD diagrams using the fundamental parameter software Autoquan (Bergmann et al., 1998). It was possible to assign between 98 to 100 % of all peaks. An accuracy of ± 3 wt% is reached with this method.

The amount of total carbon was determined using the ELTRA CS-800 analyzer. The sample (50 - 100 mg) is mixed with 1500 mg tungsten and 300 mg iron and burned in an oxygen stream. Temperatures exceed 2000°C within less than a minute, which ensure total release of carbon as CO₂. The gas is carried through an IR cell where absorbance is measured. Measurements of standards at the start and end of a measuring series ensure good calibration. The ELTRA CS-800 is especially adjusted to detect ppm amounts of carbon. Total C analysis confirms small amounts of carbon in both buffers, resulting in 309 ± 31 ppm (= 0.77 ± 0.08 $\mu\text{mol C}$ per 30 mg buffer) for the PPM and 104 ± 10 ppm (= 0.26 ± 0.02 $\mu\text{mol C}$ per 30 mg buffer) for the HM buffer. The analytical uncertainty is 10%.

3.6 THERMODYNAMIC CALCULATIONS

3.6.1 ACTIVITIES OF AQUEOUS H₂ AND H₂S REGULATED BY THE HM AND PPM BUFFERS

Under hydrothermal conditions, the HM and PPM buffer regulate the hydrogen activity ($a_{H_2(aq)}$), via Reactions (14) and (15) respectively. In addition to that, the PPM minerals have the ability to buffer the activity of aqueous hydrogen sulfide ($a_{H_2S(aq)}$) according to Reaction (16).



Thermodynamic calculations can be used to predict the activity of aqueous hydrogen and aqueous hydrogen sulfide, which are adjusted by the buffer minerals at a given temperature if the equilibrium state is attained. The subscripts (s), (aq) in the buffer reactions denote the gas and aqueous state respectively. The subscript (l) is used for pure water. It is important to define the phase states for thermodynamic calculations.

The first step for calculating aqueous hydrogen and hydrogen sulfide activities is to establish laws of mass action for the buffer reactions:

$$\log K_{(14)} = 3 \log a_{\text{Fe}_2\text{O}_3(s)} + \log a_{\text{H}_2(aq)} - 2 \log a_{\text{Fe}_3\text{O}_4(s)} \quad (17)$$

$$\log K_{(15)} = 3 \log a_{\text{FeS}_2(s)} + \log a_{\text{Fe}_3\text{O}_4(s)} + 4 \log a_{\text{H}_2(aq)} - 6 \log a_{\text{FeS}(s)} - 4 \log a_{\text{H}_2\text{O}(l)} \quad (18)$$

$$\log K_{(16)} = \log a_{\text{Fe}_3\text{O}_4(s)} + 4 \log a_{\text{H}_2\text{S}(aq)} - \log a_{\text{FeS}_2(s)} - 2 \log a_{\text{FeS}(s)} - 4 \log a_{\text{H}_2\text{O}(l)} \quad (19)$$

As the next step, the equilibrium constants ($\log K$) at experimental temperature and pressure need to be calculated. I used the SUPCRT92 computer program (Johnson et al., 1992) for the calculation, together with thermodynamic data consistent with the SPRONS92.DAT database (see Johnson et al., 1992 for original sources) or, in case of aqueous H_2S with thermodynamic data provided by Schulte et al. (2001). Following the procedure of Seewald (2001), the standard states adopted for water and minerals are unit activity of the pure liquid and solid at any temperature and pressure. Note that pyrrhotite forms an exception because its activity is reduced due to a deficit of iron in the structure (see below). The standard state for aqueous species other than water is a hypothetical 1 molal solution referenced to infinite dilution at any temperature and pressure (Seewald, 2001). Accordingly, the mass action expressions for the buffer reactions reduce to:

$$\underline{\text{HM}}: \quad \log a_{\text{H}_2(aq)} = \log K_{(14)} \quad (20)$$

$$\underline{\text{PPM}}: \quad \log a_{\text{H}_2(aq)} = (\log K_{(15)} + 6 \log a_{\text{FeS}})/4 \quad (21)$$

$$\underline{\text{PPM}}: \quad \log a_{\text{H}_2\text{S}(aq)} = (\log K_{(16)} + 2 \log a_{\text{FeS}})/4 \quad (22)$$

The activity of pyrrhotite can be derived from XRD data obtained for the PPM buffer after the experiments. Note that XRD measurements were only conducted for 350°C samples in the present PhD thesis, but the approach described below is universal.

The calibration of Yund and Hall (1969) is used to calculate the iron content in pyrrhotite according to:

$$Fe_{\text{pyrrhotite}} = 45.212 + 72.68 (d_{102} - 2.04) + 311.5 (d_{102} - 2.04)^2 \quad [\text{at \%}] \quad (23)$$

d_{102} refers to the lattice plane spacing [Å] determined from the strongest pyrrhotite reflection in the X-ray diffractogram. According to Yund and Hall (1969), the calculated iron content is accurate to ± 0.13 atomic percent iron (2σ). The atomic percentage of iron can then be used to calculate the real stoichiometric factor of iron in pyrrhotite (Fe_{1-x}S):

$$(1 - x) = \frac{Fe_{pyrrhotite} [at\%]}{(100 - Fe_{pyrrhotite} [at\%])} \quad (24)$$

The activity of pyrrhotite ($a_{FeS(s)}$) is then calculated using the calibration of Toulmin and Barton (1964):

$$\begin{aligned} \log_{10} a_{FeS} = & 85.83 \left(\frac{1000}{T} - 1 \right) (1 - N + \ln N) + 39.30 \sqrt{1 - 0.9981N} \\ & - 39.23 \tanh^{-1} \sqrt{1 - 0.9881N} - 0.002 \end{aligned} \quad (25)$$

with T as temperature in K, and N being equal to twice the atom fraction of iron in pyrrhotite ($N = 2 \cdot ((1-x)/(1+(1-x)))$), with $(1-x)$ being the stoichiometric factor of iron in pyrrhotite \rightarrow cf. Equation 24). According to Toulmin and Barton (1964), the maximal uncertainty in $\log_{10} a_{FeS}$ is ± 0.03 .

Regarding the 350°C PPM samples processed in the course of the present PhD thesis, d_{102} was determined to $2.065 \pm 0.002 \text{ \AA}$, resulting in a $\log_{10} a_{FeS}$ of -0.254 ± 0.03 . Now, the equilibrium activities of aqueous hydrogen and hydrogen sulfide at 350°C and 35 MPa can be calculated based on Equations 20 to 22, using the equilibrium constants for the buffer reactions at the experimental conditions (Table 5). The results are displayed in the phase diagram for the HM and PPM mineral buffers, which is shown in Fig. 16.

Table 5: Equilibrium constants calculated for the hematite-magnetite (HM) and pyrite-pyrrhotite-magnetite (PPM) buffer reactions at 350°C and 35 MPa. Subscript numbers refer to the corresponding buffer reactions, which are presented in the text.

	log K
HM buffer	$\log K_{(14)} = -4.25$
PPM buffer	$\log K_{(15)} = -11.32$
	$\log K_{(16)} = -7.54$

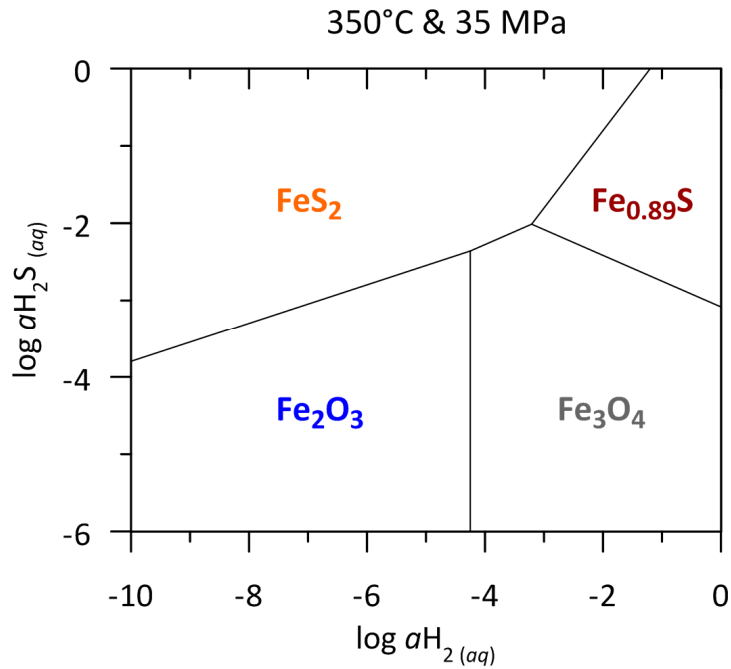
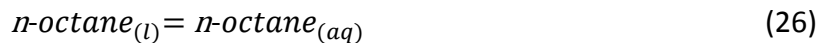


Fig. 16: Stability fields of hematite (Fe₂O₃), magnetite (Fe₃O₄), pyrite (FeS₂) and pyrrhotite (Fe_{0.89}S) plotted as function of the aqueous H₂S and H₂ activities at 350°C and 35 MPa. These minerals are the constituents of the hematite-magnetite (HM) and the pyrite-pyrrhotite-magnetite (PPM) buffers. At equilibrium, redox conditions adjusted by the PPM buffer are one order of magnitude more reducing than those with the HM buffer. This is indicated by the activities of aqueous hydrogen. At equilibrium, these are $\log a_{\text{H}_2(\text{aq})} = -3.21$ for the PPM buffer and $\log a_{\text{H}_2(\text{aq})} = -4.25$ for the HM buffer, resulting in H₂ concentrations of 0.62 mmol/kg_{H₂O} and 0.06 mmol/kg_{H₂O} respectively if an activity coefficient of 1 is assumed. Owing to presence of sulfur in the PPM buffer minerals this buffer also has the potential to regulate the activity of aqueous hydrogen sulfide. Under equilibrium conditions, a hydrogen sulfide activity of $\log a_{\text{H}_2\text{S}(\text{aq})} = -2.01$ is obtained. An error of ± 0.2 log units seems realistic for the calculated values, being attributed to uncertainties in thermodynamic data (Hentscher, personal communication).

3.6.2 AQUEOUS SOLUBILITY OF *n*-OCTANE AT EXPERIMENTAL CONDITIONS

The aqueous solubility of *n*-octane at experimental conditions can be calculated from the equilibrium constants for the following reaction:



the subscript (*l*) denotes the pure *n*-octane liquid, whereas (*aq*) refers to aqueous *n*-octane. Equilibrium constants were calculated with the SUPCRT92 computer program (Johnson et al., 1992) for the temperature range 25-400°C. Calculations were carried out by Laurent Richard. He used thermodynamic data from Shock and Helgeson (1990) and Helgeson et al. (1998) for aqueous and liquid *n*-octane respectively. The standard state adopted for liquid *n*-

octane is unit activity of the pure liquid at any temperature and pressure. The standard state adopted for aqueous *n*-octane is a hypothetical 1 molal solution referenced to infinite dilution at any temperature and pressure. Thus, calculated equilibrium constants for Reaction (26) directly represent solubility constants (K_s) for aqueous *n*-octane in the unit mol/kg H_2O (Fig. 17). The calculated maximum solubility of *n*-octane in water ranges from 0.06 mol/kg H_2O at 300°C to 0.52 mol/kg H_2O at 350°C.

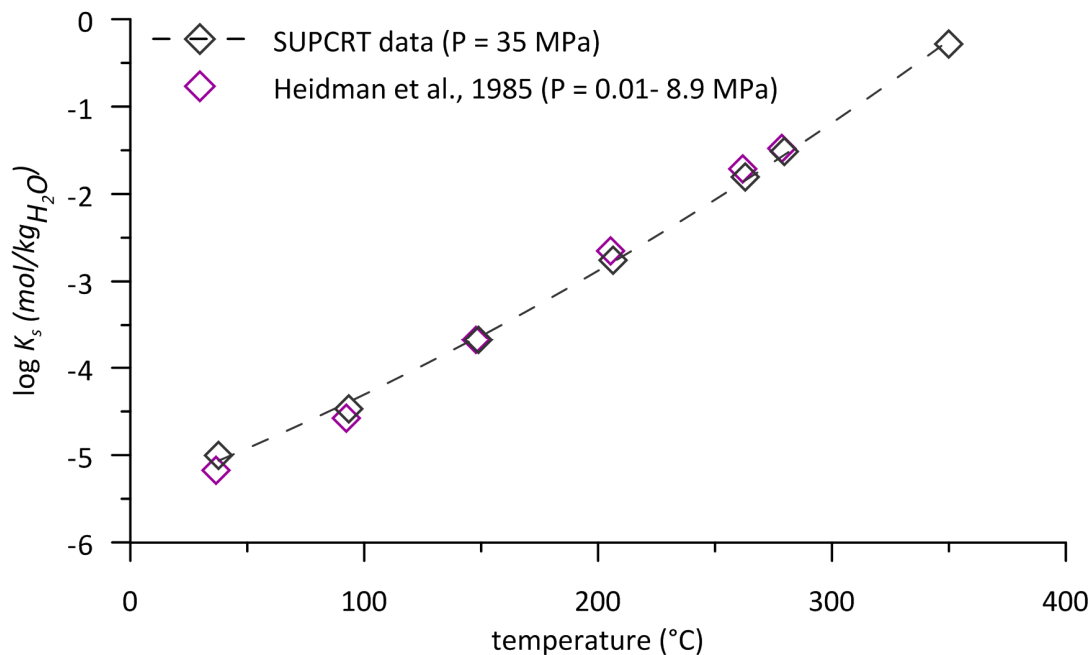


Fig. 17: Solubility constants for aqueous *n*-octane calculated by Laurent Richard with the SUPCRT computer program (Johnson et al., 1992) for the temperature range 25 to 400°C and a constant pressure of 35 MPa. Experimental data taken from Heidman et al. (1985) is plotted for comparison. The pressure in Heidman's experiments varies because it corresponds to the three phase equilibrium pressure in the H_2O - C_8H_{18} system, with the three phases being an excess water phase, a hydrocarbon rich liquid phase and a vapor phase. The good agreement of both data sets indicates that pressure does not seem to have much effect on the aqueous solubility of *n*-octane.

3.6.3 AQUEOUS SOLUBILITY OF METAL SULFATES AT EXPERIMENTAL CONDITIONS AND MODELING OF IN SITU pH

Michael Hentscher provided modeled values of the initial pH at experimental conditions (*in situ* pH) as well as values for the maximum solubility of the metal sulfates (Na_2SO_4 , $FeSO_4$, $Fe_2(SO_4)_3$, $NiSO_4$, $CuSO_4$ and $ZnSO_4$) at experimental conditions. The modeling was performed using the Geochemist's Workbench™ (GWB) (Bethke, 1996).

In order to match the experimental system, Hentscher first created a database of equilibrium constants for use in GWB, which is valid for temperatures between 0 and 350°C. The required equilibrium constants were calculated with SUPCRT92 (Johnson et al., 1992) and the corresponding OBIGT database (Dick, 2008). Requisite data for solid metal sulfates were taken from Chase (1998) for Na₂SO₄ and FeSO₄, and from Robie and Hemingway (1995) for all the other metal sulfates used. Following the procedure of Seewald (2001), the standard states adopted for water and minerals are unit activity of the pure liquid and solid at any temperature and pressure. Activity coefficients⁴ of aqueous charged species were calculated with the B-dot equation with hard core diameters, B-dot and Debye-Hückel parameters from Wolery and Jove-Colon (2004). Activity coefficients for dissolved neutral species are assumed to be unity at any temperature and pressure, except for aqueous non-polar gases (e.g. H₂ and H₂S). Here, the approach of Drummond (1981) was followed, assuming that activity coefficients are equal to the activity coefficients of aqueous CO₂. The Drummond (1981) equation takes into account that the activities are dependent on temperature and the salt concentration in the system.

The model mimics the experimental procedure by the following steps: initial water speciation, adding the pure metal sulfate and buffer minerals of interest at 25°C, subsequent heating of the sulfate solution to experimental conditions. For the modeling of mineral-buffered experiments, redox reactions in between the minerals of the buffers, like the oxidation of Fe²⁺ to Fe³⁺, were allowed. Oxidation and reduction of sulfate and *n*-octane are suppressed. Complex formation of the metals and the sulfate anions is considered, but not that of possible organometal complexes. The formation of the metal-sulfate complexes were calculated on basis of the complexes in the database from Dick (2008) (NaSO₄⁻, HSO₄⁻, NaOH, FeO, FeOH⁺, etc). This procedure has the advantage that the external conditions of the buffers are achieved and that the influence of the association and disassociation of aqueous sulfate complexes to the pH can be modeled. Note, that the HPLC grade water, which was used to prepare the sulfate solutions in the laboratory is slightly acidic (pH 5.6), which is

⁴ The activity coefficient is a dimensionless factor that accounts for differences to ideal behavior. An alternative definition of activity that includes the activity coefficient compared to the definition presented in chapter 2.2.2.1 → Equation 5) is: $\alpha_i = \gamma_i * c_i / (\text{mol/kg H}_2\text{O})$, where α_i , γ_i and c_i designate the activity, activity coefficient and molality of the species *i* in solution.

probably due to dissolved CO₂ from air⁵. To fit these starting conditions, a CO₂ fugacity of 0.002 bar was used to model the starting solution. In addition to that, a small amount of NaCl (10⁻¹² mol) was added for charge balance.

For a first quality check of the modeling, modeled and measured pH values at room temperature were compared (Fig. 18). The data are in good agreement except for FeSO₄ and CuSO₄. The strong offset between measured and modeled pH for the FeSO₄ solution suggests that a large amount of Fe(II) has been oxidized to Fe(III) during preparation of the stock solution. For CuSO₄, it is rather proposed that inconsistencies in thermodynamic data are responsible for observed differences (Hentscher, personal communication). The measured pH values are regarded to be reliable, because laboratory measurements of pH were executed several times with different equipment (pH meter and pH sticks) and always showed the same value ±0.2 units. Thus, if differences exist, modeled pH values were adjusted to the measured values prior to heating the solution to the experimental temperature during the modeling.

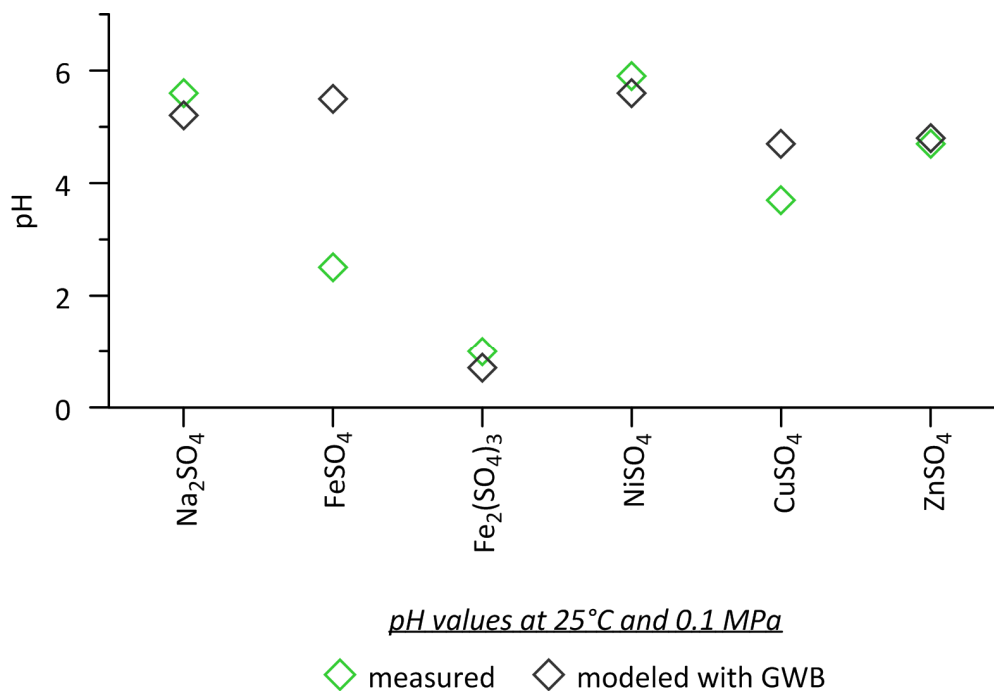


Fig. 18: Comparison of modeled and measured pH values for different metal sulfate solutions employed in this study. See text for details on the modeling of pH with the Geochemist’s Workbench (GWB). Uncertainties for measured and modeled pH values are ±0.2 units.

⁵ This does not show up in gas chromatography measurements of pure water and PPM+H₂O samples. So the amount of CO₂ dissolved in the water is small and its contribution to the measured amount of CO₂ from *n*-octane is negligible.

4.

PART I-A

INVESTIGATING THE EFFECT OF THE PPM AND HM MINERAL BUFFERS, AND THE EFFECT OF DISSOLVED SULFATE ON THE PRODUCT DISTRIBUTION GENERATED FROM *n*-OCTANE UNDER HYDROTHERMAL CONDITIONS

In this chapter results from the first and second experimental series are presented and discussed, i.e. results for experiments processed at 300 and 350°C for 168 h in presence and absence of the HM and PPM mineral buffer, with and without sodium sulfate. The main focus is on the data for the 350°C experiments. This is because of the low product yield obtained at 300°C, which makes it difficult to resolve variations in generated products caused by the inorganic components. In addition to the data for the 168 h experiments, results from time series (72-336h) experiments of the type PPM+H₂O+C₈H₁₈+Na₂SO₄ processed at 350°C are presented.

The primary objective of this chapter is to characterize the effect of the employed inorganic components on the product distribution generated from *n*-octane in order to elucidate their effect on the reaction network and processes associated with the conversion of *n*-octane. In this context, a central point is to test if the reaction scheme proposed by Seewald (2001) for aqueous oxidation of hydrocarbons is also transferable to hydrocarbon conversion in a sulfate-containing system.

Apart from the analysis of organic reaction products, this chapter provides a characterization of the solid phase in order to identify background contributions from the minerals, as well as compositional changes in the PPM and HM mineral buffers after the experiments. In this context, the question of effectiveness with respect to the buffering ability of the mineral assemblages is addressed.

It was decided to present results first in order to provide a clear overview of available data. The discussion then follows in a separate chapter, which addresses the main findings (cf. *chapter 4.3*).

4.1 RESULTS – SOLID PHASE

XRD results are summarized in Fig. 19. XRD measurements of the pre-mixed initial mineral assemblages show 52 wt% hematite (Fe_2O_3) and 48 wt% magnetite (Fe_3O_4) for the HM buffer (single measurement), and 41 wt% magnetite, 27 wt% pyrite (FeS_2), 18 wt% troilite (FeS), 12 wt% pyrrhotite (Fe_{1-x}S) and 2 wt% native iron (Fe°) for the PPM buffer (average of four samples). Troilite is the iron rich endmember of the pyrrhotite (Fe_{1-x}S) group. Detection of troilite and native iron in the initial PPM buffer is attributed to impurities in the starting compounds. XRD measurements indicate that initial pyrrhotite consists of 59 wt% troilite, 33 wt% pyrrhotite and 8 wt% native iron. Note that the amount of native iron in the pre-mixed PPM buffer is very small and scratches the quantification limit of the method, wherefore this information is rather qualitative than quantitative.

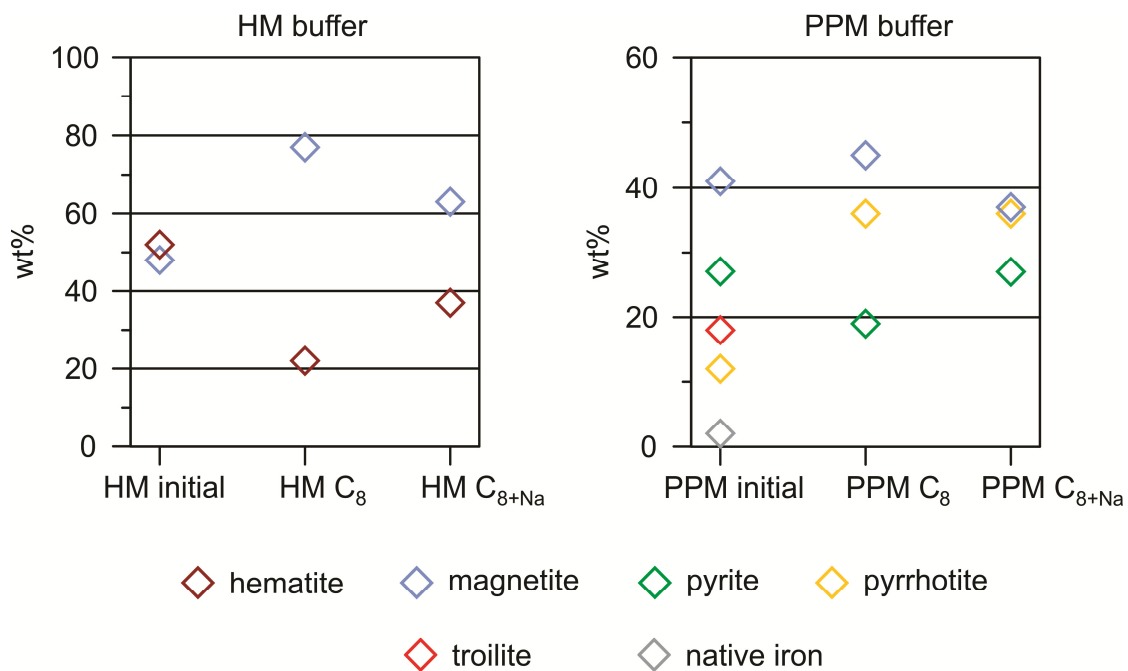


Fig. 19: Changes in mineral buffer composition for the hematite-magnetite (HM) and the pyrite-pyrrhotite-magnetite (PPM) mineral buffers after experiments processed at 350°C and 35 MPa for 168 h. The label *initial* refers to the composition of the mineral buffer before the experiment, “C₈” denotes presence of *n*-octane and “+Na” presence of sodium sulfate in the experimental charge. Symbol sizes correspond to the analytical error of ±3 wt%.

XRD measurements on solid run products were only performed on 350°C samples. Results show that the solid phase consists of pyrite, pyrrhotite and magnetite in the case of the PPM and of hematite and magnetite in the case of the HM mineral buffer assemblage. In the sulfate-containing samples, thernadite (Na_2SO_4) was detected as additional phase. In

order to directly compare the buffer composition in sulfate-free and sulfate-containing samples, amounts of thernadite were ignored and only the amounts of the buffer minerals were then normalized to 100 wt%.

HM Samples

The amount of magnetite increases from 48 wt% to 77 wt%, and that of hematite decreases from 52 wt% to 22 wt% in the sulfate-free 350°C HM sample (*HM C₈ 350°C*) compared to the initial HM buffer (Fig. 19). The sulfate-containing HM sample (*HM C_{8+Na} 350°C*) shows the same trend. However, the increase for magnetite (from 48 wt% to 63 wt%) and the decrease for hematite (from 52 wt% to 36 wt%) abundances are less pronounced.

PPM Samples

The mixture of the mineral phases in the initial PPM buffer reduces to pyrite, pyrrhotite and magnetite in all PPM samples processed at 350°C (Fig. 19). The amount of pyrrhotite is identical (36 wt%) in the sulfate-free (*PPM C₈ 350°C*) and sulfate-containing (*PPM C_{8+Na} 350°C*) PPM samples. The quantity of magnetite slightly decreases from 45 wt% to 37 wt% and the amount of pyrite slightly increases from 19 wt% to 27 wt%, if sulfate is present. However, changes are significantly smaller than observed for the HM samples.

4.2 RESULTS – ORGANIC PRODUCTS

Generated products quantified via headspace gas chromatography, comprise the following:

CO₂, *n*-alkanes (C_{1 to 7}), alkenes (C_{2 to 4}), *iso*-alkanes (*i*C₄ and *i*C₅),
ketones (C₃ and C₄) and aromatic compounds (C₆H₆ and C₇H₈)

Fig. 20 A and B illustrate the results for the 300°C and 350°C samples, which were processed for 168 hours. All results, including those of the time series experiments, are summarized in Table A1 in the appendix. Analyzed quantities are expressed as millimol of products generated per mol of initial *n*-octane.

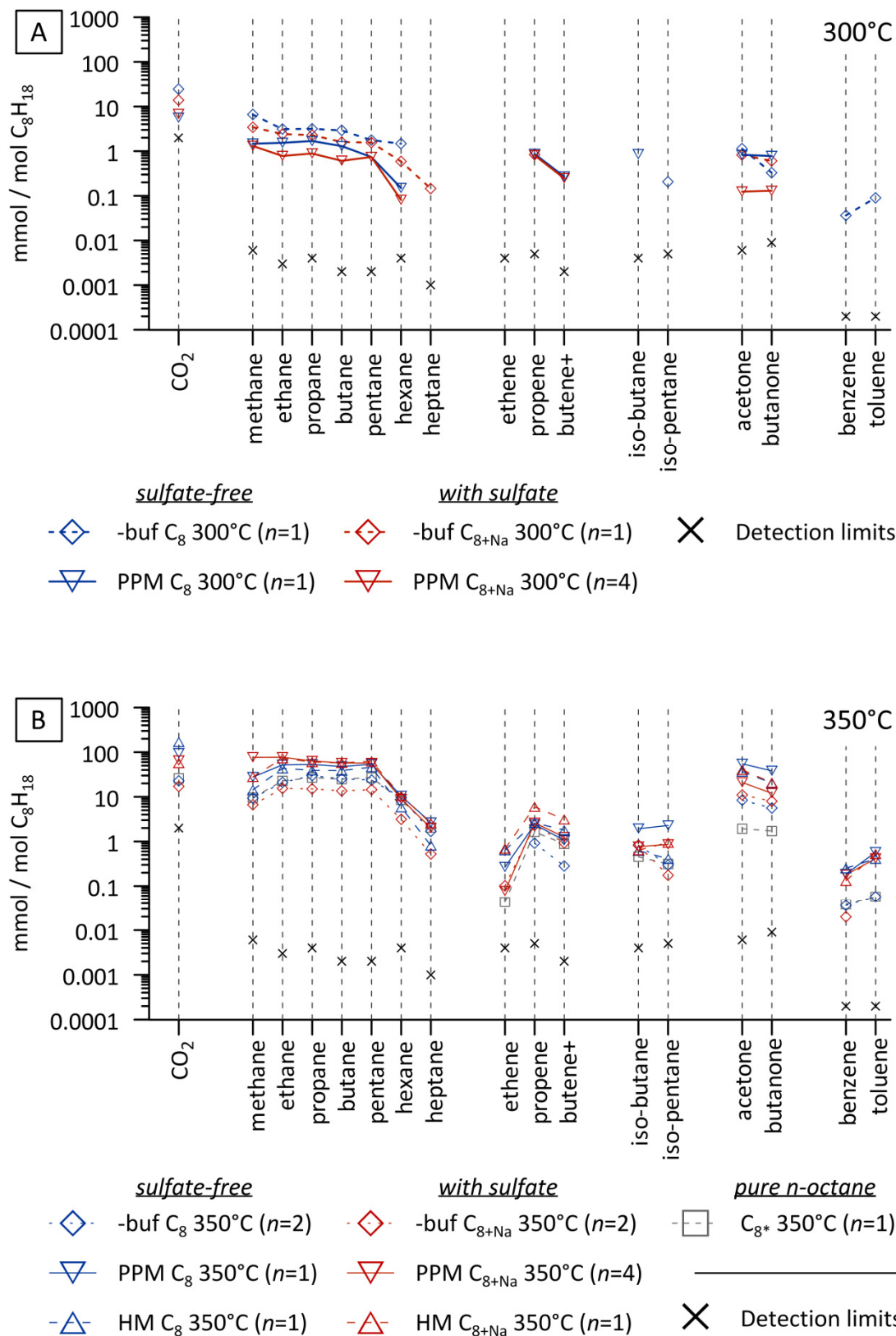


Fig. 20: Overview illustrating the variation of all quantified products generated from aqueous *n*-octane decomposition after 168 h at (A) 300°C and (B) 350°C in presence and absence of sulfate. Pressure was kept constant at 35 MPa during the experiments. The graphs show data for samples without any mineral buffer (-buf), with the pyrite-pyrrhotite-magnetite (PPM) and the hematite-magnetite (HM) mineral buffer assemblage. At 350°C one sample was processed, which only contained pure *n*-octane. Detection limits for the headspace gas chromatography method are also shown. Butene+ = mixture of 1-butene and 2-butene

The error was calculated via error propagation from the analytical uncertainty and the total weighing error of initial *n*-octane (5%). Mean values are presented for repeated experiments. For these values, the standard deviation (1σ) is given as total error, if it is above the propagated error (values are explicitly marked in Table A1). Usually, the standard deviation is considerably below the propagated error. This indicates a good reproducibility of the experiments. Although generated amounts of products at 300°C are 1 to 2 orders of magnitude lower than at 350°C, the reproducibility of the experiments is good at both temperatures (Fig. B1 & B2 in the appendix). In the following sections, results are addressed in more detail.

4.2.1 300 °C EXPERIMENTS PROCESSED FOR 168 H

Concentrations of generated products at 300°C range from 0.04 to 25 mmol/mol C_8H_{18} . The values are one to three orders of magnitude above the detection limit (Fig. 20 A). Mass balance considerations⁶ on analyzed products indicate that 0.24 mol% to 1.2 mol% of initial *n*-octane were converted during the experiments. In presence of the PPM mineral buffer, the conversion of *n*-octane is only one third of the corresponding values for the buffer free samples. This observation is in contrast to the trend for the corresponding 350°C samples. Here, addition of mineral-buffers, i.e. HM and PPM significantly enhances the yield of reaction products.

CO₂ and *n*-Alkanes

In all samples processed at 300°C, CO₂ is the most abundant single component out of all organic reaction products (Fig. 20 A). In presence of the PPM buffer, the measured concentration is the same for the sulfate-free (*PPM C₈ 300°C*) and sulfate-containing (*PPM C_{8+Na} 300°C*) samples. In the buffer-free system, addition of sulfate cuts the generated amount of CO₂ in half.

⁶ In order to estimate the amount of initial *n*-octane, which was converted during the experiments, the mass balance for carbon was calculated. The molar amount of carbon in the reaction products was summed and normalized to the initial amount of carbon provided by *n*-octane ($245 \pm 12 \mu\text{mol C}$). The resulting value is an estimate for the minimum conversion of *n*-octane. Error propagation taking into account the analytical uncertainty and the weighing uncertainty, leads to a relative error for this calculation of 17% for the 300°C samples and 7% for the 350°C samples. This “detour” was necessary owing to the fact that *n*-octane concentrations remaining after the experiments were too high to be accurately measured with the headspace gas chromatograph.

The most abundant product group, which was generated, is that of the *n*-alkanes. In all samples, they show the same trend, i.e. increase in concentration with decreasing chain length (Fig. 20 A). In the buffer-free system, generated amounts of *n*-alkanes are very similar, with slightly lower values for the sulfate-containing sample (*-buf C_{8+Nα} 300°C*) than for the one without sulfate (*-buf C₈ 300°C*). In presence of the PPM buffer, this difference is more obvious.

Alkenes and Ketones

In all samples, measured concentrations of alkenes and ketones are in the same range as generated amounts of *n*-alkanes (Fig. 20 A). A closer look reveals, however, that variations exist. Generated amounts of propene and butene, are four to six times below that for corresponding *n*-alkanes. Ethene was not detected. Propene amounts are roughly three times higher than those for butene. Interestingly, the absolute amount of the individual alkenes is about the same in all samples. Only in the sulfate- and buffer-free sample (*-buf C₈ 300°C*) and in the sulfate-containing PPM sample, which was processed for 336 hours (*PPM C₈ 300°C, 336 h*), no alkenes could be detected (Fig. 20 A and Tabel A1). Due to the close similarity of the other products, it is, however, suggested that alkenes were also generated in these samples, but possibly in low quantity.

Regarding the ketones (Fig. 20 A), acetone is generated in similar quantity than propene, with the exception of the sulfate-containing PPM samples (*PPM C_{8+Nα} 300°C*). Here, the acetone concentration is one order of magnitude below that for propene, and thus one order of magnitude below the acetone amount in the other samples. Acetone and butanone concentrations are usually comparable; only in the buffer-free sample without sulfate (*-buf C_{8+Nα} 300°C*) the butanone concentration reduces to one quarter of that for acetone.

4.2.2 350 °C EXPERIMENTS PROCESSED FOR 168 H

Data for the 350°C samples (Fig. 20 B) show more variation than at 300°C (Fig. 20 A). Product concentrations cover a range from 0.04 to 170 mmol/C₈H₁₈ (Fig. 20 B). The amount of generated products is up to one order of magnitude higher at the higher temperature. Mass balance considerations on analyzed products of the mineral buffered experiments

processed with and without sulfate indicate that a minimum of 13-16 mol% of initial *n*-octane decomposed after 168 h. In the buffer free samples and in the pure *n*-octane sample (C_8 , 350°C), the values are three times smaller (4-6 mol%). After the experiment, reaction products in all samples are characterized by a strong dominance of *n*-alkanes (C_{1-7}). They add up to 56-80 mol% of analyzed products, except for the sulfate-free HM sample, which shows a slightly lower value of 45 mol%. Acetone and butanone reach a comparable concentration as CO_2 , and as corresponding *n*-alkanes (Fig. 20 B). In contrast to the 300°C samples, the CO_2 concentration in the 350°C samples only rises above the concentration of individual *n*-alkanes in the sulfate-free HM and PPM samples (Fig. 20 B). The concentration of generated alkenes is usually one order of magnitude lower compared to that of corresponding *n*-alkanes.

Fig. 20 B illustrates that a strong positive effect of water addition is observed for ketone formation. Presence of mineral buffers further promotes ketone formation, but the strongest positive effect is observed for quantified aromatic compounds, indicating that aromatization is promoted by the HM and PPM mineral buffer. The most prominent effect of sulfate addition is that it lowers the yield of CO_2 in all three investigated systems (-buf, HM and PPM). The overall product distribution only shows minor, but non-negligible changes. Data for *n*-alkanes, alkenes, ketones and CO_2 are described in more detail below, because they form the central part of the discussion.

***n*-Alkanes**

The distribution pattern for the *n*-alkanes is very similar for all samples (Fig. 21 A & B). The trend shows a characteristic steep increase from *n*-hexane to *n*-pentane and rather equal amounts of *n*-pentane, *n*-butane and propane. The concentration of ethane is usually comparable to that of propane. Only in the sulfate-containing HM (HM C_{8+N_G} 350°C) and PPM (PPM C_{8+N_G} 350°C) samples an increase from propane to ethane is observed. A drop in concentration from ethane to methane is characteristic for all samples, except for the sulfate-containing PPM samples. Here, methane reaches the same concentration as ethane. The higher methane production is also manifested in the gas dryness ($C_1/\sum C_{1-4}$), which is twice as high in the sulfate-containing PPM sample as for the other sulfate-containing samples (Fig. 22).

The absolute abundance of n -alkanes (C_{1-7}) produced from pure n -octane pyrolysis under dry (sample labeled by C_8^* 350°C) and hydrous (-buf C_8 350°C) conditions are equal (Fig. 21 A). In the sulfate-free system (Fig. 21 A), addition of the HM and PPM mineral assemblages roughly doubles the amount of generated n -alkanes. In presence of sulfate (Fig. 21 B), n -alkane concentrations are quadrupled if the mineral buffers are added.

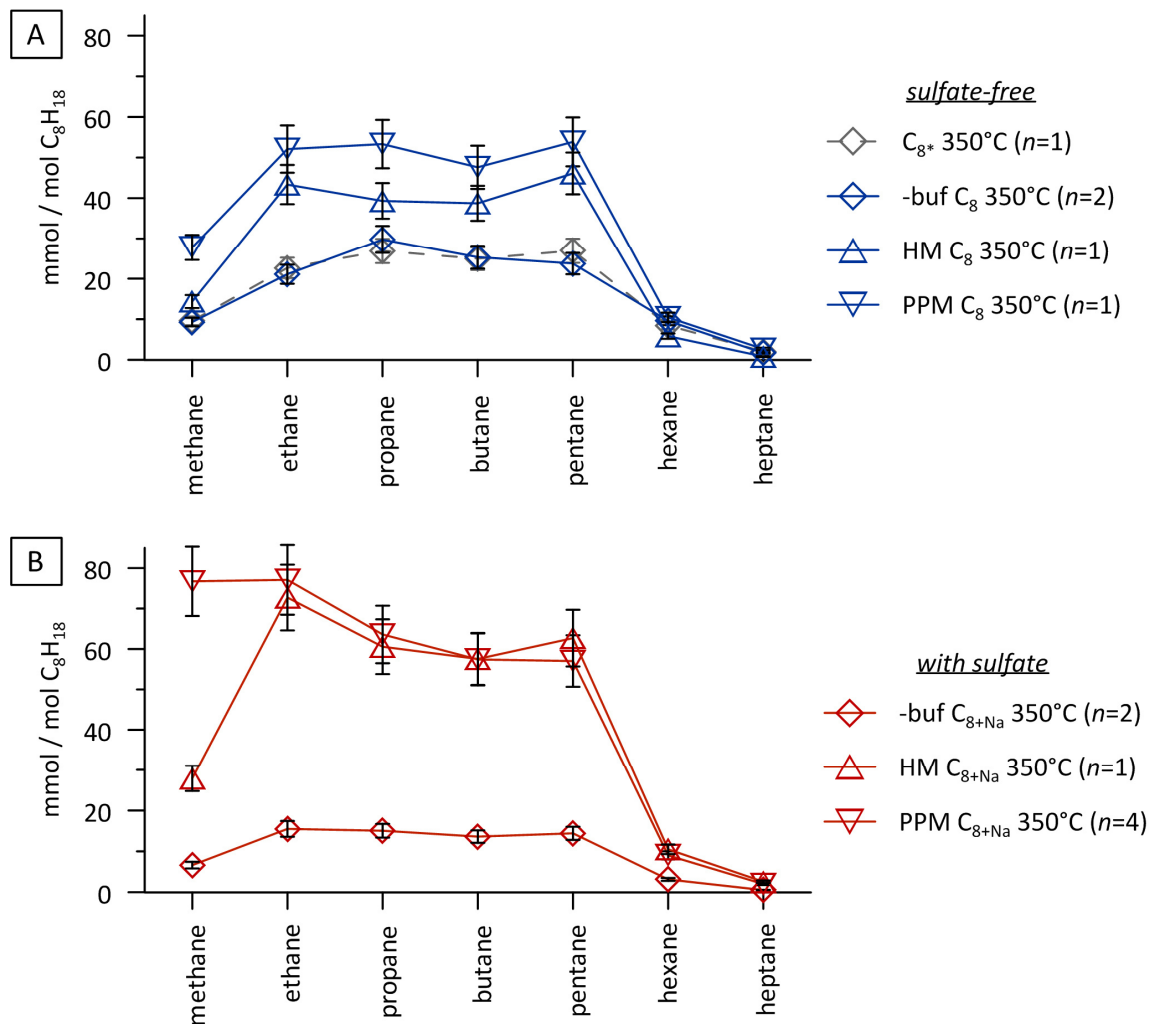


Fig. 21: Comparison of n -alkane yields from (A) sulfate-free and (B) sulfate-containing (labeled by the suffix “+Na”) simulation experiments of aqueous n -octane decomposition after 168 h at 350°C and 35 MPa. Experiments were performed in presence of the hematite-magnetite (HM) or pyrite-pyrrhotite-magnetite (PPM) mineral assemblage, or without any mineral buffer (-buf). In addition, data for one sample, which contained only n -octane (labeled by C_8^*) is presented. Error bars represent uncertainties, which results from error propagation of the analytical error and the total weighing error of initial n -octane.

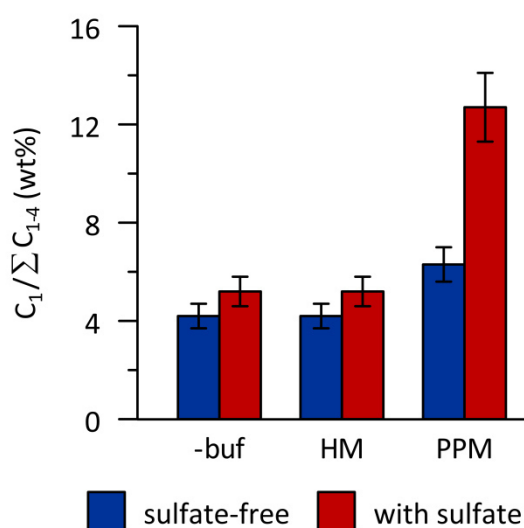


Fig. 22: Gas dryness ($C_1/\sum C_{1-4}$) for sulfate-free and sulfate-containing samples, which were processed at 350°C and 35 MPa for 168 h. Buffer conditions are indicated as: -buf = no mineral buffer, PPM = pyrite-pyrrhotite-magnetite, and HM = hematite-magnetite. For the sulfate-containing PPM samples, the average of four samples is given. Otherwise, only one sample existed per series. Error bars display values that result from error propagation of the analytical uncertainty.

Alkenes, Ketones and CO₂

Similar CO₂ concentrations are observed for the pure *n*-octane (C_8 , 350°C) and the *n*-octane + water (-buf C_8 , 350°C) samples (Fig. 20 B and Table A1 in the appendix). It is, however, apparent that presence of water boosts the yield of ketones, which increases by a factor of 3 to 4 if water is added. Generated amounts of alkenes, on the other hand, decrease by a factor of 2 to 3 in presence of water (Fig. 20 B and Table A1 in the appendix).

In accordance with observations for *n*-alkanes, addition of HM and PPM in the sulfate-free and sulfate-containing systems generally increases the yield of alkenes (ethene, propene and butene), ketones (acetone and butanone) and CO₂ (Fig. 23 A-E). In the sulfate-free system, the amount of generated alkenes in presence of the HM buffer (HM C_8 , 350°C) is between 1.6 (butene) to 2.4 (ethene) times higher than in presence of the PPM buffer (PPM C_8 , 350°C). Propene is present in equal quantity in presence of both buffers.

The amount of acetone and butanone are 1.5 and 1.9 times lower in presence of HM than in presence of the PPM minerals. Despite lower ketone concentrations, the sulfate-free HM sample shows a higher concentration of CO₂, which is in fact the highest CO₂ content among all experiments (170 ± 19 mmol/mol _{C_8H_{18}}). Only half the amount of CO₂ was observed in the sulfate-free PPM sample (95 ± 11 mmol/mol _{C_8H_{18}}).

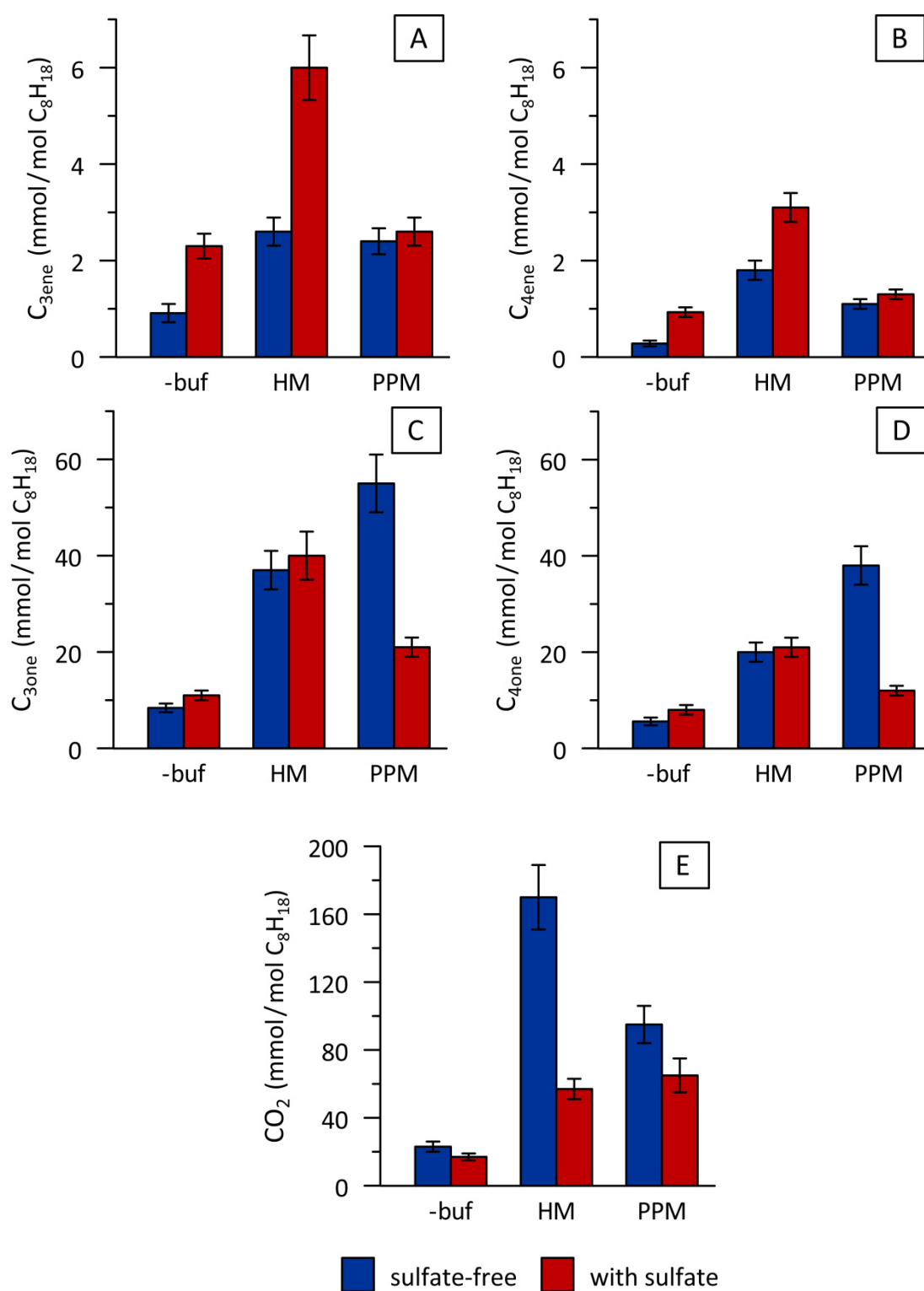


Fig. 23: Variation in the concentrations of (A) propene, (B) butene (includes 1- and 2-butene), (C) acetone, (D) butanone and (E) CO₂ generated from heating of *n*-octane, in dependence on sulfate availability and presence of mineral buffers (-buf = no buffer; PPM = pyrite-pyrrhotite-magnetite, HM = hematite-magnetite). Experiments were performed at 350°C and 35 MPa for 168 h. Regarding the mineral-free samples with and without sulfate, in each case the average of two samples is displayed. For the sulfate-containing PPM samples, the average of four samples is given. Otherwise, only one sample existed per series. Error bars display values that results from error propagation of the analytical error and the total weighing error of initial *n*-octane. It is apparent that C₃ and C₄ compounds show the same relative variations.

The most prominent effect of sulfate addition is that it lowers the yield of CO₂ in all three investigated systems (Fig. 23 E). The strongest decrease is observed in presence of the HM mineral assemblage. Here the CO₂ value is lowered by a factor of 3. In presence of the PPM buffer, sulfate addition lowers the CO₂ concentration by a factor of 1.5. In the system without any mineral buffer, the CO₂ concentration decreases by a factor of 1.4.

Regarding the alkene and ketone data, addition of sulfate has different effects on the product distribution in the three investigated systems (Fig. 23 A-E). In the buffer-free and HM samples, generated amounts of propene and butene increase by a factor of roughly 2 to 3 upon sulfate addition (Fig. 23 A & B), whereas acetone and butanone values remain constant or nearly constant (Fig. 23 C & D). In contrast, addition of sulfate in the PPM system does not affect generated amounts of propene and butene. It lowers, however, the concentration of ketones by a factor of approximately 3 in these samples (Fig. 23 A & B).

4.2.3 TIME SERIES DATA FOR SAMPLES OF THE TYPE PPM+H₂O+C₈H₁₈+NA₂SO₄ PROCESSED AT 350 °C

Time series data for the sulfate-containing PPM samples (Fig. 24) show that C₁ to C₅ *n*-alkanes are at a comparable concentration after 72 h, but they show more variation with increasing reaction time. Methane shows the strongest increase and *n*-hexane the lowest. At all times, the concentration of *n*-hexane is significantly below that of C₁ to C₅ *n*-alkanes. The offset increases with increasing reaction time (Fig. 24). The enhanced methane production with time is also mirrored by the gas dryness (C₁/∑C₁₋₄), which increases from 9.3 ± 1.0 wt% at 72 h to 16.0 ± 1.8 wt% after 336 h experiment duration (Table A1 in the appendix).

In the time frame 72 to 168 hours, ethene (average = 0.07 ± 0.01 mmol/mol C₈H₁₈) and propene (average = 2.3 ± 0.4 mmol/mol C₈H₁₈) concentrations remain constant within the uncertainty, but drop by approximately one order of magnitude between 168 and 336 hours (Table A1 in the appendix). In contrast, butene concentration increases from 1.3 ± 0.1 mmol/mol C₈H₁₈ to 2.2 ± 0.2 mmol/mol C₈H₁₈ between 168 and 336 hours .

Data for acetone and butanone are only available for the 168 h samples. Out of all quantified products, CO₂ shows the strongest increase with time. After 72 h the amount of generated CO₂ was below the detection limit and increases to 241 ± 17 mmol/mol C₈H₁₈

after 336 h (Fig. 24). The graph shows that the rate of formation (= slope in Fig. 24) for CO₂ significantly increases after 168 h, whereas variations in the rate of formation for C₁ to C₆ *n*-alkanes is rather small between 72 to 336 hours experiment duration.

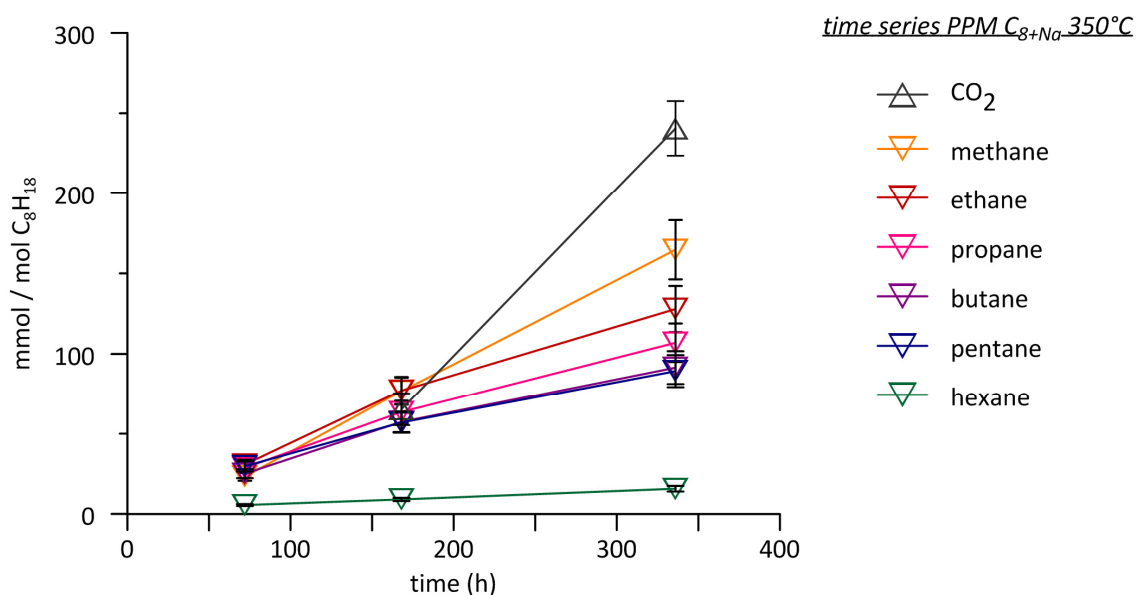


Fig. 24: Evolution of *n*-alkane and CO₂ concentrations as a function of time for experiments simulating aqueous *n*-octane decomposition in presence of the pyrite-pyrrhotite-magnetite mineral assemblage and Na₂SO₄. Experimental conditions were 350°C and 35 MPa. Error bars represent the uncertainty, calculated from error propagation of the analytical error and the total weighing error of initial *n*-octane.

4.3 DISCUSSION

4.3.1 STARTING CONDITIONS

For the interpretation of the experimental data, it is necessary to constrain the state of the system at the start of the experiments with respect to the following questions: How high is the amount of atmospheric oxygen added to the experimental charge during sample preparation and, in case of the mineral containing samples, how much carbon is introduced by these minerals? Furthermore it needs to be clarified whether the fluid is composed of a single phase or not. Information on the starting pH is also given.

Oxygen Contamination from Air

The oxygen contamination from air can be estimated from oxygenated compounds generated in the pure *n*-octane sample (C₈* 350°C, Table A1 in the appendix). Here, air and

oxygen dissolved in *n*-octane represent the only two possible oxygen sources. It is suggested that the latter can be neglected, because *n*-octane was always freshly taken from the container, i.e. it was never in contact with air for a long time. During the experiments oxygen from air seems to preferentially react with hydrocarbons to CO₂. In the pure *n*-octane samples (*C*₈* 350°C) the CO₂ concentration reaches 26 ± 3 mmol/mol_{C₈H₁₈} after the experiment. Acetone and butanone could also be quantified, but their concentrations are one order of magnitude smaller. The total amount of oxygen incorporated in the reaction products for the pure *n*-octane sample adds up to 28 ± 4 mmol_{O₂}/mol_{C₈H₁₈} (= 0.84 ± 0.12 μmol O₂ absolute).

In order to calculate the percentage of entrained air from this value, some basic considerations need to be made. First of all, the volume of the free gas phase in the sample container needs to be determined. The initial volume of the container was 440 μl, but the free volume is slightly lowered due to presence of 5 μl of *n*-octane in this sample. Furthermore, the free volume may be lowered during the welding process, because of the weld seam. This is hard to quantify, but the length of the capsule was usually not reduced by more than 1-2 mm. Based on these two factors, a free volume of 400 μl is expected to exist in the pure *n*-octane sample. If the free volume was completely filled with air, 21 % of O₂ would be introduced, which equals a volume of 16.35 μl in this case. The value can then be converted in a molar amount using the molar volume of an ideal gas, which is 24.46 l/mol at 0.1 MPa and 25°C. The resulting value is 3.43 μmol O₂. This value represents 100% air in the free volume. Thus, the 0.84 ± 0.12 μmol O₂ incorporated in the organic reaction products represent 21 to 28 vol% of residual air. This seems to be a realistic value for the argon flushing method. Because the amount of residual air in the sample container may not be constant, data cannot be corrected for this error.

The contamination by oxygen from air has to be kept in mind during data interpretation. Especially for samples without any mineral buffer (*-buf C*₈ 350°C and *-buf C*_{8+Na} 350°C) and for the 300°C PPM samples (*PPM C*₈ 300°C and *PPM C*_{8+Na} 300°C) contamination by air is critical, because here the total amount of oxygen incorporated in organic products is equal to or even below the value of the pure *n*-octane sample (Table A1 in the appendix). Nevertheless, the ketone data reveal a clear influence of water on *n*-octane decomposition if these samples are compared to the pure *n*-octane sample (cf. *chapter 4.2.2*).

Possible Carbon Input from Buffer Minerals

The HM and PPM mineral assemblages initially contain 104 ± 10 ppm ($= 0.26 \pm 0.02$ μmol) and 309 ± 31 ppm ($= 0.77 \pm 0.08$ μmol) carbon respectively. Gas chromatography measurements for the PPM blanks show that no detectable amounts of CO_2 and hydrocarbons were generated. In case of the HM samples, no blank was processed. However, from the data for the PPM blanks and from the fact that the carbon content in the HM minerals is three times lower than in the PPM ones, it can be inferred that no significant amounts of CO_2 and hydrocarbons should be generated from carbon in the HM minerals. Thus, possible hydrocarbon contaminations generated from carbon in the buffer minerals is supposed to be negligible.

pH

Initial *in situ* pH values at the specific experimental conditions were modeled by Michael Hentscher using the Geochemist's Workbench software. A brief description of the procedure is given in *chapter 3.6.3*.

Owing to an enhanced auto-dissociation of water with increasing temperature, the neutral point of water shifts from 7 at room temperature and pressure to a pH of 5.5 to 5.7 at experimental conditions (300 to 350°C, 35 MPa). Thus, the modeled *in situ* pH values for the samples (Table 6) reflect slightly acidic to alkaline conditions. They are similar to typical pHs encountered in petroleum reservoirs, which range from 5.5 to 7 (cf. Helgeson et al., 1993, Fig. 10). Cross et al. (2004) showed that the rate of TSR is

Table 6: Modeled starting pH values at experimental conditions. Values were calculated by Michael Hentscher using the Geochemist's Workbench. The error is estimated to be ± 0.2 units.

	Sample name	300°C	350°C
no buffer	-buf C_8 350°C	4.9	5.0
	buf C_{8+Na} 350°C	7.0	7.3
HM buffer	HM C_8 350°C	na	5.0
	HM C_{8+Na} 350°C	na	7.3
PPM buffer	PPM C_8 350°C	4.7	4.7
	PPM C_{8+Na} 350°C	6.5	6.7

-buf – no mineral buffer present, HM – hematite, magnetite, PPM – pyrite, pyrrhotite, magnetite ; na – not applicable, i.e. that no experiments were performed at these conditions

independent of pH at formation water pH. Only if the pH dropped below 3.5, an increase in the TSR rate would be expected (Zhang et al., 2012).

Solubility of *n*-Octane and Na₂SO₄ and Mixing Behavior of Fluids

For the simple *n*-octane-H₂O system, the thermodynamic calculations by Laurent Richard indicate a maximum solubility of *n*-octane in water of 0.52 mol/kg_{H₂O} at 350°C and 35 MPa. This value is significantly higher than the initial concentration of *n*-octane in samples of the first and second experimental series, which all contained 0.34 mol/kg_{H₂O}. The solubility of *n*-alkanes in water reduces in presence of salts (Price, 1976). Owing to this so-called salting-out effect, the addition of sodium sulfate probably results in the separation of two fluid phases – an octane- and water-dominated phase – at our experimental pressure and temperature. The coexistence of these two fluid phases is also expected for all samples processed at 300°C and 35 MPa because the aqueous solubility of *n*-octane reduces to 0.06 mol/kg_{H₂O}. The mixing behaviour of *n*-octane and water under the experimental conditions may affect the kinetics of conversion reactions, i.e. transport in fluids may become an important parameter if two or more fluid phases coexist. It is, however, assumed that the system is dynamically mixed due to fluid convection in the sample container during the experiments.

Sodium sulfate shows an inverse solubility with temperature, which means that the solubility decreases with temperature. Solubility data from Pablan and Pitzer (1988) indicate that 1.7 mol/kg_{H₂O} can be dissolved at 300°C and 35 MPa, which equals the initial concentration of the sodium sulfate solution in the samples, which were process at 300 and 350°C. Thus, a highly saturated Na₂SO₄ solution exists during the 300°C experiments. At 350°C the solubility of Na₂SO₄ in water reduces to 0.29 (Khan and Rogak, 2004). This means that only 17% of the initial sulfate are dissolved at the higher temperature, wherefore solid Na₂SO₄ is also present under experimental conditions. Solid Na₂SO₄ does not seem to have a catalytic effect, as indicated by similar results for the buffer-free samples with and without sulfate. Moreover, generated amounts of quantified products are rather lower in presence of sulfate.

4.3.2 CHANGES IN MINERAL BUFFER COMPOSITION

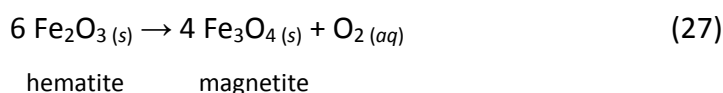
Comparison of buffer compositions before and after the experiment indicates whether the buffer is capable to adjust to chemical changes of the system or not. This is a prerequisite for the buffering ability of such mineral assemblages. For individual minerals present in the samples, μmol amounts (Table 7) were calculated from the wt% data (Fig. 19).

Table 7: Comparison of μmol amounts of individual minerals in the hematite-magnetite (HM) and pyrite-pyrrhotite-magnetite (PPM) mineral buffer samples before and after the respective experiment. Values are calculated from XRD results. Usually one measurement per sample type exists, with the exception of the initial PPM buffer. Here the calculation is based on the average of four samples.

Sample name	Minerals (μmol per 30 mg buffer)					
	hematite	magnetite	pyrite	pyrrhotite	troilite	$\alpha\text{-Fe}$
<i>Absolute error</i>	± 6	± 4	± 8	± 11	± 10	± 16
HM <i>initial</i>	98	62				
HM C_8 350°C	41	100				
HM C_{8+Na} 350°C	69	81				
PPM <i>initial</i>		53	73	44	60	11
PPM <i>initial_corrected</i>		52	64	121		
PPM C_8 350°C		58	48	132		
PPM C_{8+Na} 350°C		48	68	132		

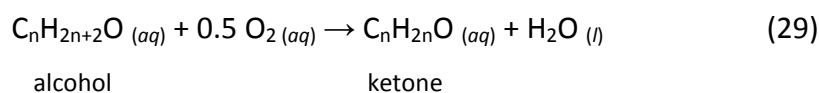
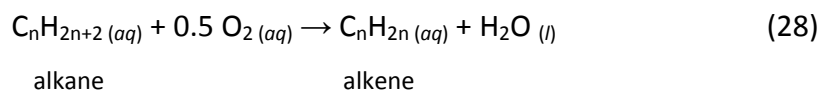
HM Samples

Comparison of the sulfate-free ($HM C_8$ 350°C) and sulfate-containing ($HM C_{8+Na}$ 350°C) HM samples with the initial HM buffer composition shows that 57 μmol and 29 μmol , respectively, of hematite were reduced to magnetite during these experiments (Table 7):



This reaction can only proceed if a suitable sink for oxygen exists, like for example the decomposition products from *n*-octane. This observation is supported by mass balance considerations:

The total amount of oxygen (O₂) incorporated in quantified organic reaction products – namely CO₂, acetone and butanone – in the sulfate-free and sulfate-containing HM samples equals 6.1 ± 0.9 μmol⁷ and 2.7 ± 0.4 μmol respectively. These amounts are significantly higher than for the corresponding buffer-free samples (0.92 ± 0.14 μmol and 0.82 ± 0.12 μmol), which points to an additional oxygen input apart from the obvious one stemming from residual air and water. As indicated by Reaction (27), reduction of hematite to magnetite is a suitable way to supply extra oxygen. During the sulfate-free HM experiment reduction of hematite produces 9.5 μmol O₂. In presence of sulfate only 29 μmol hematite are reduced, which results in the generation of 5 μmol O₂. The estimation shows that oxygen gain in organic products and oxygen supply by hematite correlate well. Smaller oxygen amounts in organic reaction products can probably be attributed to oxygen-bearing reaction products, which were not quantified (pentanone) or analyzed (e.g. C₅₊-ketones and organic acids), as well as to the formation of water during hydrothermal *n*-alkane oxidation. The latter is for example possible during oxidation of alkanes to alkenes (Reaction 28) or alcohols to ketones (Reaction 29):

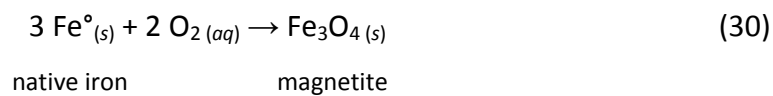


The key message from the data is that hematite initiates and promotes oxidation of *n*-octane. These observations are in line with previous studies that point out the role of hematite as oxidant in hydrocarbon systems (Surdam et al., 1989; Surdam et al., 1993; Bell et al., 1994). In presence of sulfate, the oxidizing effect of hematite is attenuated, which might be due to precipitated sulfate or mineral coating. Results for organic reaction products do, however, support the hypothesis that the buffers were not passivated (further discussed in *chapters 4.3.2.1 & 4.3.2.2*) and that a change in the reaction network has the potential to account for the observed decrease in oxidation (*c.f. chapter 4.3.4.2*).

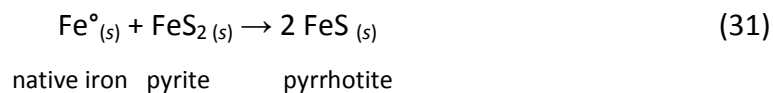
⁷ The μmolar amounts were calculated from results presented in Table A1 in the appendix, by multiplying these values with 30.64 μmol C₈H₁₈ (= initial amount of *n*-octane).

PPM Samples

The observation that native iron and troilite present in the initial PPM buffer are absent in any of the experimental samples (Fig. 19) is not surprising, because troilite and native iron are unstable under the experimental conditions (Toulmin and Barton, 1964 and McCollom et al., 2010 respectively). Troilite converts into the equilibrium modification pyrrhotite. Native iron readily reacts during heating, with two reactions being favorable. First, native iron may react with oxygen from air that prevails after capsule preparation, with a likely reaction being:



Second, native iron may react with pyrite to generate pyrrhotite:



Oxidation of native iron by water might also be possible under reducing conditions (see Reaction 2 in McCollom et al., 2010), but is rather unlikely under the conditions of the experiments performed here. The reaction would generate significant amounts of hydrogen, which contradicts results of Hinze (bachelor thesis 2012 → *cf. appendix C*), who performed similar experiments in an organic-free system with the PPM buffer at 350°C and 35 MPa. His results show that the amount of hydrogen generated in the sulfate-free PPM system is $0.31 \pm 0.06 \text{ mmol/kg}_{\text{H}_2\text{O}}$ after 24 h and $0.43 \pm 0.09 \text{ mmol/kg}_{\text{H}_2\text{O}}$ after 168 h. These values are in the same range as the expected equilibrium concentration of $0.63 \text{ mmol/kg}_{\text{H}_2\text{O}}$, providing evidence that no excess hydrogen was generated during buffer equilibration. Thus Reaction 30 and 31 are likely the dominating reaction for conversion of native iron. Based on these considerations a corrected starting composition of the initial PPM buffer at experimental conditions can be calculated from the measured initial PPM buffer composition (Table 7). For the calculation it is assumed that Reaction 30 is the preferred reaction for native iron. However, the reaction is limited by the amount of free oxygen from air that prevails after capsule preparation. This amount might not be constant in all samples, but the amount inferred from the pure cracking sample ($\approx 1 \text{ } \mu\text{mol O}_2$) gives a first estimate

also consume excess hydrogen that is generated if water acts as oxygen source. Evidence for water as oxygen donor is provided by the observation that ketone concentrations increase when water is added to the reacting system. Although, the resolution of the XRD method is too low to provide an exact mass balance, the data provide strong evidence that minerals and water both act as oxygen sources in the sulfate-free PPM experiments.

XRD data for the sulfate-containing PPM samples (*PPM C_{8+Na} 350°*) show that the absolute amounts of both sulfur-containing minerals, i.e. pyrite and pyrrhotite, increase if compared to the corrected mineral buffer composition (Table 7). This points to sulfur input from sulfate into the buffer minerals. An increase of pyrite by 4 μmol and of pyrrhotite by 11 μmol equals a net sulfur gain of 19 μmol . This implies that 38 $\mu\text{mol O}_2$ would be coproduced from sulfate. Access oxygen, does not seem to be stored in the minerals, because the amount of magnetite, the only oxygen-containing mineral, decreases if compared to the corrected buffer composition (Table 7). Moreover, a decrease of magnetite amount by 4 μmol would generate additional 8 $\mu\text{mol O}_2$. At this point, it remains unclear what the sink for oxygen could be. The formation of minor additional oxygen-containing mineral phases, which could not be resolved with the XRD method, might be possible. Apart from additional mineral phases, organic reaction products can be a sink of oxygen in the reacting system. The amount of oxygen incorporated in CO_2 , acetone and butanone in the sulfate-containing PPM samples is $2.5 \pm 0.4 \mu\text{mol O}_2$. The large difference to the above mass balance considerations may be accounted for by the fact that some oxygen-containing reaction products were not quantified (pentanone) or analyzed (e.g. C_{5+} -ketones and organic acids). The formation of water during hydrothermal *n*-alkane oxidation (Reaction 28 and 29) may also lower the concentration of free oxygen in the system. Of course the presented mass balance considerations only represent a rough estimation due to the low resolution of the XRD method, but the general trend is obvious.

4.3.2.1 IS THE BUFFER CAPABLE OF CONTROLLING REDOX?

A prerequisite for the buffering ability of mineral buffer assemblages is that the minerals are accessible and that they adjust to chemical changes of the reacting system. A crucial question that needs to be considered in this context is, whether kinetics of the

mineral buffer reactions is rapid enough to actually control the hydrogen activity of the fluid to the nominal equilibrium value.

Literature Information on HM and PPM Buffer Kinetics

Results from Seewald (2001) show that the HM and PPM mineral buffers are capable of controlling the redox conditions in a sulfate-free system at the experimental conditions employed in the present study. For experiments performed in the temperature range of 300 to 350°C and at 35 MPa, he could show that hydrogen concentrations readjust to (or at least close to) the equilibrium concentration within 25 h after perturbation of the chemical system. Based on these findings he states that the exchange of hydrogen and oxygen between water, the HM and PPM minerals, and alkanes, alkenes, alcohols and ketones in aqueous solution, is a rapid process with low kinetic barriers under hydrothermal conditions (Seewald, 2001, 2003). Mineral buffers used in the experiments were composed of the same synthetic minerals as used for the present study. Thus, mineral buffers employed by Seewald should be comparable to the ones used here.

Data from the Present Study

One difference between Seewald's experiments and those of the present study is, however, that Seewald has equilibrated the buffer together with water prior to hydrocarbon injection. The equilibration was performed for 200 to 500 h at a temperature, which was 25-50°C above the desired run temperature. This different procedure seems to have an effect for the buffering ability of the mineral assemblages. Results presented by Hinze⁸ (bachelor thesis 2012) for experiments of the type PPM+H₂O indicate that the aqueous hydrogen concentration adjusted in the system without prior equilibration is 0.31 ± 0.06 mmol/kg_{H₂O} after 24h, and 0.43 ± 0.09 mmol/kg_{H₂O} after 168 h. Corresponding hydrogen activities were calculated based on the assumption of Seewald (2001) that activity coefficients are equal to unity. Results indicate that the hydrogen activity during the sulfate-free experiments performed by Hinze (bachelor thesis 2012), was up to 0.3 log units below the expected equilibrium value for the PPM buffer. The increasing trend of the hydrogen concentration with time indicates that the buffer is still equilibrating.

⁸ A brief summary of the work by Hinze can be found in *appendix C*.

For sulfate-containing experiments of the type PPM+H₂O+Na₂SO₄, results from Hinze (bachelor thesis 2012) show that the measured hydrogen concentration after 24 h (0.18 ± 0.04 mmol/kg_{H₂O}) and 168 h (0.23 ± 0.05 mmol/kg_{H₂O}) is only half as high as in the corresponding sulfate-free samples. Lower hydrogen concentrations in presence of sulfate are in line with the expected oxidizing effect of sulfate. Calculated hydrogen activities from results of Hinze (bachelor thesis 2012) indicate that the actual hydrogen activity in presence of sulfate may be 0.4 to 0.5 log units below the expected equilibrium value for the PPM buffer. An increasing hydrogen concentration with time indicates that the buffer is also moving toward equilibrium, despite the large sulfate reservoir.

Data like those provided by Hinze for the PPM system are not available for the HM experiments, but alkane/alkene data may indicate that equilibrium was attained during the course of the sulfate-free and sulfate-containing HM experiments, which were run for 168h (cf. *chapter 5.2*).

Even though, the buffers might not have adjusted redox condition to equilibrium values, results for the organic reaction products reflect more oxidizing conditions for HM samples compared to PPM samples (Fig. 23). In the sulfate-free system, this is indicated by a higher CO₂ concentration for HM compared to PPM samples. In the sulfate-containing system, the generated amount of CO₂ is the same in presence of both mineral buffers, but ketone concentrations are higher in presence of the HM buffer. This demonstrates that even in presence of sulfate, a regulating effect of the HM and PPM mineral buffers on generated products is evident.

4.3.2.2 MINERAL BUFFERS AS CATALYSTS AND REACTANTS

In addition to the buffering effect of the minerals, results for organic reaction products at 350°C indicate that addition of the HM and PPM minerals to the experimental charge significantly promotes decomposition of *n*-octane. The conversion increases by a factor of 2 to 3 if minerals are added, and is in the same range for sulfate-free and sulfate-containing samples (Table A1 in the appendix). This provides further support for the hypothesis that the minerals are not passivated. The observed increase in conversion points to the catalytic activity of the employed minerals, which is in line with previous studies (Bell et al., 1994; Shipp et al., 2010). Observed compositional changes of the mineral buffers do, however, indicate that minerals also actively participate as reactants.

In contrast, at 300°C, the conversion of *n*-octane is lowered by a factor of three if the PPM buffer is added in the sulfate-free and sulfate-containing samples, indicating that the catalytic effect of the minerals is hampered.

4.3.3 EVALUATING CONTRIBUTIONS FROM CRACKING AND AQUEOUS OXIDATION

The distribution of organic reaction products can be used to investigate, which processes might have contributed to the decomposition of *n*-octane. In order to elucidate by which processes *n*-octane degradation is controlled in the experiments, a three step procedure was followed. First, contributions from pure cracking at the experimental conditions were estimated by evaluating the data for the sample containing pure *n*-octane (C_8^* 350°C) and comparing it to the sample, which additionally contained water. Second, experimental results are compared to results from Seewald (2001) in order to evaluate the contributions from aqueous oxidation. Third, the possibility that additional processes contribute to the degradation of *n*-octane in the experiments is explored.

4.3.3.1 CRACKING

The sample C_8^* 350°C only contained *n*-octane and thus serves as a reference for pure thermal decomposition of *n*-octane at 350°C. Cracking of pure *n*-octane is expected to yield products that only contain carbon and hydrogen. Thus, small amounts of CO₂ and ketones observed for this sample are viewed as “contaminations” that are produced from reaction with oxygen from air that is entrained during sample preparation.

Identical amounts of generated *n*-alkanes for the pure *n*-octane sample (C_8^* 350°C) and the sample with additional water (*-buf* C_8 350°C) indicate that water does not alter the formation rate of *n*-alkanes under these experimental conditions (Fig. 21 A). The distribution pattern of the *n*-alkanes is in good agreement with results of Zhang et al. (2007; 2008a) for experiments with *n*-octane and water under nearly identical conditions⁹ (Fig. 25). The difference in absolute abundances can be attributed to different run durations, but the distribution pattern is the same.

⁹ Zhang et al. (2007 and 2008a) performed hydrous pyrolysis experiments with *n*-octane at 350°C and 24 MPa, with a run duration of 24 h. They also used gold capsules as sample containers.

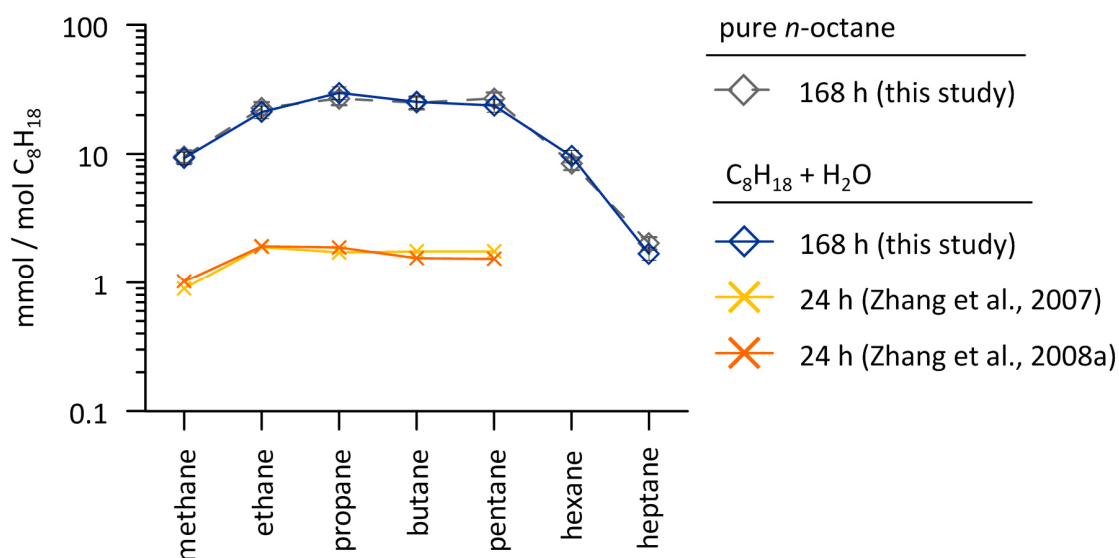


Fig. 25: Comparison of *n*-alkane amounts generated from aqueous *n*-octane decomposition after 24 h (data from Zhang et al., 2007 and 2008a) and after 168 h (this study). Experiments of Zhang et al. (2007, 2008a) were conducted at 350°C and 24 MPa. Samples contained 220 μmol *n*-octane and either 1388 μmol (2007) or 280 μmol (2008a) water. The pure *n*-octane sample (referred to as *C*₈* 350°C in the text) contained 31 μmol *n*-octane. The hydrous pyrolysis samples (referred to as -buf *C*₈ 350°C in the text) additionally contained 5 mmol water. The average of two samples is presented for this sample type. Samples of this study were processed at 350°C and 35 MPa for 168 h. Error bars (mostly covered by data points) represent uncertainties, which results from error propagation of the analytical error and the total weighing error of initial *n*-octane. Zhang et al. (2007 and 2008a) do not address the uncertainty of the data, but it is suggested that the error should be in a same range.

If the 168 h samples of this study are compared to the 24 h samples of Zhang et al. (2007; 2008a), an increase in propane, butane and pentane concentrations by a factor of 15-16 is observed. Concentrations of ethane and methane only increase by a factor of 11 and 10 respectively. The lower increase for methane and ethane, as well as the lower yield of methane relative to the other *n*-alkanes, is consistent with expectations for cracking. This is because *n*-octane is less likely to be split at the terminal C-C bond and the probability for cleavage between carbon position 2 and 3 or 6 and 7 is also lower than at interior carbon bonds (cf. *chapter 2.1*). From this, and especially from the excellent agreement of the *n*-alkane yield for the dry and hydrous pyrolysis samples in this study, it is concluded that cracking is the controlling process for aqueous *n*-octane decomposition in the buffer- and sulfate-free sample (-buf *C*₈ 350°C). The distribution pattern for *n*-alkanes in this sample is referred to as “typical cracking pattern” in the proceeding chapters. It is characterized by a steep increase from hexane to pentane, rather equal amounts for pentane, butane and propane, slightly lower ethane concentrations, and a drop towards lower methane values.

4.3.3.2 AQUEOUS OXIDATION

Although water does not affect the amount of produced *n*-alkanes, it does influence alkene and ketone abundances. Results for the hydrous pyrolysis samples indicate that alkene yields ($\sum C_{2ene-4ene}$) are halved and ketone concentrations ($\sum C_{3one+4one}$) increase by a factor of 4 when water is added (Table A1 in the appendix). One reason for this can be that water promotes hydration of alkenes to ketones. According to Seewald (2001) the reaction proceeds via alcohols as intermediate products:



However, additional reactions need to be involved due to stoichiometric reasons. The formation of oxygen-containing compounds itself is already a first sign that *n*-octane decomposition is probably influenced by aqueous oxidation in addition to cracking. Acetone, butanone and CO₂ were not only detected in the buffer-free samples, but also in those containing the HM and PPM mineral buffer, which were processed with or without sulfate (Table A1 in the appendix).

Comparison of the 300°C Data to Results from Seewald (2001)

Seewald (2001) conducted time-series experiments at 300°C and 35 MPa in a sulfate-free system in presence of the PPM buffer. During the experiments, Seewald collected a first sample after 70 h, followed by samples after 312, 741, 2229 and 3022 h. From the results he concluded that aqueous oxidation significantly contributes to *n*-heptane degradation during the experiments. The 300°C PPM samples without sulfate (PPM C₈ 300°C), which were processed for 168 h in the course of this study provide a direct comparison to Seewald's (2001) experiments.

Generated *n*-alkanes generally show the same trend in both studies, i.e. increasing abundance with decreasing chain length (Fig. 26). Two main differences are, however, apparent. First of all, the *n*-alkane curve cuts the data of Seewald. Second, concentrations of methane, ethane, propane and *n*-butane are about the same in the *n*-octane sample, whereas a continuous increase in concentration with decreasing chain length is observed for the *n*-heptane experiments at all times. A possible explanation for the latter observation is that aqueous oxidation might be enhanced during Seewald's experiments. In order to

explain this, a brief explanation of the experimental setup used by Seewald (2001) is necessary. He used a flexible gold-titanium cell for his experiments, which allows withdrawal and injection of fluids during the experiments. This setup was used to perform multiple experiments sequentially. The aqueous phase was not completely removed before injection of new reactants. Thus, previously injected reactants and their products persisted in solution for subsequent experiments. Prior to injection of new reactants, water was added to dilute the abundance of aqueous “contaminants” in the reaction cell. Nevertheless, these species prevailed in the reacting system and it is hypothesized that they might have had a “catalyzing” character. This means that they may have facilitated all reactions associated with aqueous oxidation right away, whereas some reactions might first have to be initiated in the samples, which started off with pure *n*-octane. In order to facilitate comparison of both studies and to only investigate newly formed products, the contaminant values at time of educt injection are subtracted from concentrations measured at the time of sampling in Seewald’s experiments. These values are plotted in Fig. 26.

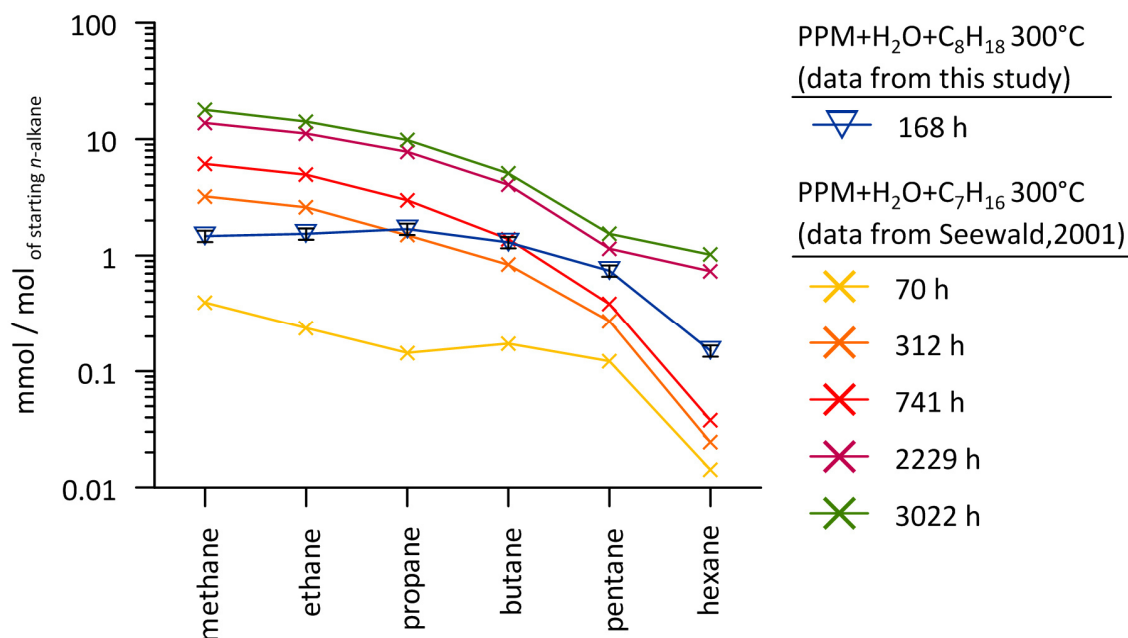


Fig. 26: Comparison of *n*-alkane amounts generated from aqueous *n*-heptane decomposition after 70 to 3022 h (data from Seewald, 2001), and from aqueous *n*-octane decomposition after 168 h (this study). All samples contained the pyrite-pyrrhotite-magnetite (PPM) mineral assemblage and water. Experiments were run at a temperature of 300°C and a pressure of 35 MPa. Seewald’s data is corrected for background concentrations of hydrocarbons present at time of *n*-heptane injection. The initial *n*-heptane concentration was 12.7 mmol/kg_{H₂O}. Error bars plotted for the sample of this study represent uncertainties, which results from error propagation of the analytical error and the total weighing error of initial *n*-octane. Seewald (2001) does not address the uncertainty of the data, but the uncertainty is expected to be in the same range.

The other difference observed for the two data sets, i.e. the intersection of the *n*-alkane curves of the two studies, is suggested to be due to the different chain length of the starting compounds. This has implications for cracking as well as for aqueous oxidation. During cracking cleavage at the terminal C-C bond is rather unlikely, which explains why significantly lower amounts of *n*-hexane compared to the other *n*-alkanes, as well as compared to the *n*-octane sample are observed in the *n*-heptane samples. With prolonged reaction times (2229 and 3022 h samples) the concentration of *n*-hexane increases significantly, which points to an increasing influence of other processes than primary cracking. The observation that methane is present as one of the most abundant compounds in all samples contradicts expectations for primary cracking. The reason for this cannot unequivocally be determined from the data. A possible reason might be that C₂₊ hydrocarbons generated during cracking are degraded by aqueous oxidation more heavily than methane. This is in line with Seewald (2001), who stated that the drive for reactions associated with aqueous oxidation increases with increasing chain length. This correlates well with the observed pattern in Fig. 26. The effect of aqueous oxidation on the *n*-alkane distribution is quite strong due to low overall conversion.

During aqueous oxidation, the chain length of the starting compound also plays a role. In the case of *n*-octane, degradation can proceed via formation of acetic acid and hexanoic acid that may decarboxylate to form CH₄ and *n*-pentane. Formation of formic acid is not a preferred option because alkene oxidation at terminal carbons is rather unlikely (see *chapter 2.2.1.1* for more details). Accordingly, the longest chain hydrocarbon generated through aqueous oxidation is *n*-pentane. During the *n*-heptane experiments presented in Seewald (2001), *n*-butane was the largest molecule produced through aqueous oxidation, consistent with the starting reactant containing one less carbon. These considerations for aqueous oxidation explain the “jump” from *n*-hexane to *n*-pentane in the *n*-octane experiment, and from *n*-pentane to *n*-butane in Seewald’s experiments.

The discussion shows that the degradation of *n*-heptane and *n*-octane seems to be influenced by the same processes, namely cracking and aqueous oxidation. The contribution of aqueous oxidation to the overall conversion is further strengthened by the close similarity of the suite of reaction products that were generated in both studies. Significant amounts of CO₂ were produced during the experiments of both studies. The CO₂ concentrations is usually comparable to the methane concentration, but may exceed it by a factor of 4 (PPM

C_8 300°C). Concentrations of quantified ketones (acetone and butanone) reach the same range as corresponding n -alkanes in the n -octane sample (PPM+H₂O+C₈H₁₈). Seewald (2001) did not measure ketones in the n -heptane samples, but he provides data for aqueous acetate (C₂H₃O₂⁻_(aq)). In all experiments, the acetate concentration is in a similar range than that of propane. The formation of oxygen-containing compounds like CO₂, ketones and organic acids provides clear evidence that aqueous oxidation contributed to the overall conversion of n -heptane and n -octane in both experimental studies.

Discussion of the 350°C Data

The n -alkane distribution of all 350°C samples (Fig. 21 A & B) generally shows a good agreement with the typical cracking pattern (cf. *chapter 4.3.3.1*). This observation suggests that cracking may also be the dominating process for aqueous n -octane decomposition in the mineral-buffered samples.

If the minerals only catalyzed primary cracking of n -octane, an increase by the same factor for propane, butane and n -pentane, and slightly lower increases for ethane and methane would be expected in comparison to the reference sample (C_8^* 350°C). This assumption is based on the comparison of the generated n -alkane amounts (C₁ to C₅) from n -octane cracking after 24 h (data from Zhang et al., 2007; Zhang et al., 2008a) and after 168 h at 350°C (cf. *chapter 4.3.3.1*). A closer look at the results shows that this is not completely the case (Fig. 27 A & B). Instead, methane and ethane show the same or higher enrichment factors than the other n -alkanes (C₃ to C₅), which is more obvious in presence of sulfate. This, and especially the selective enrichment of C₁-C₅ n -alkanes relative to C₆ and C₇ n -alkanes observed for all, except the hydrous pyrolysis (*-buf* C_8 350°C) samples, is exactly the result predicted for oxidative degradation via the reaction path described in Seewald (2001) (see *chapter 2.2.1.1* for details). During this process, longer chain n -alkanes degrade oxidatively by forming two C₂₊ carboxylic acids as intermediate products, which subsequently degrade via decarboxylation and/or oxidation. In the case of n -octane, the largest carboxylic acid that is expected to be produced in significant quantity is hexanoic acid (C₆H₁₂O₂) together with acetic acid (C₂H₄O₂). The formation of formic (CH₂O₂) and heptanoic acid (C₇H₁₄O₂) is rather unlikely because alkene oxidation (*step 2* of the Seewald model) at terminal carbons may only proceed at a very subordinate rate (Seewald, 2001). Hexanoic acid could decarboxylate to form methane and n -pentane. Accordingly, the longest chain

alteration product from oxidative degradation of *n*-octane is *n*-pentane. As a result, the steep increase from C₆ to C₅ characteristic for the typical cracking pattern is amplified.

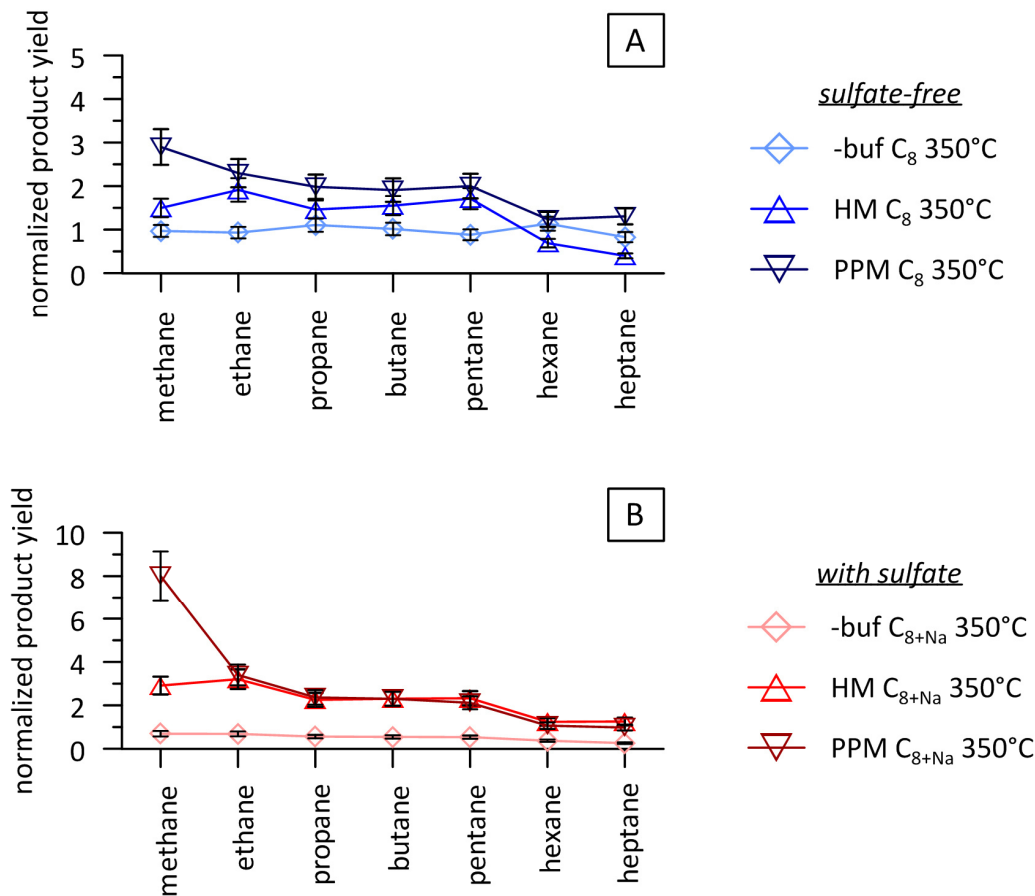


Fig. 27: Normalized product for *n*-alkanes generated from aqueous *n*-octane decomposition at 350°C and 35 MPa after 168 h in (A) sulfate-free and (B) sulfate-containing samples. The normalized product yield is calculated by dividing *n*-alkane concentrations of each sample by respective *n*-alkane concentrations for the pure *n*-octane sample (C₈ 350°C). This sample serves as reference for pure thermal cracking under the experimental conditions. Values >1 represent enrichment and values <1 depletion of individual *n*-alkanes. Buffer conditions are indicated as: -buf = no mineral buffer, HM = hematite-magnetite, PPM = pyrite-pyrrhotite-magnetite. Uncertainties are calculated by error propagation of absolute errors listed in Table A1.

Based on the results, it is suggested that *n*-alkane data for the HM and PPM samples with and without sulfate, as well as for the sulfate-containing buffer-free sample, provide compelling evidence for decomposition of *n*-octane via oxidative degradation in addition to cracking. As noted earlier in this chapter, this is also supported by the observation that the samples are characterized by an alteration assemblage that consists of *n*-alkanes, alkenes, ketones and CO₂. These are all reaction products, which are consistent with those generated by oxidative degradation (Seewald, 2001). The strongly elevated methane yield (Fig. 22), which is observed for the sulfate-containing PPM samples (labeled by PPM C_{8+Na} 350°C) needs, however, further explanation.

4.3.4 EFFECT OF THE PPM AND HM MINERAL BUFFERS, AS WELL AS THE EFFECT OF DISSOLVED SULFATE ON THE HYDROTHERMAL DEGRADATION OF *N*-OCTANE

4.3.4.1 ELEVATED GAS DRYNESS FOR THE SULFATE-CONTAINING PPM SAMPLES

The elevated methane yield in the sulfate-containing PPM samples is reflected by the gas dryness ($C_1/\sum C_{1-4}$). It increases from 6.3 ± 0.7 wt% to 18 ± 6 wt% in presence of sulfate in the PPM samples. In contrast, the gas dryness for the HM and buffer-free samples remains constant within the uncertainty, if sulfate-free and sulfate-containing samples are compared (Fig. 22). Interestingly, the gas dryness of the sulfate-free PPM sample is already 2 wt% higher than for the respective HM and buffer-free sample, which both show a gas dryness of 4.2 ± 0.5 wt% (Fig. 22). The question arises why the gas dryness shows a different behavior in the three investigated systems, and especially in the two mineral-buffered systems.

One possible explanation could be the different redox conditions adjusted by the HM and PPM buffers. At more reducing conditions, as for example encountered with the PPM mineral buffer, decarboxylation may dominate at the terminal step of the reaction sequence proposed for aqueous oxidation of hydrocarbons (Seewald, 2001). According to Seewald (2001, 2003), this can be an effective mechanism to generate dry, i.e. methane dominated, gas from C_{2+} hydrocarbons. In addition to that, the different minerals in the two buffers may display different catalytic potential with respect to methane generation. These two explanations may be valid to some extent, but they cannot fully account for the significant increase in gas dryness following sulfate addition in the PPM system, mainly because of two reasons. First of all, the same PPM minerals are present in the sulfate-free as well as in the sulfate-containing systems. Based on the discussion in chapter 4.3.2, it was inferred that the minerals were not passivated and should therefore have the same catalytic potential in sulfate-free and sulfate-containing samples. Secondly, sulfate is expected to have an oxidizing effect and would therefore promote oxidation instead of decarboxylation in the terminal step of the reaction sequence for aqueous oxidation. This would not lead to a significantly increased methane yield.

I rather propose that the crucial difference is that the PPM buffer initially provides H_2S , which can have a great impact in presence of sulfate (see paragraph below). The selective enrichment of methane observed for the PPM samples, and thus an increase of the

gas dryness, is very consistent with results expected for TSR, especially if catalyzed by H₂S (Amrani et al., 2008; Zhang et al., 2008a; Zhang et al., 2008b). Results from Zhang et al. (2008a) for experiments investigating the effect of H₂S on the reaction of *n*-octane and MgSO₄ under hydrothermal conditions are presented in (Fig. 28).

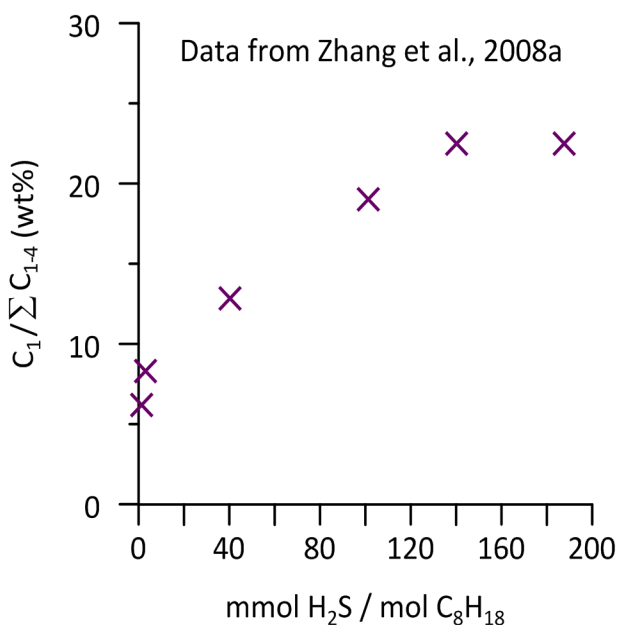


Fig. 28: Evolution of the gas dryness ($C_1/\sum C_{1-4}$) in dependence on the amount of H₂S generated from reaction of MgSO₄ and *n*-octane with varying water contents at 350°C and 24.1 MPa after 24 h experiment duration (data from Zhang et al., 2008a).

During the experiments H₂S was generated from reduction of sulfate. The thermochemical reduction of sulfate (TSR) is catalyzed by H₂S, sustaining an auto-catalyzed process (Zhang et al., 2008b). With increasing H₂S yield, and thus increasing TSR, the gas dryness sharply increases at low H₂S concentrations and seems to approach a constant value at higher H₂S levels. This finding indicates that TSR, especially if catalyzed by H₂S, is a possible mechanism for selectively enriching methane relative to C₂, C₃ and C₄.

Theoretical Background on H₂S-Catalyzed TSR

Experiments performed by Zhang et al. (2008b) had the objective to elucidate potential controls for H₂S initiation of TSR. Experiments were run at 300-370°C and 24.1 MPa for 24 h, using CaSO₄ and a C₂₁-C₃₅ paraffin mixture¹⁰ or hexadecane. The pH was adjusted to 3 or 5, employing a talc-silica and dolomite pH mineral buffer respectively. Based on their results they proposed a three-step reaction scheme for TSR initiation by H₂S (Fig. 29):

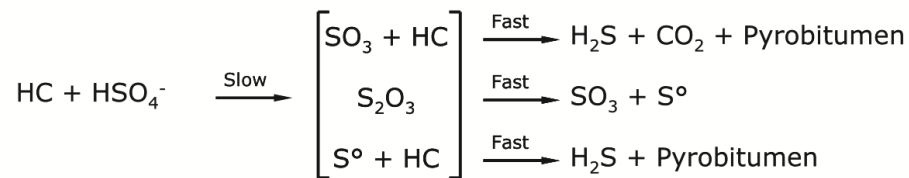
1. In absence of H₂S or other low valence sulfur species, sulfate reduction with hydrocarbons may proceed at a slow rate. The critical step is the activation of the free sulfate ion to form, for example, HSO₄⁻. According to Zhang et al. (2008b), the reaction produces lower valence sulfur species including SO₃, S₂O₃, S₈ and H₂S.

¹⁰ Research grade paraffin was composed of C₂₁ to C₃₅ normal alkanes, with a melting point of 52-58°C.

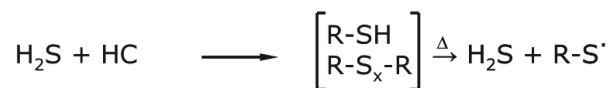
2. H₂S and other low valence sulfur species produced in the first step may rapidly react with hydrocarbons to generate labile organosulfur compounds including thiols, sulfides and disulfides. H₂S originating from other sources, like from the PPM mineral buffer, may directly enter the sequence at this step.
3. Generated LSCs are likely to react with sulfate and are significantly more effective in increasing the rate of sulfate reduction than inorganic sulfur species like H₂S or elemental S (on a mole basis) (Amrani et al., 2008). According to Zhang et al. (2008b), the lower valence sulfur species generated in this step may react with hydrocarbons to form more H₂S and LSC (second step), sustaining an auto-catalyzed reaction.

Proposed mechanism of H₂S-catalyzed sulfate reduction (adapted from Zhang et al., 2008b)

Step 1: Sulfate reduction with hydrocarbons prior to H₂S presence



Step 2: Sulfur incorporation to hydrocarbons by reacting with H₂S



Step 3: Sulfate reduction by reactive labile sulfur compounds oxidation

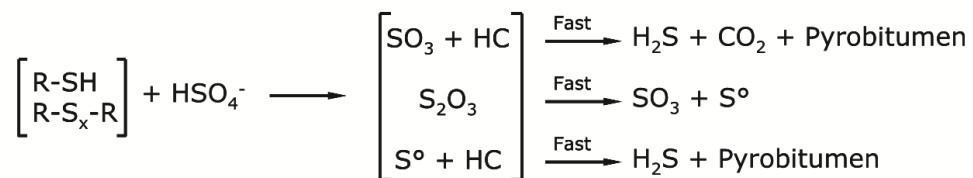
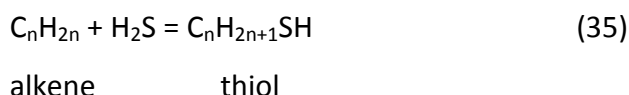


Fig. 29: Proposed reaction scheme for H₂S-catalyzed thermochemical sulfate reduction, with labile organosulfur compounds as key intermediates (modified after Zhang et al., 2008b). R represents an alkyl group, HC stands for hydrocarbons. Pyrobitumen refers to an organic network that forms by polymerization of hydrocarbons. Pyrobitumen is characterized by a low H/C ratio, indicating hydrogen depletion compared to the starting material.

In addition to the experiments mentioned above, Zhang et al. (2008b) performed experiments with the same C₂₁-C₃₅ paraffin mixture and varying initial amounts of H₂S (in absence of sulfate!) at 300°C and 24.1 MPa for 192 h. The results indicate that with increasing amounts of initially loaded H₂S, the amount of analyzed thiols (methanethiol, ethanethiol, propanethiol and iso-propanethiol) continuously increases (Fig. 30). Zhang et al. (2008b) propose that alkenes are probably the reactive hydrocarbons toward H₂S during formation of LSCs:



Results from Amrani et al. (2008)¹¹, support the findings of Zhang et al. (2008b) that LSCs significantly promote the TSR reaction and thus the formation of methane. The exact mechanisms how TSR selectively enhances methane formation is hitherto not understood, but considering findings from Zhang et al. (2008b), a possible reaction could be (Amrani, personal communication):

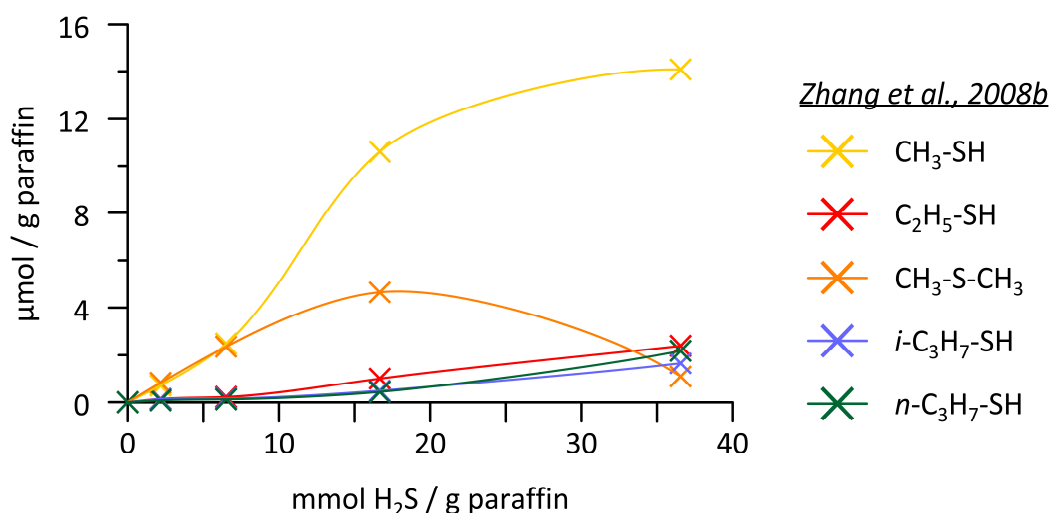


Fig. 30: Yield of five different labile sulfur compounds generated from reaction of a C₂₁₋₃₅ paraffin with variable initial H₂S amounts (data from Zhang et al., 2008b). Experiments were conducted at 300°C and 24.1 MPa for 192 h. Note that H₂S concentrations on the x-axis refer to initially loaded H₂S amounts, whereas H₂S concentrations shown in Fig. 28 refer to generated amounts of H₂S during the experiments.

¹¹ Amrani et al. (2008) performed experiments with *n*-octane and CaSO₄ in the presence of reduced sulfur (H₂S, S⁰, organic S, but no sulfur-containing minerals were tested) at 330 and 356°C at 24.1 MPa. In-situ pH was buffered to 3.5 with talc and silica.

Interpretation of the Results for the Sulfate-Containing PPM Samples

Hanin (2002) performed experiments with *n*-octadecane ($C_{18}H_{38}$) and pyrite at 300°C. Her results indicate that sulfur from pyrite gets incorporated into organic reaction products. Evidence for sulfur incorporation from minerals into organic reaction products is also provided by preliminary measurements¹² for the sulfate-free PPM sample, which show that 1-propanethiol (C_3H_8S) was generated. This is not surprising, because thiols are likely formed from the reaction of alkenes and H_2S (Reaction 35). The PPM buffer can be the source of H_2S . Such a reaction is analogue to the Markownikoff addition of water in the second step of the Seewald model (*cf. chapter 2.2.1.1*). Thus, I hypothesize that both reactions would be competing and that an alternative reaction pathway involving organosulfur compounds may open up at this step of the reaction sequence (Fig. 31). Observations for the sulfate-containing PPM samples provide compelling evidence for the possible involvement of such a LSC pathway:

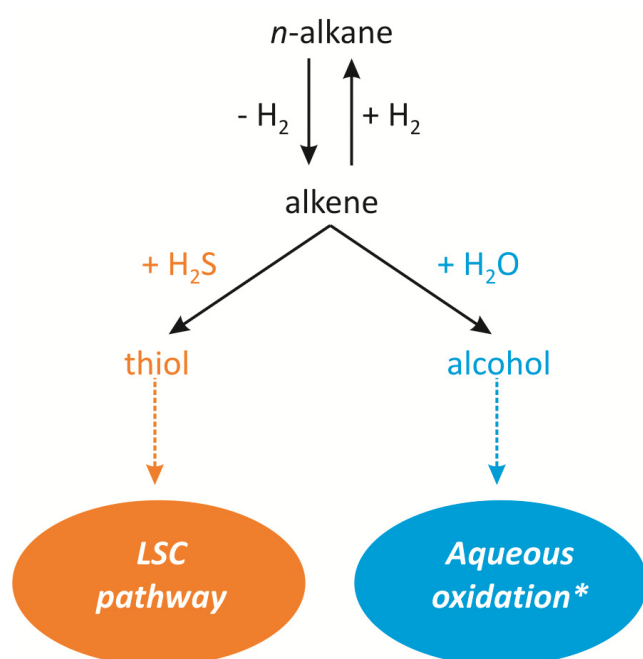


Fig. 31: Visualization of the proposed hypothesis that an alternative pathway in addition to aqueous oxidation may be initiated during hydrothermal *n*-alkane decomposition if H_2S is present in the reacting system. Analogue to the reaction $\text{alkene} + H_2O = \text{alcohol}$, $H_2S_{(aq)}$ may react with alkenes to form thiols. This could first initiate and then enhance the labile sulfur compound (LSC) pathway. Alkenes are probably not the only organic compounds that can react with $H_2S_{(aq)}$. It is rather hypothesized that all reactions postulated by Seewald (2001) for aqueous oxidation involving water, may also be possible with $H_2S_{(aq)}$. This needs, however, support of further experimental investigations.

*A detailed reaction network for aqueous oxidation of hydrocarbons was presented by Seewald (2001). His work is summarized in *chapter 2.2.1.1* of the present thesis.

¹² The analytical protocol was not set for detection of organosulfur compounds at time of sample analysis. However, recent method developments allow qualitative detection of selected thiols, whereof only 1-propanethiol shows no coelution problems in case of the PPM samples.

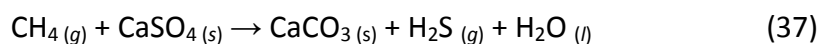
If sulfate is added, generated amount of CO₂ (Fig. 23 E) and ketones (Fig. 23 C & D) decrease, although amounts of generated C₃ to C₇ *n*-alkanes (Fig. 21 A & B) and concentrations of propene and butene (Fig. 23 A & B) remain constant. The strongest decrease is observed for ketones. These observations point to a mechanism, which seems to hinder ketone formation from alkenes. This could for example be the case, if the reaction network is shifted toward the LSC pathway. As noted above, LSCs can be generated from reaction of alkenes and H₂S. H₂S generated from the mineral buffer may initiate this reaction. Sulfate, once activated, can be reduced by the LSCs, generating more H₂S and other low valence sulfur species (Fig. 29). This would enhance the overall rate of LSC formation and sustain an auto-catalyzed reaction (Zhang et al., 2008b).

Results from Zhang et al. (2008a) show that an enhanced methane formation is expected with an increasing extent of H₂S-, or more precisely, LSC-catalyzed TSR. This is in line with observations for the sulfate-containing PPM samples. Although LSC compounds could not be quantified with the analytical protocol, the possibility that LSC- catalyzed TSR in addition to cracking and oxidative degradation may successfully explain the results for the sulfate-containing PPM samples cannot be dismissed. Further support for the possible occurrence of sulfate reduction is given by XRD data, which show that the total amount of sulfur stored in the mineral buffer increases in presence of sulfate (cf. *chapter 4.3.2*).

4.3.4.2 SULFATE ADDITION LOWERS TOTAL OXIDATION TO CO₂

Generally, sulfate is expected to have an oxidizing effect on hydrocarbons and should promote their total oxidation to CO₂ (Orr, 1977; Goldstein and Aizenshtat, 1994; Machel, 2001). Thus, the decrease in CO₂ concentration observed for all three investigated systems (-buf, PPM and HM) upon sulfate addition seems contradictory. However, results of the present PhD study do not stand alone. Pan et al. (2006) compared oxidation of gaseous hydrocarbons by pure hematite, and by hematite+MgSO₄ at nearly identical experimental conditions (350°C, 50 MPa, 72-288 h), with the same result: sulfate addition lowers the total oxidation to CO₂. In the previous paragraph it was proposed that a change in the reaction network toward a preferred generation of LSCs could offer a possible explanation. Another possibility could be that carbonates formed. Mineralogical and geochemical data for natural

samples from the Khuff Formation, Abu Dhabi, indicate that this may be a result of sulfate reduction with hydrocarbons (Worden and Smalley, 1996; Worden et al., 2000):



In the present study, Na_2SO_4 was used as sulfate source. Precipitations of Na_2CO_3 (=soda) is, however, unlikely due to its high aqueous solubility. Significant concentrations of aqueous carbonate species (CO_3^{2-} and HCO_3^-) are also not expected, because thermodynamic calculations with the Geochemist Workbench indicate that CO_2 would be the dominating aqueous species at the experimental conditions (Hentscher, personal communication).

In the mineral-buffered systems siderite (FeCO_3) represents another carbonate mineral that could precipitate. This could explain why the observed decrease in CO_2 concentration upon sulfate addition is higher in the mineral-buffered system if compared to the buffer-free samples. Especially in the HM system a strong decrease in the CO_2 concentration from $170 \pm 19 \text{ mmol/mol}_{\text{C}_8\text{H}_{18}}$ to $57 \pm 6 \text{ mmol/mol}_{\text{C}_8\text{H}_{18}}$ is observed. Under the assumption that the total decrease of CO_2 in the HM samples was attributed to siderite precipitation, formation of $3.4 \text{ } \mu\text{mol}$ of siderite (= 0.4 mg) would be expected. This amount would be detectable by XRD analysis, but it would be close to the lower limit of the method. Thus, if only half the amount had formed, it would not be resolvable. In order to verify that lacking detection of siderite was not an issue of resolution, thermodynamic calculations were performed to test the potential of siderite formation during the experiments.

Thermodynamic Calculations – Evaluating the Potential of Siderite Formation

Regarding the HM and PPM buffer minerals, different reactions for siderite formation are possible. McCollom et al. (2010)¹³ showed, for example, that siderite formation from magnetite is possible during hydrothermal experiments under highly reducing conditions (Reaction 38). In addition to that, Seewald (2001) proposed that siderite formation from pyrite may be possible in nature (Reaction 39), but he does not explicitly investigate this

¹³ McCollom et al. (2010) used native iron to adjust highly reducing conditions during experiments performed at 250°C and 17 MPa in the course of their study. The corresponding reaction is: $3 \text{ Fe} (s) + 4 \text{ H}_2\text{O} (l) \rightarrow \text{Fe}_3\text{O}_4 (s) + 4 \text{ H}_2 (aq)$. At 350°C and 35 MPa the calculated hydrogen activity at equilibrium ($\log a_{\text{H}_2 (aq)} = 1.1$), would be four orders of magnitude more reducing than the hydrogen activity in equilibrium with the pyrite-pyrrhotite-magnetite mineral buffer at identical conditions ($\log a_{\text{H}_2 (aq)} = -3.2$).

$$\log K_{(38)} = 3 \log a_{\text{FeCO}_3(s)} + \log a_{\text{H}_2\text{O}(l)} - \log a_{\text{Fe}_3\text{O}_4(s)} - \log a_{\text{H}_2(aq)} - 3 \log a_{\text{CO}_2(aq)} \quad (43)$$

$$\log K_{(39)} = \log a_{\text{FeCO}_3(s)} + 2 \log a_{\text{H}_2\text{S}(aq)} - \log a_{\text{FeS}_2(s)} - \log a_{\text{H}_2(aq)} - \log a_{\text{CO}_2(aq)} \quad (44)$$

$$\log K_{(40)} = 2 \log a_{\text{FeCO}_3(s)} + \log a_{\text{H}_2\text{O}(l)} - \log a_{\text{Fe}_2\text{O}_3(s)} - \log a_{\text{H}_2(aq)} - 2 \log a_{\text{CO}_2(aq)} \quad (45)$$

$$\log K_{(41)} = \log a_{\text{FeCO}_3(s)} + \log a_{\text{H}_2\text{S}(aq)} - \log a_{\text{FeS}(s)} - \log a_{\text{H}_2\text{O}(l)} - \log a_{\text{CO}_2(aq)} \quad (46)$$

In order to determine Q , measured amounts of products and reactants present during the reaction at a particular point in time are converted to corresponding activities (see below) and are included in the calculation. In line with the other thermodynamic calculations in this study, the standard state adopted for liquid H_2O and stoichiometric minerals is 1 of unit activity. As noted in chapter 3.6.1, pyrrhotite is a non-stoichiometric mineral, wherefore its activity is smaller than 1 and needs to be included in the calculation. In case of the PPM samples of this study the activity of pyrrhotite was determined to be 0.56 ± 0.03 at 350°C and 35 MPa (cf. *chapter 3.6.1*). Thus, Equations (38) - (42) reduce to:

$$\log Q_{(38)} = -\log a_{\text{H}_2(aq)} - 3 \log a_{\text{CO}_2(aq)} \quad (47)$$

$$\log Q_{(39)} = 2 \log a_{\text{H}_2\text{S}(aq)} - \log a_{\text{H}_2(aq)} - \log a_{\text{CO}_2(aq)} \quad (48)$$

$$\log Q_{(40)} = -\log a_{\text{H}_2(aq)} - 2 \log a_{\text{CO}_2(aq)} \quad (49)$$

$$\log Q_{(41)} = \log a_{\text{H}_2\text{S}(aq)} - \log a_{\text{FeS}(s)} - \log a_{\text{CO}_2(aq)} \quad (50)$$

Even though aqueous concentrations of hydrogen and hydrogen sulfide were not measured for the HM and PPM samples, a first estimate of reaction quotients can be made based on the assumption that equilibrium values were attained. Calculations of hydrogen activities in equilibrium with the HM ($\log a_{\text{H}_2(aq)} = -4.2$) and PPM ($\log a_{\text{H}_2(aq)} = -3.2$) mineral buffers, as well as of the hydrogen sulfide activity in equilibrium with the PPM ($\log a_{\text{H}_2\text{S}(aq)} = -2.0$) mineral buffer at 350°C and 35 MPa , are described in *chapter 3.6.1*. The activity of CO_2 was calculated from measured molal CO_2 concentrations under the assumption that the

activity coefficient is equal to unity (cf. *chapter 3.6.3* → footnote 4), which is consistent with the approach of Seewald (2001). Reaction quotients calculated based on these assumptions, are listed in (Table 8).

Table 8: Values for the logarithmic reaction quotient ($\log Q$ → first number) and the chemical affinity (A in Kcal/mol → second number) calculated for siderite formation from magnetite (Reaction 38), pyrite (Reaction 39), hematite (Reaction 40) and pyrrhotite (Reaction 41) during sulfate-free (labeled by C_8) and sulfate-containing (C_{8+Na}) experiments. Calculated values are specific for the experimental conditions, i.e. 350°C and 35 MPa, and run duration of 168 h. The uncertainty for the affinity values is ± 1 kcal/mol.

<i>HM C₈ 350°C</i>	<i>HM C_{8+Na} 350°C</i>	<i>PPM C₈ 350°C</i>	<i>PPM C_{8+Na} 350°C</i>
<i>Molal CO₂ concentrations* used to calculate Q</i>			
0.058	0.020	0.032	0.022
<i>Reaction (38) – Fe₃O_{4(s)} + H_{2(aq)} + 3 CO_{2(aq)} = 3 FeCO_{3(aq)} + H_{2O(l)}</i>			
8 -24	9.4 -28	7.7 -23	8.2 -25
<i>Reaction (39) – FeS_{2(s)} + H_{2(aq)} + CO_{2(aq)} + H_{2O(l)} = FeCO_{3(s)} + 2H_{2S(aq)}</i>			
		0.7 -8	0.8 -8
<i>Reaction (40) – Fe₂O_{3(s)} + H_{2(aq)} + 2 CO_{2(aq)} = 2 FeCO_{3(s)} + H_{2O(l)}</i>			
6.7 -16	7.7 -19		
<i>Reaction (41) – FeS_(s) + CO_{2(aq)} + H_{2O(l)} = FeCO_{3(s)} + H_{2S(aq)}</i>			
		-0.3 -8	-0.1 -8

PPM = pyrite-pyrrhotite-magnetite; HM = hematite-magnetite

*The molal (mol/kg H₂O) concentrations for CO₂ are obtained from concentrations listed in Table A1 in the appendix through division by 1000 subsequent multiplication by the molar amount of initial *n*-octane (3.064 x 10⁻⁵ mol), and final division by the amount of water (9 x 10⁻⁵ kg).

For the HM and PPM samples processed at 350°C and 35 MPa, calculated affinities for Reactions 38 to 41 are all negative (Table 8), indicating that no thermodynamic drive for siderite formation exists during the experiments. Siderite formation could be promoted if hydrogen and/or CO₂ concentrations rose, but even if hydrogen and CO₂ activities were one order of magnitude higher, chemical affinities would still be negative. Additionally, the

actual hydrogen activity is rather up to 0.5 log units lower than the predicted value (bachelor thesis Hinze, 2012). This will also counteract siderite precipitation. Another possibility, which could promote siderite formation from iron sulfides (Reactions 39 and 41) is to lower the amount of hydrogen sulfide in the system. This might be the case, if LSC compounds formed (e.g. Reaction 35). If hydrogen and CO₂ activities remained unchanged, the activity of hydrogen sulfide would, however, have to be lowered by 1.5 or 3 log units to approach zero affinity for Reactions 39 and 41 respectively. Such a decrease is quite high and unrealistic to be reached during the experiments. Furthermore, siderite precipitation could only be initiated if chemical affinities actually switched to positive values.

The thermodynamic consideration in conjunction with the XRD data, indicate that siderite precipitation is not expected during experiments performed at 350°C and 35 MPa. Thus, the drop in CO₂ concentration that was observed as consequence of sulfate addition cannot be accounted for by this mechanism.

4.3.4.3 SIMILARITY OF THE SULFATE-CONTAINING BUFFER-FREE AND HM SAMPLES

Interestingly, despite differences in concentrations, relative abundances of reaction products generated in the sulfate-containing buffer-free samples (*-buf C_{8+N_α} 350°C*) and the sulfate-containing HM (*HM C_{8+N_α} 350°C*) samples are very similar. The trend for the *n*-alkane distribution is for example identical. It agrees with the typical cracking pattern, showing an increase from C₅ to C₆, rather equal amounts for C₅ to C₂ and a drop towards lower methane concentrations. A closer look reveals, however, that C₁₋₅ *n*-alkanes are stronger enriched relative to C₆ and C₇ than in the cracking reference sample (Fig. 27 B). This points to an influence of oxidative degradation (Seewald, 2001). It is striking that the curve for the sulfate-containing buffer free samples (*-buf C_{8+N_α} 350°C*) depicted in Fig. 27 B plots directly on the curve for the sulfate-containing HM sample (*HM C_{8+N_α} 350°C*) if values were multiplied by a factor of 4. In addition to that, molar alkane/alkene, ketone/alkene and CO₂/C₁ ratios are identical or at least very similar in both samples (Table A1 in the appendix). Good correlation of results for the sulfate-containing buffer-free and sulfate-containing HM samples provide compelling evidence that aqueous *n*-octane decomposition is influenced by

the same processes in both samples. The main processes being cracking and oxidative degradation.

In addition to that, some results point to the possibility of small contributions from TSR at its initial stage. One indication for this is given by the gas dryness data. HM and buffer-free samples in absence of sulfate are characterized by a gas dryness of 4.2 ± 0.5 wt%, and corresponding samples with sulfate by a gas dryness of 5.2 ± 0.6 wt%. Data are the same within uncertainty, but absolute values seem to be a sign of an increase. In fact, the presented error is regarded to be an overestimation of the uncertainty. This assumption is based on the results for five identical sulfate-containing PPM samples that were processed at 350°C. Here the gas dryness ranges from 12.4 to 13.5 wt%, with an arithmetic mean of 12.9 ± 0.4 wt% (Fig. B3 in the appendix). The double standard deviation of the arithmetic mean (= 0.8 wt%) covers the whole range of the data. It equals a relative uncertainty of 7%. If this was applied for the gas dryness values of the HM and buffer-free samples, the results would change to 4.2 ± 0.3 wt% and 5.2 ± 0.3 wt% for the sulfate-free and sulfate-containing samples respectively. Based on this discussion, the observed increase for the gas dryness is considered to be reliable.

This, together with the observation that sulfate addition seems to hamper ketone and CO₂ formation in the buffer-free and HM experiments, is consistent with the observations for the PPM samples. Here, a change in the reaction network associated with H₂S-catalyzed TSR was proposed as a possible hypothesis to explain the findings (cf. *chapter 4.3.4.1*). A crucial difference between the buffer-free and HM systems on the one hand, and the PPM system on the other hand, is, however, that the first two initially do not contain any H₂S or other low valence sulfur species. Thus, the first step of the reaction scheme proposed by Zhang et al. (2008b) for sulfate reduction initiated by H₂S (cf. Fig. 29) could not be jumped over in these two systems, which would explain the lower TSR rate. Here, the activation of the free sulfate ion to a more reactive species (e.g. HSO₄⁻) is the critical step for TSR initiation. Regarding the experiments performed in the course of the present study, thermodynamic modeling with the Geochemist Workbench shows that NaSO₄⁻ is the dominant aqueous sulfate species (Hentscher, personal communication). It is, however, unknown if this species is reactive towards hydrocarbons.

Alkane and alkene data do, however, provide further evidence for possible TSR involvement in the thermal decomposition of *n*-octane, at least for the buffer-free system. Here, the molar alkane/alkene ratio is lowered if sulfate is added (Table A1 in the appendix and Fig. 32 in the next chapter). This is consistent with expectations for TSR controlled reactions (Ma et al., 2008):



A lowering of the alkane/alkene ratio upon sulfate addition is not obvious for the mineral-buffered systems. Here, the influence of TSR on the conversion of alkanes to alkenes seems to be masked by the buffering influence of the mineral assemblages on the reaction. In presence of the HM buffer, a decreasing trend of the molar alkane/alkene ratio may be spotted with some courtesy, if absolute values for the sulfate-free and sulfate-containing HM samples are compared (Fig. 32 in the next chapter).

4.4 CONCLUSIONS

The thermal degradation of *n*-octane in presence or absence of the hematite-magnetite (HM), the pyrite-pyrrhotite-magnetite (PPM) mineral assemblages and dissolved sulfate was studied at 300 and 350°C. Gas chromatographic analyses of organic reaction products generated during the experiments reveal insights into the effect of these inorganic components on the distribution of reaction products. Measured data were used to evaluate, which processes contributed to the degradation of *n*-octane and which implications presence of the inorganic components has on the reaction network. The results contribute to an improved understanding of the reaction of hydrocarbons with inorganic components. Principal findings for the experiments are:

1. Cracking is the dominating primary reaction controlling *n*-alkane decomposition in all experiments.

2. In all water-containing samples aqueous oxidation contributes to *n*-octane degradation in addition to cracking. This is consistent with observations for similar experiments with *n*-heptane in a sulfate-free system (Seewald, 2001). However, this is the first time that the reaction network for aqueous oxidation has been verified in such detail for hydrocarbon degradation in sulfate-containing experiments.
3. Data for sulfate-containing PPM samples (*PPM C_{8+N_a} 350°C*), especially the strongly elevated methane yield, cannot be explained by cracking and aqueous oxidation only, and require further explanation. Results suggest that additional contributions from H₂S-catalyzed TSR, may successfully explain the findings with the source of H₂S being the PPM mineral buffer. It is hypothesized that an alternative reaction pathway involving organosulfur compounds (LSC pathway) is initiated, which may proceed simultaneously to the aqueous oxidation pathway.
4. The product distribution of the sulfate-containing buffer-free (*-buf C_{8+N_a} 350°C*) and sulfate-containing HM (*HM C_{8+N_a} 350°C*) samples show compelling similarity despite differences in the absolute abundance. As noted in point 2, aqueous oxidation and cracking are the main processes responsible for *n*-octane degradation. However, results for these sulfate-containing samples point to the possibility that TSR proceeded at a very subordinate rate as well.
5. Interestingly, sulfate addition lowers the total oxidation of *n*-octane to CO₂ in all three investigated systems (buffer-free, HM and PPM), which contradicts expectations for TSR. XRD analyses as well as a thermodynamic evaluation verify that siderite (FeCO₃) precipitation is not an explanation for this observation. A change in the reaction network toward an LSC pathway could, however, offer a suitable explanation for the observed decrease in the oxidation of hydrocarbons to CO₂ upon sulfate addition.

6. Presence of minerals (HM and PPM) influence the reaction network to various extents:
 - a. Results confirm findings of other studies suggesting that individual minerals of the hematite-magnetite and pyrite-pyrrhotite-magnetite buffers can act as catalysts and reactants. However, this study expands the understanding by investigating mineral mixtures and not single minerals only.
 - b. Apart from the ability to act as catalyst and reactant, investigated mineral assemblages effectively acted as redox buffers during the experiments. Distribution of reaction products reflects more oxidizing conditions in presence of the HM than in presence of the PPM mineral buffers. This is the first time that the regulating influence of redox mineral buffers has been demonstrated in experiments investigating the reaction of hydrocarbons with sulfate.

5.

PART I-B

METASTABLE THERMODYNAMIC EQUILIBRIUM OF THE ALKANE-ALKENE AND ALKENE-KETONE REACTIONS

In *chapter 4* it has been shown that aqueous oxidation in addition to cracking are the dominating processes for aqueous *n*-octane decomposition in the water-containing experiments. In this chapter the results are evaluated with respect to equilibration of the alkane-alkane and alkene-ketone reactions. Experimental studies in a sulfate-free system by Seewald (1994, 2001) demonstrated that mineral redox buffers may influence redox-dependent organic-organic reactions in the way that they are pushed toward a metastable thermodynamic equilibrium state. A brief summary of his studies was presented in chapter 2.2.2, where a definition of the term “metastable thermodynamic equilibrium” can also be found. If *alkenes* were used as starting compounds, equilibration of alkanes and alkenes (Reaction 9), as well as equilibration of alkenes and ketones (Reaction 10) is possible in the experiments under hydrothermal conditions (300-350°C) in presence of the HMP and PPM buffers. In contrast, neither equilibration of alkanes and alkenes nor equilibration of ketones and alkenes is observed in presence of the HM mineral buffer under the same experimental conditions. If an *n-alkane*, e.g. *n*-heptane, was used as starting compound attainment of equilibrium for these compounds was also not observed in experiments, which were processed at 300°C in presence of the HMP and PPM buffers.

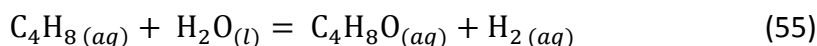
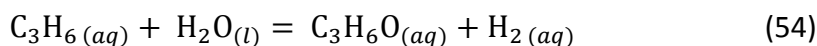
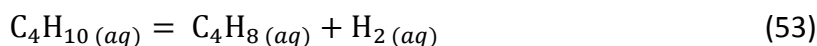
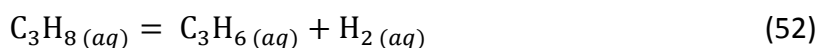
Reeves et al. (2012) showed, however, that at a slightly higher temperature of 323°C and in presence of the PPM mineral buffer, equilibration of ethane-ethene and propane-propene is possible if a mixture of C₁ to C₅ *n*-alkanes is used as starting compound. However, equilibrium states were only reached after 100 days experiment duration. Unfortunately, Reeves et al. (2012) do not provide data for ketones.

Based on this literature review, open questions remain like for example: Which role does the starting compound play? Is it possible to reach alkane-alkene equilibria within shorter run duration, if the temperature is raised in experiments using an *n*-alkane as starting compound, and is it possible to reach alkene-ketone equilibria in such experiments? It also remains unanswered, which effect the HM buffer has on equilibration of *n*-alkanes,

alkenes and corresponding ketones, if an *n*-alkane is used as starting compound. Last but not least, the effect of sulfate on the metastable thermodynamic equilibrium of *n*-alkanes, alkenes and corresponding ketones has not yet been investigated.

Experiments with *n*-octane performed in the course of the present PhD thesis extend the work of Seewald (1994, 2001) and Reeves et al. (2012), and offer a consistent data set to elucidate these points. In order to evaluate whether the alkane-alkene (Reaction 9, p. 17) and the alkene-ketone (Reaction 10, p. 17) reactions attained metastable equilibrium states during the experiments with the HM and PPM mineral buffers at 350°C, the molar propane/propene and butane/butene, as well as the molar acetone/propene and butanone/butene ratios were compared to corresponding equilibrium ratios predicted from thermodynamic calculations for the two buffer systems (Fig. 32).

The predicted ratios were calculated from expressions of the law of mass action for the propane-propene (Reaction 52), butane-butene (Reaction 53), propene-acetone (Reaction 54) and butene-butanone (Reaction 55) reactions:



with the general equations for the alkane/alkene (Equation 56) and ketone/alkene (Equation 57) ratios being as follows:

$$\log[\text{alkane}_{(aq)}/\text{alkene}_{(aq)}]_{\text{predicted}} = \log a_{\text{H}_2(aq)} - \log K \quad (56)$$

$$\log[\text{ketone}_{(aq)}/\text{alkene}_{(aq)}]_{\text{predicted}} = \log K - \log a_{\text{H}_2(aq)} \quad (57)$$

The equilibrium constants (K) for Reaction 52 to 55 are listed in Table 9. They were calculated using the SUPCRT92 computer program (Johnson et al., 1992) together with thermodynamic properties consistent with the SPRONS92.DAT database (see Johnson et al., 1992 for original sources) or taken from Amend and Helgeson (1997) for aqueous propane and *n*-butane. The standard state adopted for aqueous organic species is a hypothetical 1 molal solution referenced to infinite dilution at any temperature and pressure (Seewald, 2001). The standard state adopted for water is unit activity of the pure liquid at any temperature and pressure (Seewald, 2001).

As a first estimate, the equilibrium hydrogen activities that would be adjusted by the mineral buffers at 350°C are used to calculate predicted alkane/alkene and ketone/alkene ratios. The corresponding $\log a_{\text{H}_2(aq)}$ values are -4.3 and -3.2 for the HM and PPM buffer respectively (see *chapter 3.6.1* for details on the calculation). An uncertainty of ± 0.2 log units for predicted ratios is assumed to be realistic taking uncertainties in thermodynamic data in consideration (Hentscher, personal communication). Furthermore, the potential implication of lower hydrogen concentrations is evaluated in the discussion, because the aqueous hydrogen concentration might be up to 0.5 log units below expected equilibrium values (see discussion for details).

Table 9: Equilibrium constants calculated with SUPCRT92 for individual alkane-alkene and alkene-ketone reactions at 350°C and 35 MPa.

Reactions of interest		log K
alkane-alkene	$\text{C}_3\text{H}_8(aq) = \text{C}_3\text{H}_6(aq) + \text{H}_2(aq)$	-5.64
	$\text{C}_4\text{H}_{10}(aq) = \text{C}_4\text{H}_8(aq) + \text{H}_2(aq)$	-5.66
alkene-ketone	$\text{C}_3\text{H}_6(aq) + \text{H}_2\text{O}(l) = \text{C}_3\text{H}_6\text{O}(aq) + \text{H}_2(aq)$	-0.67
	$\text{C}_4\text{H}_8(aq) + \text{H}_2\text{O}(l) = \text{C}_4\text{H}_8\text{O}(aq) + \text{H}_2(aq)$	-0.29

5.1 RESULTS

5.1.1 MOLAR ALKANE/ALKENE RATIOS

Regarding the experimental data for the alkane/alkene ratios, the same relative variations between individual samples can be observed, if the propane/propene and the butane/butene ratios are compared (Fig. 32 A & B). In contrast to the buffer-free system, alkane/alkene ratios remain constant in the HM and PPM mineral buffered system, if sulfate is added. In the HM system, experimental alkane/alkene ratios are in good agreement with predicted ones. In the PPM system, alkane/alkene ratios for experimental samples are one order of magnitude below predicted values. Time series data for the sulfate-containing PPM samples (*PPM C_{8+N₀} 350°C*) show that the molar propane/propene ratio increases with time, from a log ratio of 1.1 ± 0.1 mol/mol after 72 hours to a log ratio of 1.7 ± 0.1 mol/mol after 336 hours (Table A1 in the appendix).

5.1.2 MOLAR KETONE/ALKENE RATIOS

In contrast to the alkane/alkene ratios, molar ketone/alkene ratios for the experimental samples do not remain constant in the HM and PPM samples if sulfate is added. Instead they decrease in all three investigated systems if sulfate is present (Fig. 32 C & D). The strongest decrease is observed for the PPM samples, with -0.45 log units for the acetone/propene and -0.58 log units for the butanone/butene ratio. Interestingly, the molar ketone/alkene ratios are the same within uncertainty for all sulfate-containing samples in the three investigated systems (-buf, HM and PPM). In absence of sulfate, these ratios do, however, show slight variations. Note that experimental ketone/alkene ratios are one to three orders of magnitude below predicted values with the deviation being the strongest in case of the HM buffer.

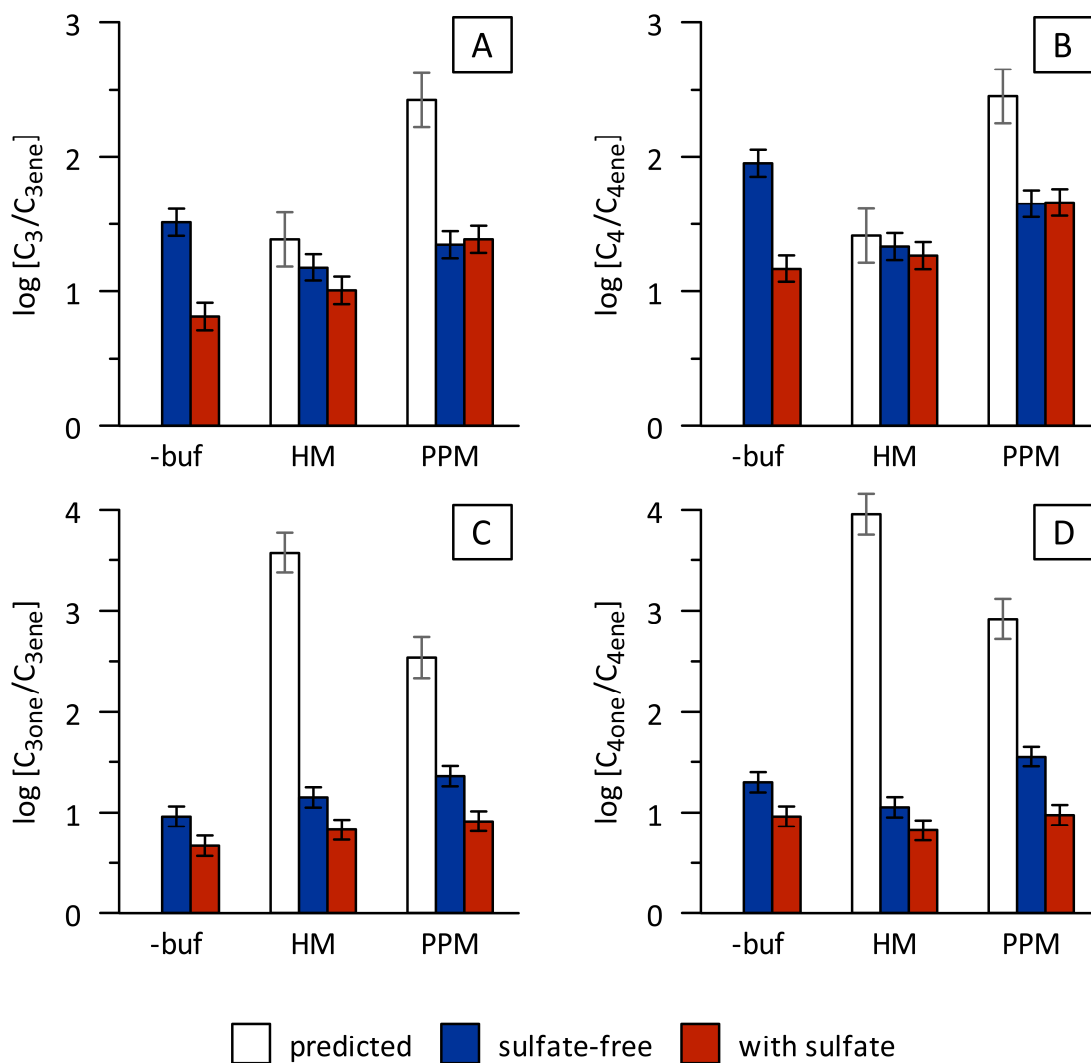


Fig. 32: Molar alkane/alkene (A and B) and ketone/alkene ratios (C and D) for sulfate-free and sulfate-containing samples in the three investigated systems (-buf = no mineral buffer, PPM = pyrite-pyrite-magnetite, HM = hematite-magnetite) after 168 h at 350°C and 35 MPa. For comparison predicted ratios calculated for mineral-buffered conditions at equilibrium in a sulfate-free system are shown. The uncertainty for the predicted ratios is ± 0.2 log units, and 0.1 log units for ratios calculated from experimental data.

5.2 DISCUSSION

5.2.1 EVALUATING THE ATTAINMENT OF EQUILIBRIUM FROM COMPARISON OF PREDICTED AND EXPERIMENTAL RATIOS

Alkane-Alkene Reactions

Regarding the HM samples, molar alkane/alkene ratios for the sulfate-free and sulfate-containing samples are in good agreement with predicted ratios (Fig. 32 A & B). This suggests that the HM buffer effectively controlled the hydrogen concentration to, or if sulfate is present at least close to the expected equilibrium value. Results indicate that reaction rates for the propane-propene and butane-butene reaction seem to be sufficiently fast at 350°C for alkanes to attain a redox-dependent metastable thermodynamic equilibrium state with corresponding alkenes within 168 h.

In contrast to the HM system, results for the PPM samples show that predicted and experimental alkane/alkene ratios do not agree (Fig. 32 A & B). It is however conspicuous why *n*-alkanes and alkenes seem to equilibrate in the HM system and not in the PPM system. Especially, because results presented by Seewald (2001) for experiments with alkenes as starting compounds show that equilibration of alkenes with corresponding *n*-alkanes should be promoted in sulfur-containing systems rather than in the HM system without initial sulfur being present (Table 2, p. 19). Regarding results of the present study, we see that the difference between experimental alkane/alkene ratios for the HM and PPM samples are smaller than expected. This is in line with results presented by Hinze (bachelor thesis 2012), which show that the hydrogen activity adjusted by the PPM mineral buffer under the experimental conditions may be up to 0.3 and 0.5 log units below the expected equilibrium value for the sulfate-free and respectively sulfate-containing experiments. Consequently, predicted alkane/alkene ratios for the PPM system can drop to a value of 2. As a result, the difference between the values for predicted and experimental ratios would decrease. Based on these observations, it is hypothesized that *n*-alkanes may have reached, or almost approached equilibrium with corresponding alkenes in dependence on the actual hydrogen activity prevailing during the experiments, which is not necessarily the equilibrium one.

One possible explanation why the HM buffer might reach equilibrium during the experiments, but not the PPM buffer, is that both are characterized by different

equilibration kinetics. In case of the HM buffer only two minerals have to equilibrate, whereas there are three in the PPM system. Results from Hinze (bachelor thesis 2012) for sulfate-free and sulfate-containing experiments with the same PPM buffer and water (no hydrocarbons!) show that the PPM buffer does move toward equilibrium in the investigated time frame ranging from 24 to 168 h (Fig. C1). This is supported by the increase of the propane/propene ratio with time, which is observed for the sulfate-containing PPM samples processed at 350°C (Table A1 in the appendix).

In the buffer-free experiments (Fig. 32 A & B) the activity of aqueous hydrogen is not controlled. In contrast to the mineral-buffered systems, sulfate addition lowers the alkane/alkene ratios. A lowering of the alkane/alkene ratio is in line with expectations for TSR controlled reactions (cf. *chapter 4.3.2.1*). The observation that the alkane/alkene ratio remains very similar upon sulfate addition in the mineral-buffered systems, but is lowered significantly in absence of mineral buffers if sulfate is added, provides further evidence that presence of mineral buffers influences the reaction network.

Alkene-Ketone Reactions

In contrast to the dataset obtained for alkane/alkene ratios, decreasing ketone/alkene ratios (Fig. 32 C & D) upon sulfate addition indicate that the alkene-ketone reactions do not seem to be controlled by the mineral buffers. This is also confirmed by the observation that experimental ketone/alkene ratios are one to three orders of magnitude below predicted ratios. The deviation would even be greater, if we consider that the actual hydrogen activity might be up to 0.5 log units lower than expected. Results from the present study provide evidence that the alkane-alkene reaction equilibrate faster than the alkene-ketone reaction, if an *n*-alkane is used as starting compound. This is right the opposite for Seewald's (2001) findings for experiments with an alkene as starting compound. Observed differences are further elucidated below.

5.2.2 EVALUATING THE THERMODYNAMIC DRIVE FOR THE REACTIONS

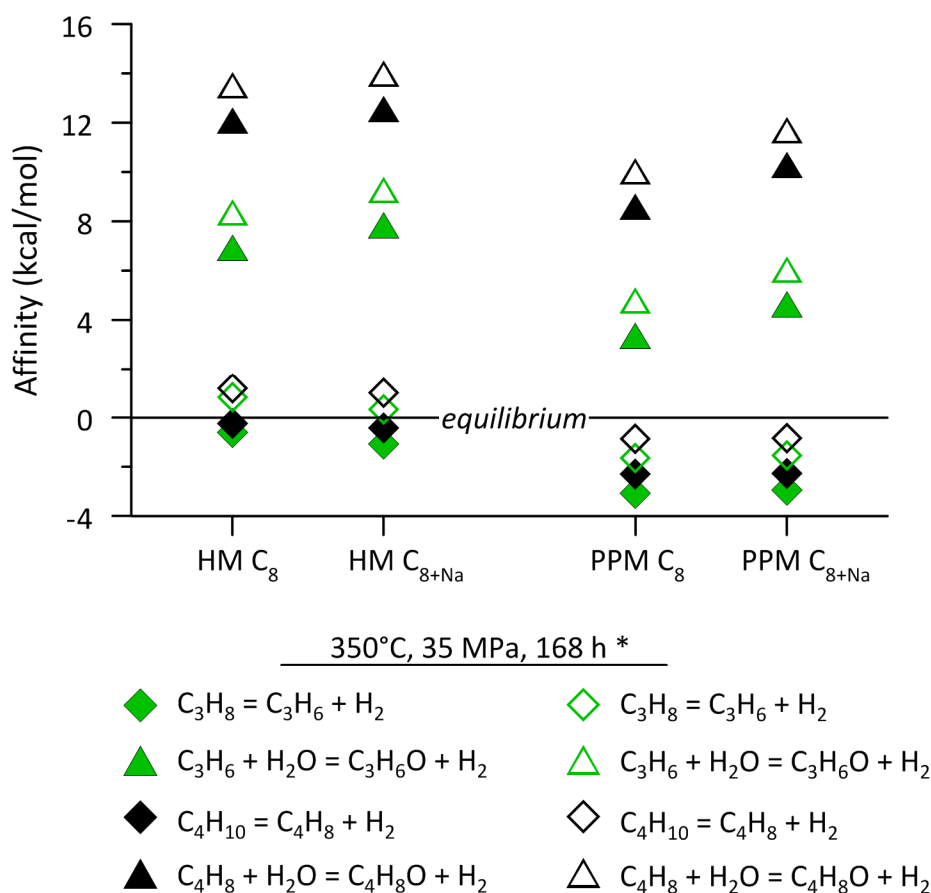
Comparison of predicted and experimental ratios provides compelling evidence that redox-dependent metastable thermodynamic equilibrium seems possible for alkane-alkene reactions but not for the alkene-ketone reactions, if *n*-octane is used as starting compound

(cf. *chapter 5.2.1*). However, the comparison cannot reveal the state of the reaction systems, i.e. the driving force of individual reactions as well as information on their preferred direction. This information is, however, crucial to understand the reaction network. In order to get more insight into the driving force and preferred direction of reactions, results were evaluated thermodynamically in greater detail. For this purpose, chemical affinities (Reaction 42) were calculated for the propane-propene (Reaction 52), butane-butene (Reaction 53), propene-acetone (Reaction 54) and butene-butanone (Reaction 55) reactions from results for the sulfate-free and sulfate-containing HM and PPM samples that were processed at 350°C for 168 h (Fig. 33). Positive affinities indicate that a thermodynamic drive for a reaction exists to proceed from left to right. Negative affinities indicate the opposite. A chemical affinity of 0 ± 1 kcal/mol reflects thermodynamic equilibrium. Equilibrium constants for the investigated reactions are listed in Table 9. Corresponding reaction quotients (Q) were calculated from measured aqueous concentrations¹⁴ of n -alkanes, alkenes and ketones, and the assumption that activity coefficients for these species are equal to unity. This is in accordance with Seewald (2001). The standard state adopted for liquid H₂O is assumed to be one of unit activity of the pure liquid at any temperature and pressure (Seewald, 2001). For hydrogen, expected equilibrium activities adjusted by the mineral buffers were taken as a first estimate for the calculation of Q , i.e. $\log a_{\text{H}_2(aq)}$ values of -4.25 and -3.21 for the HM and PPM buffer respectively. Owing to potential disequilibrium and resulting hydrogen activities that may be up to 0.5 log units lower (cf. *chapter 4.3.2.1*), reaction quotients and corresponding affinities are also calculated for this incidence. General formulas for the reaction quotient for the alkane-alkene and alkene-ketone reactions are as follows:

$$\log Q = \log a_{\text{alkene}(aq)} + \log a_{\text{H}_2(aq)} - \log a_{\text{alkane}(aq)} \quad (58)$$

$$\log Q = \log a_{\text{ketone}(aq)} + \log a_{\text{H}_2(aq)} - \log a_{\text{alkene}(aq)} \quad (59)$$

¹⁴Molal (mol/kg H₂O) concentrations for aqueous compounds are obtained from concentrations listed in Table A1 in the appendix through division by 1000 subsequent multiplication by the molar amount of initial n -octane (3.064×10^{-5} mol), and final division by the amount of water (9×10^{-5} kg).



*Chemical affinities were calculated for two different hydrogen activities.

Filled symbols represent values, which were calculated using the hydrogen activities, which are expected to adjust if the buffers reach equilibrium at the experimental conditions ($\log a_{\text{H}_2(\text{aq})} = -3.21$ for PPM and -4.25 for HM)

Blank symbols represent values, which were calculated using the hydrogen activities, which are 0.5 log units below expected equilibrium values for the two buffers.

Fig. 33: Calculated chemical affinities for selected alkane-alkene (diamonds) and alkene-ketone (triangles) reactions. Calculated values are specific for the experimental conditions, i.e. 350°C and 35 MPa, and run duration of 168 h. Positive affinities indicate that a thermodynamic drive for a reaction exists to proceed from left to right. Negative affinities indicate the opposite. A chemical affinity of 0 ± 1 kcal/mol is obtained if the reaction under investigation reached the metastable thermodynamic equilibrium state. Chemical affinities were calculated for two different hydrogen activities, because the actual hydrogen concentration during the experiments may be up to 0.5 log units lower than expected equilibrium values for the mineral buffers (cf. *chapter 4.3.2.1*). According to Seewald (2001), an uncertainty of ± 1 kcal/mol is realistic for calculated affinity values.

Alkane-Alkene Reactions

Calculated chemical affinities of 0 ± 1 kcal/mol provide support for the attainment of a metastable thermodynamic equilibrium state for the propane-propene and butane-butene reactions in the sulfate-free and sulfate-containing HM experiments, which were processed for 168 h at 350°C (Fig. 33). Corresponding values for the sulfate-free PPM samples are slightly negative, but are very close to equilibrium if it is considered that the actual hydrogen activity during the experiments may be 0.3 to 0.5 log units lower. Based on these findings, it

can be inferred that a thermodynamic drive exists for alkane-alkene equilibration and that reaction kinetics are sufficiently fast for the propane-propene and butane-butene reactions to attain or closely approach the metastable thermodynamic equilibrium state after 168 h at 350°C.

Alkene-Ketone Reactions

The more interesting picture is, however, provided by calculated affinities for the propene-acetone and butene-butanone reactions for the sulfate-free and sulfate-containing HM and PPM experiments, which were run at 350°C for 168 h. Here, all affinities are positive, ranging from 3 to 13 kcal/mol (Fig. 33). Thus, a strong thermodynamic drive should exist for the conversion of alkenes to ketones in presence and absence of sulfate, but no equilibration of these compounds was observed. The simplest explanation could be that reaction kinetics represents the limiting factor. Results from Seewald (2001) and Reeves et al. (2012) indicate, however, that reaction kinetics for the alkane-alkene and alkene-ketone reactions should be sufficiently fast at 350°C.

5.2.3 THE ROLE OF THE STARTING COMPOUND AND OF THE REACTION NETWORK

It has been shown that the reaction scheme proposed by Seewald (2001) for aqueous oxidation can be used as a first estimate to describe the reaction network responsible for *n*-octane decomposition during the water-containing experiments (cf. *chapter 4*). In this sequence the formation and transformation of *n*-alkanes, alkenes and ketones are interdependent. This can have important implications for possible alkane-alkene and alkene-ketone equilibration if an *n*-alkane or an alkene is used as starting compound, which will be discussed below.

Results from this study, in combination with the results from Seewald (2001) and Reeves et al. (2012), provide evidence that the alkene-ketone reaction equilibrate faster than the alkane-alkene reaction, if an alkene is used starting compound in contrast to experiments, which initially contained an *n*-alkane. In experiments with 1-butene, for example, which were processed in presence of the PPM buffer and in the temperature range of 300 to 350°C, at a pressure of 35 MPa and for a total run duration of 8000 h, Seewald (2001) observed that the propene-acetone as well as the butene-butanone reactions reach

thermodynamic equilibrium at all temperatures within 200 h (Fig. 34 A & B). In contrast, the butane-butene and the propane-propene reactions only reach thermodynamic equilibrium after 4 months at the highest temperature during the same experiments (Fig. 34 C).

Data from Seewald, 2001

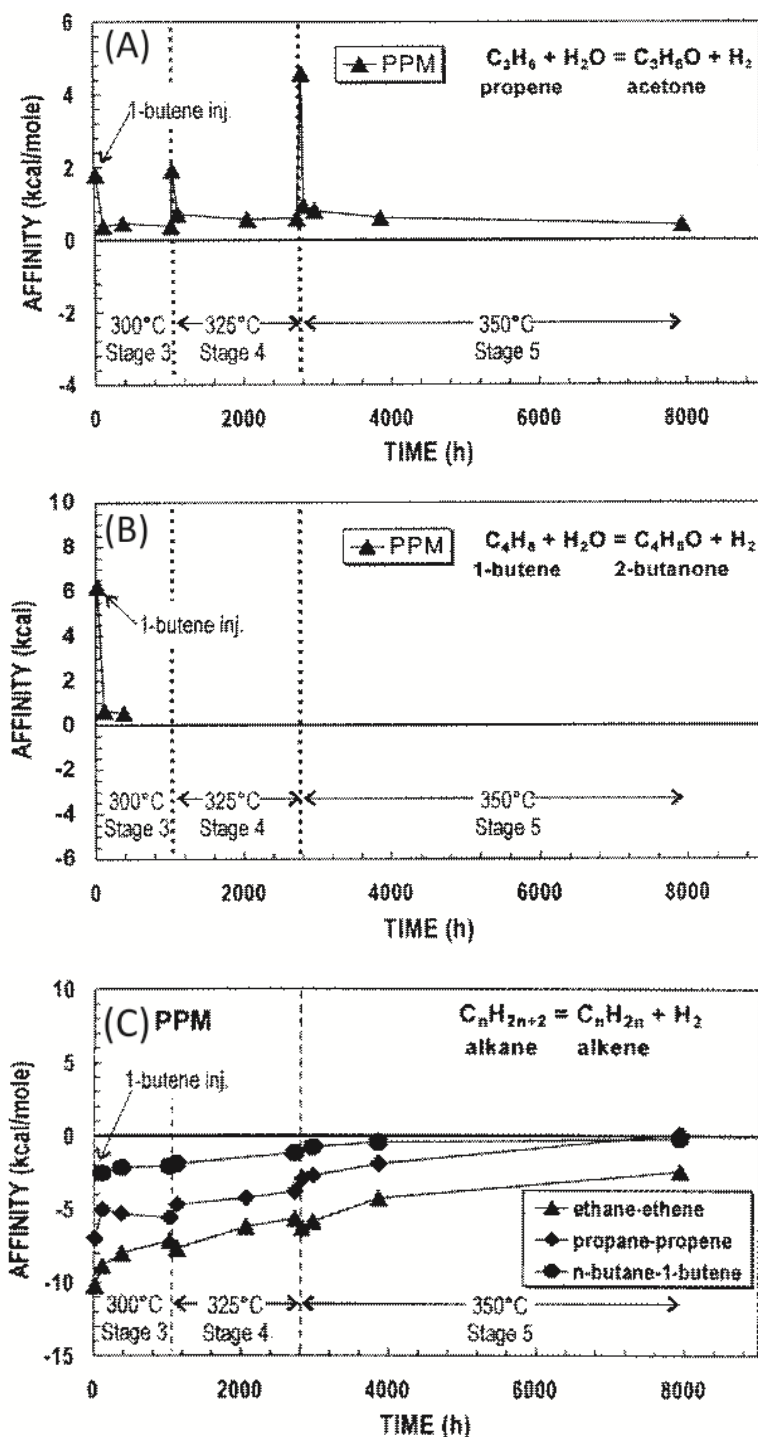


Fig. 34: Data from Seewald (2001), showing calculated chemical affinities for individual (A) alkane-alkene and alkene-ketone (B and C) reactions. Positive affinities indicates a thermodynamic drive for a reaction to proceed from left to right as written, whereas negative affinities indicate the opposite. A chemical affinity of 0 ± 1 kcal/mol indicates metastable thermodynamic equilibrium for the reaction of interest. Adapted from Seewald (2001) with kind permission of Pergamon.

Based on these observations, it seems to be crucial at which step the reaction network is entered. If an *n*-alkane is used as starting compound, alkenes are the first products generated by aqueous oxidation. Only then, ketones may be produced involving alcohols as intermediates. Consequently, the formation of ketones will depend on the rate of the alkane-alkene, the rate of the alkene-alcohol and finally the rate of the alcohol-ketone reactions. This dependency on preceding reactions seems to hamper alkene-ketone equilibration if an *n*-alkane is used as starting compound. In contrast, if an alkene is used as starting compound, the initial step can be skipped, facilitating alkene-ketone equilibration. Furthermore, results for organic reaction products (cf. *chapter 4*), show that the relative abundance of alkenes and especially of ketones, and therefore the molar ketone/alkene ratios, may be significantly affected by a change in the reaction network if sulfate is added. Sulfate addition lowers, for example, the conversion of alkenes to ketones and CO₂ in all three investigated systems (-buf, HM and PPM). This obviously affects the relative abundance of alkenes and ketones, and may therefore amplify disequilibrium of these compounds.

5.3 CONCLUSIONS

Results for experiments with *n*-octane processed with and without sulfate in presence of the HM and PPM buffers indicate that metastable thermodynamic equilibrium of *n*-alkanes and corresponding alkenes is reached or closely approached within 168 h at 350°C, whereas this is not the case for alkenes and corresponding ketones. This is the first time that the regulating influence of redox mineral buffers on equilibration of organic reactions has been demonstrated experimentally in a sulfate-containing system.

Observations from the experiments in this study are right opposite to those of Seewald (2001), who performed similar experiments in a sulfate-free system, in which alkenes were used as starting compounds. Here, alkene-ketone reactions equilibrate faster than corresponding alkane-alkene reactions. In order to interpret findings of this study, observations from Seewald (2001) and Reeves et al. (2012) were taken into consideration with the following results:

1. The starting compound plays a critical role because it determines at which step the reaction network for aqueous oxidation is entered. If it is entered at the second step, as in the case of alkenes, the alkane-alkene reaction, which seems to be rate-limiting for alkene-ketone equilibration, may be jumped over, facilitating equilibration of alkenes and ketones.
2. It is crucial to consider the reaction of interest in the context of the whole reaction network because preceding, subsequent and parallel reactions can strongly influence the reaction of interest. This observation is in agreement with Seewald (2001). As highlighted in the first point, this may explain why metastable equilibrium can be reached in one case but not in the other.
3. Findings indicate that alkenes, or possibly their precursors, seem to have a bottleneck character for the thermal decomposition of *n*-alkanes. This confirms the suggestion of Seewald (2001), who stated that “alkene formation may represent the rate limiting step during *n*-alkane oxidation”.
4. Interestingly, in presence of sodium sulfate a very similar degree of equilibration was observed for alkanes and alkenes in the mineral buffered systems if compared to corresponding sulfate-free experiments. In contrast, the alkane/alkene ratio is significantly lowered if sulfate is added in absence of mineral buffers, which is in line with expectations for TSR controlled reactions. From these observations it is inferred that the influence of redox mineral buffers on equilibration of organic reactions has implications for the TSR process and the associated reaction network.

6.

PART II

EFFECT OF DISSOLVED TRANSITION METAL SULFATES ON THE DEGRADATION OF *N*-OCTANE UNDER HYDROTHERMAL CONDITIONS

The reactivity of dissolved alkali (Na_2SO_4) and alkaline (MgSO_4 and CaSO_4) earth metal sulfates toward hydrocarbons has been investigated in numerous studies (e.g. Cross et al., 2004; Zhang et al., 2007; Zhang et al., 2008a; Zhang et al., 2008b; Lu et al., 2010b; Lu et al., 2011). However, such data have not yet been published for transition metal sulfates.

Solid and dissolved transition metals are ubiquitous in sedimentary basins, like for example in minerals (Mango, 1997a and references therein; Seewald, 2001), oil field brines (Kharaka et al., 1977; Saunders and Swann, 1990) or petroleum (Manning and Gize, 1993). Thus, it seems likely that hydrocarbons can be altered by transition metals during different stages of reservoir formation, i.e. during petroleum generation, expulsion, migration and storage. Furthermore, reaction of dissolved transition metals and dissolved sulfate with organic matter can be of fundamental importance during sulfide ore formation (Fig. 35). This has been demonstrated by studies investigating Mississippi-Valley type deposits (Leventhal, 1990) and the Kupferschiefer (Sun and Püttmann, 2000).

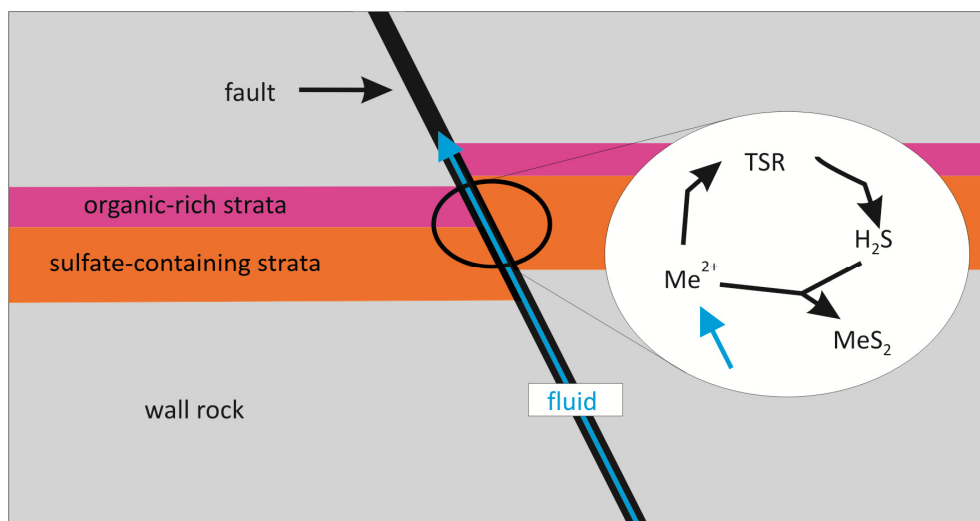


Fig. 35: Simplified geological block diagram illustrating a possible scenario for thermochemical sulfate reduction (TSR) in the environment of sulfide ore deposits that are associated with organic matter. A fluid, which contains transition metals migrates along a fault. If it passes sulfate-containing strata on its way, the fluid may dissolve sulfate. If this fluid reaches strata, rich in organic matter, TSR may occur with the result of metal sulfide precipitation. In order to achieve massive sulfide precipitation it is likely that the fluid is captured near the organic facies.

In order to investigate the reaction of dissolved transition metal cations with hydrocarbons in presence of sulfate, a consistent experimental series with *n*-octane and five transition metal sulfate (TMS) solutions (FeSO_4 , $\text{Fe}_2(\text{SO}_4)_3$, NiSO_4 , CuSO_4 and ZnSO_4) was conducted. For each metal three different dilutions were studied. Furthermore, duplicate samples containing the pure Na_2SO_4 solution were processed as reference for 0 % TMS. These samples and the pure transition metal sulfate solution (100 % TMS) set the two end points in the dilution series. In the samples, which are labeled by TM_mix1 and TM_mix2, both solutions were mixed in a ratio of 1:4 and 1:1 (TMS:Na, volumetric basis) respectively (Table 10). Thus, the molar fraction of the transition metal sulfate in the experimental charge steadily increases from 0 to 1 according to the following sequence:

Dilution series: $\text{TM} > \text{TM_mix2} > \text{TM_mix 1} > \text{Na}$

All samples were processed at 315°C and 13 MPa for 168 h. In this chapter, first results are presented.

6.1 STARTING CONDITIONS

Starting conditions for the transition metal sulfate experiments need to be evaluated to address the reacting system and to facilitate data interpretation. The following points are considered: What is the amount of atmospheric oxygen added to the experimental charge during sample preparation? Furthermore it needs to be clarified whether the fluid is composed of a single phase, and whether the transition metal sulfates remain soluble under the experimental conditions. Last but not least, information on the starting pH is given to determine, if TSR may have been catalyzed during the experiments.

Oxygen Contamination from Air

Based on the results for the pure *n*-octane sample, which was processed at 350°C for 168 h it was calculated that up to 28 vol% of residual air remain in the samples once the sample container is sealed (cf. *chapter 4.3.1*). The amount of air in the sample container may not be constant. However, the calculated percentage is considered to be a realistic value for

air contamination during sample preparation with the argon flushing method and can therefore be taken as first estimate for the transition metal sulfate samples. In order to calculate the molar concentration of oxygen in the samples from this percentage, the free gas volume in the sample containers needs to be determined. Two different gold tube sizes were used for the transition metal sulfate experiments, with one having the dimension (inner diameter x length) 5 mm x 25 mm, and the other one having the dimension 4 mm x 40 mm, resulting in a total volume of 491 and 503 μl respectively. All samples contained a total fluid volume of 205 μl (5 μl *n*-octane + 200 μl sulfate solution). Thus, the resulting free volume is 286 and 298 μl respectively. It may be further reduced during welding of the sample container, but this is neglected here because we want to quantify the maximal possible oxygen contamination. If the free volume contained 28 vol% of air, the absolute amount of oxygen (O_2) introduced would equal 0.7 μmol . In addition to that, water, which is the solvent for the sulfate solutions, may dissolve up to 3 vol% O_2 at room temperature (Holleman and Wiberg, 1995). This could introduce up to 0.2 additional μmol of oxygen (O_2), if a fluid volume of 200 μl is considered. It is suggested that oxygen dissolved in *n*-octane can be neglected, because *n*-octane was always freshly taken from the container, i.e. it was never in contact with air for a long time. Furthermore, the fluid volume of the organic phase is very small compared to the free gas volume and that of the aqueous phase. Based on these considerations it is inferred that up to 0.9 μmol O_2 may be introduced as contamination into the sample container during sample preparation. This might be critical for all samples with low conversion ($\leq 2\%$), because in this case the total amount of oxygen incorporated in the reaction products is either very similar to or even smaller than the possible oxygen input from air (Table A2 in the appendix; 0.9 μmol O_2 would equal 29 $\text{mmol}_{\text{O}_2}/\text{mol}_{\text{C}_8\text{H}_{18}}$).

Aqueous Solubility of Transition Metal Sulfates and Na_2SO_4 at 315°C and 13 MPa

It is necessary to estimate the aqueous sulfate and transition metal cation concentrations, because educt concentrations may influence the reaction rate. Furthermore, it is valuable to know if the transition metal sulfates are completely soluble under the experimental conditions or if a precipitate may form that could possibly act as surface catalyst.

At room temperature, the concentration of Na_2SO_4 and of all transition metal sulfates in the stock solutions does not exceed the maximum solubility. With increasing temperature a decreasing solubility is, however, observed for all employed transition metal sulfates with the exception of NiSO_4 (Table 10). Due to a lack of appropriate solubility data published in literature for high temperatures, solubilities of transition metal sulfates at experimental temperature (315°C) and pressure (13 MPa) were calculated by Michael Hentscher using the Geochemist's Workbench (for details see *chapter 3.6.3*). The objective of the modeling was to determine initial conditions of the reacting system at experimental conditions. Modeled values are regarded to closely match the starting conditions, but should only be viewed as rough estimate for solubilities during the course of the experiments. One reason for this is that organometallic complexes with organic acid anions (Manning and Gize, 1993) might form, which would lower the activity of dissolved transition metals. Another factor that could lower the activity of dissolved transition metals is the precipitation of metal sulfides, which could be a consequence if TSR occurred (Machel et al., 1995). Both possibilities are not considered in the model.

Pure Metal Sulfate Solutions

In samples that contain the pure metal sulfate solutions, the initial sulfate and metal cation concentrations in solution are controlled by the solubilities of the metal sulfates at experimental conditions. Only for Na_2SO_4 and NiSO_4 saturation is not reached at experimental conditions, meaning that the modeled solubility at 315°C and 13 MPa is well above the metal sulfate concentration of the stock solution at room temperature and pressure (Table 10). In contrast, saturation for the other transition metal sulfates is reached under experimental conditions and only 0.14 % (FeSO_4) to 31 % (ZnSO_4) of the initial amount can be dissolved at 315°C and 13 MPa (Table 10).

In addition to that, modeling with the Geochemist's Workbench indicate that hematite (Fe_2O_3) and goethite ($\alpha\text{-FeO(OH)}$) can precipitate at experimental conditions in samples containing Fe(III) sulfate (Hentscher, personal communication).

Mixed Solutions of Na_2SO_4 and Transition Metal Sulfates

Mixed sulfate solutions were not modeled by Michael Hentscher. The initial sulfate and metal cation concentrations in solution can, however, be estimated from the modeled

solubilities of the pure metals sulfate solutions under the requirement that chemical interactions between the metals are negligible. This is appropriate for a first estimation. The procedure is described below and results are summarized in Table 10.

If the transition metal sulfate is completely soluble at experimental conditions, the dilution by the sodium sulfate solution is considered to be the only factor that determines the metal cation concentration in solution. Out of all investigated metal sulfates, this is only the case for NiSO₄. Here, the aqueous concentration of Ni²⁺ increases by a factor of 2 in each dilution step, except in the first one (*Na* → *Ni_mix1*). The aqueous sulfate concentration remains constant at (0.5 mmol_{SO₄⁻²}/kg_{H₂O}) in all Ni-containing samples.

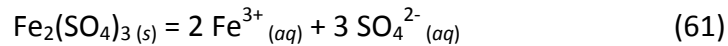
In contrast, solubilities for FeSO₄, CuSO₄ and Fe₂(SO₄)₃ are extremely low under experimental conditions, wherefore their sulfate input to the solution is negligible compared to that of sodium sulfate. Thus, the initial sulfate concentration in the mixed solutions (*c_{initial}SO₄²⁻_(aq)*) is controlled by Na₂SO₄ and varies from 0.25 to 0.40 mmol_{SO₄⁻²}/kg_{H₂O} (Table 10).

ZnSO₄ has an intermediate solubility, which implies that the possible sulfate contribution stemming from ZnSO₄ needs to be taken into account. Here, the initial sulfate concentration in the mixed solutions under experimental conditions is:

$$\text{For ZnSO}_4 \text{ samples: } c_{\text{initial}} \text{SO}_4^{2-}(\text{aq}) = c\text{Na}_2\text{SO}_4(\text{aq}) + c\text{ZnSO}_4(\text{aq}) \quad (60)$$

with the aqueous concentration of Na₂SO₄ and ZnSO₄ being those at experimental conditions. For Na₂SO₄ this corresponds to the modeled value at 315°C and 13 MPa. For ZnSO₄ the actual solubility under experimental is, however, lower than the modeled value. This is because sulfate introduced from Na₂SO₄ can have a significant effect on the solubility of transition metal sulfates. This needs to be taken into account for all investigated transition metal sulfates, which reach saturation at experimental conditions (ZnSO₄, Fe₂(SO₄)₃, CuSO₄ and FeSO₄). In order to evaluate this aspect, solubility products at experimental conditions were calculated using the transition metal sulfate solubilities modeled for 315°C and 13 MPa. Solubility products for FeSO₄, CuSO₄ and ZnSO₄ were calculated analogue to the following example for Fe₂(SO₄)₃:

1. Establish Dissociation Reaction



Prerequisite is the assumption that metal sulfate is completely dissociated.

2. Establish Law of Mass Action

$$K_{\text{Fe}_2(\text{SO}_4)_3} = \frac{(c\text{Fe}^{3+} (aq))^2 \times (c\text{SO}_4^{2-} (aq))^3}{a_{\text{Fe}_2(\text{SO}_4)_3 (s)}} \quad (62)$$

Note: The activity of a pure solid is, by definition, equal to one.

3. Calculate Solubility Product (K_{sp})

$$K_{sp_Fe_2(SO_4)_3} = (c\text{Fe}^{3+} (aq))^2 \times (c\text{SO}_4^{2-} (aq))^3 \quad (63)$$

with $c\text{Fe}^{3+} (aq) = 2 \times c\text{Fe}_2(\text{SO}_4)_3 (aq)$ and $c\text{SO}_4^{2-} (aq) = 3 \times c\text{Fe}_2(\text{SO}_4)_3 (aq)$. The aqueous solubility of Fe(III) sulfate ($c\text{Fe}_2(\text{SO}_4)_3 (aq)$) under experimental conditions is given in Table 10. With that, the calculated solubility product of $\text{Fe}_2(\text{SO}_4)_3$ at 350°C and 13 MPa is $1.78 \times 10^{-10} \text{ mol}^5/\text{kg H}_2\text{O}^5$.

The concentration of the transition metal cation (TM) in solution under experimental conditions can then be calculated from the solubility product (K_{sp}):

$$\text{For } \text{FeSO}_4, \text{CuSO}_4 \text{ and } \text{ZnSO}_4 \text{ samples: } c\text{TM}^{2+} (aq) = \frac{K_{sp_TMS}}{c_{\text{initial}} \text{SO}_4^{2-} (aq)} \quad (64)$$

$$\text{For } \text{Fe}_2(\text{SO}_4)_3 \text{ samples: } c\text{Fe}^{3+} (aq) = \sqrt{\frac{K_{sp_Fe_2(SO_4)_3}}{(c_{\text{initial}} \text{SO}_4^{2-} (aq))^3}} \quad (65)$$

with the aqueous sulfate concentration being the initial one at experimental conditions.

Table 10: Expected solubilities of Na₂SO₄ and transition metal sulfates at 315°C and 13 MPa, and resulting estimates on initial concentrations of aqueous sulfate and aqueous transition metal cations at experimental conditions. Values marked in **orange** indicate that saturation for the transition metal sulfates is reached at experimental conditions (maximum solubility at 315°C and 13 MPa < concentration in stock solution), whereas values in **green** indicate that transition metal sulfates remain completely soluble.

Transition Metal Sulfate (TMS)	Concentration of stock solution (mol/kg H ₂ O)	Maximum solubility at 315°C and 13 MPa (mol/kg H ₂ O)	Solubility product at 315°C and 13 MPa	Sample ID	Volume of stock solution in the sample		Calculated initial concentration at 315°C and 13 MPa (mol/kg H ₂ O)		Expected solubility of initial TMS at experimental conditions
					TMS (μl)	Na ₂ SO ₄ (μl)	SO ₄ ²⁻ _(aq)	TM cation _(aq)	
Na ₂ SO ₄	0.50	1.3	8.8 mol ² /kg ²	Na	0	200	0.50	0	-
FeSO ₄	0.27	3.8 × 10 ⁻⁴	1.4 × 10 ⁻⁷ mol ² /kg ²	Fe(II)_mix1	40	160	0.40	3.5 × 10 ⁻⁷	6.5 ppm
				Fe(II)_mix2	100	100	0.25	5.6 × 10 ⁻⁷	4.2 ppm
				Fe(II)	200	0	3.8 × 10 ⁻⁴	3.8 × 10 ⁻⁴	0.14 %
Fe ₂ (SO ₄) ₃	0.17	4.4 × 10 ⁻³	1.8 × 10 ⁻¹⁰ mol ⁵ /kg ⁵	Fe(III)_mix1	42	158	0.40	5.4 × 10 ⁻⁵	753 ppm
				Fe(III)_mix2	84	116	0.29	8.5 × 10 ⁻⁵	598 ppm
				Fe(III)	200	0	0.013	8.8 × 10 ⁻³	2.59 %
NiSO ₄	0.50	40	1600 mol ² /kg ²	Ni_mix1	40	160	0.50	0.10	100 %
				Ni_mix2	100	100	0.50	0.25	100 %
				Ni	200	0	0.50	0.50	100 %
CuSO ₄	0.48	2.5 × 10 ⁻³	6.3 × 10 ⁻⁶ mol ² /kg ²	Cu_mix1	40	160	0.40	1.6 × 10 ⁻⁵	163 ppm
				Cu_mix2	100	100	0.25	2.5 × 10 ⁻⁵	104 ppm
ZnSO ₄	0.45	0.14	0.020 mol ² /kg ²	Zn_mix1	40	160	0.43	0.046	51 %
				Zn_mix2	100	100	0.32	0.061	27 %
				Zn	200	0	0.14	0.14	31 %

As noted above, these considerations only provide estimates because they do not account for possible organic or inorganic metal complexing, which would affect the metal solubility during the experiments. In order to address the complexing issue, extensive geochemical modeling would be needed. This is beyond the scope of the study at this stage, and considerations presented here are suggested to be an appropriate first estimation.

To sum up, the sulfate concentration remains in a comparable range at experimental conditions for all samples (0.14 - 0.50 mmol_{SO₄²⁻}/kg_{H₂O}), except for those that contain the pure transition metal sulfates with very low solubilities (Table 10). In contrast, the aqueous concentration of transition metal cations shows large variations ranging from 0.35 μmol/kg_{H₂O} (Fe(II)_mix1) to 0.50 mol/kg_{H₂O} (pure Ni). This is due to significant solubility variations of transition metal sulfates at experimental conditions, which complicate a one-to-one comparison of samples with different metals, but the same dilution. General trends can, however, be addressed.

Aqueous Solubility of *n*-Octane at 315°C and 13 MPa

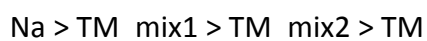
The aqueous solubility of *n*-octane at experimental conditions was calculated using SUPCRT 92 (cf. chapter 3.6.2). It is calculated that 0.15 mol of *n*-octane can be dissolved in 1 kg of water at a temperature of 315°C and a pressure of 13 MPa. This is exactly the concentration, which was added during sample preparation. Thus, the solution is close to saturation with respect to *n*-octane at experimental conditions.

The aqueous solubility of *n*-octane may be reduced due to presence of sulfate (Price, 1976). Owing to this so-called salting-out effect, addition of metal sulfates probably results in the separation of two fluid phases – an octane- and a water-dominated liquid phase. Phase separation could possibly affect kinetics of reactions controlling the decomposition of *n*-octane. The extent of this effect is unknown, but it is assumed that the system is dynamically mixed due to fluid convection in the sample container during the experiments.

pH

The *in situ* pH values of the pure metal sulfate solutions at the start of the experiments were modeled by Michael Hentscher (2013) using the Geochemist's Workbench software (see *chapter 3.6.3* for details). *In situ* pH refers to the initial pH at experimental conditions (315°C, 13 MPa). Owing to an enhanced auto-dissociation of water with increasing temperature, the neutral point of water shifts from 7 at room temperature and ambient pressure to a pH of 5.7 at experimental conditions (315°C and 13 MPa). Thus, the modeled *in situ* pH values for the transition metal samples (Table 11) reflect very acidic to alkaline conditions.

Modeled pH data for the mixed samples are not available at present, but work is underway to provide these data. It is, however, expected that *in situ* pH values for all mixed samples increase with increasing amounts of Na₂SO₄ added to the experimental charge (Hentscher, personal communication). This is confirmed by preliminary modeling results. Thus it is inferred that the following sequence for *in situ* pH values can be established in each transition metal (TM) series:



Zhang et al. (2008b; 2012), showed that low pH (≤ 3.5) can enhance TSR of MgSO₄ and CaSO₄. Thus, the low *in situ* pH of the pure Fe(II) and Fe(III) solutions and of the iron-containing mixed solutions with *in situ* pH values below 3.5, may have catalyzed TSR during the experiments.

Table 11: Modeled *in situ* pH values for pure transition metal sulfate solutions at 315°C and 13 MPa. Values were calculated by Michael Hentscher using the Geochemist's Workbench. Uncertainties are estimated to be ± 0.2 units.

Sample ID	315°C & 13 MPa
Na	7.3
Fe(II)	2.4
Fe(III)	0.6
Ni	3.8
Cu	4.2
Zn	3.8

6.2 RESULTS AND DISCUSSION

6.2.1 PRODUCT DISTRIBUTION AND ESTIMATE OF CONVERSION

Fig. 36 A – E give an overview of all quantified products generated from *n*-octane after 168 h at 315°C in experiments with transition metal sulfates. The data is also listed in Table A2 in the appendix. Although, the transition metal concentration affects the abundance of reaction products to various degrees, the overall product distribution is comparable for all samples. The most abundant product group is that of the *n*-alkanes, and the single most abundant product component is CO₂. Alkenes and ketones are also generated, with ketone concentrations reaching those of corresponding *n*-alkanes. This is perfectly in line with observations for the 350°C samples with Na₂SO₄ (cf. chapter 4, Fig. 20). Based on this, it is inferred that cracking, and aqueous oxidation are also the major controlling factors for *n*-octane degradation in presence of transition metal sulfates.

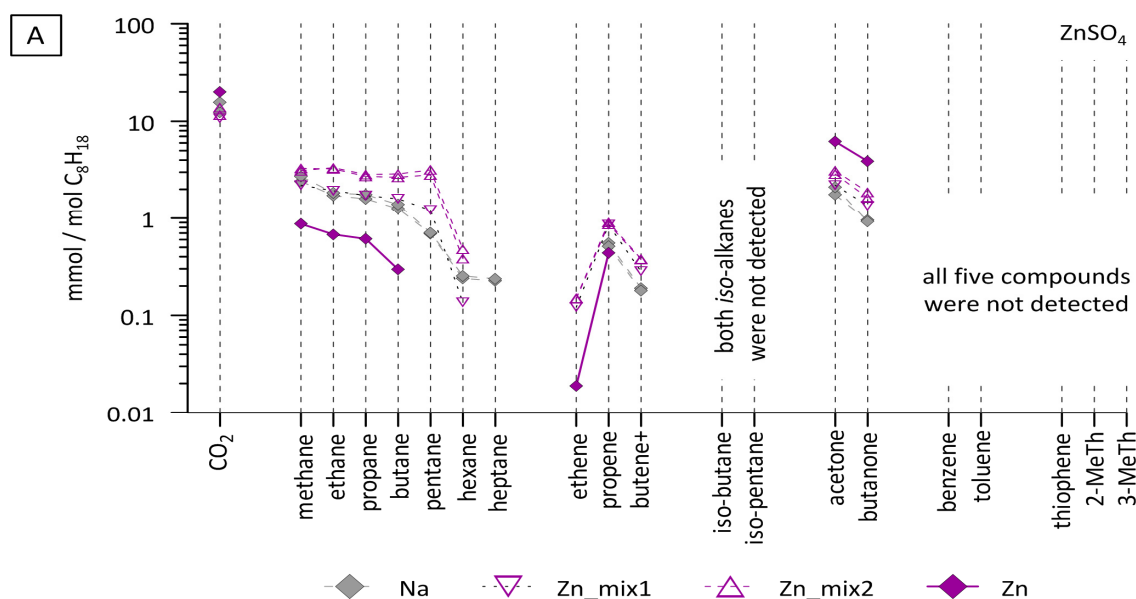


Fig. 36 A-E (Continued on next page): Overview of organic reaction products that were quantified for transition metal (TM) sulfate samples (A-E: ZnSO₄, NiSO₄, CuSO₄, FeSO₄ and Fe₃(SO₄)₃ respectively), which were processed at 315°C and 13 MPa for 168 h. All samples initially contained the same amount of *n*-octane (30.64 μmol) and the same volume of an aqueous sulfate solution (200 μl). This was either a pure Na₂SO₄ solution (indicated by Na in the sample name), a pure transition metal sulfate solution (indicated by Zn, Ni, Fe(II) and Fe(III) in the sample name), or a mixture of both (labeled by mix_1 and mix_2, see Table A2 in the appendix for details). Data points for the Na samples are the same in all five graphs. They represent results for duplicate Na samples, which serve as reference for *n*-octane degradation in a sulfate-containing, but transition metal (TM) free system. If duplicate TM samples were processed, results for both samples plotted as well (see individual graphs). Duplicate samples generally indicate an excellent reproducibility. The detection limits were ≤ 0.01 mmol/mol C₈H₁₈ for all compounds, and the analytical uncertainty is 10 % for most compounds, but may increase to 20 % at low concentrations (see Table A2 for details). Butene+ = mixture of 1- and 2-butene; 2-MeTh = 2-methylthiophene; 3-MeTh = 3-methylthiophene

A) ZnSO₄ series:

Data for one sample of the type Zn and Zn_mix1, and data for two samples of the type Zn_mix2 are shown.

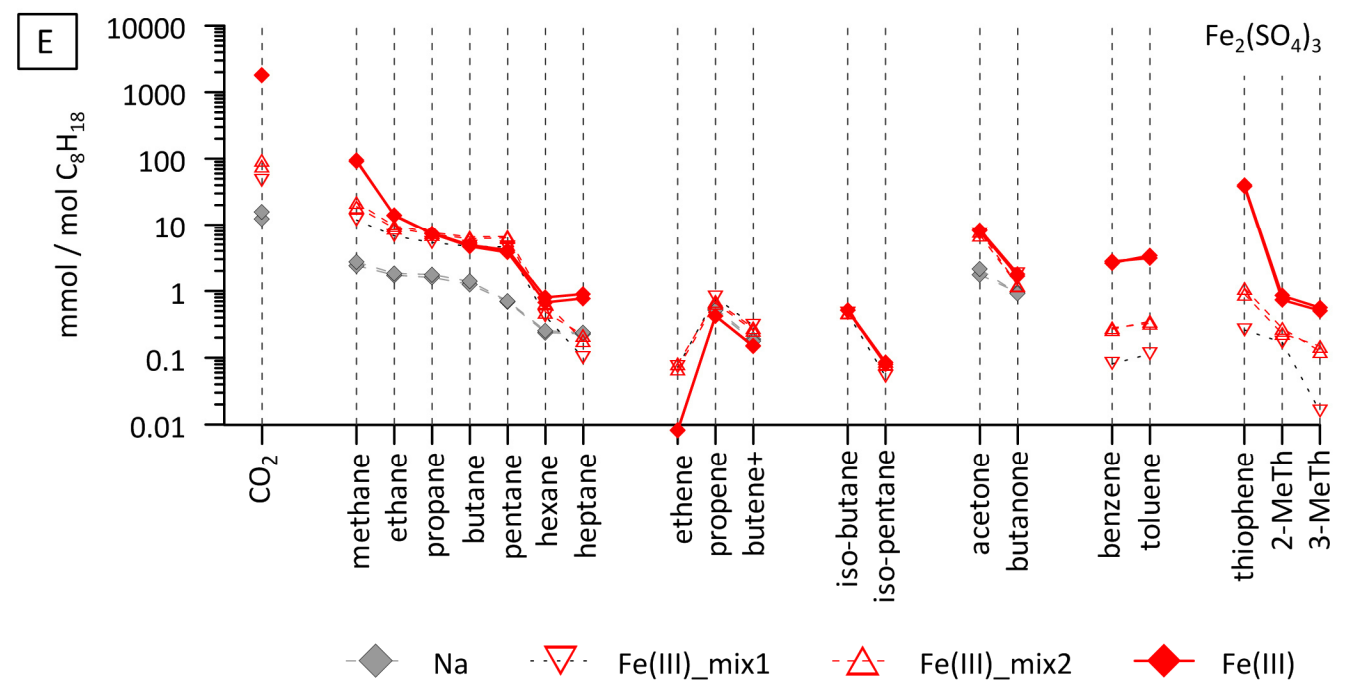
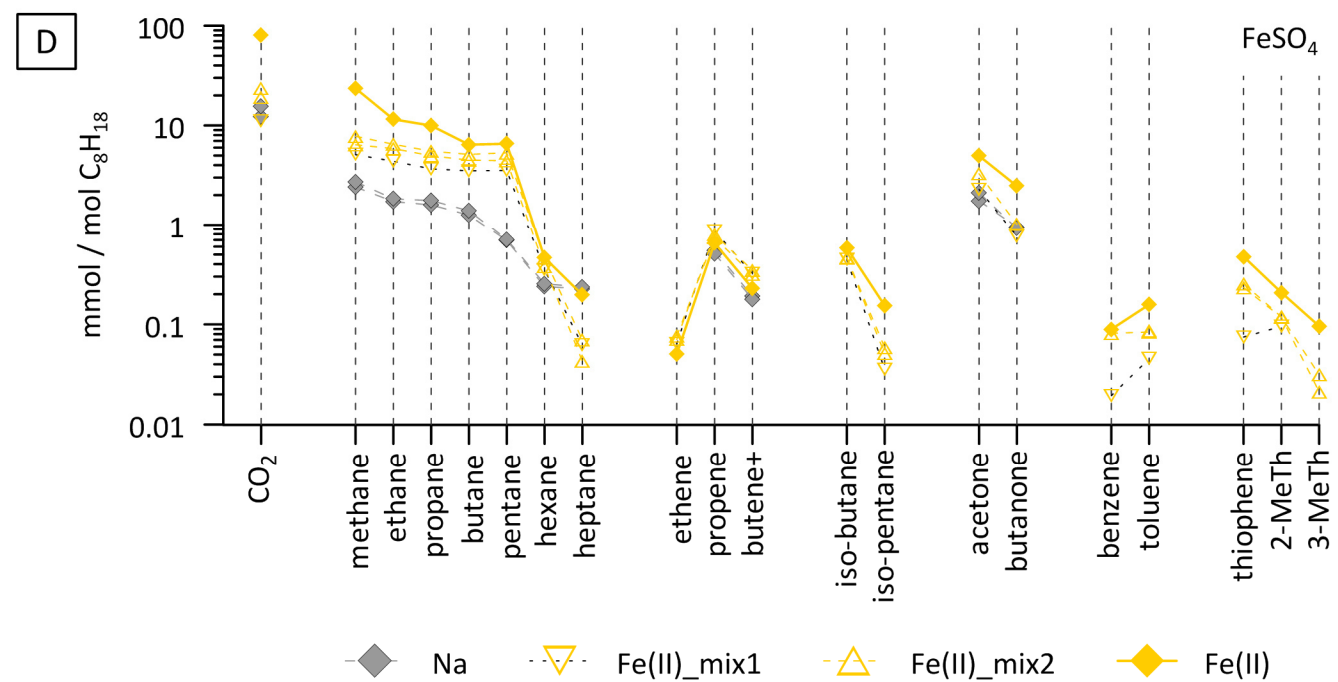
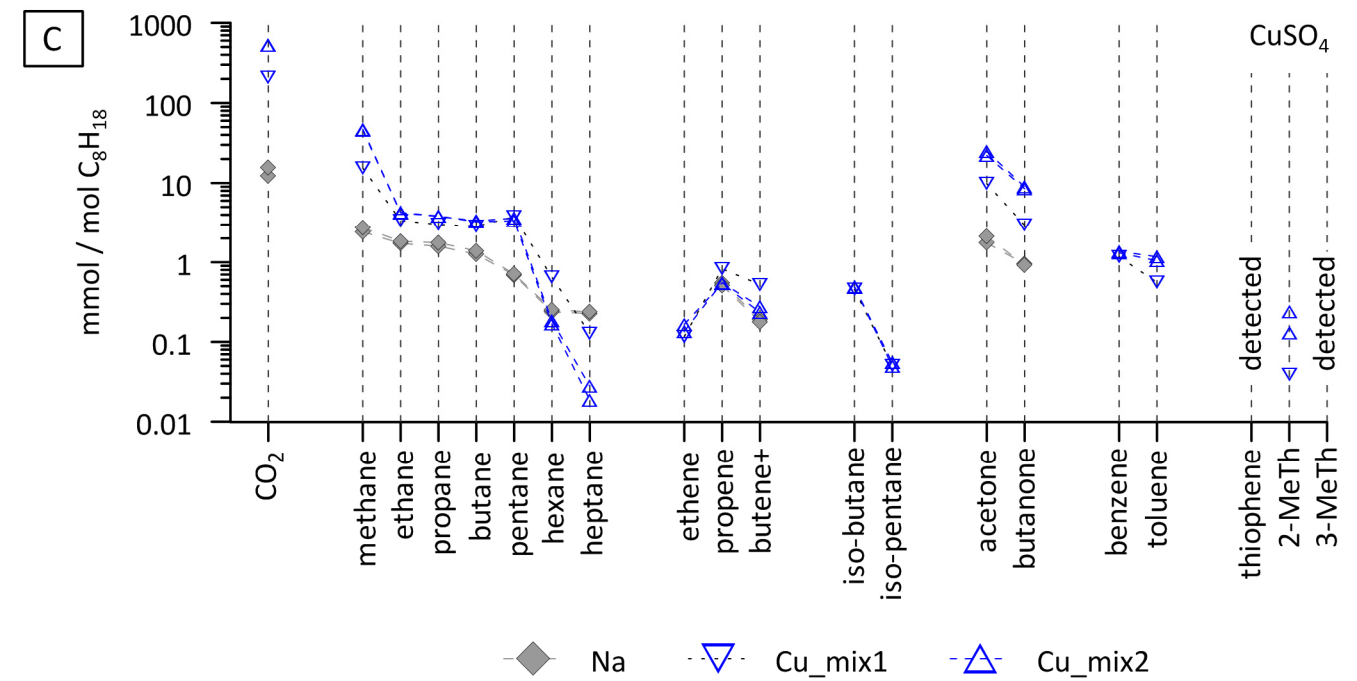
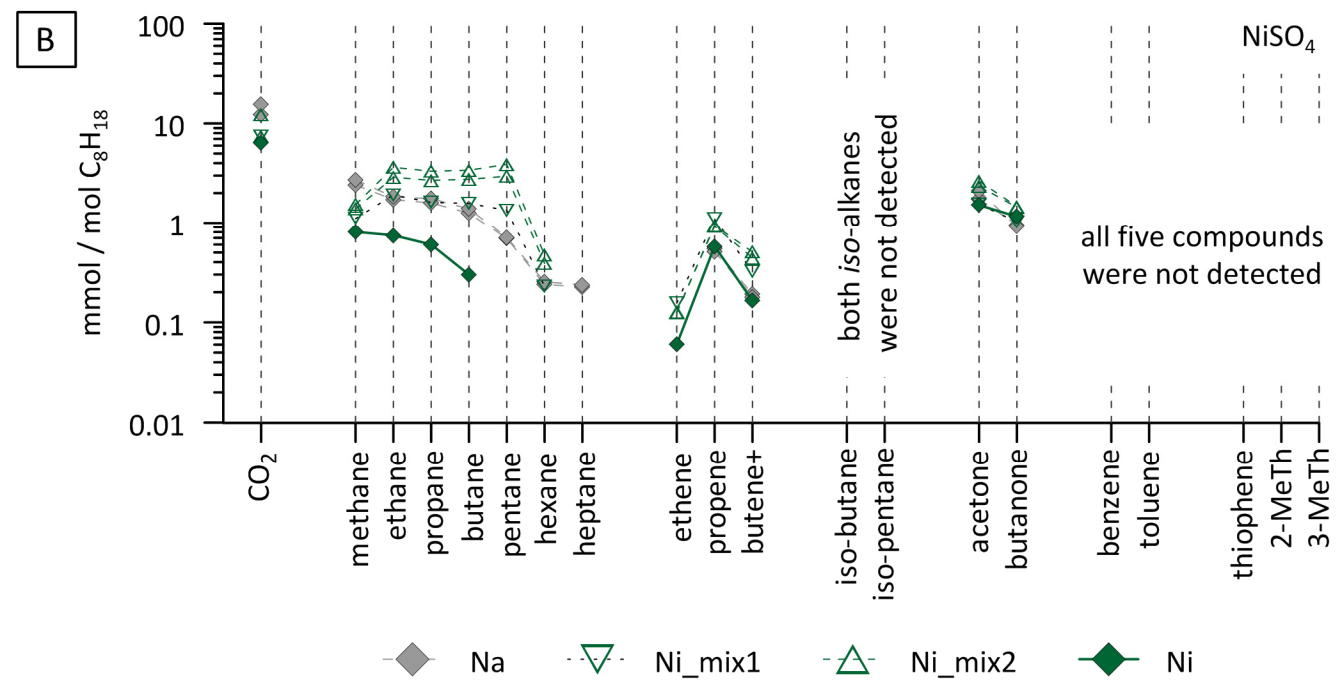


Fig. 36 B-E (Continuation of previous page):

B) NiSO₄ series:

Data for one sample of the type *Ni* and *Ni_mix1*, and data for two samples of the type *Ni_mix2* are shown.

D) FeSO₄ series:

Data for one sample of the type *Fe(II)* and *Fe(II)_mix1*, and data for two samples of the type *Fe(II)_mix2* are shown.

C) CuSO₄ series:

Data for one sample of the type *Cu_mix1* and for two samples of the type *Cu_mix2* are shown.

E) Fe₂(SO₄)₃ series:

Two samples per each dilution step were processed. Thus, data for two samples of the type *Fe(III)*, *Fe(III)_mix1* and *Fe(III)_mix2* are shown.

Despite this general agreement, significant differences exist between the Fe(II), Fe(III) and Cu containing samples, on the one hand, and the Ni and Zn containing samples, on the other hand. The most striking observation is that organosulfur compounds (thiophene, 2- and 3-methylthiophene), aromatics (benzene and toluene) and *iso*-alkanes (*iso*-butane and *iso*-pentane) were detected for the former, but not for the latter. In the sodium sulfate samples, which serve as reference to investigate transition metal free reactions, *iso*-alkanes and aromatic compounds were detected, but concentrations were too low to be quantified. Furthermore, 2- and 3-methylthiophene, as well as thiophene are lacking in the sodium sulfate samples.

The generated amounts of *iso*-alkanes are comparable in the Fe(II), Fe(III) and Cu containing samples, with concentrations of *iso*-butane and *iso*-pentane ranging from 0.44 to 0.58 mmol/mol_{C₈H₁₈} and 0.036 to 0.15 mmol/mol_{C₈H₁₈} respectively. In contrast aromatics and organosulfur compounds show more variation. Benzene and toluene concentrations are usually below 0.60 mmol/mol_{C₈H₁₈} and only reach above this value in the Cu-containing and pure Fe(III)-sulfate samples. Aromatization is strongest in the samples with the pure Fe(III)-sulfate solution. Here benzene and toluene reach a concentration of 2.8 mmol/mol_{C₈H₁₈} and 3.4 mmol/mol_{C₈H₁₈}. The highest concentration of organosulfur compounds was observed in presence of the pure Fe(III)-sulfate solution. Here, the thiophene concentration (40 mmol/mol_{C₈H₁₈}) reaches above that for most *n*-alkanes. The sample with the pure Fe(III)-sulfate solution is also characterized by an extraordinary high CO₂ concentration (1.8 mol/mol_{C₈H₁₈}). This is consistent with expectations, because hematite, which is predicted to form as precipitate in these samples, has been demonstrated to catalyze oxidation of hydrocarbons to CO₂ (cf. *chapter 4*). Furthermore, it is hypothesized that the reduction of dissolved Fe(III) to Fe(II) by organic matter promotes the oxidation to CO₂. An indication for this is that the CO₂ concentration significantly increases in the sample with the pure Fe(III) sulfate solution compared to the Fe(III)_mix1 and Fe(III) mix samples. The concentration of dissolved Fe(III) in the pure Fe(III) sample is two orders of magnitude higher than in the mixed Fe(III) samples.

The second and third highest concentration of CO₂ is observed for the Cu_mix2 (530 mmol/mol_{C₈H₁₈}) and Cu_mix1 (210 mmol/mol_{C₈H₁₈}) samples. Analog to the Fe(III) samples, it is hypothesized that reduction of Cu(II) to Cu(I) has promoted the oxidation of *n*-octane to CO₂. In all the other samples, the CO₂ concentration is below 100 mmol/mol_{C₈H₁₈},

with the sodium sulfate samples showing a CO₂ concentration of 12 to 16 mmol/mol_{C₈H₁₈} (see Table A2 for details).

Based on these observations, it is not surprising that the estimated conversion¹⁵ of *n*-octane is the highest in the sample with the pure Fe₂(SO₄)₃ solution (28 ± 2 mol%), followed by the Cu_mix2 (9.5 ± 0.1 mol%) and Cu_mix1 samples (4.2 ± 0.3 mol%). In all the other samples, the estimated conversion of *n*-octane is ≤4 mol%. In presence of transition metal sulfates the conversion is, however, at least 1.6 times higher compared to the sodium sulfate samples, which show a conversion of 0.58 to 0.65 mol%.

6.2.2 EVIDENCE FOR TSR

Formation of Organosulfur Compounds

A very interesting feature of the results, which were presented in the previous section, is the formation of organosulfur compounds. This is because it reflects incorporation of reduced sulfur in the reaction products. The oxidation state of sulfur in thiophene, 2- and 3-methylthiophene is -2 and that of sulfur in sulfate +6. Due to the fact that sulfate is the only sulfur source in the transition metal sulfate

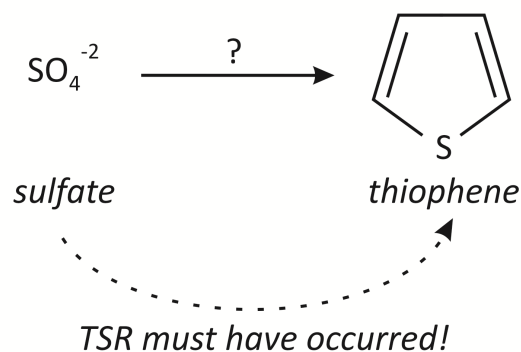


Fig. 37: Formation of organosulfur compounds is a direct indicator for TSR, if sulfate is the only sulfur source in the reacting system. This is illustrated for thiophene. Detailed reaction mechanisms and possible reactants are, however, unclear.

samples, the formation of these organosulfur compounds implies that reduction of sulfate must have occurred (Fig. 37). Formation of organosulfur compounds was observed for the Fe(III), Fe(II) and Cu containing samples (Fig. 36). The observation is most interesting, because these samples represent one of the few examples reported for TSR without the initial presence of low valence sulfur (Toland, 1960; Kiyosu, 1980; Kiyosu and Krouse, 1990;

¹⁵ Mass balance considerations on analyzed products (Table A2 in the appendix) were conducted to estimate the minimum amount of *n*-octane, which was converted during the experiments. Calculations were performed in the same manner as described in *chapter 4.2.1 (footnote 6)*, with the exception that amounts of three organosulfur compounds (i.e. thiophene, 2- and 3-methylthiophene) were also taken into account. This was possible because of an extended calibration of the gas chromatograph.

Yue et al., 2006; Chen et al., 2009; Truche et al., 2009; Lu et al., 2010a; Lu et al., 2010b; Lu et al., 2011; Truche et al., 2011; Zhang et al., 2012). Moreover, the results represent the first published example of TSR with transition metal sulfates, and the first published example of TSR without initial presence of low valence sulfur at a pH >4 (CuSO₄ samples). Based on the generated amount of organosulfur compounds (thiophene, 2- and 3-methylthiophene), the following relative reactivity of the transition metal sulfates can be inferred:



Under the assumption that reduced sulfur is dominantly stored in the organic phase and not in metal sulfides, the generated amount of organosulfur compounds would mirror the extent of TSR. However, results for the CuSO₄ containing samples point to the possibility that metal sulfides precipitated (see below). Absence of organosulfur compounds in the Na₂SO₄, NiSO₄ and ZnSO₄ containing samples (Fig. 36) does not necessarily mean that no TSR occurred, as was revealed by the results for the first and second experimental series (cf. *chapter 4*).

Gas Dryness

A positive correlation is observed between the organosulfur compound concentration and the gas dryness (Fig. 38), which is consistent with expectations for TSR (cf. *chapter 2.2.3* and *chapter 4.3.4.1*). Only the copper containing samples significantly deviate from the trend. A hypothesis, which is further evaluated at present, is that copper sulfide precipitated during the experiments, which lowered the amount of H₂S in the system, wherefore the formation of organosulfur compounds was hampered. In this context, the possibility of metal sulfide precipitation in presence of the other transition metals will also be considered. Furthermore, it needs to be evaluated if metal sulfide precipitates may catalyze methane generation. At least for iron, results for the 350°C experiments with the PPM buffer indicate that the aqueous concentration of low valence sulfur species is more critical for enhancing methane formation than the solid sulfides (cf. *chapter 4*).

The gas dryness of all Ni and Zn containing samples is close to or below that of the samples with the pure Na₂SO₄ solution (Fig. 38). This is also the case for the Fe(II)_mix1 and Fe(II)_mix2 samples, although clear evidence for TSR (=detection of organosulfur compounds) was observed in these samples. Interestingly, a significant increase in gas

dryness is observed in presence of Ni, Zn and Fe(II) if the sample with the pure metal sulfate solution is compared to the respective mix_2 sample. This correlates with an increase in the amount of the transition metal sulfate in the experimental charge (see Table 10 for details). Based on these observations it is hypothesized that TSR proceeded at a subordinate rate, at least in the samples containing the pure metal sulfate solutions. This needs further investigation and a more in depth analysis of the product distribution, which is out of scope at this stage.

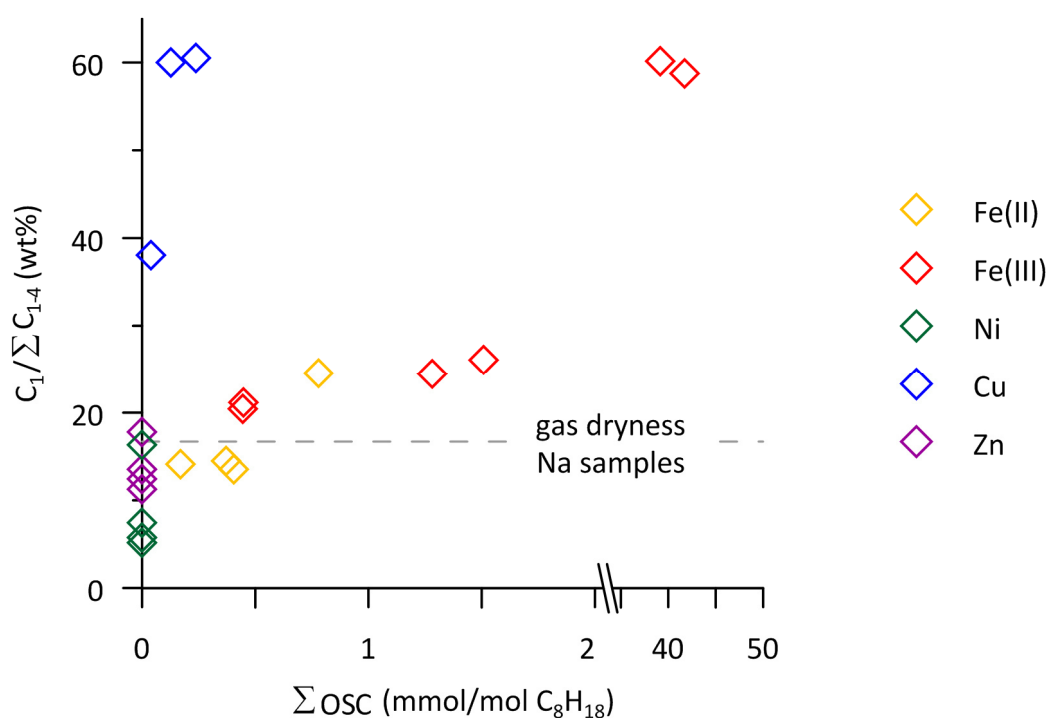
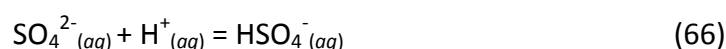


Fig. 38: Correlation of gas dryness and quantified organosulfur compounds for transition metal sulfate samples, which were processed at 315°C and 13 MPa for 168 h. All samples initially contained 30.64 μmol *n*-octane and 200 μl sulfate solution. This was either a pure Na₂SO₄ solution, a pure transition metal sulfate solution or a mixture of both (see Table A2 in the appendix for details). It was decided to display all samples of one series with the same symbol, because the main objective is to illustrate the difference between individual metals. Fe(II), Fe(III), Ni, Cu and Zn reflect the type of metal sulfate present in the sample, i.e. ZnSO₄, NiSO₄, CuSO₄, FeSO₄ and Fe₃(SO₄)₃ respectively. The relative error for the OSC sum is 11% and that for the gas dryness 7%. The gas dryness for the samples with the pure sodium sulfate solution is shown as dashed grey line for reference. Note, however, that no organosulfur compounds were detected in these samples.

6.2.3 EFFECT OF PH AND ADDITIONAL FACTORS ON TSR

Based on the discussion in the preceding chapter, the question arises why variations in the extent of TSR are observed if different metal sulfates are used. One controlling factor can be the pH. Previous TSR studies show that it can strongly influence the rate of TSR

(cf. *chapter 2.2.3*). This is due to an increase of the HSO_4^- concentration with decreasing pH according to:



Geochemical modeling show that the in situ pH of the samples with the pure Fe(II)-sulfate solution is acidic (= 2.4) and that the value for the pure Fe(III)-sulfate solution is even more acidic (= 0.6). The in situ pH of the other pure transition metal sulfate solutions (CuSO_4 , NiSO_4 and ZnSO_4) is higher (4.2, 3.8 and 3.8 respectively). Thus, it is not surprising that the highest amount of organosulfur compounds was observed in the Fe(III) containing samples, and that TSR was also significantly promoted in the Fe(II) containing samples. The observation that the Cu containing samples showed a significantly lower concentration of organosulfur compounds is also consistent with the lower pH in these samples. It is expected to be above that of the pure CuSO_4 solution (in situ pH = 4.2), because only samples of the type *Cu_mix1* and *Cu_mix2* were processed (cf. *chapter 6.1*). This raises, however, the question why evidence for TRS, i.e. detection of organosulfur compounds, was observed for the CuSO_4 containing mix1 and mix2 samples, but not in presence of NiSO_4 and ZnSO_4 , even though the *in situ* pH of the pure metal sulfate solutions are comparable. Thus the pH in the samples with the pure NiSO_4 and ZnSO_4 solutions should be below that of the Cu mix samples (cf. *chapter 6.1*), wherefore a higher TSR rate would be expected. These observations call for additional factors besides pH that control the initiation and extent of TSR, at least at pH \geq 3.8. Metal sulfide precipitation has been proposed as one hypothesis that may explain why generated amounts of organosulfur compounds in the Cu containing samples are low although the gas dryness points to a strong TSR influence in these samples. It needs to be clarified if this could preferentially occur in presence of Cu, and possibly Ni and Zn.

Even though precipitation of metal sulfides may be possible during the experiments, a positive correlation between the concentration of generated organosulfur compounds and the modeled initial concentration of dissolved transition metal cations is observed in the Fe(II), Fe(III) and Cu series (Fig. 39). The trend is most pronounced in presence of Fe(III), which can probably be attributed to the extremely low in situ pH (= 0.6) in the samples with the pure $\text{Fe}_2(\text{SO}_4)_3$ solution. From the results of this study it cannot unequivocally be

determined if the concentration of the dissolved metal cation in solution or the pH have a more dominant effect on TSR. This is also complicated by the fact that these two factors are interdependent.

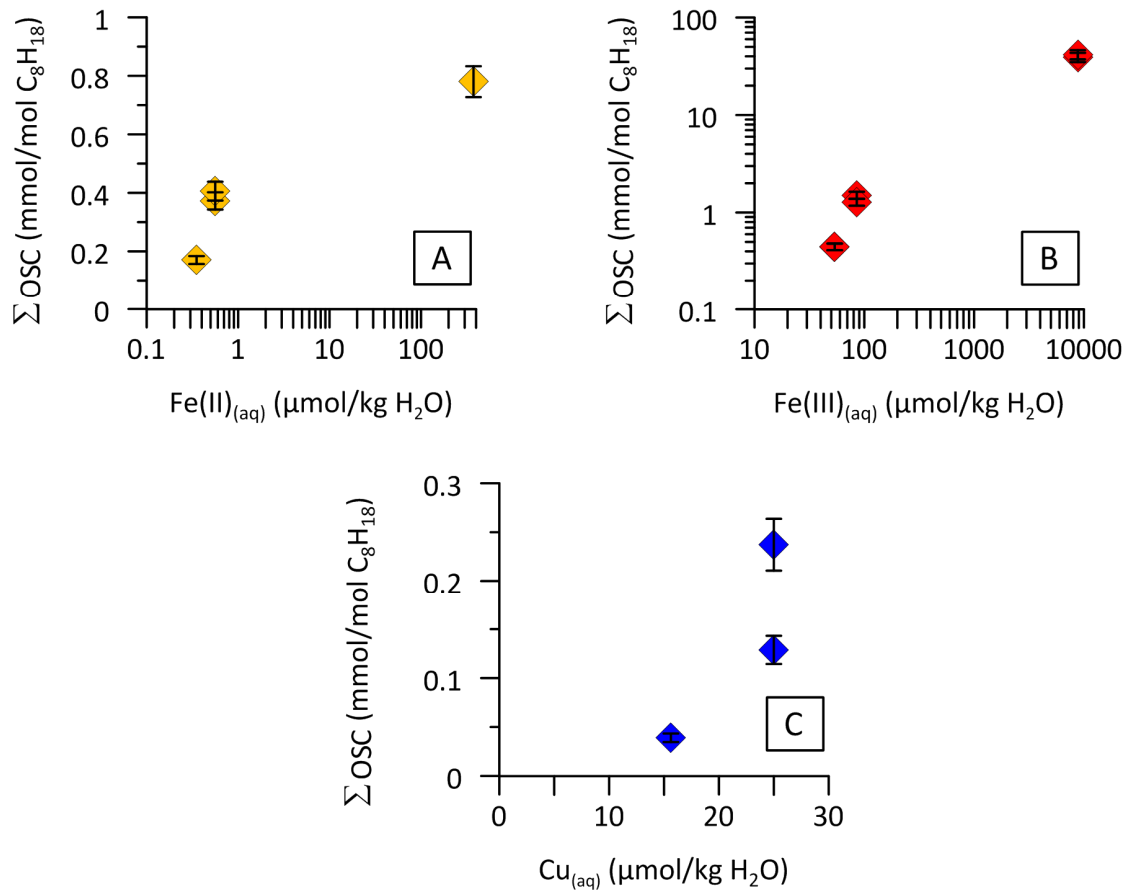
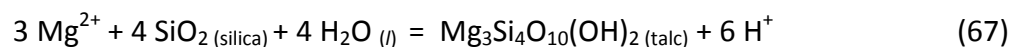


Fig. 39: Correlation of the sum of quantified organosulfur compounds (thiophene, 2- and 3-methylthiophene) and the calculated initial concentration of transition metal cations in solution at 315°C and 13 MPa for: (A) the Fe(III), (B) the Fe(II) and (C) the Cu series. Details on the calculation of the initial concentration of the dissolved metal cations are provided in *chapter 6.1*. Error bars reflect the propagated error taking into account the analytical uncertainty and the uncertainty in the weighed in quantity *n*-octane.

The interdependence of pH and dissolved metal cation is also highlighted by Zhang et al. (2012) for a transition metal free system. They performed a series of experiments to investigate the reaction of aqueous CaSO₄ and a research-grade paraffin wax mixture (composed of C₂₁ to C₃₅ normal *n*-alkanes) without initial presence of low valence sulfur species. Experiments were conducted at 329, 340, 360°C under a constant confined pressure of 24.1 MPa. Run duration of experiments ranged from 5 to 853 h. Gold capsules were used as sample containers, which was also the case in this study. Zhang et al. (2012) used a talc-silica mineral to regulate the pH of the solution during the experiments. The buffer reaction

is suggested to proceed rapidly at the experimental conditions, and regulates the pH via the precipitation of talc according to (Zhang et al., 2012 and references therein):



The initial amount of talc and silica were constant (30 mg each). The initial $\text{Mg}^{2+}_{(\text{aq})}$ concentration was varied to adjust different pH, ranging from 3 to 4 at experimental conditions (Table 13). The initial sulfate concentration was constant (0.04 mol/l). Based on the amount of hydrogen sulfide, which was generated during the experiments the extent of TSR was estimated, with increasing amounts reflecting an increase in the TSR reaction. Based on their results, Zhang et al. (2012) conclude that the pH is the controlling factor for the extent of TSR reaction in the investigated pH range (3 to 4).

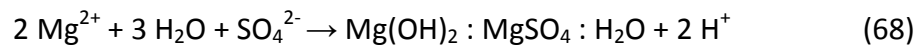
Table 12: Magnesium concentration and *in situ* pH of the aqueous solutions used by Zhang et al. (2012) for experiments simulating TSR with CaSO_4 and a paraffin mixture in the temperature range 320-360°C (see text for details). The amount of H_2S generated during the experiments was used to estimate the extent of TSR.

Solution no.	Mg^{2+} (mmol/l)	<i>in situ</i> pH	Extent of TSR estimated from generated amount of H_2S
1	620	3	Strong TSR
2	26	3.5	Medium TSR
3	2.6	4	No TSR

Measured concentrations of organosulfur compounds in the Fe(II) series indicate, however, that TSR still proceeds at a subordinate rate at pH 2.4 (=pure FeSO_4 solution) and is only catalyzed significantly at a pH < 1 (= pure $\text{Fe}_2(\text{SO}_4)_3$ solution). Apart from pH, the concentration of the dissolved metal cation is suggested to have an affect on the TSR rate. As noted above, results for each metals series indicate that the extent of TSR increases with increasing metal in solution (Fig. 39). This is further supported by the observation that the concentration of quantified organic sulfur compounds in the Fe(II), Fe(III) and Cu series stays in the range 0.04 - 1.5 mmol/mol C_8H_{18} if metal concentrations are below 100 $\mu\text{mol/kg}$ H_2O (even at an *in situ* pH of 2.4!), and only increase significantly if the concentration of the

dissolved metal reaches approximately 10 mmol/kg H₂O (Fig. 39). These observations show striking similarities with the results of Zhang et al. (2012). Here, H₂S (=indication for TSR) is only observed if the aqueous Mg²⁺ concentration exceeds 10 mmol/l (at pH 3.5), and an even greater extent of TSR is observed if the magnesium concentrations¹⁶ reaches 620 mmol/l (at pH 3). Furthermore, the increase in the magnesium concentration is eight times higher than the increase in H⁺ concentration if solution 1 is compare to solution 2 (calculated from *in situ* pH), which also points to the possibility that the magnesium concentration may be more critical than the *in situ* pH in the investigated pH range of 3 to 4.

In general, an increasing concentration of aqueous Mg²⁺ is expected to promote the formation of magnesium-sulfate contact ion-pairs, which are know to be highly reactive during TSR (Ma et al., 2008; Zhang et al., 2012). Zhang et al. (2012, and references therein), argues, however that aqueous Mg²⁺ and SO₄²⁻ form a magnesium-hydroxide-sulfate-hydrate complex (MHSH) at temperatures above 200°C, according to:



I suggest that this might be buffered by the talc-silica assemblage. In any case, the positive correlation of dissolved metal concentration and extent of TSR cannot be dismissed. Based on the discussion in this chapter, I hypothesize that the metal cation concentration may play a more important role for controlling the extent of TSR than the *in situ* pH, at least in a system without initial presence of low valence sulfur and with pH values above 2. This hypothesis stresses the importance of the metal itself, wherefore additional factors influencing the reactivity of dissolved metals are considered to be crucial. Especially the complexing behavior of the transition metals in presence of organic matter, which is for example observed during ore transport in nature (Manning and Gize, 1993), opens a whole new field to be explored in the context of TSR reaction mechanisms. A factor that controls the complexing behavior of the metals is their electronic structure (Weisshaar, 1993). This takes, for example, the electron configuration into account. Interestingly, the electron configuration of Cu²⁺ ([Ar]3d⁹) is significantly different from that of the other transition metals in the way that only one electron is needed to reach a completely filled *d* subshell.

¹⁶ Note that the units mmol/kg H₂O and mmol/l are comparable, because the density of the solution has a negligible effect at these salt concentrations.

This reflects a particularly stable arrangement of electrons and should therefore be favored. I hypothesize that differences in electronic structure of the dissolved transition metal cations are an additional factor that controls the reactivity of the transition metal sulfates during TSR. This provides promising opportunities for future research, but is beyond the scope of the present PhD thesis.

6.3 CONCLUSIONS

The distribution of organic reaction products generated in experiments with *n*-octane, transition metal sulfates (FeSO_4 , $\text{Fe}_2(\text{SO}_4)_3$, NiSO_4 , CuSO_4 and ZnSO_4) and Na_2SO_4 at 315°C and 13 MPa is very similar in all samples, showing a strong dominance of *n*-alkanes. CO_2 is the single most abundant component. Alkenes and ketones were also generated with ketone concentrations reaching those of corresponding *n*-alkanes. The product distribution shows that *n*-octane degradation is dominated by cracking and aqueous oxidation during the experiments.

Despite the good agreement, differences in the product distribution do, however, exist if transition metal samples are compared to samples, which were processed with the pure sodium sulfate solution and *n*-octane. Significant difference in the product distribution obtained with the different transition metal sulfates also exist. The most striking observation is the detection of organosulfur compounds in the $\text{Fe}_2(\text{SO}_4)_3$, FeSO_4 and CuSO_4 containing samples, which provides clear evidence for TSR. The results represent one of the few examples for successful simulation of TSR without the initial presence of low valence sulfur, wherefore a special focus was to evaluate possible factors that control the different reactivity of the transition metal sulfates.

The highest extent of TSR was observed in the sample containing $\text{C}_8\text{H}_{18}+\text{H}_2\text{O}+\text{Fe}_2(\text{SO}_4)_3$, which can be attributed to the low pH (≈ 0.6) in this sample at experimental conditions. The increase in TSR rate at low pH is consistent with observations of previous TSR studies. Results for the Cu containing experiments demonstrate, however that TSR without initial presence of low valence sulfur at $\text{pH} \geq 4$ is also possible. Based on the results of the transition metal sulfate experiments, it is hypothesized that additional factors besides pH control the extent of TSR. These are, for example the concentration of the dissolved transition metal, the redox potential and the electron configuration.

Based on the results and comparison with data from Zhang et al. (2012), it is hypothesized that the concentration of the dissolved transition metals is one of the main parameters controlling the extent of TSR at $\text{pH} > 1$. The redox potential, or more specifically the reduction potential of the metals, may have a positive effect on TSR. This is indicated by the observation that conversion is highest in presence of Fe(III) and Cu(II) the only two metal cations, which can easily be reduced under experimental conditions. Last but not least the electron configuration is suggested to play an important role, because it determines the complexing behavior of the transition metals and therefore its reactivity during TSR.

The findings, which were derived from these first results are promising and a more detailed analysis of the distribution of organic reaction products will help to evaluate the effect of the transition metals on the whole reaction network and not only TSR. The factors, which were proposed to determine the extent of TSR (pH, dissolved transition metal concentration, the redox potential of the metal cations and their electron configuration), are also considered to be crucial for reactions associated with aqueous oxidation and possibly cracking.

7.

IMPLICATIONS FOR NATURAL SYSTEMS

In the introduction it was noted that inorganic-organic interactions can be relevant in a variety of geologic environments, like in association with petroleum systems, sulfide ore deposits and submarine hydrothermal systems. Results from the present study demonstrate that laboratory experiments can be a powerful tool to investigate such reactions under well constrained conditions. Obviously, natural environments are more complex. Thus, some limitations but also the potential for extrapolating experimental results to natural systems are addressed in this chapter.

7.1 PETROLEUM SYSTEMS

7.1.1 TRANSFERABILITY OF EXPERIMENTAL RESULTS

Economic deposits of oil and natural gas are generally believed to form at temperatures ranging from 50-150°C and from 150-220°C, respectively (Seewald, 1994 and references therein). This is significantly below the experimental temperatures employed in the present study, which ranged from 300-350°C. A common approach in experimental studies is to use higher temperature in order to simulate processes that would take place over much longer time periods at lower temperature in nature (e.g. McCollom and Seewald, 2003; Zhang et al., 2012). This assumption bears the risk of false conclusions because reactions, which proceed at higher temperature, might not proceed at lower temperatures and/or other reaction mechanisms might dominate. Thus, results extrapolated to lower temperatures must be examined critically.

Petroleum-geochemical analyses of samples from ultra-deep wellbores (7-10 km) provide, however, evidence for the existence of hydrocarbon deposits at temperatures approaching 300°C (Price, 1993 and references therein). In this case, experimental results might be directly applicable.

Regarding the reactants, water is the dominant compound in the experiments. The molar ratio of *n*-octane and water is 6.1 mmol C₈H₁₈/mol H₂O. In contrast, the dominant components in oil and gas reservoirs are hydrocarbons. At the oil-water contact and the gas-water contact the ratio of hydrocarbons and water increases and aqueous alteration of

petroleum may be possible. In addition to that, chemical reactions between hydrocarbons and water can become very critical during enhanced oil recovery operations if water steam is used (Hoffmann et al., 1995; Kapadia et al., 2011). Steam temperatures of up to 320°C have been reported (Hoffmann et al., 1995). The steam may not only chemically react with petroleum, but also with the rock matrix. In doing so, it can introduce contaminants to the target formation, like for example sulfate. In this case, TSR may be initiated and promoted, thus increasing the hydrogen sulfide concentration in the reservoir, which is undesirable (Hoffmann et al., 1995; Kapadia et al., 2011).

In order to get an estimate of possible sulfate concentrations in petroleum systems, the study by Kharaka et al. (1977) was taken into consideration. They report data from detailed chemical analyses of 48 formation-water samples from 10 oil and gas fields in the Houston-Galveston and Corpus Christi areas, Texas. Here, the SO_4^{2-} concentrations reach up to 1.2 mmol/kg $_{\text{H}_2\text{O}}$, which is several orders of magnitude below the sulfate concentration for most experiments performed in the course of the present study (290 - 1700 mmol $_{\text{SO}_4^{2-}}$ /kg $_{\text{H}_2\text{O}}$). Only, in experiments with pure FeSO_4 , CuSO_4 and $\text{Fe}_2(\text{SO}_4)_3$ solutions, sulfate concentrations are in a range (0.38 - 13 mmol $_{\text{SO}_4^{2-}}$ /kg $_{\text{H}_2\text{O}}$) that is directly comparable to natural formation waters. According to Zhang et al. (2012) sulfate concentration or more precisely the concentration of reactive sulfate species play, however, a significant role in controlling the rate of TSR for example. Thus, differences in sulfate concentration might limit the extrapolation of experimental results to natural petroleum systems. Published kinetic rate data for TSR suffer, however, from large uncertainties and further investigations are urgently needed to improve geochemical models (Ostertag-Henning et al., 2010; Zhang et al., 2012; Peters et al., 2013).

The study by Saunders and Swann (1990) was used to estimate possible concentrations of dissolved transition metals in oil field brines. They report data for 34 formation water samples from central Mississippi. Overall, the study by Saunders and Swann (1990) represents a snap shot of possible trace metal concentrations in oil filed brines and many other scenarios might be possible. The concentration of trace metals can be highly variable, especially, because “the composite effects of the reduced sulfur content and physiochemical characteristics of the brine (i.e., salinity, temperature, redox state and pH), along with formation metal sources and brine migration history” affect the concentrations of

the trace metals. Trace metals may for example precipitate with sulfide generated by TSR (Cross, 1999; Worden et al., 2003). Despite possible variations, it is interesting that Fe and Zn concentrations reported by Saunders and Swann (1990) are comparable to those in the $\text{Fe}_2(\text{SO}_4)_3$ and ZnSO_4 containing samples of the present study (Table 13).

Presence of transition metals can have implications for hydrocarbon transformation, as indicated by results from the present study (*cf. chapter 6*). Results also show that the type of the transition metal as well as the concentration of dissolved transition metal cation may significantly affect the rates of reactions associated with the transformation of organic matter.

Table 13: Transition metal concentrations in formation water samples from central Mississippi (Saunders and Swann, 1990) compared to the respective concentrations in experimental samples (this study).

Metal in solution ¹	Saunders and Swann (1990) (mmol/kg H ₂ O)	This study ² (mmol/kg H ₂ O)
Fe	1.13 - 7.71	Fe(II): 3.5×10^{-4} - 0.38
		Fe(III): 0.054 - 8.8
Ni	na	Ni(II): 0.10 - 0.50
Cu	3.5×10^{-6} - 6.3×10^{-5}	Cu(II): 0.016 - 2.5
Zn	0.033 - 4.77	Zn(II): 0.046 - 0.14

¹ Element symbols are used here, because Saunders and Swann (1990) do not differentiate between different valences of metal cations in solution.

² Concentrations of transition metal cations in solution were calculated from maximum solubilities of the transition metal sulfates under experimental conditions (*cf. chapter 6.1*). Note that the range of concentrations represents aqueous transition metal concentrations in mix1, mix2 and the pure transition metal sulfate samples.

In addition to formation waters, transition metals can be present in organic sediments, like in oxide (e.g. Fe_3O_4) or sulfide (e.g. FeS_2) minerals. In a side note, Orr (1974) already states that “the effect of catalytic activity of reservoir rock on the maturation

processes is possibly an important variable about which we have little information". Little has changed during the last four decades, stressing the urgent need for studies investigating inorganic-organic interactions in petroleum reservoirs. Regarding, the minerals examined in the present study, the question is, if these are representative for petroleum systems. Surely, some of the buffer minerals might be absent in source and reservoir rocks. However, if petroleum reservoirs are spatially separated from their source rocks, ample opportunity exists for hydrocarbons to interact with various minerals along the migration conduit (Seewald, 2001). Seewald (2001) noted



Fig. 40: Partial bleaching of sandstone due to hydrocarbon invasion. Zion National Park, Utah. (photo taken by R. Gaupp, University of Jena)

that the buffer minerals investigated in the present study (i.e. hematite, magnetite, pyrite and pyrrhotite), are all present to varying degrees in sedimentary basins. One example, where interaction of minerals and organic matter has been confirmed in nature is the bleaching of hematite-bearing sandstones by hydrocarbons (Surdam et al., 1993; Schöner and Gaupp, 2005; Meier, 2012) (Fig. 40). According to Schöner and Gaupp (2005), hydrocarbon oxidation by water and minerals within reservoir sandstones can create considerable amounts of organic acids and CO₂. This may significantly enhance reservoir porosity due to dissolution of carbonate cements and detrital feldspars (Schöner and Gaupp, 2005 and references therein).

Based on this discussion, it is inferred that experimental results are directly transferable to natural petroleum systems only, if boundary conditions are comparable. If this is not the case, extrapolation of experimental results to nature should be examined critically. In any case, the main finding is that inorganic components can significantly affect hydrocarbon decomposition, which is often neglected. This is considered to be a relevant factor that influences hydrocarbon stability in nature. The next two subchapters provide

exemplarily two possible implications on natural petroleum systems, derived from the experimental results.

7.1.2 IMPLICATION I: THERMOCHEMICAL SULFATE REDUCTION

Geological observations as well as geochemical investigations of natural samples present evidence that TSR can occur in petroleum systems. Two well studied *TSR laboratories* are for example the Smackover Formation in the United States of America (Sassen, 1988; Rooney, 1995) and the Khuff Formation in Abu Dhabi (Worden and Smalley, 1996; Worden et al., 2000). As a consequence of TSR, both locations are characterized by high amounts of sour gas. This is problematic during recovery, because H₂S is very corrosive, toxic and increases production costs. Thus, accurate TSR modeling becomes more and more important, but the understanding of the reaction and influencing factors is still limited (Zhang et al., 2012; Peters et al., 2013).

It is generally assumed, that the critical step during TSR is the activation of sulfate (Amrani et al., 2008; Ma et al., 2008). Results from the present study show that minerals and dissolved transition metals may have a positive effect on this. The PPM buffer may for example supply reduced sulfur species, which may initiate and promote LSC-catalyzed TSR (cf. *chapter 4.3.4.1*). Moreover, results of the present study provide evidence that the type and concentration of dissolved transition metal cations may significantly affect the rate of TSR (cf. *chapter 6.2.2*). In presence of dissolved Fe₂(SO₄)₃, FeSO₄ and CuSO₄ TSR was initiated without initial presence of low valence sulfur. Geochemical modeling indicate that the pH of the Fe(III) and Fe(II) containing samples might be too acidic for typical petroleum formation waters (pH 5.5. - 7, cf. Helgeson et al., 1993, Fig. 10), but the pH of the Cu containing samples is comparable to that in petroleum systems.

Based on the results of the present study, it is suggested that incorporation of inorganic-organic reactions in modeling studies that consider reaction of petroleum with minerals, transition metals and sulfate will strongly improve prediction of the occurrence, stability and alteration of hydrocarbons in nature.

7.1.3 IMPLICATION II: CONVERSION OF HYDROCARBONS TO DRY GAS

The formation of dry (methane dominated) thermogenic gas is one of the most controversial issues discussed in petroleum geochemistry (Mango, 1997a; Price, 2001; Seewald, 2003). The methane content in such gases can vary from 50 to 100 wt% in the C₁-C₄ fraction (Mango et al., 1994) and the CO₂ content of these gases is usually less than 10% (Seewald, 2003 and references therein). Phase partitioning in reservoirs and fractionation during migration (Price and Schoell, 1995), have been presented as possible explanations for the origin of dry gas. However, Mango and Hightower (1997b) argue that it is unlikely that dry gas with methane concentrations ≥ 60 wt% can be produced from oil and kerogen pyrolysis without catalytic assistance by transition metals. This is in good agreement with results of the present study. Only in presence of dissolved Fe(III) and Cu the measured gas dryness (C₁/ Σ C₁₋₄) after the experiment increases from ≤ 20 wt% to > 59 wt% (Table A2 in the appendix). However, a significant amount of CO₂ was always co-produced, with molar amounts usually being one order of magnitude above the methane values. This is untypical for natural dry gas, but Seewald (2001, 2003) stated that CO₂ may be removed from natural gas by mineral precipitation.

7.2 SUBMARINE HYDROTHERMAL SYSTEMS

Submarine hydrothermal systems represent another potential environment for inorganic-organic interactions. A simplified cross-section of a submarine hydrothermal is illustrated in Fig. 41. Submarine hydrothermal systems are manifold and very difficult to understand. This is mainly due to the variety and complexity of mineral compositions as well as the various alteration processes occurring in these systems. These may either be purely inorganic or may also involve organic matter (Konn et al., 2009). Under certain circumstances, conditions in submarine hydrothermal systems can show compelling similarities with the experiments performed in the course of the present study, as demonstrated in the next paragraph. Excellent overviews on submarine hydrothermal systems are presented by Von Damm (1990) and Hannington et al. (2005).

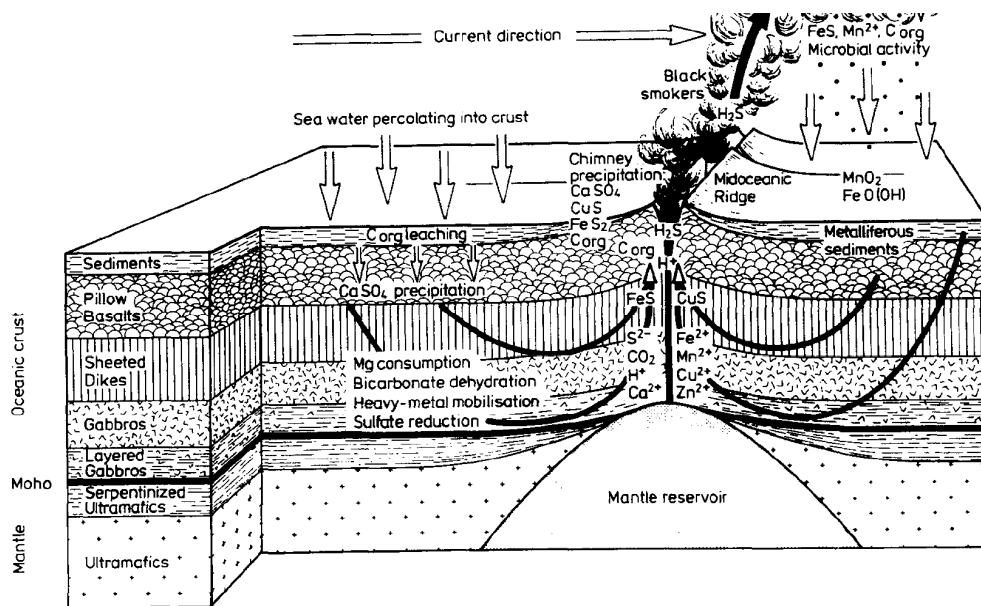


Fig. 41: Simplified cross-section of a submarine hydrothermal system at a Mid Ocean Ridge. The main petrographical features are shown on the left side of the graph. The Moho, which is located approximately 8-11 km below the sea surface, represents the transition of the oceanic crust to the upper mantle. Seawater can circulate to various depths through the “porous” and cracked oceanic crust. At depths approaching 1.3 km, i.e. deep down into the sheeted dikes, redox conditions correspond to those adjusted by the PPM mineral (Alt et al., 1989). Deeper in the circulating systems, closer to the ultramafic zone, it is likely that redox conditions are fixed by the quartz-fayalite-magnetite mineral assemblage (Shock, 1990), which adjusts more reducing than PPM. If the oceanic crust is covered by organic-rich sediments, sea water percolating through the sediments into the crust may leach organic matter from the sediment layer and carry it along down into the crust. Physicochemical changes and complex reactions may occur in the subsurface, including but not limited to: redox and pH changes, mineral precipitation, metal leaching and ion extractions. Zones where this may occur are roughly sketched. Figure adapted from Degens (1989) with kind permission of Springer.

7.2.1 TRANSFERABILITY OF EXPERIMENTAL RESULTS

Known submarine hydrothermal systems are usually situated at water depths of 2,000 - 3,600 m (Hannington et al., 2005), which corresponds to a hydrostatic pressure of 20 - 36 MPa. Temperature of venting fluids can vary between 10 to >350°C depending on venting type, but temperatures of 300 to 350°C are not uncommon (Hannington et al., 1995). In fact, 100 out of the 300 submarine hydrothermal systems that have been discovered until 2005 are associated with high-temperature ($\geq 350^\circ\text{C}$) venting. Such systems are usually referred to as black smokers (Hannington et al., 2005). The discussion shows that pressure and temperature conditions in high-temperature submarine hydrothermal systems can directly mirror the experimental conditions.

Interestingly, most vent solutions show constant fluid composition throughout the lifetime of a vent field (Von Damm, 1990). This hints at some controlling mechanism at depth, which influences the composition of the fluids. Most fluids associated with black

smokers are strongly buffered close to equilibrium with pyrite, pyrrhotite and magnetite with respect to oxygen and sulfur fugacity (Bowers et al., 1988; Von Damm, 1990). The PPM minerals are present in the upper part of the oceanic crust and buffer the redox conditions at depths approaching 1.3 km (Alt et al., 1989) (Fig. 41). At the deeper parts of the circulation system fluids are rather buffered close to the quartz-fayalite-magnetite (QFM) buffer. The QFM mineral assemblage adjusts conditions, which are approximately one order of magnitude more reducing than with PPM. Based on this discussion, it is inferred that at least the results from experiments with the PPM mineral buffer are directly applicable to high-temperature submarine hydrothermal systems.

The sulfate concentration of bottom seawater (28 mmol/kg_{H₂O} Hannington et al., 2005) is one order of magnitude below the dissolved sulfate concentration in the 350°C experiments (290 mmol/kg_{H₂O}), which were performed in the course of the present study. Furthermore, the sulfate concentration in venting fluids can be significantly lower than in the seawater due to anhydrite precipitation along the circulation conduit (Fig. 41). Differences in initial sulfate concentration might negatively affect the transferability of the results for the sulfate-containing experiments performed at this temperature, because it is generally assumed that the rate of sulfate reduction is dependent on the concentration of reactive sulfate species (Cross et al., 2004; Truche et al., 2009; Zhang et al., 2012). As already stated for petroleum systems (cf. *chapter 7.1.1*), published kinetic rate data are, however, related with large uncertainties. Thus, it is not clear at present, which difference in initial sulfate concentration may actually be critical to evoke a significant change in product distribution if a sample with lower and one with higher sulfate concentration are compared. In contrast to the 350°C, the dissolved sulfate concentration in the 315°C experiments with FeSO₄, CuSO₄ and Fe₂(SO₄)₃ solutions (≤ 13 mmol/kg_{H₂O}) is in the same range as reported by Hannington et al. (2005) for the venting fluids, which facilitates the comparability of the experimental and natural system. Regarding the concentration of dissolved transition metals, data reported by Hannington et al. (2005) show that concentrations in venting fluids are highly variable. In some cases, the concentrations of dissolved transition metals fall, however, in the same range as in the experimental samples of the present study. Thus, results of the transition metal sulfate samples may directly be transferable. Another distinct characteristic of submarine hydrothermal systems is that the dominating phase is water. This facilitates the direct application of the experimental results, because water was also the dominating

phase during the experiments. Furthermore, significant amounts of hydrocarbons can be present in these systems, as will be addressed in the next section.

The above discussion stresses the close similarity that high-temperature submarine hydrothermal systems can have with the experimental system. This emphasizes the potential that submarine hydrothermal systems have to serve as a natural analogue for the experiments performed in the course of this study. One specific example is discussed in the next section.

7.2.2 IMPLICATIONS III: PETROLEUM ALTERATION IN SUBMARINE HYDROTHERMAL SYSTEMS

High-temperature (300-350°C) petroleum formation is a “widespread process in hydrothermal systems” (Simoneit, 1990, 2013). A well studied site where this occurs is the Guayamas Basin located in the central part of the Gulf of California (Simoneit, 1985; Kawka and Simoneit, 1987; Didyk and Simoneit, 1989). Seawater circulates through the sediment layer, leaches the organic matter and carries it further down into the crust (Fig. 41). In the Guayamas Basin, “the oil expulsion and migration mechanisms are provided by the hydrothermal fluids under pressures of 200 bars and temperature conditions up to and exceeding 315°C at some vent outlets” (Didyk and Simoneit, 1989). If the circulation reaches down into the QFM-buffered ultramafic zone of the crust (Fig. 41), abiotic synthesis of hydrocarbons may also contribute to expelled petroleum (Konn et al., 2009). The biomarker signature of the generated petroleum in the Guayamas Basin provides, however, evidence that the sediments are the main source of the organic matter at this location (Simoneit, 1990).

Hydrothermal oils show striking similarity to conventionally exploited crude oils (Simoneit, 1985; Didyk and Simoneit, 1989; Simoneit, 2013). Hydrothermal oil in the Guayamas Basin has a young geological age (< 5,000 yr). This is significantly below that of conventional oils, which are usually several million years old (Simoneit, 2013). According to Simoneit (1990, 2013), the “instantaneous” (on a geological timescale) oil generation in hydrothermal systems is an efficient process for petroleum generation, expulsion and migration. This could have a considerable impact on our understanding of petroleum

formation mechanisms and eventually assist us in tapping resources in new high-temperature environments (Didyk and Simoneit, 1989; Simoneit, 2013).

Conditions in the Guayamas Basin show striking similarities to the experimental systems used in the present study. All inorganic and organic components under investigation are present to various degrees. Thus, ample opportunity for inorganic-organic interactions should exist. The inorganic reduction of sulfate by minerals, like for example during serpentinization of olivine, is a well-documented process in submarine hydrothermal systems (Seyfried and Dibble, 1980; Shanks et al., 1981; Alt et al., 1989). In contrast, true TSR, i.e. sulfate reduction with the involvement of organic matter, has not been studied in this context. It may, however, have implications for the composition of expelled petroleum.

7.3 SULFIDE ORE DEPOSITS

Last but not least, inorganic-organic interactions can play an important role for the formation of sulfide ore deposits. Here, organic matter, and more specifically organic acid anions, play an important role for the transportation of metals in ore-forming solutions (Manning and Gize, 1993; McCollom and Seewald, 2003a). Furthermore, organic matter can be an important controlling factor for the precipitation of ore minerals. A relevant inorganic-organic reaction, which has been studied in this context, is TSR. It is well documented for Mississippi Valley type deposits (Powell and Macqueen, 1984; Leventhal, 1990) and the Kupferschiefer (Sun, 1998; Sun and Püttmann, 2000; Bechtel et al., 2001; Sun and Püttmann, 2003). A case study of the latter is briefly discussed below.

7.3.1 IMPLICATION IV: THERMOCHEMICAL SULFATE REDUCTION IN THE KUPFERSCHIEFER

Sun and Püttmann (2000) investigated possible contributions of TSR during Kupferschiefer mineralization in the Sangerhausen basin, Germany. Petrological and geochemical analyses of the Kupferschiefer show that Cu was precipitated by replacement of biogenic pyrite and by TSR. Their results indicate that TSR contributed up to 60 % of the total Cu mineralization. With increasing copper content in the ore, they observe a stronger TSR

signature in the organic matter, which is characterized by an increase in the amounts of aromatic hydrocarbons and organosulfur compounds (Fig. 42 A & B). This correlates well with results of the present study. For the Cu-containing samples the concentration of aromatic hydrocarbons increases with increasing generation of organosulfur compounds, i.e. increasing TSR (Fig. 42 C & D).

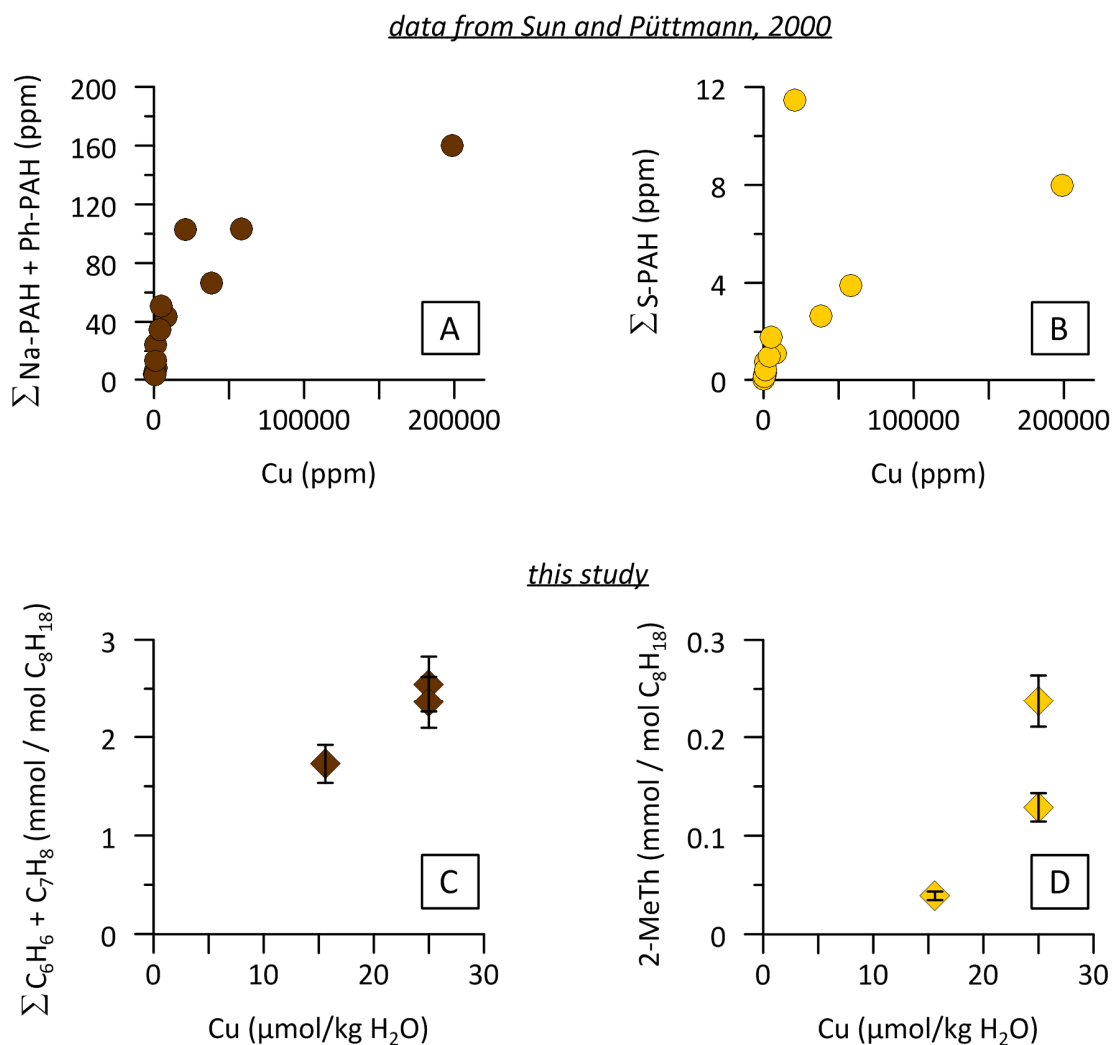


Fig. 42: Sulfur-free aromatic hydrocarbon and organosulfur compound concentrations in natural Kupferschiefer samples from the Sangerhausen basin, Germany (**A & B**, data from Sun and Püttmann (2000)), and those produced in CuSO₄-containing samples, which were processed at 315°C and 13 MPa for 168 h in presence of *n*-octane and water (**D & E**, data from this study). Results from both studies show the same trend, i.e. increasing concentrations of sulfur-free aromatic hydrocarbons with increasing Cu content (**A & C**), as well as increasing concentrations of organosulfur compounds with increasing Cu content (**B & D**). In detail, the graphs show: (**A**) correlation of the sum of quantified naphthalenes and alkylated naphthalenes (Na-PAH = 16 compounds), and phenanthrenes and alkylated phenanthrenes (Ph-PAH = 18 compounds) vs. Cu contents, and (**B**) correlation of the sum of quantified S-containing aromatic hydrocarbons (S-PAH = 10 compounds) vs. Cu contents. A detailed list of all quantified Na-PAH, Ph-PAH and S-PAH compounds is presented by Sun and Püttmann (2000). For the CuSO₄-containing samples, benzene and toluene were quantified as sulfur-free aromatic hydrocarbons (**C**) and 2-methylthiophene as organosulfur compound (**D**).

The typical temperatures involved in the formation of the Kupferschiefer and other sediment-hosted sulfide deposits associated with organic matter, are below 200°C (Manning and Gize, 1993; Sun and Püttmann, 2000). This might limit direct extrapolation of the experimental results, as discussed in *chapter 7.1.1*. Good correlation of experimental results with natural observations from Sun and Püttmann (2000) is, however, compelling. This highlights the potential, which experimental studies can have to simulate ore-forming processes in sulfide deposits like those of the Kupferschiefer type.

8.

CONCLUSIONS

In this study, the reaction of *n*-octane with a variety of inorganic compounds under hydrothermal conditions was investigated in well constrained laboratory experiments. This included the use of purely synthetic compounds. Investigated inorganic additives comprise iron-containing minerals (hematite-magnetite and pyrite-pyrhotite-magnetite), dissolved sodium sulfate (Na_2SO_4) and dissolved transition metal sulfates (FeSO_4 , $\text{Fe}_2(\text{SO}_4)_3$, NiSO_4 , CuSO_4 and ZnSO_4). Gold capsules were used as inert sample containers. Experiments were conducted at temperatures ranging from 300 to 350°C, at pressures of 13 and 35 MPa for 72-366 h. The run duration for most experiments was 168 h (= 1 week). After the experiments, solids were analyzed using X-ray diffraction and organic reaction products were analyzed via headspace gas chromatography. Results of the experiments provide insight into the effect of inorganic components on hydrocarbon transformation and associated processes at hydrothermal conditions. Main findings comprise the following:

1. Overall, the distribution pattern of organic products is very similar for all samples. The most abundant product group are *n*-alkanes, and the single most abundant product component is CO_2 . Generated amounts of ketones reach those of corresponding *n*-alkanes. The results show that cracking, and aqueous oxidation are the major controlling factors for *n*-octane decomposition in all samples.

The results show that oxygen-containing products play a significant role for hydrocarbon degradation under hydrothermal conditions, as has already been pointed out by Seewald (2001). Hence, it is surprising that CO_2 and organic acids are usually quantified in experimental and natural fluids, but not ketones although they may reveal interesting insight into degradation processes.

2. Despite a general agreement of the distribution pattern for the organic products, results clearly show that the examined inorganic compounds can affect the distribution and abundance of generated products to various, non-negligible degrees. This is illustrated by, but not limited to the following observations:

- a. Different additives cause a varying *n*-octane conversion, which ranges from 0.24 mol% (PPM+C₈H₁₈+H₂O 300°C) to 28 mol% (C₈H₁₈+H₂O+CuSO₄ 315°C).
 - b. Despite a complex reaction network, generated products reflect more oxidizing conditions in presence of HM than in presence of the PPM minerals, which is in agreement with the redox buffering ability of these mineral assemblages. Thermodynamic evaluations of the results provide evidence that the buffers can also control the equilibrium of redox dependent organic-organic reactions. Evidence is provided that alkanes and alkenes, but not alkenes and ketones, attained thermodynamic equilibrium with respect to the aqueous hydrogen concentration, which was regulated by the mineral buffers during the experiments.
 - c. Addition of sodium sulfate reduces the oxidation of *n*-octane to CO₂ in the buffer-free, HM and PPM systems, although TSR may have proceeded (*see below*). Thermodynamic evaluations show that this cannot be attributed to carbonate precipitation. An alternative explanation might be a change in the reaction network (*see next point*).
3. Results for the sulfate-containing PPM experiments (PPM+C₈H₁₈+H₂O+Na₂SO₄ 350°C), show an elevated methane yield if compared to corresponding buffer-free and HM samples, which were processed at the same temperature. This cannot be explained by cracking and aqueous oxidation alone and calls for further explanation. The results show striking similarity with observations for H₂S-catalyzed TSR of Zhang et al. (2008a; 2008b). This process involves labile sulfur compounds (LSC) as intermediate species and may produce methane as one end product. Based on the results it is hypothesized that H₂S derived from the PPM mineral buffer may initiate this process at a subordinate rate and, at this initial stage, evoke a shift in the reaction network toward an LSC pathway. This may also explain the observed decrease in oxidation of *n*-octane to CO₂. Similar observations for the buffer-free and HM samples may indicate that TSR might also have occurred upon sulfate addition, but with a rate substantially below that in the sulfate-containing PPM samples.

The involvement of TSR in the Na₂SO₄ containing experiments is speculative at this stage, and calls for further investigation. However, the fact that H₂S-catalyzed

TSR may successfully explain the observations cannot be dismissed. To test the hypothesis it is suggested to repeat the PPM experiments and analyze the samples in the same way as in the present study, with additional quantification of organosulfur compounds.

4. Due to an extended calibration of the gas chromatograph, this was enabled for transition metal sulfate samples. Here, three organosulfur compounds (thiophene, 2- and 3-methylthiophene) could be quantified with the following results:
 - a. Organosulfur compounds (OSCs) were identified for $\text{Fe}_2(\text{SO}_4)_3$, FeSO_4 and CuSO_4 containing samples, which were processed at 315°C . Due to the fact that sulfate is the only sulfur source in these experiments, formation of OSCs is a direct indicator for TSR. No OSCs were detected in presence of ZnSO_4 and NiSO_4 , although this does not necessarily exclude the occurrence of TSR (see *point 3*). The observation that an increase in gas dryness with increasing concentration of the metal sulfate was observed for all transition metal sulfate samples may be an indication for TSR, even if no organosulfur compounds were detected.
 - b. Results represent one of the few examples for TSR without the initial presence of low valence sulfur. Moreover, results for CuSO_4 samples represent the first published example of TSR at $\text{pH} \geq 4$.
 - c. Under the assumption that no metal sulfides precipitated, the following extent of TSR can be estimated from the generated amount of OSCs: $\text{Fe}_3(\text{SO}_4)_2 \gg \text{FeSO}_4 > \text{CuSO}_4$.
 - d. The observation that the extent of TSR is highest in presence of $\text{Fe}_3(\text{SO}_4)_2$ is consistent with the low pH of these samples at experimental conditions.
 - e. Based on the results and comparison with data from Zhang et al. (2012), it is hypothesized that the concentration of the dissolved transition metals is one of the main parameters controlling the extent of TSR at $\text{pH} > 1$.
Furthermore, the results provide evidence that the redox potential, or more specifically the reduction potential of the metals, may have a positive effect

on TSR. This is indicated by the observation that conversion is highest in presence of Fe(III) and Cu(II) the only two metal cations, which can easily be reduced under experimental conditions. Last but not least the electron configuration is suggested to play an important role, because it determines the complexing behavior of the transition metals and therefore its reactivity during TSR.

Results of the present study demonstrate the potential, which laboratory experiments have to study inorganic-organic interactions under well-constrained conditions. Results clearly show that the reaction network and associated processes responsible for hydrocarbon conversion at hydrothermal conditions can be significantly influenced by the inorganic components that were investigated. This demonstrates that hydrocarbon stability at elevated temperature and pressure is not limited to the two controlling factors time and temperature, which is often assumed in conventional petroleum and basin models. Recent advances in petroleum system modeling (Peters et al., 2013) try to overcome this problem, but knowledge of the effect of inorganic components on organic matter transformation is still inadequate, stressing the need for further research.

I propose that experimental studies similar to the present one will contribute to an improved understanding in this context. An in depth analysis of experimental results, in conjunction with thermodynamic evaluations has the potential to reveal most interesting insights into the effect of inorganic component on hydrocarbon conversion. This could have a considerable impact on our understanding of organic-inorganic interactions and may eventually help to tune conventional basin and petroleum models.

References

- Alt, J.C., Anderson, T.F., Bonnell, L., 1989. The geochemistry of sulfur in a 1.3 km section of hydrothermally altered oceanic crust, DSDP Hole 504B. *Geochimica et Cosmochimica Acta* 53, 1011-1023.
- Amrani, A., Deev, A., Sessions, A.L., Tang, Y., Adkins, J.F., Hill, R.J., Moldowan, J.M., Wei, Z., 2012. The sulfur-isotopic compositions of benzothiophenes and dibenzothiophenes as a proxy for thermochemical sulfate reduction. *Geochimica et Cosmochimica Acta* 84, 152-164.
- Amrani, A., Zhang, T., Ma, Q., Ellis, G.S., Tang, Y., 2008. The role of labile sulfur compounds in thermochemical sulfate reduction. *Geochimica et Cosmochimica Acta* 72, 2960-2972.
- Bechtel, A., Sun, Y., Püttmann, W., Hoernes, S., Hoefs, J., 2001. Isotopic evidence for multi-stage base metal enrichment in the Kupferschiefer from the Sangerhausen Basin, Germany. *Chemical Geology* 176, 31-49.
- Behar, F., Vandenbroucke, M., 1996. Experimental Determination of the Rate Constants of the n-C₂₅ Thermal Cracking at 120, 400, and 800 bar: Implications for High-Pressure/High-Temperature Prospects. *Energy & Fuels* 10, 932-940.
- Bell, J.L.S., Palmer, D.A., Barnes, H.L., Drummond, S.E., 1994. Thermal decomposition of acetate: III. Catalysis by mineral surfaces. *Geochimica et Cosmochimica Acta* 58, 4155-4177.
- Bergmann, J., Friedel, P., Kleeberg, R., 1998. BGMN - a new fundamental parameter based Rietveld program for laboratory X-ray sources, its use in quantitative analysis and structure investigations. Commission of Powder Diffraction. *International Union of Crystallography, CPD Newsletter*, 5-8.
- Bethke, C., 1996. *Geochemical reaction modeling: Concepts and applications*. Oxford University Press New York.
- Bowers, T.S., Campbell, A.C., Measures, C.I., Spivack, A.J., Khadem, M., Edmond, J.M., 1988. Chemical controls on the composition of vent fluids at 13°-11° N and 21° N, East Pacific Rise. *Journal of Geophysical Research: Solid Earth* 93, 4522-4536.
- Carothers, W.W., Kharaka, Y.K., 1978. Aliphatic acid anions in oil-field waters - Implications for origin of natural gas. *AAPG BULLETIN* 62, 2441-2453.
- Chase, M.W., 1998. *NIST-JANAF Thermochemical Tables, Parts I and II*. J. Phys. Chem. Ref. Data, Monograph.
- Chen, T.S., He, Q., Lu, H., Peng, P.A., Liu, J.Z., 2009. Thermal simulation experiments of saturated hydrocarbons with calcium sulfate and element sulfur: Implications on origin of H₂S. *Science in China Series D: Earth Sciences* 52, 1550-1558.
- Cross, M.M., 1999. *Rates and Mechanisms of Thermochemical Sulphate Reduction*, Department of Earth Sciences. University of Manchester, Manchester, p. 314.
- Cross, M.M., Manning, D.A.C., Bottrell, S.H., Worden, R.H., 2004. Thermochemical sulphate reduction (TSR): experimental determination of reaction kinetics and implications of the observed reaction rates for petroleum reservoirs. *Organic Geochemistry* 35, 393-404.
- Dick, J., 2008. Calculation of the relative metastabilities of proteins using the CHNOSZ software package. *Geochemical Transactions* 9.
- Didyk, B.M., Simoneit, B.R.T., 1989. Hydrothermal oil of Guaymas Basin and implications for petroleum formation mechanisms. *Nature* 342, 65-69.
- Drummond, S.E., 1981. PhD thesis: Boiling and mixing of hydrothermal fluids: chemical effects on mineral precipitation PhD thesis. Pennsylvania State University.
- Dry, M., 1990. Fischer-Tropsch synthesis over iron catalysts. *Catalysis Letters* 7, 241-251.

- Fabuss, B.M., Smith, J.O., Satterfield, C.N., 1964. Thermal cracking of pure saturated hydrocarbons. *Advances in Petroleum Chemistry and Refining* 9, 157-201.
- Giuliani, G., France-Lanord, C., Cheilletz, A., Coget, P., Branquet, Y., Laumonnier, B., 2000. Sulfate Reduction by Organic Matter in Colombian Emerald Deposits: Chemical and Stable Isotope (C, O, H) Evidence. *Economic Geology* 95, 1129-1153.
- Goldstein, T.P., Aizenshtat, Z., 1994. Thermochemical sulfate reduction a review. *Journal of Thermal Analysis and Calorimetry* 42, 241-290.
- Greensfelder, B.S., Voge, H.H., Good, G.M., 1949. Catalytic and Thermal Cracking of Pure Hydrocarbons: Mechanisms of Reaction. *Industrial & Engineering Chemistry* 41, 2573-2584.
- Hanin, S., 2002. PhD thesis : Thermoréduction des sulfates dans les réservoirs pétroliers: Approche moléculaire. Université Strasbourg, p. 250.
- Hannington, M.D., de Ronde, C.D.J., Petersen, S., 2005. Sea-floor tectonics and submarine hydrothermal systems. *Economic Geology 100th Anniversary Volume*, 111-141.
- Hannington, M.D., Jonasson, I.R., Herzig, P.M., Petersen, S., 1995. Physical and Chemical Processes of Seafloor Mineralization at Mid Ocean Ridges. *Seafloor hydrothermal systems: physical, chemical, biological, and geological Interactions*, 115-157.
- Harrison, A.G., Thode, H.G., 1957. The kinetic isotope effect in the chemical reduction of sulphate. *Transactions of the Faraday Society* 53, 1648-1651.
- Heidman, J.L., Tsonopoulos, C., Brady, C.J., Wilson, G.M., 1985. High temperature mutual solubilities of hydrocarbons and water. Part II: Ethylbenzene, ethylcyclohexane, and n-octane. *AIChE journal* 31, 376-384.
- Helgeson, H.C., Knox, A.M., Owens, C.E., Shock, E.L., 1993. Petroleum, oil field waters, and authigenic mineral assemblages: Are they in metastable equilibrium in hydrocarbon reservoirs? *Geochimica et Cosmochimica Acta* 57, 3295-3339.
- Hinze, M., 2012. BSc thesis: Stabilität und Verfügbarkeit des Pyrit-Pyrrhotin-Magnetit-Puffers in Hydrothermalen Systemen, Institute for Mineralogy. Leibniz Universität Hannover, Hannover.
- Hoffmann, G.G., Steinfatt, I., Strohschein, A., 1995. Thermal recovery processes and hydrogen sulfide formation, *SPE International Symposium on Oilfield Chemistry*.
- Holleman, A.F., Wiberg, E., 1995. *Lehrbuch der anorganischen Chemie*. Walter de Gruyter & Co, Berlin.
- Holm, N.G., Andersson, E.M., 1995. Abiotic synthesis of organic compounds under the conditions of submarine hydrothermal systems: a perspective. *Planetary and Space Science* 43, 153-159.
- Horsfield, B., Douglas, A.G., 1980. The influence of minerals on the pyrolysis of kerogens. *Geochimica et Cosmochimica Acta* 44, 1119-1131.
- Huc, A.Y., 2003. *Petroleum Geochemistry at the dawn of the 21st Century*. *Oil & Gas Science and Technology - Rev. IFP* 58, 233-241.
- Johnson, J.W., Oelkers, E.H., Helgeson, H.C., 1992. SUPCRT92: A software package for calculating the standard molal thermodynamic properties of minerals, gases, aqueous species, and reactions from 1 to 5000 bar and 0 to 1000°C. *Computers & Geosciences* 18, 899-947.
- Kapadia, P.R., Wang, J.Y.J., Kallos, M., Gates, I.D., 2011. Reactive Thermal Reservoir Simulation: Hydrogen Sulphide Production in SAGD, *Canadian Unconventional Resources Conference*. Society of Petroleum Engineers.
- Kawka, O.E., Simoneit, B.R.T., 1987. Survey of hydrothermally-generated petroleums from the Guaymas Basin spreading center. *Organic Geochemistry* 11, 311-328.

- Khan, M.S., Rogak, S.N., 2004. Solubility of Na₂SO₄, Na₂CO₃ and their mixture in supercritical water. *The Journal of supercritical fluids* 30, 359-373.
- Kharaka, Y.K., Callender, E., Carothers, W.W., Meriwether, J., 1977. Geochemistry of geopressed geothermal waters from the Texas Gulf Coast.
- Kissin, Y.V., 1987. Catagenesis and composition of petroleum: Origin of n-alkanes and isoalkanes in petroleum crudes. *Geochimica et Cosmochimica Acta* 51, 2445-2457.
- Kiyosu, Y., 1980. Chemical reduction and sulfur-isotope effects of sulfate by organic matter under hydrothermal conditions. *Chemical Geology* 30, 47-56.
- Kiyosu, Y., Krouse, H.R., 1990. The role of organic acid in the abiogenic reduction of sulfate and the sulfur isotope effect. *Geochemical Journal* 24, 21-27.
- Kiyosu, Y., Krouse, H.R., 1993. Thermochemical reduction and sulfur isotopic behavior of sulfate by acetic acid in the presence of native sulfur. *Geochemical Journal* 27, 49-57.
- Konn, C., Charlou, J.L., Donval, J.P., Holm, N.G., Dehairs, F., Bouillon, S., 2009. Hydrocarbons and oxidized organic compounds in hydrothermal fluids from Rainbow and Lost City ultramafic-hosted vents. *Chemical Geology* 258, 299-314.
- Kossiakoff, A., Rice, F.O., 1943. Thermal Decomposition of Hydrocarbons, Resonance Stabilization and Isomerization of Free Radicals¹. *Journal of the American Chemical Society* 65, 590-595.
- Leif, R.N., Simoneit, B.R.T., 1995. Ketones in hydrothermal petroleum and sediment extracts from Guaymas Basin, Gulf of California. *Organic Geochemistry* 23, 889-904.
- Leif, R.N., Simoneit, B.R.T., 2000. The role of alkenes produced during hydrous pyrolysis of a shale. *Organic Geochemistry* 31, 1189-1208.
- Leventhal, J.S., 1990. Organic matter and thermochemical sulfate reduction in the Viburnum Trend, Southeast Missouri. *Economic Geology* 85, 622-632.
- Lewan, M.D., 1997. Experiments on the role of water in petroleum formation. *Geochimica et Cosmochimica Acta* 61, 3691-3723.
- Lewan, M.D., Spiro, B., Illich, H., Raiswell, R., Mackenzie, A.S., Durand, B., Manning, D.A.C., Comet, P.A., Berner, R.A., Leeuw, J.W.D., 1985. Evaluation of petroleum generation by hydrous pyrolysis experimentation [and discussion]. *Philosophical Transactions of the Royal Society of London. Series A, Mathematical and Physical Sciences* 315, 123-134.
- Lu, H., Chen, T., Liu, J., Peng, P.a., Lu, Z., Ma, Q., 2010a. Yields of H₂S and gaseous hydrocarbons in gold tube experiments simulating thermochemical sulfate reduction reactions between MgSO₄ and petroleum fractions. *Organic Geochemistry* 41, 1189-1197.
- Lu, H., Chen, T., Peng, P.A., 2010b. Effect of brine on the TSR and generation of H₂S revealed by gold-tube simulation experiments. *Geochimica et Cosmochimica Acta* 74, A634.
- Lu, H., Greenwood, P., Chen, T., Liu, J., Peng, P.a., 2011. The role of metal sulfates in thermochemical sulfate reduction (TSR) of hydrocarbons: Insight from the yields and stable carbon isotopes of gas products. *Organic Geochemistry* 42, 700-706.
- Ma, Q., Ellis, G.S., Amrani, A., Zhang, T., Tang, Y., 2008. Theoretical study on the reactivity of sulfate species with hydrocarbons. *Geochimica et Cosmochimica Acta* 72, 4565-4576.
- Machel, H.G., 2001. Bacterial and thermochemical sulfate reduction in diagenetic settings - old and new insights. *Sedimentary Geology* 140, 143-175.
- Machel, H.G., Krouse, H.R., Sassen, R., 1995. Products and distinguishing criteria of bacterial and thermochemical sulfate reduction. *Applied Geochemistry* 10, 373-389.

- Mango, F.D., 1992. Transition metal catalysis in the generation of petroleum and natural gas. *Geochimica et Cosmochimica Acta* 56, 553-555.
- Mango, F.D., 1997a. The light hydrocarbons in petroleum: a critical review. *Organic Geochemistry* 26, 417-440.
- Mango, F.D., Hightower, J., 1997b. The catalytic decomposition of petroleum into natural gas. *Geochimica et Cosmochimica Acta* 61, 5347-5350.
- Mango, F.D., Hightower, J.W., James, A.T., 1994. Role of transition-metal catalysis in the formation of natural gas. *Nature* 368, 536-538.
- Mango, F.D., Jarvie, D.M., Herriman, E., 2010. Natural catalytic activity in a marine shale for generating natural gas. *Proceedings of the Royal Society A: Mathematical, Physical and Engineering Science*.
- Manning, D.A.C., Gize, A.P., 1993. The role of organic matter in ore transport processes. *Organic Geochemistry—Principles and Applications*, 547-563.
- McCullom, T., 2010. Investigations into the Roles of Minerals in Hydrothermal Organic Geochemistry, Abstract. *Goldschmidt Conference 2010, Knoxville*, p. A686.
- McCullom, T.M., Lollar, B.S., Lacrampe-Couloume, G., Seewald, J.S., 2010. The influence of carbon source on abiotic organic synthesis and carbon isotope fractionation under hydrothermal conditions. *Geochimica et Cosmochimica Acta* 74, 2717-2740.
- McCullom, T.M., Seewald, J.S., 2003. Experimental study of the hydrothermal reactivity of organic acids and acid anions: II. Acetic acid, acetate, and valeric acid. *Geochimica et Cosmochimica Acta* 67, 3645-3664.
- McCullom, T.M., Seewald, J.S., 2003a. Experimental constraints on the hydrothermal reactivity of organic acids and acid anions: I. Formic acid and formate. *Geochimica et Cosmochimica Acta* 67, 3625-3644.
- McCullom, T.M., Seewald, J.S., 2007. Abiotic Synthesis of Organic Compounds in Deep-Sea Hydrothermal Environments. *Chemical Reviews* 107, 382-401.
- Meier, A., 2012. PhD thesis: Experimentelle Untersuchungen zu Reaktionen von Erdölverbindungen (n-Alkanen) mit Hämatit-Kutanen in klastischen Erdölspeichergesteinen. Friedrich-Schiller-Universität Jena.
- Moldoveanu, S.C., 2010. *Pyrolysis of organic molecules with application to health and environmental issues*, 1st ed. Elsevier, Amsterdam.
- Nöth, S., 1997. High H₂S contents and other effects of thermochemical sulfate reduction in deeply buried carbonate reservoirs: a review. *Geologische Rundschau* 86, 275-287.
- Olah, G.A., Molnár, Á., 2003. *Hydrocarbon chemistry*, 2nd ed. Wiley-interscience.
- Orr, W.L., 1974. Changes in sulfur content and isotopic ratios of sulfur during petroleum maturation - study of Big Horn basin Paleozoic oils. *AAPG BULLETIN* 58, 2295-2318.
- Orr, W.L., 1977. Geologic and geochemical controls on the distribution of hydrogen sulfide in natural gas, in: Campos, R., Goni, J. (Eds.), *Advances in organic geochemistry*. Enadimsa, Madrid, pp. 572-597.
- Ostertag-Henning, C., Scheeder, G., Hentscher, M., Bach, W., 2010. Reassessing reaction rates for TSR by experiments and modelling. *Geochimica et Cosmochimica Acta* 74, A780.
- Ott, L., Lehr, V., Urfels, S., Bicker, M., Vogel, H., 2006. Influence of salts on the dehydration of several biomass-derived polyols in sub- and supercritical water. *The Journal of supercritical fluids* 38, 80-93.
- Pabalan, R.T., Pitzer, K.S., 1988. Heat capacity and other thermodynamic properties of Na₂SO_{4(aq)} in hydrothermal solutions and the solubilities of sodium sulfate minerals in the system Na-Cl-SO₄-OH-H₂O to 300° C. *Geochimica et Cosmochimica Acta* 52, 2393-2404.
- Palmer, D.A., Drummond, S.E., 1986. Thermal decarboxylation of acetate. Part I. The kinetics and mechanism of reaction in aqueous solution. *Geochimica et Cosmochimica Acta* 50, 813-823.

- Pan, C., Yu, L., Liu, J., Fu, J., 2006. Chemical and carbon isotopic fractionations of gaseous hydrocarbons during abiogenic oxidation. *Earth and Planetary Science Letters* 246, 70-89.
- Peters, K.E., Hantschel, T., Kauerauf, A.I., Tang, Y., Wygrala, B., 2013. Recent Advances in Petroleum System Modeling of Geochemical Processes: TSR, SARA, and Biodegradation. Search and Discovery Article #41261, AAPG Annual Convention and Exhibition, Pittsburgh, Pennsylvania.
- Pokrovskii, V.A., Helgeson, H.C., 1994. Solubility of petroleum in oil-field waters as a function of the oxidation state of the system. *Geology* 22, 851-854.
- Powell, T.G., Macqueen, R.W., 1984. Precipitation of Sulfide Ores and Organic Matter: Sulfate Reactions at Pine Point, Canada. *Science* 224, 63-66.
- Price, L.C., 1976. Aqueous solubility of petroleum as applied to its origin and primary migration. AAPG BULLETIN 60, 213-244.
- Price, L.C., 1993. Thermal stability of hydrocarbons in nature: Limits, evidence, characteristics, and possible controls. *Geochimica et Cosmochimica Acta* 57, 3261-3280.
- Price, L.C., 2001. A possible deep-basin high-rank gas machine via water-organic matter redox reactions. U.S. Geological Survey Electronic Bulletin.
- Price, L.C., DeWitt, E., 2001. Evidence and characteristics of hydrolytic disproportionation of organic matter during metasomatic processes. *Geochimica et Cosmochimica Acta* 65, 3791-3826.
- Price, L.C., Schoell, M., 1995. Constraints on the origins of hydrocarbon gas from compositions of gases at their site of origin. *Nature* 378, 368-371.
- Proskurowski, G., Lilley, M.D., Seewald, J.S., Früh-Green, G.L., Olson, E.J., Lupton, J.E., Sylva, S.P., Kelley, D.S., 2008. Abiogenic Hydrocarbon Production at Lost City Hydrothermal Field. *Science* 319, 604-607.
- Pryor, W.A., 1962. Mechanisms of sulfur reactions. McGraw-Hill.
- Reeves, E.P., Seewald, J.S., Sylva, S.P., 2012. Hydrogen isotope exchange between n-alkanes and water under hydrothermal conditions. *Geochimica et Cosmochimica Acta* 77, 582-599.
- Rice, F.O., 1931. The thermal decomposition of organic compounds from the standpoint of free radicals. I. Saturated hydrocarbons. *Journal of the American Chemical Society* 53, 1959-1972.
- Rice, F.O., Herzfeld, K.F., 1934. The Thermal Decomposition of Organic Compounds from the Standpoint of Free Radicals. VI. The Mechanism of Some Chain Reactions. *Journal of the American Chemical Society* 56, 284-289.
- Robb, L., 2009. Introduction to ore-forming processes. John Wiley & Sons.
- Robie, R.A., Hemingway, B.S., 1995. Thermodynamic properties of minerals and related substances at 298.15 K and 1 bar (10⁵ Pascals) pressure and at higher temperatures. US Geol. Survey Bull., vol. 2131, p. 461-461 (1995). 2131, 461-461.
- Rooney, M.A., 1995. Carbon isotope ratios of light hydrocarbons as indicators of thermochemical sulfate reduction, in: Grimalt, J.O., Dorronsoro, C. (Eds.), *Organic Geochemistry: Developments and Applications to Energy, Climate, Environment and Human History*, Donostia-San Sebastian, Spain, pp. 523-525.
- Safarik, I., Strausz, O., 1996. The thermal decomposition of hydro-carbons. Part 1. n-alkanes (C > 5). *Research on Chemical Intermediates* 22, 275-314.
- Sassen, R., 1988. Geochemical and carbon isotopic studies of crude oil destruction, bitumen precipitation, and sulfate reduction in the deep Smackover Formation. *Organic Geochemistry* 12, 351-361.
- Saunders, J.A., Swann, C.T., 1990. Trace-metal content of Mississippi oil field brines. *Journal of Geochemical Exploration* 37, 171-183.

- Schöner, R., Gaupp, R., 2005. Contrasting red bed diagenesis: the southern and northern margin of the Central European Basin. *International Journal of Earth Sciences* 94, 897-916.
- Seewald, J.S., 1994. Evidence for metastable equilibrium between hydrocarbons under hydrothermal conditions. *Nature* 370, 285-287.
- Seewald, J.S., 2001. Aqueous geochemistry of low molecular weight hydrocarbons at elevated temperatures and pressures: constraints from mineral buffered laboratory experiments. *Geochimica et Cosmochimica Acta* 65, 1641-1664.
- Seewald, J.S., 2003. Organic-inorganic interactions in petroleum-producing sedimentary basins. *Nature* 426, 327-333.
- Seyfried, W.E., Dibble, W.E., 1980. Seawater-peridotite interaction at 300°C and 500 bars: implications for the origin of oceanic serpentinites. *Geochimica et Cosmochimica Acta* 44, 309-321.
- Shanks, W.C., Bischoff, J.L., Rosenbauer, R.J., 1981. Seawater sulfate reduction and sulfur isotope fractionation in basaltic systems: Interaction of seawater with fayalite and magnetite at 200-350°C. *Geochimica et Cosmochimica Acta* 45, 1977-1995.
- Shipp, J., Gould, I.R., Herckes, P., Shock, E.L., Williams, L.B., Hartnett, H.E., 2013. Organic functional group transformations in water at elevated temperature and pressure: Reversibility, reactivity, and mechanisms. *Geochimica et Cosmochimica Acta* 104, 194-209.
- Shipp, J.A., Hartnett, H.E., Gould, I.R., Shock, E.L., Williams, L.B., 2010. Minerals affect the interconversion between alkanes and alkenes in hydrothermal systems, Abstract. *Goldschmidt Conference 2010*, Knoxville, p. A954.
- Shock, E.L., 1988. Organic acid metastability in sedimentary basins. *Geology* 16, 886-890.
- Shock, E.L., 1989. Corrections to "Organic acid metastability in sedimentary basins". *Geology* 17, 572-573.
- Shock, E.L., 1990. Geochemical constraints on the origin of organic compounds in hydrothermal systems. *Origins of Life and Evolution of Biospheres* 20, 331-367.
- Shock, E.L., 1992. Chapter 5 Chemical environments of submarine hydrothermal systems. *Origins of Life and Evolution of Biospheres* 22, 67-107.
- Simoneit, B.R.T., 1985. Hydrothermal petroleum: genesis, migration, and deposition in Guaymas Basin, Gulf of California. *Canadian Journal of Earth Sciences* 22, 1919-1929.
- Simoneit, B.R.T., 1990. Petroleum generation, an easy and widespread process in hydrothermal systems: an overview. *Applied Geochemistry* 5, 3-15.
- Simoneit, B.R.T., 2013. Natural hydrous pyrolysis - Petroleum generation in submarine hydrothermal systems, Productivity, Accumulation and Preservation of Organic Matter in Recent and Ancient Sediments, Chapter 16, pp. 368-402.
- Siskin, M., Katritzky, A.R., 1991. Reactivity of organic compounds in hot water: Geochemical and technological implications. *Science(Washington)* 254, 231-237.
- Stalker, L., Farrimond, P., Larter, S.R., 1994. Water as an oxygen source for the production of oxygenated compounds (including CO₂ precursors) during kerogen maturation. *Organic Geochemistry* 22, 477-484.
- Sun, Y.-Z., 1998. Influences of secondary oxidation and sulfide formation on several maturity parameters in Kupferschiefer. *Organic Geochemistry* 29, 1419-1429.
- Sun, Y.-Z., Püttmann, W., 2000. The role of organic matter during copper enrichment in Kupferschiefer from the Sangerhausen basin, Germany. *Organic Geochemistry* 31, 1143-1161.

- Sun, Y., Püttmann, W., 2003. The role of organic matter during metal enrichment in Permian Kupferschiefer of the Rudna mine, Southwest Poland. *Chinese Journal of Geochemistry* 22, 1-10.
- Surdam, R.C., Crossey, L.J., Hagen, E.S., Heasler, H.P., 1989. Organic-inorganic interactions and sandstone diagenesis. *AAPG BULLETIN* 73, 1-23.
- Surdam, R.C., Jiao, Z.S., MacGowan, D.B., 1993. Redox reactions involving hydrocarbons and mineral oxidants: A mechanism for significant porosity enhancement in sandstones. *AAPG BULLETIN* 77, 1509-1509.
- Toland, W.G., 1960. Oxidation of organic compounds with aqueous sulfate. *Journal of the American Chemical Society* 82, 1911-1916.
- Toulmin, P., Barton, P.B., 1964. A thermodynamic study of pyrite and pyrrhotite. *Geochimica et Cosmochimica Acta* 28, 641-671.
- Truche, L., Berger, G., Cartigny, P., 2011. Sulphate reduction induced by hydrogen under hydrothermal conditions. *Mineralogical Magazine* 75, 2034. Abstract for poster presentation at the Goldschmidt Conference 2011 in Prague.
- Truche, L., Berger, G., Destriigneville, C., Pages, A., Guillaume, D., Giffaut, E., Jacquot, E., 2009. Experimental reduction of aqueous sulphate by hydrogen under hydrothermal conditions: Implication for the nuclear waste storage. *Geochimica et Cosmochimica Acta* 73, 4824-4835.
- Trudinger, P.A., Chambers, L.A., Smith, J.W., 1985. Low-temperature sulphate reduction: biological versus abiological. *Canadian Journal of Earth Sciences* 22, 1910-1918.
- Vollhardt, K.P.C., Schore, N.E., 2005. *Organische Chemie*. John Wiley & Sons.
- Von Damm, K.L., 1990. Seafloor Hydrothermal Activity: Black Smoker Chemistry and Chimneys. *Annual Review of Earth and Planetary Sciences* 18, 173-204.
- Wei, Z., Walters, C.C., Michael Moldowan, J., Mankiewicz, P.J., Pottorf, R.J., Xiao, Y., Maze, W., Nguyen, P.T.H., Madincea, M.E., Phan, N.T., Peters, K.E., 2012. Thiadiamondoids as proxies for the extent of thermochemical sulfate reduction. *Organic Geochemistry* 44, 53-70.
- Weisshaar, J.C., 1993. Bare transition metal atoms in the gas phase: reactions of M, M⁺, and M²⁺ with hydrocarbons. *Accounts of chemical research* 26, 213-219.
- Winters, J.C., Williams, J.A., Lewan, M.D., 1981. A laboratory study of petroleum generation by hydrous pyrolysis. *Advances in organic geochemistry*, 524-533.
- Wolery, T.J., Jove-Colon, C.F., 2004. Qualification of thermodynamic data for geochemical modeling of mineral-water interactions in dilute systems. Yucca Mountain Project, Las Vegas, NV (United States). Funding organisation: US Department of Energy (United States).
- Worden, R.H., Smalley, P.C., 1996. H₂S-producing reactions in deep carbonate gas reservoirs: Khuff Formation, Abu Dhabi. *Chemical Geology* 133, 157-171.
- Worden, R.H., Smalley, P.C., Barclay, S.A., 2003. H₂S and diagenetic pyrite in North Sea sandstones: due to TSR or organic sulphur compound cracking? *Journal of Geochemical Exploration* 78, 487-491.
- Worden, R.H., Smalley, P.C., Cross, M.M., 2000. The influence of rock fabric and mineralogy on thermochemical sulfate reduction: Khuff Formation, Abu Dhabi. *Journal of Sedimentary Research* 70, 1210-1221.
- Yue, C., Li, S., Ding, K., Zhong, N., 2006. Thermodynamics and kinetics of reactions between C₁-C₃ hydrocarbons and calcium sulfate in deep carbonate reservoirs. *Geochemical Journal* 40, 87-94.
- Yund, R.A., Hall, H.T., 1969. Hexagonal and monoclinic pyrrhotites. *Economic Geology* 64, 420-423.
- Zhang, T., Amrani, A., Ellis, G.S., Ma, Q., Tang, Y., 2008b. Experimental investigation on thermochemical sulfate reduction by H₂S initiation. *Geochimica et Cosmochimica Acta* 72, 3518-3530.

- Zhang, T., Ellis, G.S., Ma, Q., Amrani, A., Tang, Y., 2012. Kinetics of uncatalyzed thermochemical sulfate reduction by sulfur-free paraffin. *Geochimica et Cosmochimica Acta* 96, 1-17.
- Zhang, T., Ellis, G.S., Walters, C.C., Kelemen, S.R., Wang, K.-S., Tang, Y., 2008a. Geochemical signatures of thermochemical sulfate reduction in controlled hydrous pyrolysis experiments. *Organic Geochemistry* 39, 308-328.
- Zhang, T., Ellis, G.S., Wang, K.-s., Walters, C.C., Kelemen, S.R., Gillaizeau, B., Tang, Y., 2007. Effect of hydrocarbon type on thermochemical sulfate reduction. *Organic Geochemistry* 38, 897-910.

Appendix

A. Tables A1 & A2	I
B. Figures B1 – B4	VI
C. Summary of the Bachelor Thesis from Hinze (2012)	VIII
Curriculum Vitae • Svenja Erdmann (née Germerott)	x
List of Publications	xII

A. TABLES A1 & A2

Table A1: Concentrations of generated products from *n*-octane at 300 and 350°C in presence of the pyrite-pyrrhotite-magnetite (PPM), the hematite-magnetite (HM), and without any mineral buffer (-buf). Samples were processed for 72 to 336 h.

		Experimental conditions			Sample composition					Reaction products (mmol/mol C ₈ H ₁₈)									
Sample name		<i>n</i>	<i>t</i> (h)	<i>T</i> (°C)	<i>P</i> (MPa)	PPM (mg)	HM (mg)	H ₂ O (μmol)	C ₈ H ₁₈ (μmol)	Na ₂ SO ₄ (μmol)	CO ₂	methane	ethane	propane	butane	pentane	hexane	heptane	
Detection limits and blanks											1.8	0.0062	0.0034	0.0044	0.0020	0.0021	0.0044	0.0014	
PPM blank 300°C		1	168	300	35	29		4992		148	-	-	-	-	-	-	-	-	
PPM blank 350°C		1	168	350	35	30		5154		150	-	-	-	-	-	-	-	-	
SERIES 1 sulfate-free	300°C	-buf C ₈ 300°C	1	168	300	35			4951	29		25 (±3)	6.6 (±0.7)	3.1 (±0.3)	3.2 (±0.4)	2.9 (±0.3)	1.8 (±0.2)	1.5 (±0.16)	+
		PPM C ₈ 300°C	1	168	300	35	30		4972	30		5.6 (±1.2)	1.5 (±0.2)	1.5 (±0.2)	1.7 (±0.2)	1.3 (±0.1)	0.74 (±0.08)	0.15 (±0.02)	+
	350°C	C ₈ + 350°C	1	168	350	35				31		26 (±3)	10 (±1)	23 (±3)	27 (±3)	25 (±3)	27 (±3)	8.5 (±0.9)	2.0 (±0.2)
		-buf C ₈ 350°C	2	168	350	35			5010	30		23 (±3)	9.3 (±1.0)	21 (±2)	30 (±3)	25 (±3)	24 (±3)	9.6 (±1.1)	1.7 (±0.2)
		PPM C ₈ 350°C	1	168	350	35	29		5004	29		95 (±11)	28 (±3)	52 (±6)	53 (±6)	48 (±5)	54 (±6)	10.5 (±1.2)	2.7 (±0.3)
HM C ₈ 350°C	1	168	350	35		30	4968	31		170 (±19)	14 (±2)	43 (±5)	39 (±4)	39 (±4)	46 (±5)	5.8 (±0.7)	0.81 (±0.09)		
SERIES 2 with sulfate	300°C	-buf C _{8+Na} 300°C	1	168	300	35			5031	30	156	14 (±2)	3.4 (±0.4)	2.4 (±0.3)	2.3 (±0.3)	1.6 (±0.2)	1.6 (±0.2)	0.59 (±0.07)	0.15 (±0.02)
		PPM C _{8+Na} 300°C	4	168	300	35	31		5023	29	159	6.8 (±2.6) ^b	1.3 (±0.1)	0.78 (±0.09)	0.89 (±0.10)	0.61 (±0.07)	0.74 (±0.08)	0.14 (±0.02) ^b	+
		PPM C _{8+Na} 300°C, 336 h	1	336	300	35	30		5070	29	159	na	na	0.51 (±0.06)	0.54 (±0.06)	0.62 (±0.07)	0.63 (±0.07)	0.17 (±0.02)	+
	350°C	-buf C _{8+Na} 350°C	2	168	350	35			4988	30	157	17 (±2)	6.6 (±0.8) ^b	16 (±2) ^b	15 (±2)	14 (±2)	14 (±2)	3.1 (±0.3)	0.53 (±0.06)
		PPM C _{8+Na} 350°C, 72 h	1	72	350	35	30		4990	30	167	-	23 (±3)	31 (±3)	29 (±3)	25 (±3)	30 (±3)	5.5 (±0.6)	+
		PPM C _{8+Na} 350°C	5	168	350	35	30		4981	29	155	65 (±10) ^b	77 (±9)	77 (±9)	64 (±7)	57 (±6)	57 (±6)	9.0 (±1.0)	2.0 (±0.22)
		PPM C _{8+Na} 350°C, 336 h	1	336	350	35	31		5061	30	158	241 (±17)	165 (±18)	128 (±14)	107 (±12)	91 (±10)	89 (±10)	16 (±2)	+
HM C _{8+Na} 350°C	1	168	350	35		30	4979	31	157	57 (±6)	28 (±3)	73 (±8)	61 (±7)	58 (±6)	63 (±7)	10.5 (±1)	2.6 (±0.29)		

Table A1
Continued

Sample name		<i>n</i>	ethene	propene	butene+	iso-butane	iso-pentane	acetone	butanone	benzene	toluene	1-PTH	
Detection limits and blanks			0.0040	0.0048	0.0019	0.0044	0.0045	0.0063	0.0089	0.00018	0.00016		
PPM blank 300°C		1	-	-	-	-	-	na	na	na	na	na	
PPM blank 350°C		1	-	-	-	-	-	na	na	na	na	na	
SERIES 1 sulfate-free	300°C	-buf C ₈ 300°C	1	-	-	-	+	0.21 (±0.02)	1.14 (±0.13)	0.33 (±0.04)	0.036 (±0.008)	0.090 (±0.010)	na
		PPM C ₈ 300°C	1	+	0.87 (±0.18)	0.27 (±0.05)	0.86 (±0.09)	+	0.83 (±0.09)	0.78 (±0.09)	-	-	na
	350°C	C ₈ + 350°C	1	0.043 (±0.005)	1.6 (±0.2)	0.88 (±0.10)	0.45 (±0.05)	0.31 (±0.04)	1.9 (±0.2)	1.7 (±0.2)	0.038 (±0.008)	0.057 (±0.006)	na
		-buf C ₈ 350°C	2	+	0.91 (±0.19)	0.28 (±0.06)	0.83 (±0.09)	0.30 (±0.03)	8.4a (±0.9)	5.6 ^a (±0.8) ^b	0.036 (±0.007)	0.057 (±0.006)	na
		PPM C ₈ 350°C	1	0.27 (±0.03)	2.4 (±0.3)	1.1 (±0.1)	1.9 (±0.2)	2.3 (±0.3)	55 (±6)	38 (±4)	0.19 (±0.02)	0.58 (±0.06)	+
HM C ₈ 350°C	1	0.64 (±0.07)	2.6 (±0.3)	1.8 (±0.2)	0.62 (±0.07)	0.41 (±0.05)	37 (±4)	20 (±2)	0.25 (±0.03)	0.41 (±0.05)	-		
SERIES 2 with sulfate	300°C	-buf C _{8+Na} 300°C	1	-	0.83 (±0.17)	+	-	-	0.83 (±0.09)	0.60 (±0.07)	-	-	na
		PPM C _{8+Na} 300°C	4	-	0.81 (±0.17)	0.25 (±0.05)	-	-	0.12 (±0.04) ^b	0.13 (±0.04) ^b	-	-	na
		PPM C _{8+Na} 300°C, 336 h	1	-	-	-	-	-	na	na	na	na	na
	350°C	-buf C _{8+Na} 350°C	2	0.10 (±0.03) ^b	2.3 (±0.3)	0.93 (±0.10)	0.81 (±0.09)	0.17 (±0.02)	11 ^a (±1)	8 ^a (±1)	0.020 (±0.004)	+	na
		PPM C _{8+Na} 350°C, 72 h	1	0.058 (±0.004)	2.0 (±0.2)	+	0.16 (±0.03)	+	na	na	na	na	na
		PPM C _{8+Na} 350°C	5	0.077 (±0.010)	2.6 (±0.3)	1.3 (±0.1)	0.77 (±0.09)	0.86 (±0.10)	21 ^a (±2)	12 ^a (±1)	0.18 (±0.02)	0.41 (±0.05)	+
PPM C _{8+Na} 350°C, 336 h	1	+	0.095 (±0.020)	2.2 (±0.2)	2.4 (±0.3)	+	na	na	na	na	na		
HM C _{8+Na} 350°C	1	0.68 (±0.08)	6.0 (±0.7)	3.1 (±0.3)	0.64 (±0.07)	0.95 (±0.11)	40 (±5)	21 (±2)	0.13 (±0.01)	0.52 (±0.06)	-		

n = number of samples processed with the same composition

butene+ = mixture of 1-butene and 2-butene

1- PTH = 1-propanethiol

- quantification/detection not possible; due to low concentration and/or strong coelution

+ detected, but concentration too low for quantification

na not analyzed

^a ketone values are corrected for dilution (see chapter 3.5 for details)

^b Error represents the single standard deviation of the arithmetic mean. Errors for the other values reflect the error that is calculated from error propagation of the analytical error and the total weighing error of initial *n*-octane.

Table A1 continued: Calculated values from quantified organic reaction products.

		Experimental conditions			Sample composition					Conversion, gas dryness, oxygen content			log ratios (mol/mol), uncertainty is ± 0.1 log units for all values					
Sample name		<i>n</i>	<i>t</i> (h)	<i>T</i> (°C)	<i>P</i> (MPa)	PPM (mg)	HM (mg)	H ₂ O (μmol)	C ₈ H ₁₈ (μmol)	Na ₂ SO ₄ (μmol)	Conversion of <i>n</i> -octane (mol%)*	C ₁ /ΣC ₁₋₄ (wt%)	O ₂ in organic products (mmol/mol C ₈ H ₁₈)	log[propane/propene]	log[butane/butene+]	log[acetone/propene]	log[butanone/butene+]	
Detection limits and blanks		Detection limits																
		PPM blank 300°C	1	168	300	35	29		4992		148							
		PPM blank 350°C	1	168	350	35	30		5154		150							
SERIES 1 sulfate-free	300°C	-buf C ₈ 300°C	1	168	300	35			4951	29		1.2 (±0.1)	21 (±2)	25 (±4)				
		PPM C ₈ 300°C	1	168	300	35	30		4972	30		0.47 (±0.03)	11 (±1)	6.0 (±1.0)	0.3			
	350°C	C ₈ + 350°C	1	168	350	35				31		6.1 (±0.4)	4.4 (±0.5)	28 (±4)	1.2	1.5	0.1	0.3
		-buf C ₈ 350°C	2	168	350	35			5010	30		6.4 (±0.4)	4.2 (±0.5)	30 (±5)	1.5	2.0	1.0	1.3
		PPM C ₈ 350°C	1	168	350	35	29		5004	29		16 (±1)	6.3 (±0.7)	142 (±22)	1.3	1.7	1.4	1.6
HM C ₈ 350°C	1	168	350	35		30	4968	31		13 (±1)	4.2 (±0.5)	198 (±31)	1.2	1.3	1.2	1.1		
SERIES 2 with sulfate	300°C	-buf C _{8+Na} 300°C	1	168	300	35			5031	30	156	0.69 (±0.05)	17 (±2)	15 (±2)	0.4			
		PPM C _{8+Na} 300°C	4	168	300	35	31		5023	29	159	0.24 (±0.02)	18 (±2)	6.9 (±2.5) ^b	0.04	0.4		
		PPM C _{8+Na} 300°C, 336 h	1	336	300	35	30		5070	29	159							
	350°C	-buf C _{8+Na} 350°C	2	168	350	35			4988	30	157	4.1 (±0.3)	5.2 (±0.6)	27 (±4)	0.8	1.2	0.7	1.0
		PPM C _{8+Na} 350°C, 72 h	1	72	350	35	30		4990	30	167	5.8 (±0.4)	9.3 (±1.0)		1.1			
350°C	PPM C _{8+Na} 350°C	5	168	350	35	30		4981	29	155	15 (±1)	13 (±1)	82 (±13)	1.4	1.7	0.9	1.0	
	PPM C _{8+Na} 350°C, 336 h	1	336	350	35	31		5061	30	158	24 (±2)	16 (±2)		1.7				
HM C _{8+Na} 350°C	1	168	350	35		30	4979	31	157	16 (±1)	5.2 (±0.6)	88 (±14)	1.0	1.3	0.8	0.8		

* In order to estimate the amount of initial *n*-octane, which was converted during the experiments, the mass balance for carbon was calculated. The molar amount of carbon in the reaction products was summed and normalized to the initial amount of carbon provided by *n*-octane (245 ± 12 μmol C). The resulting value is an estimate for the minimum conversion of *n*-octane. Error propagation taking into account the analytical uncertainty and the weighing uncertainty, leads to a relative error for this calculation of 17% for the 300°C samples and 7% for the 350°C samples. This "detour" was necessary owing to the fact that *n*-octane concentrations remaining after the experiments were too high to be accurately measured with the headspace gas chromatograph.

Table A2: Reaction products generated from reaction of *n*-octane with transition metal sulfate and sodium sulfate after 168 h at 315°C and 13 MPa. All samples initially contained 5 µl *n*-octane (= 30.6 µmol). Errors reflect the error that is calculated from error propagation of the analytical error and the total weighing error of initial *n*-octane.

Transition metal sulfate (TMS)	Concentration of stock solution (mol/kg H ₂ O)	Ratio TMS/Na ₂ SO ₄ (µl/µl)	Sample ID	Sample #	Reaction products (mmol/mol C ₈ H ₁₈)										
					CO ₂	methane	ethane	propane	butane	pentane	hexane	heptane	ethene	propene	butene+
Detection limits					2	0.0062	0.0034	0.0044	0.0020	0.0021	0.0044	0.0014	0.004	0.0048	0.0019
Na ₂ SO ₄	0.50	0/200	Na	S06-023	12 (±1)	2.4 (±0.3)	1.7 (±0.2)	1.6 (±0.2)	1.3 (±0.1)	0.69 (±0.08)	0.24 (±0.03)	0.23 (±0.025)	+	0.55 (±0.06)	0.19 (±0.02)
				S06-033	16 (±2)	2.7 (±0.3)	1.8 (±0.2)	1.8 (±0.2)	1.4 (±0.2)	0.71 (±0.08)	0.25 (±0.03)	0.24 (±0.027)	+	0.51 (±0.06)	0.18 (±0.02)
FeSO ₄	0.27	40/160	Fe(II)_mix1	S06-042	11 (±1)	5.1 (±0.6)	4.4 (±0.5)	3.7 (±0.4)	3.5 (±0.4)	3.5 (±0.4)	0.35 (±0.04)	0.062 (±0.013)	0.064 (±0.007)	0.86 (±0.10)	0.32 (±0.04)
		100/100	Fe(II)_mix2	S06-043	19 (±2)	7.8 (±0.9)	6.5 (±0.7)	5.5 (±0.6)	5.1 (±0.6)	5.3 (±0.6)	0.46 (±0.05)	0.070 (±0.014)	0.076 (±0.009)	0.73 (±0.08)	0.32 (±0.04)
				S06-044	23 (±3)	6.4 (±0.7)	5.9 (±0.7)	5.0 (±0.6)	4.5 (±0.5)	4.4 (±0.5)	0.38 (±0.04)	0.043 (±0.009)	0.071 (±0.008)	0.79 (±0.09)	0.35 (±0.04)
200/0	Fe(II)	S06-045	81 (±9)	24 (±3)	12 (±1)	10 (±1)	6.4 (±0.7)	6.6 (±0.7)	0.46 (±0.05)	0.20 (±0.02)	0.051 (±0.006)	0.65 (±0.07)	0.23 (±0.03)		
Fe ₂ (SO ₄) ₃	0.17	42/158	Fe(III)_mix1	S06-046	46 (±5)	13 (±1)	7.3 (±0.8)	5.9 (±0.7)	5.2 (±0.6)	5.1 (±0.6)	0.55 (±0.06)	0.11 (±0.01)	0.089 (±0.010)	0.90 (±0.10)	0.36 (±0.04)
				S06-100	47 (±5)	12 (±1)	6.7 (±0.8)	5.4 (±0.6)	4.7 (±0.5)	4.6 (±0.5)	0.42 (±0.05)	0.10 (±0.01)	0.072 (±0.008)	0.80 (±0.09)	0.30 (±0.03)
		84/116	Fe(III)_mix2	S06-047	94 (±11)	22 (±2)	9.6 (±1.1)	7.6 (±0.8)	6.5 (±0.7)	6.6 (±0.7)	0.68 (±0.08)	0.18 (±0.02)	0.081 (±0.009)	0.70 (±0.08)	0.28 (±0.03)
				S06-048	78 (±9)	19 (±2)	8.9 (±1.0)	7.1 (±0.8)	6.1 (±0.7)	6.3 (±0.7)	0.49 (±0.05)	0.22 (±0.02)	0.068 (±0.008)	0.66 (±0.07)	0.26 (±0.03)
		200/0	Fe(III)	S06-101	1829 (±205)	95 (±11)	14 (±2)	7.3 (±0.8)	4.7 (±0.5)	3.8 (±0.4)	0.67 (±0.08)	0.78 (±0.09)	0.0083 (±0.0017)	0.42 (±0.05)	0.15 (±0.02)
				S06-102	1804 (±202)	92 (±10)	14 (±2)	7.5 (±0.8)	4.9 (±0.5)	4.1 (±0.5)	0.80 (±0.09)	0.90 (±0.19)	0.0080 (±0.0017)	0.43 (±0.05)	0.15 (±0.02)
NiSO ₄	0.50	40/160	Ni_mix1	S06-029	7.4 (±1.5)	1.1 (±0.1)	1.9 (±0.2)	1.6 (±0.2)	1.6 (±0.2)	1.3 (±0.2)	0.23 (±0.03)	+	0.16 (±0.02)	1.1 (±0.1)	0.32 (±0.04)
		100/100	Ni_mix2	S06-030	7.4 (±1.5)	1.5 (±0.2)	3.6 (±0.4)	3.3 (±0.4)	3.4 (±0.4)	3.9 (±0.4)	0.47 (±0.05)	+	0.13 (±0.01)	0.92 (±0.10)	0.44 (±0.05)
				S06-031	12 (±1)	1.4 (±0.2)	2.9 (±0.3)	2.7 (±0.3)	2.8 (±0.3)	3.0 (±0.3)	0.39 (±0.04)	+	0.12 (±0.01)	0.94 (±0.10)	0.51 (±0.06)
		200/0	Ni	S06-032	6.4 (±1.3)	0.80 (±0.09)	0.74 (±0.08)	0.60 (±0.07)	0.30 (±0.03)	+	+	+	0.060 (±0.007)	0.58 (±0.06)	0.17 (±0.02)
CuSO ₄	0.48	40/160	Cu_mix1	S06-024	210 (±23)	15 (±2)	3.4 (±0.4)	3.0 (±0.3)	2.9 (±0.3)	3.8 (±0.4)	0.65 (±0.07)	0.13 (±0.01)	0.12 (±0.01)	0.83 (±0.09)	0.52 (±0.06)
		100/100	Cu_mix2	S06-025	532 (±59)	47 (±5)	4.2 (±0.5)	3.8 (±0.4)	3.4 (±0.4)	3.6 (±0.4)	0.18 (±0.02)	0.028 (±0.006)	0.14 (±0.02)	0.55 (±0.06)	0.28 (±0.03)
				S06-026	531 (±59)	46 (±5)	4.3 (±0.5)	3.9 (±0.4)	3.3 (±0.4)	3.4 (±0.4)	0.17 (±0.02)	0.019 (±0.004)	0.17 (±0.02)	0.54 (±0.06)	0.23 (±0.03)
ZnSO ₄	0.45	40/160	Zn_mix1	S06-034	11 (±1)	2.2 (±0.2)	1.9 (±0.2)	1.7 (±0.2)	1.6 (±0.2)	1.2 (±0.1)	0.14 (±0.02)	+	0.12 (±0.01)	0.85 (±0.10)	0.28 (±0.03)
		100/100	Zn_mix2	S06-035	12 (±1)	3.1 (±0.3)	3.3 (±0.4)	2.8 (±0.3)	2.9 (±0.3)	3.2 (±0.4)	0.48 (±0.05)	+	0.15 (±0.02)	0.87 (±0.10)	0.37 (±0.04)
				S06-036	14 (±2)	3.3 (±0.4)	3.3 (±0.4)	2.7 (±0.3)	2.7 (±0.3)	2.8 (±0.3)	0.38 (±0.04)	+	0.15 (±0.02)	0.90 (±0.10)	0.38 (±0.04)
		200/0	Zn	S06-037	20 (±2)	0.87 (±0.10)	0.68 (±0.08)	0.61 (±0.07)	0.30 (±0.03)	+	+	+	0.019 (±0.004)	0.44 (±0.05)	+

butene+ = mixture of 1-butene and 2-butene

1-PTH = 1-propanethiol

2-MeTH = 2-methylthiophene

3-MeTH = 3-methylthiophene

- quantification/detection not possible; due to low concentration and/or strong coelution

+ detected, but concentration too low for quantification

Table A2 continued: Reaction products continued.

Sample ID	Sample #	<i>iso</i> -butane	<i>iso</i> -pentane	acetone	butanone	pentanone	benzene	toluene	thiophene	2-MeTH	3-MeTH	Conversion of <i>n</i> -octane [mol%]*	C ₁ /ΣC ₁₋₄ [wt%]	O ₂ in organic products [mmol/mol C ₈ H ₁₈]
		0.0044	0.0045	0.0063	0.0089		0.00018	0.00016	0.00032	0.00014	0.00021			
Na	S06-023	+	+	1.8 (±0.2)	0.95 (±0.11)	+	+	+	-	-	-	0.58 (±0.04)	17 (±2)	14 (±2)
	S06-033	+	+	2.1 (±0.2)	0.92 (±0.10)	+	+	+	-	-	-	0.65 (±0.05)	17 (±2)	17 (±3)
Fe(II)_mix1	S06-042	0.44 (±0.05)	0.036 (±0.004)	2.3 (±0.3)	0.77 (±0.09)	+	0.019 (±0.002)	0.045 (±0.005)	0.075 (±0.008)	0.10 (±0.01)	+	1.1 (±0.1)	14 (±2)	13 (±2)
Fe(II)_mix2	S06-043	0.46 (±0.05)	0.059 (±0.007)	3.3 (±0.4)	1.0 (±0.1)	+	0.081 (±0.009)	0.084 (±0.009)	0.23 (±0.03)	0.12 (±0.01)	0.021 (±0.004)	1.6 (±0.1)	15 (±2)	21 (±3)
	S06-044	0.46 (±0.05)	0.051 (±0.006)	+	+	+	+	0.086 (±0.010)	0.26 (±0.03)	0.12 (±0.01)	0.031 (±0.006)	1.3 (±0.1)	14 (±2)	
Fe(II)	S06-045	0.58 (±0.06)	0.15 (±0.02)	5.0 (±0.6)	2.5 (±0.3)	+	0.089 (±0.010)	0.16 (±0.02)	0.48 (±0.05)	0.21 (±0.02)	0.10 (±0.01)	3.2 (±0.2)	25 (±3)	84 (±13)
Fe(III)_mix1	S06-046	0.47 (±0.05)	0.061 (±0.007)	7.8 (±0.9)	2.1 (±0.2)	+	0.092 (±0.010)	0.12 (±0.01)	0.22 (±0.02)	0.22 (±0.02)	0.009 (±0.002)	2.3 (±0.2)	20 (±3)	51 (±8)
	S06-100	0.46 (±0.05)	0.053 (±0.006)	7.3 (±0.8)	1.8 (±0.2)	+	0.081 (±0.009)	0.11 (±0.01)	0.26 (±0.03)	0.17 (±0.02)	0.016 (±0.003)	2.1 (±0.1)	21 (±3)	51 (±8)
Fe(III)_mix2	S06-047	0.49 (±0.05)	0.089 (±0.010)	8.0 (±0.9)	1.2 (±0.1)	+	0.28 (±0.03)	0.33 (±0.04)	1.1 (±0.1)	0.28 (±0.03)	0.13 (±0.01)	3.3 (±0.2)	26 (±3)	99 (±16)
	S06-048	0.47 (±0.05)	0.081 (±0.009)	6.9 (±0.8)	1.2 (±0.1)	+	0.27 (±0.03)	0.35 (±0.04)	0.90 (±0.10)	0.23 (±0.03)	0.15 (±0.02)	3.0 (±0.2)	25 (±3)	82 (±13)
Fe(III)	S06-101	0.51 (±0.06)	0.080 (±0.009)	8.0 (±0.9)	1.7 (±0.2)	+	2.8 (±0.3)	3.1 (±0.3)	38 (±4)	0.74 (±0.08)	0.51 (±0.06)	28 (±2)	60 (±8)	1834 (±290)
	S06-102	0.52 (±0.06)	0.085 (±0.010)	8.3 (±0.9)	1.8 (±0.2)	+	2.6 (±0.3)	3.4 (±0.4)	40 (±5)	0.85 (±0.10)	0.56 (±0.06)	28 (±2)	59 (±8)	1809 (±286)
Ni_mix1	S06-029	-	-	1.5 (±0.2)	1.0 (±0.1)	+	-	-	-	-	-	0.57 (±0.04)	7.5 (±1.0)	9 (±2)
Ni_mix2	S06-030	-	-	2.6 (±0.3)	1.5 (±0.2)	+	-	-	-	-	-	1.0 (±0.1)	5.2 (±0.7)	9 (±2)
	S06-031	-	-	2.4 (±0.3)	1.4 (±0.2)	+	-	-	-	-	-	0.92 (±0.06)	5.7 (±0.7)	14 (±2)
Ni	S06-032	-	-	1.5 (±0.2)	1.2 (±0.1)	+	-	-	-	-	-	0.29 (±0.02)	16 (±2)	8 (±2)
Cu_mix1	S06-024	0.45 (±0.05)	0.051 (±0.006)	9.8 (±1.1)	3.0 (±0.3)	+	1.2 (±0.1)	0.56 (±0.06)	+	0.039 (±0.004)	+	4.2 (±0.3)	38 (±5)	216 (±34)
Cu_mix2	S06-025	0.49 (±0.05)	0.055 (±0.006)	25 (±3)	9.0 (±1.0)	+	1.4 (±0.2)	1.2 (±0.1)	+	0.24 (±0.03)	+	9.6 (±0.7)	61 (±8)	549 (±87)
	S06-026	0.49 (±0.05)	0.050 (±0.006)	22 (±2)	8.5 (±1.0)	+	1.3 (±0.1)	1.0 (±0.1)	+	0.13 (±0.01)	+	9.4 (±0.7)	60 (±8)	547 (±86)
Zn_mix1	S06-034	-	-	2.2 (±0.2)	1.4 (±0.2)	+	-	-	-	-	-	0.64 (±0.04)	14 (±2)	12 (±2)
Zn_mix2	S06-035	-	-	2.9 (±0.3)	1.6 (±0.2)	+	-	-	-	-	-	1.0 (±0.1)	11 (±1)	14 (±2)
	S06-036	-	-	3.1 (±0.3)	1.9 (±0.2)	+	-	-	-	-	-	1.0 (±0.1)	12 (±2)	16 (±3)
Zn	S06-037	-	-	6.2 (±0.7)	3.9 (±0.4)	+	-	-	-	-	-	0.76 (±0.05)	18 (±2)	25 (±4)

* In order to estimate the amount of initial *n*-octane, which was converted during the experiments, the mass balance for carbon was calculated. The molar amount of carbon in the reaction products was summed and normalized to the initial amount of carbon provided by *n*-octane (245 ± 12 μmol C). The resulting value is an estimate for the minimum conversion of *n*-octane. Error propagation taking into account the analytical uncertainty and the weighing uncertainty, leads to a relative error for this calculation of 17% for the 300°C samples and 7% for the 350°C samples. This “detour” was necessary owing to the fact that *n*-octane concentrations remaining after the experiments were too high to be accurately measured with the headspace gas chromatograph.

B. FIGURES B1 – B4

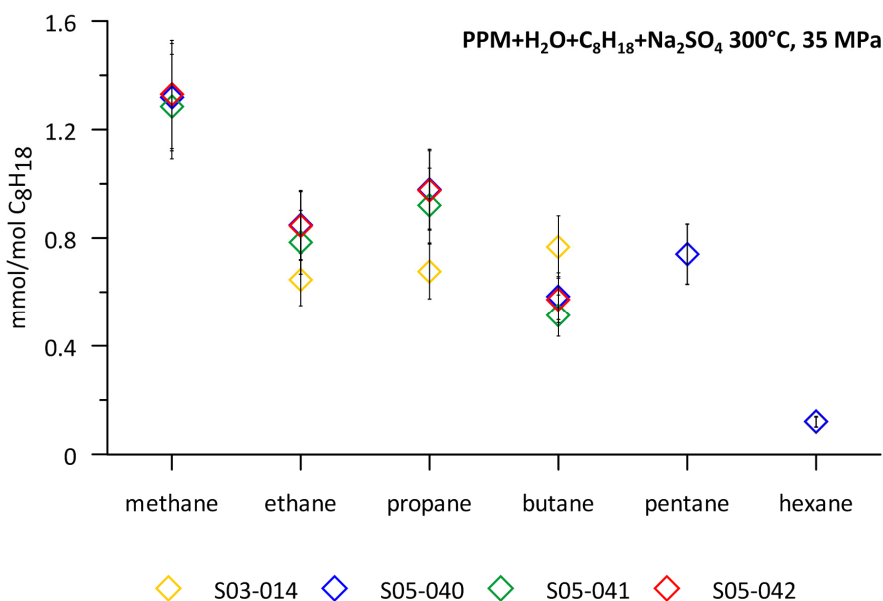


Fig. B1: Reproducibility of the sulfate-containing PPM samples at 300°C. The graphic compares the amount of *n*-alkanes produced from decomposition of *n*-octane at 300°C and 35 MPa after 168 h in the PPM-H₂O-C₈H₁₈-Na₂SO₄ system. Samples S05-040, -041 and -042 were processed in the same experiment, whereas sample S03-014 was processed 2 years prior to this. Methane data for sample S03-014, and *n*-pentane and *n*-hexane for samples S05-041 and -042 were not acquired. Detection limits were << 0.01 mmol/mol C₈H₁₈. Error bars represent the error (11 %), which was calculated via error propagation from the analytical uncertainty (10 %) and the total weighing error of initial *n*-octane (5 %).

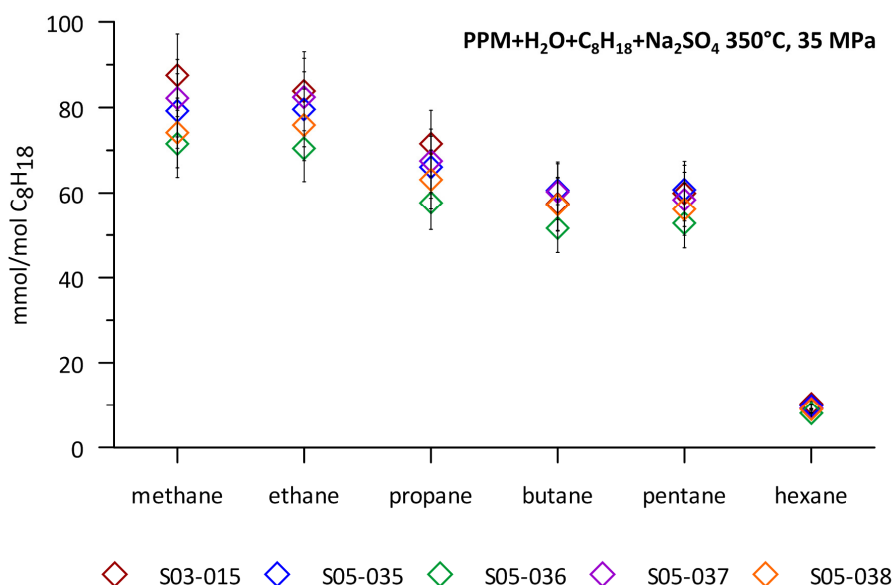


Fig. B2: Reproducibility of the sulfate-containing PPM samples at 350°C. The graphic compares the amount of *n*-alkanes produced from decomposition of *n*-octane at 350°C and 35 MPa after 168 h in the PPM-H₂O-C₈H₁₈-Na₂SO₄ system. Samples with the prefix S05 were processed in the same experiment, whereas sample S03-015 was processed 1.5 years prior to this. Depicted error bars represent a relative error of 11%, which results from error propagation taking into account the analytical error (10 %) and the total weighing error of initial *n*-octane (5 %). Note that the concentration of *n*-alkanes generated at 350°C is two orders of magnitude higher than at 300°C (Fig. B1).

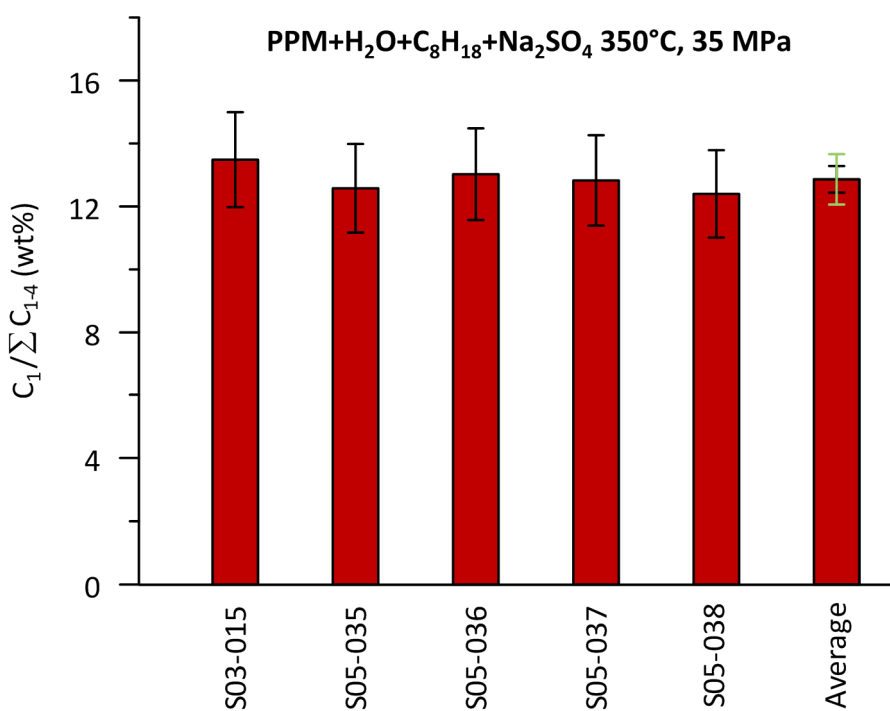


Fig. B3: Gas dryness values for five identical sulfate-containing PPM samples processed at 350°C and 35 MPa for 168 h in two different experiments (see caption of Fig. B2 for details). The uncertainty of the gas dryness values is calculated from error propagation of the analytical uncertainty, which is 10 % for each *n*-alkane. The single (black) and double (green) standard deviation of the arithmetic mean for the five samples indicate, however, that the precision for ratio considerations is significantly better ($\pm 7\%$).

C. SUMMARY OF THE BACHELOR THESIS FROM HINZE (2012)

In the course of my PhD work, I supervised the Bachelor thesis of Michael Hinze. The objective was to investigate the buffering capability of the PPM mineral buffer in presence and absence of sulfate at 350°C and 35 MPa. The experiments were planned by me. Furthermore, I provided support during laboratory work, and especially during data interpretation was. Michael Hinze performed the experiments of the type PPM+H₂O and PPM+H₂O+Na₂SO₄, using the same PPM mineral buffer that was employed in the present study. Sample preparation and the experimental procedure are analogue to this study. This means that initial quantities of all components are the same (30 mg PPM and 90 µl H₂O or Na₂SO₄ solution with a concentration of 1.7 molal) and that the CSPV was used for the experiments. Run duration was either 24 or 168 h.

Within 2 hours after the experiment, samples were analyzed by gas chromatography. In this case, a Varian CP 4900 micro gas chromatograph was used. It contains four separate analytical modules. Each module consists of an injector, a heated column compartment and a thermal conductivity detector (TCD). The first module was used for the hydrogen measurements. It consists of a molar sieve column with a length of 10 m. Column temperature and pressure were 45°C and 125 kPa respectively. The software “Galaxie Chromatography Workstation Version 1.9.3.2” was used to control the chromatograph as well as for data logging and processing. Compound identification was based on retention time as compared to analyses of certified standards. For the calibration two hydrogen standards (1.01 and 0.01 vol%) were used. Hydrogen amounts in the samples range from 0.004 to 0.009 vol% and are significantly below the calibrated range. However, it is assumed that the response of the TCD detector is linear and that the calibration can be extended to these lower concentrations. Multiple measurements of the lowest standard give an uncertainty of 20%. The reproducibility of individual sample measurements is even better, showing a relative error of 10 %.

Measured hydrogen amounts were converted to aqueous hydrogen concentrations, assuming that the analyzed hydrogen was completely dissolved in the fluid under experimental conditions. Results are illustrated in Fig. C1.

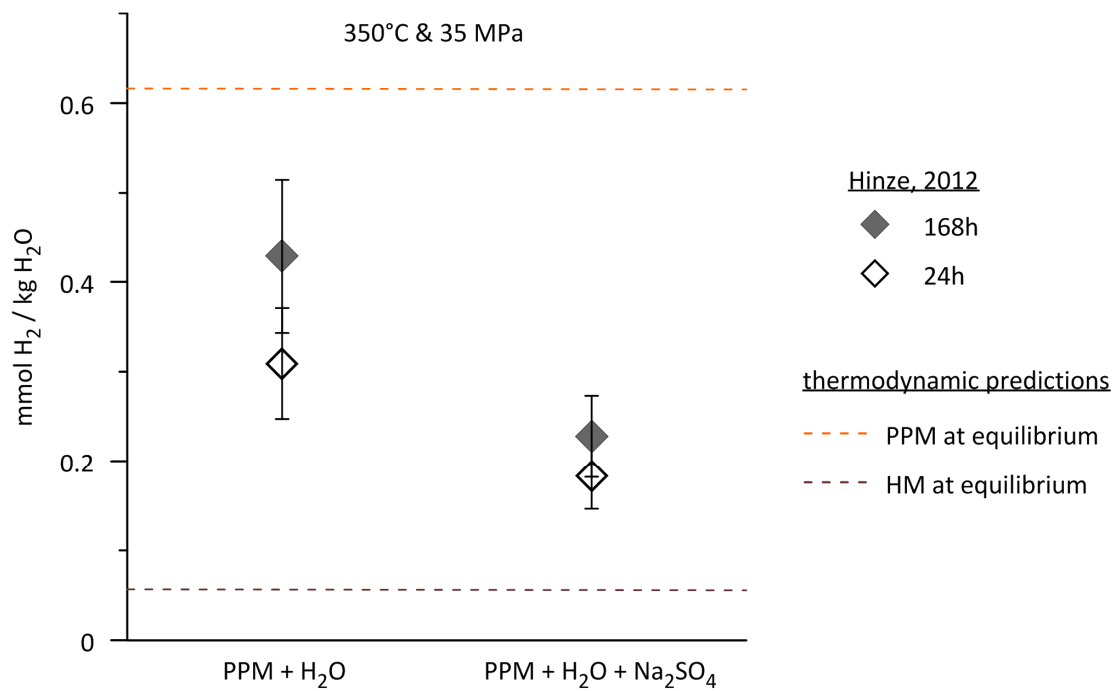


Fig. C1: Concentrations of aqueous hydrogen measured for PPM samples with (PPM+H₂O+Na₂SO₄) and without (PPM+H₂O) sulfate, which were processed at 350°C and 35 MPa for 24 and 168 h. Measured hydrogen concentrations can be converted to activity (α) values using the following equation:

$$\alpha_{H_2(aq)} = y_{H_2(aq)} \cdot c_{H_2(aq)} / \left(\frac{\text{mol}}{\text{kg H}_2\text{O}} \right)$$

with c being the molal (mol/kg H₂O) concentration of aqueous hydrogen. Following the procedure of Seewald (2001), an activity coefficient of 1 is adapted.

CURRICULUM VITAE • SVENJA ERDMANN (NÉE GERMEROTT)

■ Education

12.2009 – 01.2015

Ph.D. Geochemistry

Leibniz Universität Hannover (Germany), in cooperation with the Federal Institute for Geosciences and Natural Resources, Hannover (Germany), *final grade: magna cum laude*

Dissertation: “The Effect of Inorganic Components on Organic Matter Transformation under Hydrothermal Conditions – Constraints from Laboratory Experiments Studying the Abiotic Oxidation of *n*-Octane in Presence of Iron Mineral Assemblages, Additional Transition Metals and Dissolved Sulfate”

- Attended short courses on “Geochemistry in petroleum exploration” (Georg-August-Universität Göttingen, Germany) and “Molecular organic biogeochemistry” (NIOZ, Netherlands)
- Presentations at several conferences (e.g. Gordon Research Conference and IMOG)

11.2005 – 11.2009

M.Sc. equivalent Earth Sciences

German: “Diplom Geowissenschaftlerin”

Leibniz Universität Hannover (Germany), *final grade: 1.1, very good*

Thesis: “Experimental Investigations on Thermochemical Sulfate Reduction in Seafloor Hydrothermal Systems”

- Emphasis on mineral deposits and petroleum reservoirs

10.2003 – 11.2005

Undergraduate Studies Earth Sciences

Leibniz Universität Hannover (Germany), *final grade: 2.1, good*

■ Work Experience

since 03.2014

Geochemist – Research and Development

Baker Hughes INTEQ GmbH, Celle (Germany)

- Downhole fluid analysis and sampling
- Surface logging systems
- Formation evaluation
- Data integration

12.2009 – 05.2014

Research Assistant

Leibniz Universität Hannover (Germany)

- Experimental work with high pressure vessels
- Analytics: HSGC, HPLC, XRD, REM-EDX
- Supervision of a Bachelor thesis

04.2009 – 11.2009

Student Research Assistant – Experimental Petrology

Leibniz Universität Hannover (Germany)

- Experimental work with high pressure vessels

- 11.2007 – 05.2008 **Exploration Geologist**
 Vergenoeg Mining Company (Proprietary) Limited (South Africa)
- Supervision of drilling operations, led team of 5 people
 - Estimation of reserves and resources of the fluorspar deposit based on macroscopic, microscopic and geochemical analyses, integrated everything in a 3D model using Surpac 6.0.3
- 02.2004 – 09.2007 **Student Research Assistant – Material Sciences**
 Leibniz Universität Hannover (Germany)
- Synthesis of possible oxygen conductors
 - Analytics: XRD, IR, EMPA
- 03.2007 – 04.2007 **Internship Geothermal Energy**
 Federal Institute for Geosciences and Natural Resources, Hannover (Germany)
- 07.2006 – 09.2006 **Internship Mining Industry**
 Vergenoeg Mining Company (Proprietary) Limited (South Africa)

■ Extracurricular Activities

- 07.2014 – to date **Officer of the Society of Petroleum Engineers (SPE)**
 One out of three organizers for the SPE Student Technical Conference 2014 held in Wietze (Germany)
- 04.2012 – to date **Vice President and Founder of the Club “Freunde der Geowissenschaften Hannover e.V.”**
 Key objective is to support networking of alumni and students
- 12.2011 – to date **German Delegate for the Youth Committee of the World Petroleum Council (WPC)**
 The vision of the WPC Youth Committee is to engage young professionals from around the world to design a sustainable future
- 10.2010 – 07.2011 **“Promotion plus⁺ qualifiziert” Participant**
 Leibniz Universität Hannover (Germany), Qualifying courses for leadership skill development, selected by CV and motivation letter
- Covered topics: project management, time management, conflict management, team coaching, communication and presentation skills
- 11.2005 – 11.2009 **Elected member of the Earth Sciences’ Student Council**
 Leibniz Universität Hannover (Germany)
- Mentored and supported students

■ Language skills

Fluent: German and English Basic: French and Spanish

LIST OF PUBLICATIONS

2014

ERDMANN, S., Wessling, S., Pragt, J., Cartellieri, A. (2014). Downhole fluid analysis and sampling: Experience with a new logging-while-drilling service. Poster presentation at the Gordon Research Conference, Holderness, New Hampshire, USA

2012

GERMEROTT, S., Ostertag-Henning, C., Behrens, H. (2012). The solid interface: Effect of minerals on thermochemical sulfate reduction? – An experimental study. Oral presentation at the Gordon Research Seminar and poster presentation at the Gordon Research Conference, Holderness, New Hampshire, USA

2011

GERMEROTT, S., Ostertag-Henning, C., Behrens, H. (2011). Mechanisms of thermochemical sulfate reduction: Insights from redox buffered laboratory experiments. Abstract book of the 25th International Meeting on Organic Geochemistry, 18-23 September 2011, Interlaken, Switzerland, P-357. Poster presentation

GERMEROTT, S., Ostertag-Henning, C., Behrens, H. (2011). Geochemical signature of thermochemical sulfate reduction – Ketones and sulphur species. *Mineralogical Magazine*, Vol. 75 (3), 908. Oral presentation at the Goldschmidt Conference in Prague

2010

GERMEROTT, S., Ostertag-Henning, C., Behrens, H. (2010). Experimental investigations on thermochemical sulfate reduction (TSR) in a mineral buffered system – possible influences on sulfide ore precipitation. Oral presentation at the GeoDarmstadt Conference

GERMEROTT, S., Ostertag-Henning, C., Behrens, H. (2010): Experimental investigations on TSR in a mineral-buffered system with fixed H₂ and H₂S fugacities. *Geochimica et Cosmochimica Acta*, 74 (11), Supplement 1, A325. Poster presentation at the Goldschmidt Conference in Knoxville

GERMEROTT, S., Ostertag-Henning, C., Behrens, H. (2010): Thermochemical sulfate reduction: An experimental study – indices of oxidation. *Tagungsband der 88. Jahrestagung der Deutschen Mineralogischen Gesellschaft (DMG)*, P6-02. Poster presentation at the Annual Conference of the DMG in Münster

2008

FIEGE, A., Germerott, S., Holtz, F., Schwarz-Schampera, U., Schuette, P., Terblanche, H. (2008): Lithology and genesis of Plattekop hill as an extension of the Vergenoeg fluorspar deposit. Poster presentation at the 33rd International Geological Congress, Oslo, Norway